KfK 3815
Oktober 1984

Annual Report on Nuclear Physics Activities

July 1, 1983 - June 30, 1984

Editors:
D. C. Fries, P. Matussek, Ch. Weddigen
Institut für Kernphysik

Kernforschungszentrum Karlsruhe

KERNFORSCHUNGSZENTRUM KARLSRUHE

Institut für Kernphysik

KfK 3815

ANNUAL REPORT

on

NUCLEAR PHYSICS ACTIVITIES

July 1, 1983 - June 30, 1984

Editors:

D.C. Fries, P. Matussek, and Ch. Weddigen

Kernforschungszentrum Karlsruhe GmbH, Karlsruhe

Last Annual Reports:

1982/83: KfK 3621 (November 1983)

1981/82: KfK 3427 (November 1982)

1980/81: KfK 3280 (Februar 1982)

Als Manuskript vervielfältigt
Für diesen Bericht behalten wir uns alle Rechte vor

Kernforschungszentrum Karlsruhe GmbH
ISSN 0303-4003

ABSTRACT

This report surveys the activities in fundamental research from July 1, 1983 to June 30, 1984 at the Institute for Nuclear Physics (IK) of the Kernforschungszentrum Karlsruhe. The research program of this institute comprises laser spectroscopy, nuclear reactions with light ions, neutron physics, neutrino physics and physics at medium and higher energies.

ZUSAMMENFASSUNG

Der vorliegende Bericht gibt einen Überblick über die Arbeiten am Institut für Kernphysik (IK) des Kernforschungszentrums Karlsruhe im Zeitraum vom 1. Juli 1983 bis zum 30. Juni 1984. Das Forschungsprogramm umfaßt die Gebiete Laserspektroskopie, Kernreaktionen mit leichten Ionen, Neutronenphysik, Neutrino-Physik, sowie Mittel- und Hochenergiephysik.

PREFACE

We have the pleasure to present the fourth report on nuclear physics activities at the Kernforschungszentrum Karlsruhe. These activities are concentrated in the Institute for Nuclear Physics (IK). It consists of three sections (IK I, IK II, IK III), each of which spezializes in particular energy domains.

Three groups in Section IK I are engaged in work in various fields of nuclear physics and particle physics:

- Fast Neutron Physics: Scattering experiments on very light nuclei are carried out using the polarized neutron beam of the Karlsruhe Cyclotron (POLKA). The main goal is to determine precise phase shifts from experiments with polarized neutrons on unpolarized and also on polarized protons. Moreover, the internal structure and dynamics of the nuclei up to the A = 5 system are to be studied. The large-volume polarized proton target has been successfully used for scattering experiments with the polarized neutron beam in a number of experiments.

- High Energy Physics: This group runs the CELLO detector system at the e^+e^- storage ring, PETRA, in Hamburg within the framework of an international collaboration. The detector serves for experiments to study e^+e^- collisions at the highest energies at present attainable. CELLO, with its modern liquid-argon calorimeter, lends itself particularly well to studies of the electromagnetic component in these reactions. This allows, e.g., precise studies of quantum electrodynamics, detailed studies of quark and gluon jets and the search for new quarks. The upgraded detector is working satisfactorily and is strongly involved in the search for a new quark during the continuous energy increases in PETRA.

- Neutrino Physics: The newly founded working group is concerned with neutrino physics in the energy range between approximately 10 and 50 MeV, at the Spallation Neutron Source (SNS) under construction at the Rutherford-Appleton Laboratory (RAL) in England. This is a new field of work involving fundamental questions in the fields of elementary particle physics, nuclear physics and astrophysics. The project was proposed by KfK. In the meantime, a bilateral agreement has been signed between KfK and RAL. Several smaller working groups of the University of Oxford (Prof.Dr. N.E. Booth), Queen Mary College of London (Prof.Dr. J.A. Edgington), University of Erlangen (Prof.Dr. E. Finckh), and University of Tübingen (Prof.Dr. A. Faessler) have meanwhile joined the project. The detector system is being developed and built at KfK. It will be installed in a massive blockhouse of iron at the Rutherford SNS by the end of 1985.

Section IK II is mostly working on medium energy physics at CERN and SIN:

- One group, continuing a long tradition in the field of exotic atoms at CERN, has concentrated its activities on the LEAR Project (Low-Energy Antiproton Ring). The project, the realization of which was backed very strongly by Karlsruhe, promises to offer unique possibilities for work with slow antiprotons. Spectra of various elements were obtained. They contain new information on the strong interaction of antiproton-nucleon pairs, on the magnetic moment of the antiproton, and on the spin-orbit coupling for antiprotons. Another experiment makes use of the idea of the cyclotron trap proposed by Dr. L.M. Simons. The aim is the study of antiprotonic Hydrogen and Deuterium, the most direct approach to the antiproton-nucleon system. Karlsruhe is involved personally and financially also in a technical upgrading of LEAR, namely the use of electron cooling.

- The experiments at SIN focus on problems of pion interaction (scattering and absorption) with simple systems consisting of few nucleons. Theoretical assumptions, especially those about the existence of dibaryon states, are verified on the basis of additional information that can be obtained by using polarized targets. Also the low-energy spectrometer designed by Karlsruhe will mainly be used in studies of very simple systems at energies close to the pion threshold. The Coulomb nuclear interferences have been studied in preliminary experiments on Hydrogen. Absorption measurements of pion in ^3He study the isospin-dependence of the basic two-nucleon-absorption process. This reaction is of great theoretical significance.

Section IK III is mainly working in the following fields:

- Nuclear astrophysics: Capture cross sections of fast neutrons in the keV to MeV range are measured in order to understand in detail the build-up of heavy elements in stars. These measurements are supplemented by studies of nuclear spectroscopy on nuclei of specific importance to stellar neutron capture reactions. A new 4π scintillation gamma ray sum spectrometer is developed in order to increase the precision of capture cross section measurements.

- Nuclear reactions: Alpha particle and ^{6}Li beams from the Karlsruhe Isochronous Cyclotron are used for studying nuclear reactions at 26 MeV/nucleon. The emphasis is at present on the break-up of ^{6}Li in nuclear collisions with the aim to study the momentum distribution of its constituents.

- Laser spectroscopy: This technique is applied to sub-ng amounts of radioactive atoms in order to determine hyperfine structure and isotopic shifts of atomic transitions. The results yield information on nuclear moments and on the change of nuclear charge radii due to varying neutron number. Measurements on a long series of tin isotopes are nearing completion, and new techniques are developed to extend the experiments to transuranium elements.

- Applied gamma-ray spectroscopy: Here instruments are developed to determine concentration and isotopic composition of fissile material. The instruments make use either of the intrinsic radioactivity or of X-ray absorption and fluorescence. Their main applications are in the safeguards of nuclear fuel and in process control during fabrication and reprocessing.

- Section IK III is also responsible for the operation of the Karlsruhe Isochronous Cyclotron. The cyclotron laboratory has been considerably extended during the last years by the installation of a second cyclotron in an annex to the cyclotron building. This accelerator has gone into operation in late 1983 (after a considerable delay caused by economic difficulties of the manufacturer) and is operated on a commercial basis for producing isotopes for nuclear medicine and for irradiating machine parts for wear studies in industry.

The three sections of the Institute have been involved in common studies of future instruments in nuclear physics.

(A. Citron) (G. Schatz) (B. Zeitnitz)

CONTENTS

1. NUCLEAR PHYSICS

1.1 NUCLEAR ASTROPHYSICS

1.1.1 DESTRUCTION OF ^{26}Al VIA THE ^{26}Al(n,p)^{26}Mg REACTION

H.-P. Trautvetter^{+}, F. Käppeler, Z. Physik A 318 (1984) 121

Among the isotopic anomalies discovered in meteorites over the last years, the Mg anomaly is of particular interest. It was found that the relative ^{26}Mg enrichments correlate with the aluminium content of the respective inclusions of the Allende meteorite, and it was therefore concluded that ^{26}Al is the cosmologically short lived ($T_{1/2}$ = 7.2 • 10^{5}y) radioactive progenitor of the ^{26}Mg excess. This means that freshly produced ^{26}Al from supernova or nova events was incorporated into the premordial solar system material.

An understanding of the ^{26}Al abundance in terms of stellar nucleosynthesis requires knowledge of all processes which may create or destroy this nucleus. In the absence of neutrons ^{26}Al is destroyed mainly by the ^{26}Al(p,γ) reaction whose rate is now experimentally determined (1) after an ^{26}Al target became available (2). In explosive nucleosynthesis where free neutrons are abundant the survival of ^{26}Al depends critically on the ^{26}Al (n,p) reaction.

For this reason a first measurement of the ^{26}Al(n,p) cross section was initiated using the Maxwellian like spectrum for kT = 25 keV from the ^{7}Li(p,n) reaction near threshold (3). The experimental setup is shown in Fig. 1 together with the neutron spectrum to which the sample was exposed. This spectrum is somewhat shifted to kT = 30 keV rather than 25 keV due to the limited solid angle between neutron target and sample. Protons are detected by a 100 µm thick Si-detector with an area of 300 mm² which was placed at a distance of 6 mm from the ^{26}Al sample. This sample had an area of 616 mm² and a thickness of 1.14 • 10^{15} atoms cm^{-2}. A gold foil back to back with the ^{26}Al target served for neutron flux determination via activation.

In this first experiment we succeeded to detect the protons from the p_1-group of the ^{26}Al(n,p) reaction leading to the first excited state in ^{26}Mg. A weak p_o-group was barely visible in the proton spectrum (at Θ_p = 90 deg the 100 µm - Si-detector does not stop the P_o-group completely)

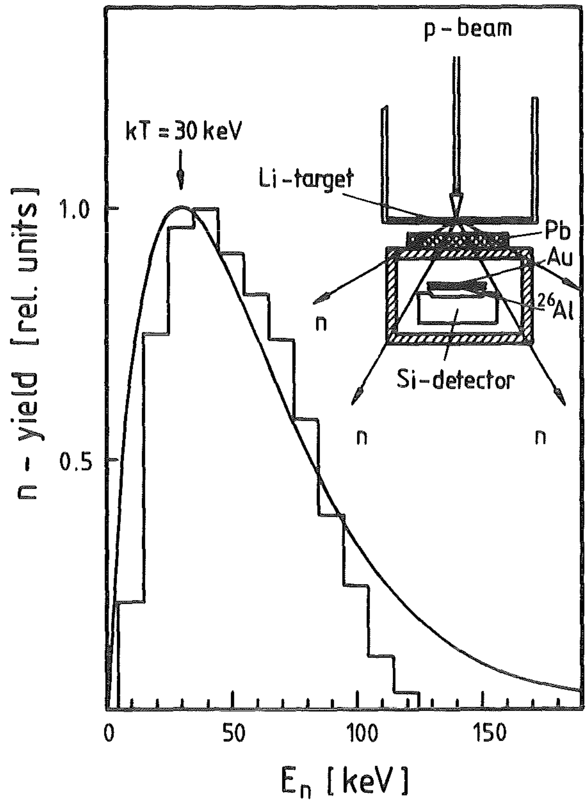

Fig.1
Experimental setup and neutron spectrum at the sample position (histogram). The solid line gives the Maxwellian spectrum at kT = 30keV for comparison.

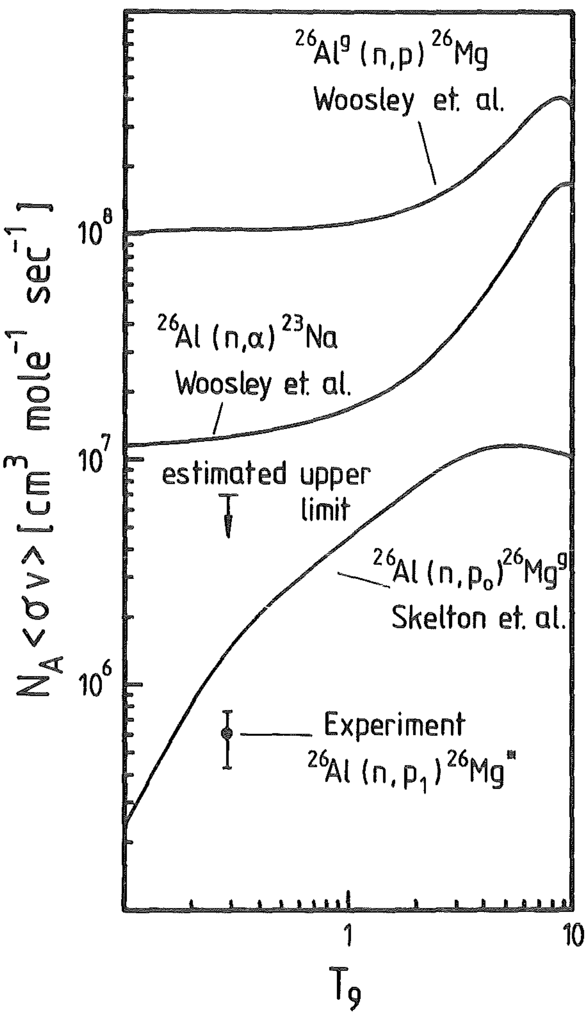

Fig.2
First experimental results for the $^{26}Al(n,p)^{26}Mg^*$ reaction and the estimated upper limit for the total (n,p) rate of ^{26}Al. These data are considerably lower than the corresponding Hauser-Feshbach calculations (4).

while the proton groups p_2, p_3, p_4, p_5 associated with the higher lying states in ^{26}Mg could not be unambiguously identified because of the intense background. For the partial cross section of the p_1-group we extracted a value of $\overline{\sigma}$ = 4.1 ± 1.2 mb. With the assumptions (based on energy and centrifugal barrier arguments) that the unobserved p_i-transitions have similar intensities as the transition to the first excited state and that the cross section varies with 1/v one estimates an upper limit of the total (n,p) rate of $N_A<\sigma v> \leq 10^6$ cm³ mol^{-1} sec^{-1} at T_q = 2.9. This limit is more than a factor of 10 smaller than the result of a Hauser-Feshbach calculation (4), as is shown in Fig. 2.

The here described first attempt to determine the ^{26}Al(n,p) rate will be complemented with measurements at different neutron energies and with an improved setup.

(1) L. Buchmann, M. Hilgemeier, A. Krauss, A. Redder, C. Rolfs, H.P. Trautvetter, T.R. Donoghue, Nucl. Phys. A 415 (1984) 93
(2) L.Buchmann, H. Baumeister, C. Rolfs, Nucl. Instr. Meth. (in print)
(3) H. Beer, F. Käppeler, Phys. Rev. C 21 (1980) 534
(4) S.E. Woosley, W.A. Fowler, J.A. Holmes, B. Zimmerman, Atomic Data and Nuclear Data Tables 22 (1978) 371

+ Institut für Kernphysik der Universität Münster

1.1.2 THE CAPTURE WIDTH OF THE 34.8 keV s-WAVE NEUTRON RESONANCE IN ^{27}Al

K. Wisshak, F. Käppeler and G. Reffo+, (1)

The neutron capture width of the s-wave resonance at 34.8 keV in ^{27}Al has been determined using a setup with extremely low neutron sensitivity. This feature is important because this resonance exhibits a very large scattering to capture ratio. A pulsed 3-MV Van de Graaff accelerator and a kinematically collimated neutron beam, produced via the ^{7}Li(p,n) reaction, was used in the experiment. Capture gamma-rays were observed by three Moxon-Rae detectors with graphite-, bismuth-graphite-, and bismuth-converter, respectively. The samples were positioned at a neutron flight path of only 9 cm. Thus events due to capture of resonance scattered neutrons in the detectors or in surrounding materials are completely discriminated by their additional time of flight. The data obtained with the individual detectors were corrected for the efficiency of the different converter materials. For that purpose, theoretical calculations of the capture gamma-ray spectra of the measured isotope and of gold, which was used as a standard, were performed. The final radiative width is $g\Gamma_{\gamma} = 1.22 \pm 0.07$ eV. The accuracy is nearly a factor of three better than in previous experiments.

(1) dito, Nucl. Sci. Eng.(in print)

+ E.N.E.A., Bologna, Italy

1.1.3 STELLAR NEUTRON CAPTURE RATES FOR ^{46}Ca AND ^{48}Ca

F. Käppeler, G. Walter, G.J. Mathews[+]

The nucleosynthetic origin of the heaviest calcium isotopes, ^{46}Ca and ^{48}Ca, has been a long standing puzzle in nuclear astrophysics. Fig. 1 shows the isotopic calcium abundances. The most abundant stable isotope, ^{40}Ca, is copiously produced in oxygen-burning zones of massive stars (1).

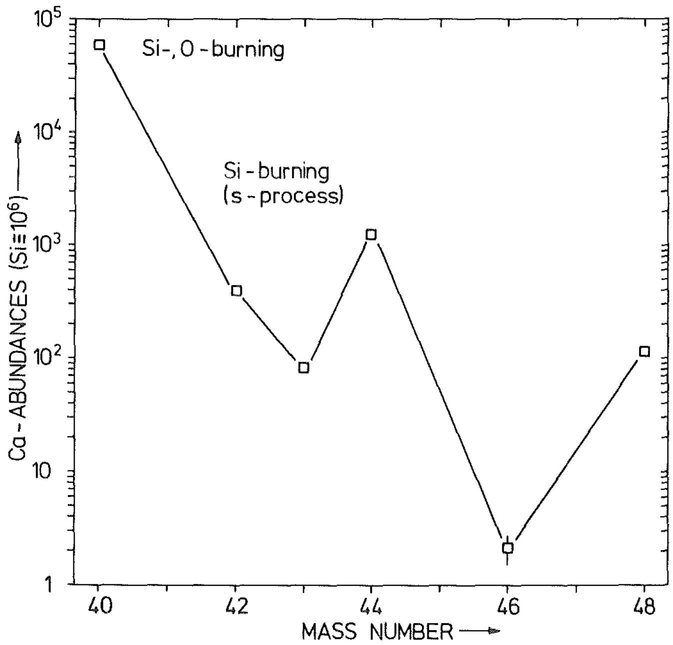

Fig. 1
The isotopic calcium abundances

Quasiequilibrium silicon burning (2,3) also contributes to the abundance of ^{40}Ca and (via the decay of ^{44}Ti) to the abundance of ^{44}Ca, as well as to the intermediate isotopes 42 and 43. These latter isotopes may also have a classical s-process component (4). The contribution of the above processes to ^{46}Ca and ^{48}Ca, however is a steeply decreasing function of isotopic mass. These processes tend to underestimate the already low ^{46}Ca and ^{48}Ca abundances as well as their large isotopic ratio of 53 ± 16. The rare heavy Ca isotopes are therefore probably the result of a separate stellar environment which can produce significant enrichments of the ^{46,48}Ca isotopes. This material can later mix with the interstellar medium to produce the observed solar-system abundances.

Numerous attempts have been made to identify the exotic origin of these isotopes. Detailed reaction network calculations in explosive nucleosynthetic environments have had some success in producing $^{46,48}Ca$ enrichments but are overestimating the ^{46}Ca abundance by factors 4 to 7. These results have been limited by a lack of experimental (n,γ) cross sections for ^{46}Ca and ^{48}Ca.

These data are equally important for the discussion of recently discovered isotopic anomalies for ^{46}Ca and ^{48}Ca in several inclusions from the Allende meteorite (5). It has been proposed (6) that these anomalies could be produced in a high-density neutron capture environment in which both neutron capture and beta-decay are in competition.

At the present time there is not enough separated isotope of ^{46}Ca for an in-beam time-of-flight measurement (with existing facilities) of the $^{46}Ca(n,\gamma)^{47}Ca$ cross section by observing the capture gamma-rays. This precludes the possibility of directly measuring neutron capture resonances in ^{46}Ca. Fortunately, however, both ^{46}Ca and ^{48}Ca are quite amenable to a measurement of the Maxwellian averaged capture cross section by the activation technique (7). This technique has been shown to yield the proper Maxwellian averaged (n,γ) cross sections with a precision of ∿ 5 - 10 %. Beside the standard spectrum corresponding to kT = 25 keV we also utilized spectra at higher energies to search for the effect of resonances and to allow for a reliable extrapolation to kT = 30 keV.

Our final results for the average capture cross sections of $^{46,48}Ca$ are listed in Table 1. The comparison with Hauser-Feshbach calculations (8) shows agreement within the 50 % error band usually quoted for these calculations. This is somewhat surprising since for these light nuclei near or at a doubly closed shell the level density is too low for the usual statistical-model assumption to be valid.

With the present cross sections a straightforward solution for the formation of $^{46,48}Ca$ via steady-state neutron capture reactions can be ruled out. The assumption of a high neutron density ($n_n \gtrsim 10^{12}$ cm^{-3}) would allow for a bridge in the neutron capture path to ^{48}Ca across the beta unstable isotopes ^{45}Ca ($t_{1/2}$ = 163d) and ^{47}Ca ($t_{1/2}$ = 4.5 d) with negligible leakage to scandium and titanium. Any steady state situation, however, can at most produce an isotopic ratio

$$\frac{N^{48}}{N^{46}} \leq \frac{\sigma_{46}}{\sigma_{48}} = 6 \pm {1.2 \atop 1.0} ,$$

which is much lower than the solar system ratio of 53. A possible way to increase the steady state value would be to selectively deplete ^{46}Ca by subsequently irradiating the steady state abundances with a sufficiently low neutron density that neutron capture on ^{45}Ca and ^{47}Ca can no longer compete with beta decay. This formal solution, however, requires that all ^{46}Ca and ^{48}Ca must be processed in this way which is not plausible. Therefore, a neutron capture origin of ^{46,48}Ca can almost certainly be ruled out. On the other hand we find that our steady state abundances for $n_n \gtrsim 10^{12}$ cm^{-3} are consistent with the anomaly reported for the high temperature inclusion EK-1-4-1 from Allende.

Table 1 Experimental results of the Maxwellian-averaged (n,γ)-cross sections for ^{46,48}Ca and comparison to model calculations.

	Average Capture Cross Section for kT = 30 keV (mb)	
	^{46}Ca	^{48}Ca
This work experimental	5.7 $\pm$ 0.5	0.95 $\pm$ 0.09
Ref. (8) calculated	3.7	1.1

(1) S.E. Woosley and T.A. Weaver in "Essays in Nuclear Astrophysics", eds. C.A. Barnes, D.D. Clayton, and D.N. Schramm (Cambridge: Cambridge University Press) 1982, p. 377

(2) D. Bodansky, D.D. Clayton, and W.A. Fowler, Ap. J. Suppl., 16 (1968) 299

(3) J.W. Truran, Ap. Sp. Sci., 18 (1972) 306

(4) F. Käppeler, H. Beer, K. Wisshak, D.D. Clayton, R.L. Macklin, and R.A. Ward, Ap. J. 257 (1982) 821

(5) F.R. Niederer, D.A. Papanastassiou, and G. Wasserburg Geochim. Cosmochim. Acta, 45 (1981) 1017

(6) D.G. Sandler, S.E. Koonin, and W.A. Fowler, Ap. J. 259 (1982) 908

(7) H. Beer, and F. Käppeler, Phys. Rev., C 21 (1980) 534

(8) S.E. Woosley, W.A. Fowler, J.A. Holmes, and B.A. Zimmerman, Atomic Data and Nuclear Data Tables, 22 (1978) 371

+ University of California, Lawrence Livermore National Laboratory

1.1.4 NEUTRON CAPTURE CROSS SECTIONS OF THE KRYPTON ISOTOPES AND THE s-PROCESS BRANCHING AT ^{79}Se

G. Walter, B. Leugers, F. Käppeler, Z.Y. Bao[+], D. Erbe, G. Rupp, G. Reffo[++], F. Fabbri[++], (1)

The input data for an analysis of the s-process branching at ^{79}Se have been significantly improved. The neutron capture cross sections for the stable krypton isotopes (except ^{86}Kr) were measured between 3 and 240 keV neutron energy. In addition, with statistical model calculations of the (n,γ)-cross sections for all isotopes and with other experimental results from literature,a recommended set of Maxwellian average cross sections was established in the mass region 77<A<85. The relevant decay parameters of the involved unstable nuclei and the parameters for the s-process model are discussed as well. On this basis the following aspects are investigated: the temperature during s-process, the decomposition into s- and r-process contributions and the solar krypton abundance.

(1) dito, KfK-Report 3652 (1984)

\+ On leave from the Institute of Atomic Energy Academic Sinica, Peking, China

++ E.N.E.A. Bologna, Italy

1.1.5 NEUTRON DENSITY AND TEMPERATURE OF THE WEAK s-PROCESS COMPONENT

G. Walter, (1)

The present work is concerned with nucleosynthesis by neutron capture. The methodology of the applied (n,γ)-experiments is described and the results of various capture cross section measurements are used for a first determination of temperature and neutron density of the weak s-process component.

The neutron capture cross sections of ^{70}Ge, ^{80}Se, ^{80}Kr, ^{82}Kr, ^{86}Kr, ^{86}Se, ^{87}Se and elemental gallium have been measured as a function of neutron energy by the time-of-flight method. From the experimental data the Maxwellian averaged capture cross sections were calculated for kT = 20 keV up to kT = 50 keV.

The activation method was applied to measure directly the 25 keV Maxwellian averaged (n,γ)-cross sections of ^{71}Ga, ^{74}Ge, ^{75}As, ^{79}Br, ^{81}Br, ^{86}Kr,

^{85}Rb, and ^{87}Rb.

With the help of the experimental data the s-process branchings at ^{79}Se and ^{85}Kr have been analysed in the framework of a model with two independent components of exponentially distributed neutron fluences. A consistent description of the solar abundances was achieved. The solar krypton abundance has been calculated from s-process systematics.

It is shown for the first time that the allowed regions for temperature and neutron density of main and weak s-process component do not overlap within the applied model.

(1) dito, KfK-Report 3706 (1984)

1.1.6 COSMOCHRONOLOGY WITH THE ^{87}Rb/^{87}Sr ISOBARIC PAIR

H. Beer, G. Walter, Astrophys. Space Sci. 100 (1984) 243

The long-lived cosmochronometer ^{87}Rb ($T_{1/2}$ = 4.8 x 10^{10}y) is studied. As its origin is partly due to s- and partly to r-process nucleosynthesis it can provide information about the time histories of these processes. The methods of using ^{87}Rb quantitatively for a chronological analysis are described. Tentative calculations based on the existing experimental data are also presented. The data indicate a larger r-process age than the s-process age.

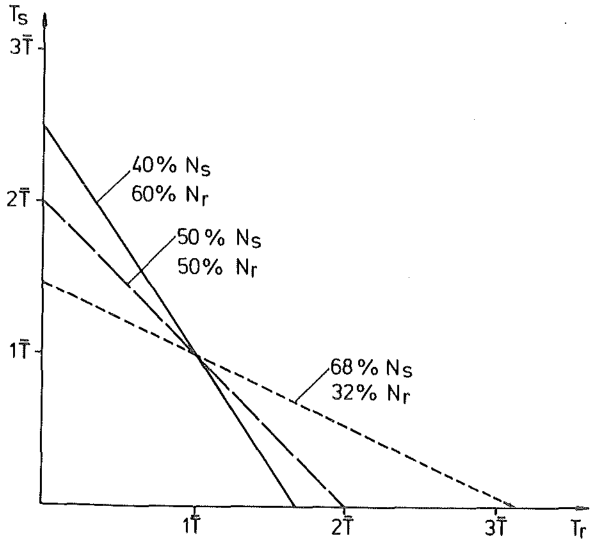

Fig. 1
The functional dependency $N_s e^{-\lambda T_s} + N_r e^{-\lambda T_r} = (N_s + N_r) e^{-\lambda \bar{T}}$ of the average s-process age T_s and the r-process age T_r for $\lambda\bar{T}$, λT_s, λT_r <<1 can be approximated by a linear relationship of T_s and T_r. The function is plotted for various assumptions about the N_s and N_r contribution of the radionuclide ^{87}Rb which can - in principle - be calculated via s-process systematics.

1.1.7 THE s-PROCESS NUCLEOSYNTHESIS OF ZIRCONIUM IN S-STARS

H. Beer, G. Walter, Astron. Astrophys. 133 (1984) 317

The abundances of $^{90,91,92,93,94}Zr$ in the S-stars R Cyg, V Cnc, and R Gem as reported by Zook (1978) are studied using the model of an exponential distribution of neutron exposures. The characteristic quantity, the average time integrated neutron flux τ_0, was determined to be $(0.0075 {+0.083 \atop -0.029}) 10^{27}$ neutrons per cm². The neutron density was estimated to be smaller than $\sim 10^8$ neutrons per cm³ due to the absence of any ^{96}Zr abundance. Implications for the pulsed s-process model of Truran and Iben (1) are discussed.

(1) J.W. Truran, and I. Iben, jr., Ap. J. 216 (1977) 797

1.1.8 ANALYSIS OF Zr AND Tc ABUNDANCES FROM S-STARS USING THE s-PROCESS WITH AN EXPONENTIAL DISTRIBUTION OF NEUTRON EXPOSURES

H. Beer, G. Walter, (1)

The abundances of Zr, Mo, Tc and Ru from S-stars were studied in the frame of the s-process with an exponential neutron fluence distribution which appears to be a natural consequence of the repeated occurrence of short neutron exposures in the He-shell of red giant stars. For quantitative analyses of the isotopic and elemental abundances the computer code SPEED has been developed. Estimates for the average time integrated neutron flux τ_0 and the s-process neutron density and temperature have been derived from the abundances of the Zr-isotopes and from Tc, respectively.

In conclusion we can state that it is possible to obtain the following information about the s-process in stars from elemental abundances (Fig. 1):

a) τ_0 can be determined if the abundances of Sr, Y, Zr, Mo are compared with Ba and the rare earths.

b) s-process temperature and neutron density can be derived from the analysis of branchings using abundance ratios like Cu/Zn, Sr/Rb, Tc/Mo, Sm/Pm and Lu/Hf.

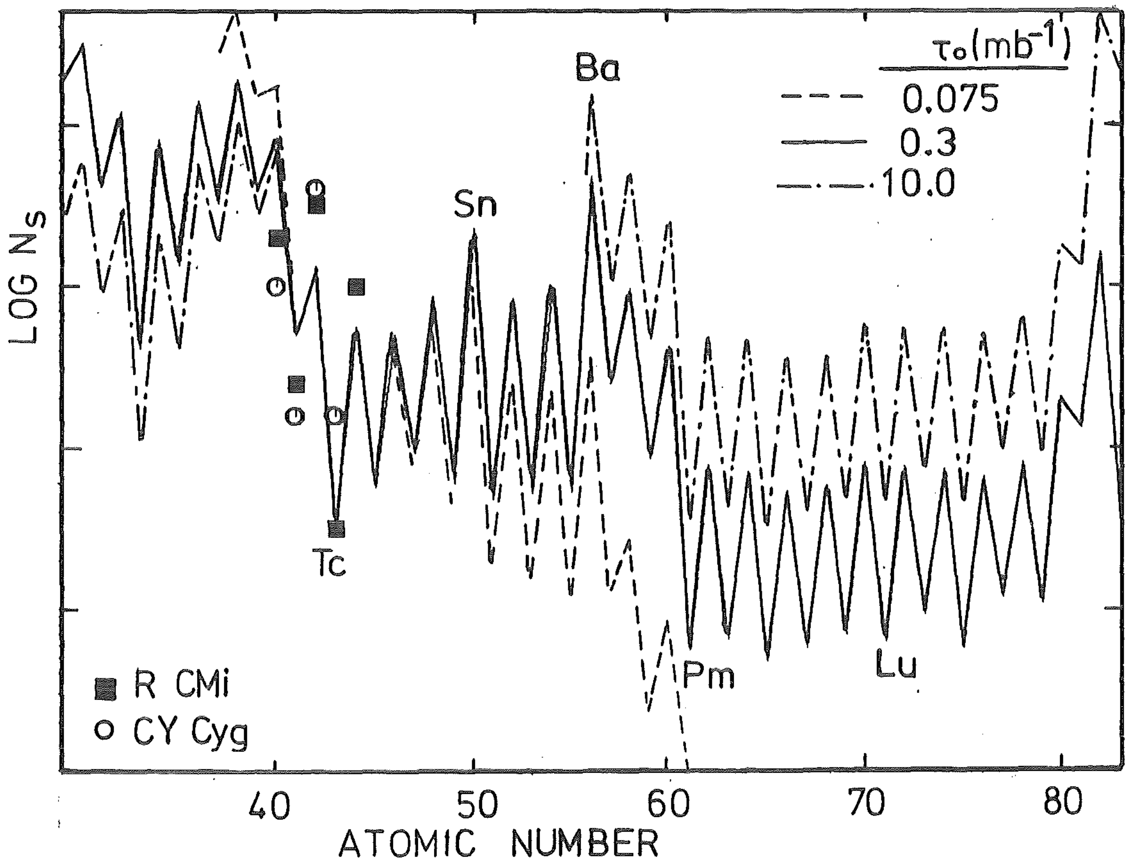

Fig. 1 The s-process abundance N_S calculated for three values of the average time integrated neutron flux τ_0 and normalized at Mo. The symbols are stellar data. The normalization between the calculation and the data was taken from Smith and Wallerstein (2). To reproduce Tc from R CMi as shown, a branching is required where half of ^{99}Tc is allowed to decay to Ru.

(1) dito, Colloquium on Cold Stars with excess of Heavy Elements July 3 - 6 1984 Strasbourg - France

(2) V.V. Smith, and G. Wallerstein, Ap. J. 273 (1983) 742

1.1.9 NEUTRON CAPTURE CROSS-SECTIONS OF STABLE XENON ISOTOPES AND THEIR APPLICATION IN STELLAR NUCLEOSYNTHESIS

H. Beer, F. Käppeler, G. Reffo[+], G. Venturini[+], Astrophysics and Space Science 97 (1983) 95

The neutron capture cross-sections of ^{124,132,134}Xe have been measured by the activation technique at 25 keV neutron energy. These data were supplemented by calculated capture cross-sections for $^{128,129,130,131}Xe$ via the statistical model. The complete set of capture cross-sections obtained in this way served to determine the solar xenon abundance through s-process systematics and to study a variety of isotopic anomalies.

+ Laboratorio Dati Nucleari, Ente Nazionale per l'Energie Alternative, Bologna, Italy

1.1.10 NEUTRON CAPTURE NUCLEOSYNTHESIS OF NEODYNIUM ISOTOPES AND THE s-PROCESS FROM A = 130 TO 150

G.J. Mathews+, F. Käppeler (1)

New measurements of neutron capture cross sections for $^{142,143,144}Nd$ are reported. These are combined with other recent measurements and applied to a detailed study of the s-process and r-process systematics for A = 130 to 150 nuclei. The influence of these results on the interpretations of isotopic anomalies observed in acid insoluble residues and inclusions from the Allende meteorite is also examined. The uncertainties in the s-process σN curve are significantly diminished in the present work and a fit is obtained which is consistent with all of the s-process-only isotopes in this region. A somewhat larger value than previous determinations is obtained for the mean neutron exposure for heavy nuclei in the s-process, $\tau_0 = 0.29 - 0.35\ mb^{-1}$. The derived r-process abundances decrease systematically from the A = 130 peak but exhibit a pronounced odd-even effect. The new results tend to confirm the hypothesis that the isotopic anomalies in materials from the Allende meteorite are the results of an unusual mixture of average solar-system s-process and r-process material, but a previously unobserved odd-even effect may be present in the r-process anomalies of inclusion EK1-4-1.

(1) Ap. J. (in press)

+ University of California, Lawrence Livermore National Laboratory

1.1.11 THE s-PROCESS BRANCHING AT ^{151}Sm

H. Beer, F. Käppeler, K. Yokoi and K. Takahashi, The Astrophysical Journal, 278 (1984) 388

The s-process branching in the mass region 150 ≦ A ≧ 154, initiated by the ^{151}Sm β^- decay, is reinvestigated, particulary in connection with the solar ^{152}Gd abundance. The Maxwellian averaged neutron capture cross sections for kT = 25 keV are measured for ^{152}Sm, ^{151}Eu (to the 9.3 hour isomeric state of ^{152}Eu), ^{152}Gd, ^{158}Gd, and ^{160}Gd. The ß-decay rates of the unstable nuclei involved in the branching are calculated theoretically. In addition, it is shown that the thermal equilibration between the ground state and the isomeric state in ^{152}Eu under plausible s-process conditions is achieved on a time scale shorter than those for β-decay and neutron capture. With these results and the neutron capture cross sections from literature for the other concerned nuclei, a branching analysis is performed within a steady flow model of the s-process. This study yields constraints for s-process models, particulary with regard to temperature and neutron density.

1.1.12 THE ^{163}Dy - ^{163}Ho BRANCHING: AN s-PROCESS BAROMETER

H. Beer, G. Walter, R.L. Macklin+, (1)

The isotope ^{163}Dy, under terrestrial conditions a stable nucleus, can become a radionuclide in the hot photon bath of a star via the electromagnetic linkings with the excited states and subsequent beta decay to ^{163}Ho. This conversion is strongly favored by the small Q-value of ^{163}Ho which lies only 2.3 to 2.6 kev above ^{163}Dy (2,3). A stellar environment where ^{163}Dy shows this behavior is the site of the s-process nucleosynthesis (He-shell of a red giant star). The synthesis path has a branching at ^{163}Dy which renders possible the s-process synthesis of ^{164}Er. This branching is sensitive to temperature, neutron density and electron density due to the efficacy of gamma-ray absorption and emission (temperature), neutron capture (neutron density) and bound state beta decay (electron density) on the ^{163}Dy-^{163}Ho half-lives (4,5). The branching has been treated quantitatively. Necessary input parameters are the capture cross sections of ^{160,163}Dy and ^{164}Er which were measured. Neutron density and s-process temperature could be taken from the analysis of other branchings (6). The experimental data and the calculations are discussed and constraints are derived for the electron density which is a measure of the density in the He-shell and can therefore act as a barometer.

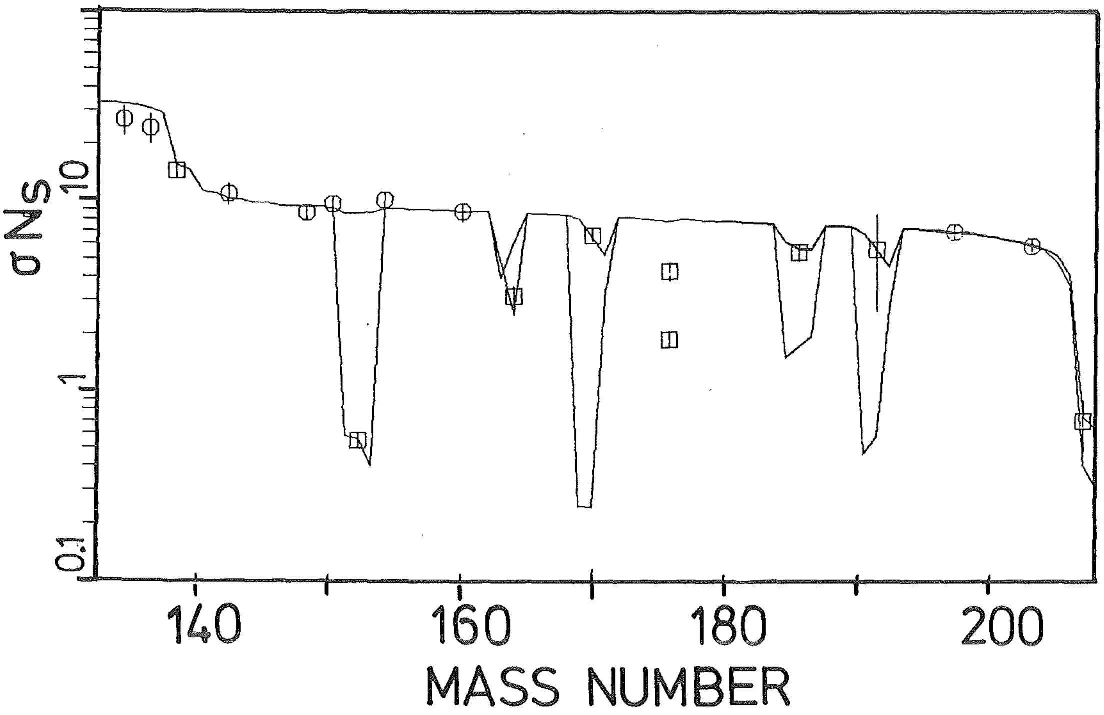

Fig. 1 The product of s-process abundance times cross section as a function of mass number. Temperature and neutron and electron density are adjusted in the branchings to reproduce ^{152}Gd, ^{164}Er, ^{186}Os and ^{192}Pt. Only in the case of ^{164}Er the branching is sensitive to the electron density. The solid curve is calculated for kT = 23 keV, $n_n = 1.3 \times 10^8$ neutrons/cm³ and $n_e = 3 \times 10^{27}$ electrons/cm³.

(1) dito, Fifth International Symposium on Capture Gamma-Ray Spectroscopy and Related Topics, Knoxville, TN, Sept. 10-14, 1984
(2) J.U. Andersen et al., Phys. Lett. 113B (1982) 72
(3) P.A. Baisden et al., Phys. Rev. C 28 (1983) 337
(4) K. Takahashi, K. Yokoi, Nucl. Phys. A404 (1983) 578
(5) K. Takahashi, K. Yokoi, private communication
(6) H. Beer, G. Walter, R.L. Macklin, P.J. Patchett, Phys. Rev. C (in press)

+ Oak-Ridge National Laboratory, Oak Ridge, USA

1.1.13 NEUTRON CAPTURE CROSS SECTIONS AND SOLAR ABUNDANCES OF ^{160,161}Dy, ^{170,171}Yb, ^{175,176}Lu and ^{176,177}Hf TO STUDY THE s-PROCESS NUCLEOSYNTHESIS OF THE RADIONUCLIDE ^{176}Lu

H. Beer, G. Walter, R.L. Macklin[+], P.J. Patchett[++]

The neutron capture cross sections and solar abundances of ^{160,161}Dy, ^{170,171}Yb, ^{175,176}Lu and ^{176,177}Hf have been measured. With this data base s-process studies have been carried out to determine the s-process neutron density and temperature and to investigate the s-process nucleosynthesis of the ^{176}Lu clock. From various branchings the neutron density was found to be $(0.8 - 1.8) \times 10^8$ neutrons per cm³ and the temperature kT to be 18 - 28 keV. On the present data basis ^{176}Lu proved not to be applicable as a cosmic clock due to the temperature sensitivity of the ^{176}Lu half life but can be used instead as a stellar thermometer. Constraints for the s-process temperature (kT = 20 to 28 keV) were found to be in good agreement with the investigated branchings.

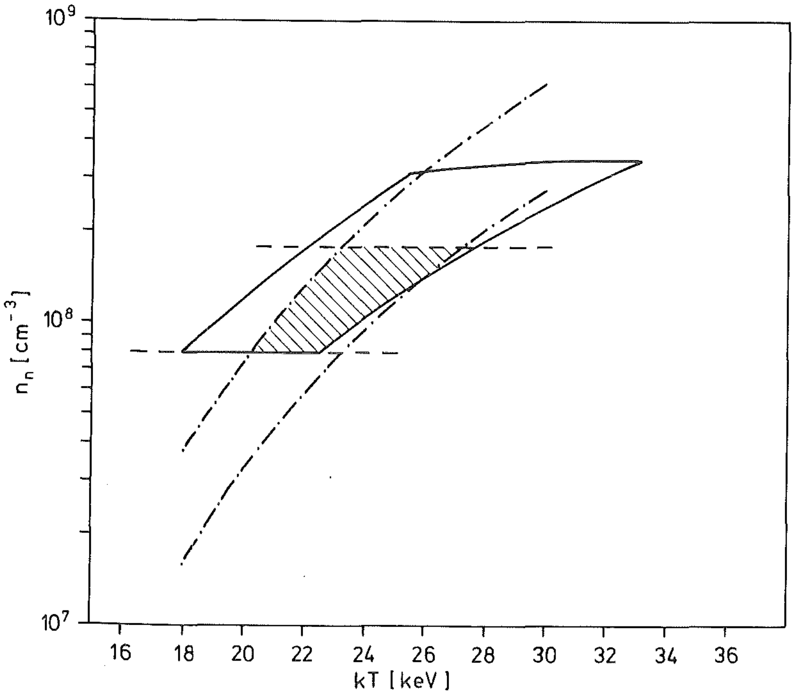

Fig. 1
The s-process neutron density n_n and temperature kT derived from the various branchings. The solid curve shows the allowed range of values calculated from the ^{151}Sm - ^{152}Eu, ^{169}Er - ^{170}Tm and ^{185}W - ^{186}Re branchings. The dashed lines indicate the limits of the neutron density reported in ref. (1). The dashed dotted lines designate the range of temperatures and neutron densities from ^{176}Lu treated as a stellar thermometer. The neutron densities and temperatures common to all investigated branchings lie in the hatched region.

(1) F. Käppeler, K. Wisshak, R.R. Winters, G. Reffo, A. Mengoni, Proc. of Int. Conf. on Nucl. Physics Florence 1983

+ Oak Ridge Nat.-Lab., Oak Ridge, USA
++ MPI für Chemie, Mainz, Saarstr. 23

1.1.14 MEASUREMENT OF THE ß-DECAY BRANCH IN ^{180}Lu to ^{180m}Hf FOR INVESTIGATION OF THE r-PROCESS NUCLEOSYNTHESIS OF ^{180m}Ta

W. Eschner[+], W.-D. Schmidt-Ott[+], K.-L. Gippert[+], E. Runte[+], H. Beer, G. Walter, R. Kirchner[++], O. Klepper[++], E. Roeckl[++], D. Schardt[++], (1)

The ß-decay branch of ^{180}Lu to ^{180m}Hf is measured by an integral method tracing the amount of ^{180m}Hf daughter activity, to be 0.46 (15) %. Samples of ^{180}Lu are prepared by on-line mass separation of ^{136}Xe-on-tungsten transfer reaction products. The amount of isobaric ^{180m}Hf in the samples is strongly suppressed by the employed separator ion source; its directly produced fraction is derived from comparison with ^{177m}Hf activity. The properties of lutetium and hafnium release from the ion source are separately determined. With this measurement r-process nucleosynthesis is estimated to account for at most 22 % of the solar ^{180m}Ta abundance.

(1) Z. Physik A (in press)

+ II. Physikalisches Institut der Universität, Göttingen
++ Gesellschaft für Schwerionenforschung mbH, Darmstadt

1.1.15 SLOW NEUTRON CAPTURE ORIGIN FOR $^{180}Ta^m$

K. Yokoi, K. Takahashi[+], Nature 305 (1983) 198

The very rare isotope ^{180}Ta (a nuclear isomeric state $^{180}Ta^m$ with a half-life $\geq 3x30^{13}$ yr) is of particular astrophysical interest because of its uncertain origin. Recently, Beer and Ward (1) have examined the $^{180}Ta^m$ (spin-parity: 9^-) processing via a small ß decay branching at $^{180}Hf^m(8^-)$ during the s-process and/or the post r-process cascade.

In the present work, it was shown that a significant amount of $^{180}Ta^m$ may be produced by another type of s-process branching mechanism: $ß^-$-decays of the ^{179}Hf excited states thermally populated at s-process temperatures, followed by neutron captures on the daughter ^{179}Ta, leading partly to $^{180}Ta^m$. This branching is essentially determined by the bound-state $ß^-$-decays of the excited states of ^{179}Hf, which enhance the net decay rate considerably. Another key quantity in this scenario is the fractional population B of $^{180}Ta^m$ by the $^{179}Ta(n,\gamma)$ reaction, which was estimated to be 0.02 - 0.09 by using a simple γ-cascade model. The B value is particularly important because it would help constrain acceptable s-process conditions.

To investigate whether the proposed mechanism is promising or not, an experimental determination or a more detailed calculation of the B value is awaited.

(1) H. Beer, R.A. Ward, Nature 291 (1981) 308

+ Centre d'Etudes Nucléaires de Saclay, France

1.1.16 ON THE VALIDITY OF THE LOCAL APPROXIMATION FOR THE s-PROCESS IN THE Os REGION, AND IMPLICATIONS FOR THE $^{187}Re-^{187}Os$ COSMOCHRONOLOGY

M. Arnould[+], K. Takahashi[++], K. Yokoi, (1)

The s-process number abundance ratio of ^{186}Os and ^{187}Os, which is of key importance for the $^{187}Re-^{187}Os$ cosmochronology, was calculated in two schematic s-process models. Special emphasis was put on possible s-process path branchings in the W-Os region, as well as on the role of ^{187}Os electron captures. It was shown that the "local approximation" commonly called for in the evaluation of the above-mentioned ratio may break down in certain seemingly realistic s-process conditions. This result and the possibly important consequences for the Re-Os chronometry were discussed in combination with the uncertain contribution of the first nuclear excited state of ^{187}Os to its stellar neutron capture cross section. It was concluded that the relative s-process yields of ^{186}Os and ^{187}Os are still uncertain enough for preventing the $^{187}Re-^{187}Os$ pair from being accepted as a reliable cosmochronometer. In particular, it was stressed that some of those predicted yields are incompatible with the results of a study of that pair in the framework of a chemical evolution model of the Galaxy which satisfies various observational (non-cosmochronological) constraints, and which predicts an age of the Galaxy in the $11 \lesssim T_G \lesssim 15$ Gyr range (2).

(1) dito, Astron. Astrophys. (in press)
(2) K. Yokoi, K. Takahashi, M. Arnould, Astron. Astrophys. 117 (1983) 65

+ Université Libre de Bruxelles, Bruxelles, Belgium
++ Centre d'Etudes Nucléaires de Saclay, Cedex, France

1.1.17 $^{198,\ 199,\ 200,\ 201,\ 202,\ 204}Hg(n,\gamma)$ CROSS SECTIONS AND THE TERMINATION OF s-PROCESS NUCLEOSYNTHESIS

H. Beer, R.L. Macklin⁺

The neutron capture cross sections of $^{198,\ 199,\ 200,\ 201,\ 202,\ 204}Hg$ were measured in the energy range 2.6 keV to 500 keV. The average capture cross sections were calculated and fitted in terms of strength functions. Resonance parameters for the observed resonances were determined by a shape analysis. Maxwellian averaged capture cross sections were computed for thermal energies kT between 5 and 100 keV. The solar mercury abundance was determined to be 0.34 ± 0.04 relative to Si = 10^6. The termination of s-process nucleosynthesis

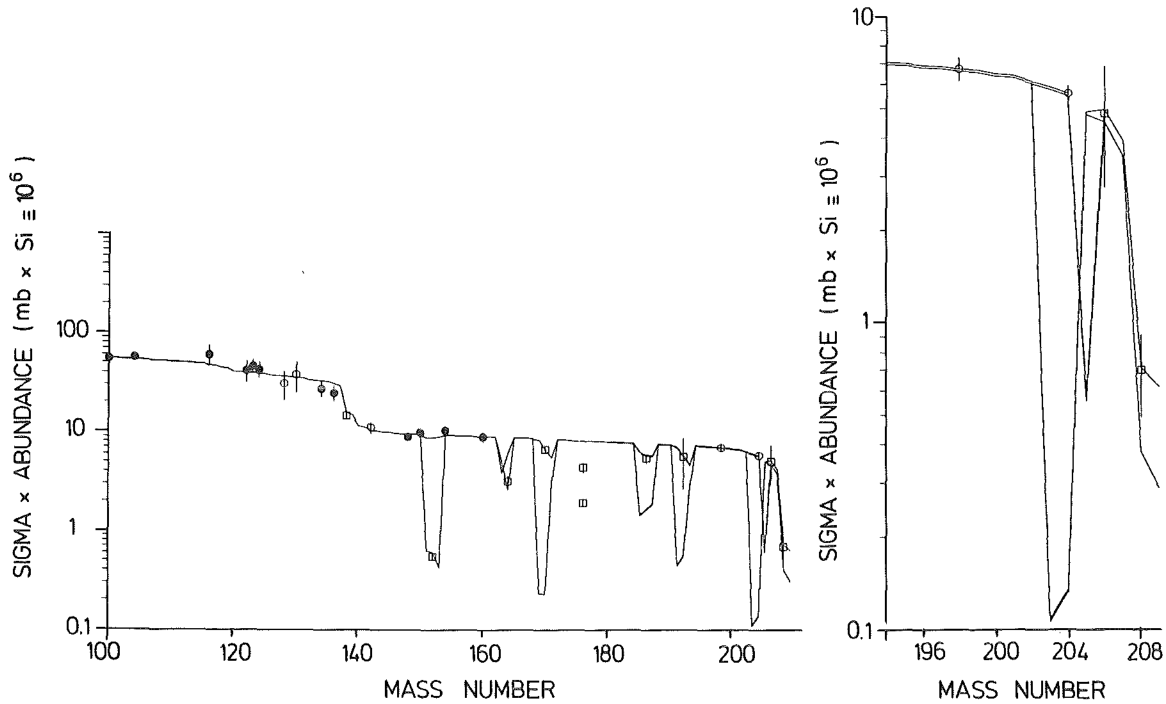

Fig. 1 The product of s-process abundance times cross section as a function of mass number for kT = 23 keV. The symbols correspond to empirical values for s-only isotopes or to s-process dominated isotopes near magic neutron shells. Significant branchings were identified due to the low empirical σN values ^{152}Gd, ^{164}Er, ^{170}Yb, ^{186}Os and ^{192}Pt. The ^{198}Hg and ^{204}Pb values are normalized to the σN curve. The branchings at ^{203}Hg, ^{204}Tl and ^{205}Pb are treated using neutron density and temperature from the other branchings. The half-life of ^{203}Hg is assumed to be terrestrial. The insert shows the influence of the strong s-process fluence component which is added to the main component.

at lead and bismuth was investigated. The abundances of $^{206,207,208}Pb$ were reproduced introducing a strong fluence component of the s-process in addition to normal s- and r-process nucleosynthesis. The radiogenic ^{207}Pb abundance was determined and the r-process age was calculated via ^{235}U. Using Fowler's exponential model an age T = 4.6 Gyr + Δ = 17.2 ± 2.6 Gyr was obtained.

+ Oak Ridge National Laboratory, Oak Ridge, USA

1.1.18 THE PRODUCTION AND SURVIVAL OF ^{205}Pb IN STARS, AND THE ^{205}Pb-^{205}Tl s-PROCESS CHRONOMETRY

K. Yokoi, K. Takahashi[+], M. Arnould[++]

The ^{205}Pb-^{205}Tl pair is interesting in two complementary respects: (i) it could help better characterizing the possible branching in the s-process path at ^{204}Tl (1,2,3), and (ii) it could very usefully complement the information provided by the other extinct radionuclide data. In particular, ^{205}Pb has the distinctive feature among the short-lived species of being (eventually) produced by the s-process only, at least if the ^{204}Tl ß-decay competes successfully with its neutron capture. Thus the ^{205}Pb-^{205}Tl pair would be a potential candidate for providing highly interesting chronometric informations about the last s-process contribution(s) to the solar system (1,2,4,5).

However, Blake and Schramm (2) express some doubts about the usefulness of ^{205}Pb-^{205}Tl as a short-lived s-process chronometer. This pessimism relates to the realization that the electron capture of the 2.3 keV first excited state of ^{205}Pb might reduce drastically the ^{205}Pb effective lifetime in a wide range of astrophysical conditions, the likelihood of a late injection of ^{205}Pb into the (proto-)solar nebula being reduced correspondingly.

The aim of this study is to shed light on some shortcomings affecting previous estimates of the s-process production of ^{205}Pb and of the possibility of its survival in stellar conditions. More specifically, we emphasize the role of the bound-state $ß^-$-decay of ^{205}Tl. This mechanism has been totally overlooked in previous studies, and is able to effectively slow down the destruction of ^{205}Pb by electron capture in a wide range of stellar conditions. This hindrance may have some important consequences for the chronometric usefulness of the ^{205}Pb-^{205}Tl pair. In fact, we stress that the ^{205}Pb yield from certain stars might be large enough to highly merit a renewed search for extinct ^{205}Pb in meteorites.

(1) J.B. Blake, T. Lee, D.N. Schramm, Nature Phys. Sci. 242 (1973) 98
(2) J.B. Blake, D.N. Schramm, Astrophys. J. 197 (1975) 615
(3) R.L. Macklin, R.R. Winters, Astrophys. J. 208 (1976) 812
(4) E. Anders, C.M. Stevens, J. Geophys. Res. 65 (1960) 3043
(5) J.M. Huey, T.P. Kohman, Earth Planet Sci. Letters 16 (1972) 401

+ Centre d'Etudes Nucléaires de Saclay, France
++ Université Libre de Bruxelles, Bruxelles, Belgium

1.1.19 BETA TRANSITION RATES OF NUCLEI IN THE s-PROCESS

K. Takahashi[+], K. Yokoi

In the canonical treatment of the s-process, it is assumed that ß transitions of radioactive nuclei always occur before neutron capture, except for some long-lived nuclei. However, several studies of the steady flow s-process model show that the consideration of competition between ß decay and neutron capture at various nuclei along the path is of great importance to evaluate the "mean" neutron density and temperature for the solar-system s-process material. Further, in the performance of a more realistic s-process network calculation, it is indispensable to consider the s-process branchings.

In the present work, we calculate ß transition rates [β^--decay and/or (bound plus free) electron capture] of 130 heavy nuclei for various temperatures ($T = 1 - 5\times10^8$ K) and electron number densities ($n_3 = 3\times10^{26} - 3\times10^{27}$ cm^{-3}) by using a recent formalism (1) of ß transitions in a plasma of electrons and ions, in which the Saha equation is solved to determine degrees of ionization with a simultaneous inclusion of the "depression of the continuum" evaluated from a finite-temperature Thomas-Fermi model. The electron ionization potentials of several ions calculated by a relativistic self-consistent mothod are used to make an approximation formula. The bound-state β^--decays are also calculated if their contributions to the total decay rates are significant.

A difficult task is to determine ft values of unknown transitions. Our procedure is as follows: 1) First, available experimental data (ft values) of ß transitions are classified by usual spin-parity selection rules (i.e. allowed, non-unique first forbidden and unique first forbidden transitions). 2) Second, from the survey of nuclear level structure which is obtained by experiments or predicted by nuclear models, the transitions are classified according to appropriate selection rules (e.g. Alaga- and K-selection rules in strongly deformed nuclei). 3) The ft values of transitions classified by 1) and 2) are corrected by pairing correlations. In order to obtain the UV factor, we solve the BCS equation by using single-particle energies calculated by nuclear models. 4) The ft values of unknown transitions are then determined by 1), 2) and 3) if the level structures of both parent and daughter nuclei are experimentally known or theoretically predicted.

Although the above mentioned procedure cannot give definite ft values (mainly due to various configuration mixings), the ft values determined in this way are expected to be much more reasonable than average ft values which were used previously for unknown transitions (2).

The influence of uncertainties of the adopted ft values on the total β transition rates will be also investigated.

(1) K. Takahashi, K. Yokoi, Nucl. Phys. A 404 (1983) 578
(2) K. Cosner, J.W. Truran, Astrophys. Space Sci. 78 (1981) 85

+ Centre d'Etudes Nucléaires de Saclay, France

1.1.20 ACCRETING WHITE DWARF MODELS FOR TYPE I SUPERNOVAE

K. Nomoto[+], F.-K. Thielemann[++], K. Yokoi, (1)

The carbon deflagration models in accreting C+O white dwarfs were presented as a plausible model for Type I supernovae. The evolution of the white dwarf was calculated from the beginning of accretion. The main numerical results are as follows:

(i) The deflagration wave synthesizes 0.5 - 0.6 $M_\odot$ ^{56}Ni in the inner layer of the star. This amount is sufficient to power the light curve of Type I supernovae by the radioactive decays of ^{56}Ni and ^{56}Co.

(ii) In the outer layers, substantial amounts of intermediate mass elements, Ca, Ar, S, Si, Mg, and O are synthesized in the decaying deflagration wave. This is consistent with the spectra of Type I supernovae near maximum light. As a result of large nuclear energy release, the star is disrupted completely leaving no compact star remnant behind. Thus the carbon deflagration model can account for many of the observed features of Type I supernovae.

(iii) The abundance ratios of synthesized elements with respect to ^{56}Fe normalized to the solar values are ∿ 1 for ^{40}Ca and ∿ 0.5 for ^{36}Ar, ^{32}S, and ^{28}Si. This indicates that Type I supernovae produce significant fractions of these elements in the Galaxy besides the iron peak elements, which may be complementary to the nucleosynthesis in massive star models for Type II supernovae.

(1) dito, Astrophys. J. (submitted)

+ University of Tokyo, Japan
++ Max-Planck-Institut für Physik und Astrophysik, Garching bei München

1.2 NEUTRON PHYSICS

1.2.1 FIRST RESULTS ON THE MEASUREMENT OF THE n-p SPIN CORRELATION-PARAMETER A_{yy}

F.P.Brady, P.Doll, R.Garrett, W.Heeringa, K.Hofmann, H.O.Klages, H.Krupp and J.Wilczynski

In the framework of systematic experimental studies of the neutron-proton interaction up to 50 MeV a measurement of the n-p spin correlation parameter A_{yy} was carried out in the energy range from 19 to 50 MeV. We scattered the polarized continuous energy neutron beam from POLKA (1) on a brute-force polarized proton target (2) and detected the scattered neutrons at 4 angles. The experimental set-up is shown in Fig. 1.

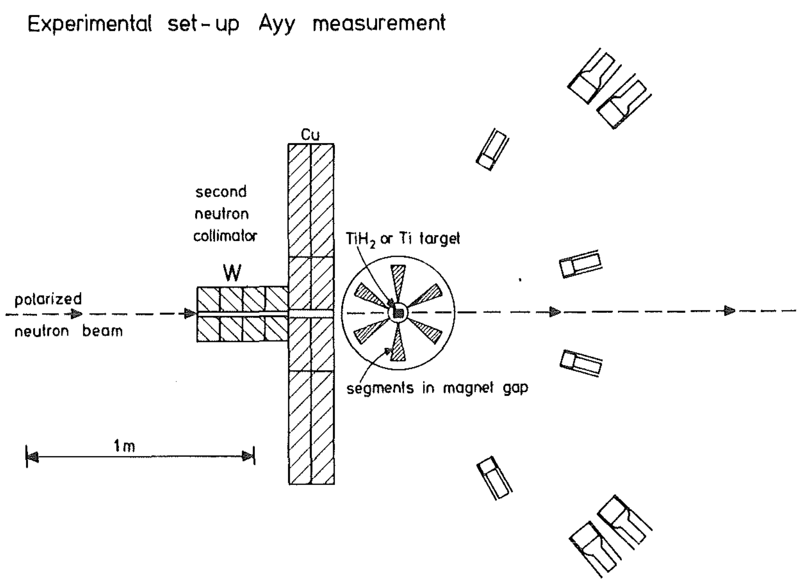

Fig. 1 Experimental set-up of the A_{yy} measurement

The neutron flux is monitored by two proton recoil telescopes at the exit of the main collimator. A second collimator is used to achieve a narrow neutron beam on the scattering sample. The neutron detectors are shielded against the collimator by a copper wall. The proton target consists of TiH_2 powder pressed into a copper tube (35mm x 25mm Ø). The sample is connected by a copper rod to the cooling stage of a ^3He - ^4He dilution refrigerator inside a cryostat. The temperature of the sample can be brought below 0.01 K. In the experiment described here a temperature of 8.6 mK was

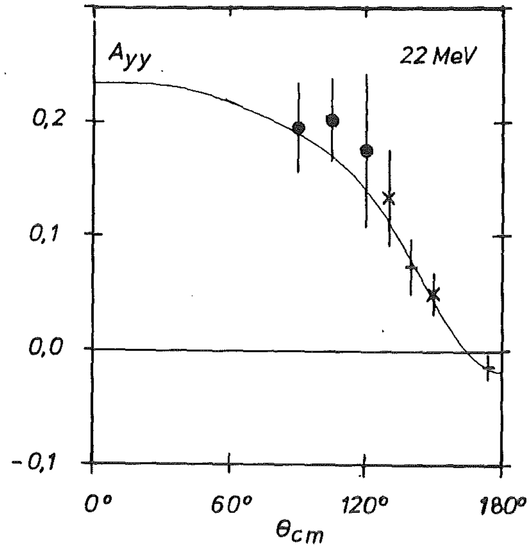

Fig. 2
Experimental results A_{yy} measurement, ● our data, x data of ref.(4), + data of ref.(3), the solid line is calculated with the Paris potential

reached. The sample is placed in the central field of a superconducting split coil magnet with a maximum field strength of 9 Tesla. In the present experiment a field of 7 Tesla was used. The proton polarisation achieved was P = 68%.

The background from elastic and inelastic scattering on titanium has to be subtracted. A dummy measurement was performed using a pure Ti sample. For this purpose the cryostat had to be opened and to be cooled down again after target change. This operation needs more than 5 days. So we have to compare measurements which were performed at different experimental periods at the cyclotron. The stability of the detectors, which have to work in a magnetic field of ~ 1000 Gauss, of the electronics and of the cyclotron operation is a crucial part of the experiment. These problems will be reduced by the fast target change apparatus described in contr. 6.2.1 and by LED-stabilisation of the neutron detectors. A more severe constraint is the low polarized neutron flux available from the cyclotron. The flux will be considerably enhanced when the new polarized ion source comes into operation in early 1985.

At present the accuracy of our data is limited mainly by statistics. Fig. 2 shows our results at 22 MeV compared to the prediction of the Paris potential and to the data from LANL (3,4). With the new ion source and some technical improvements the errors can be reduced by one order of magnitude. Then the data will have strong impact on the n-p phase shifts, especially on ε_1.

(1) H.O.Klages, H.Dobiasch, P.Doll, H.Krupp, M.Oexner, P.Plischke, B.Zeitnitz, F.P.Brady and J.C.Hiebert, Nucl.Instr.Meth. 219 (1984) 269

(2) R.Aures, Ph.D. thesis, Karlsruhe (1983)
(3) J.J.Malanify, P.J.Bendt, T.R.Roberts and J.E.Simmons, Phys.Rev. Lett. 17 (1966) 481
(4) J.E.Simmons, Rev.Mod.Phys. 39 (1967) 542

1.2.2 INCLUSION OF NEW PRECISE DATA IN n-p PHASE SHIFT ANALYSES

H.O.Klages, H.Krupp, J.Wilczynski

In the energy range below 100 MeV a unique description of the two-nucleon system, e.g. in terms of phase shifts, is still not possible. Phase shifts predicted by various models (1,2) differ from each other and do not agree with the phase shifts determined from experimental results (3). In addition, in experimental phase shift analyses the determination of several phase parameters is ambiguous due to the insufficient data base (4,5).

It is the aim of the neutron scattering programme at POLKA to provide new precise data for n-p scattering observables and to analyse all available experimental results in terms of nucleon-nucleon phase shifts. We measured the n-p analyzing power $A_y(\theta)$ in the energy range from 17 to 50 MeV (6). Additional new data were taken at backward angles (7). A recent measurement of A_y at 25 MeV (8) agrees well with our results at this ener-
MeV (6). Additional new data were taken at backward angles (7). A recent

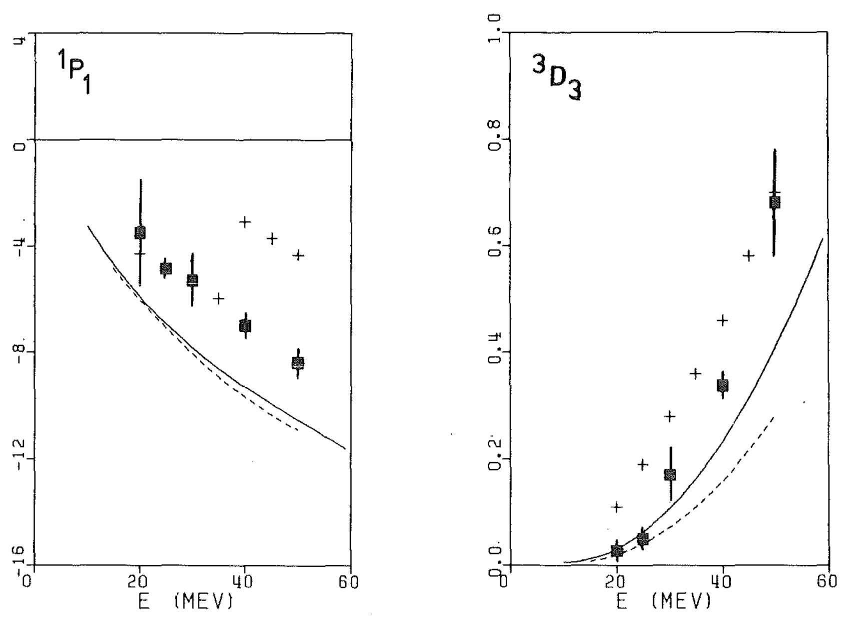

Fig.1 Experimental and theoretical scattering phases, ■ this work, + ref.(3), full curve ref.(1), dashed curve Paris potential

measurement of A_y at 25 MeV (8) agrees well with our results at this energy. All this new accurate data have been added to the data base in new phase shift analyses carried out at 20 ± 4 MeV, 25 ± 4 MeV, 30 ± 4 MeV, 40 ± 5 MeV and 50 ± 5 MeV.

Phase shifts with L $\leq$ 2 were fitted to the data. Phase shifts for J $\leq$ 6 and the energy dependence of all phase parameters were taken from the Bonn OBEP (1). In Fig. 1 a sample of our results is compared to model predictions and a previous experimental analysis. It can be seen that the energy dependence of the $^1P_1$ phase shift is smooth in contradiction to the previous analysis. The $^3D_3$ phase shift seems to be well constrained by the accurate analyzing power data. The phase parameter ε_1 which describes the mixing ε_1 $^3S_1$ and $^3D_1$ states, could not be determined in these analyses. Additional experiments are necessary to put constraints on ε_1.The measurement of the n-p spin correlation parameter A_{yy} (see 1.2.1) will be decisive if the accuracy of the data is sufficient.

The central-, tensor- and spin-orbit part of the nucleon-nucleon interaction can be represented by linear combinations of the ^{3}P- or the ^{3}D-phase shifts (9). Whereas for the 1 = 1 case all models and experimental results agree, Fig. 2 shows that our new analyses confirm the discrepancy for the ^{3}D waves. The experiments are not in agreement with the model predictions for the central and spin-orbit part of the interaction in this

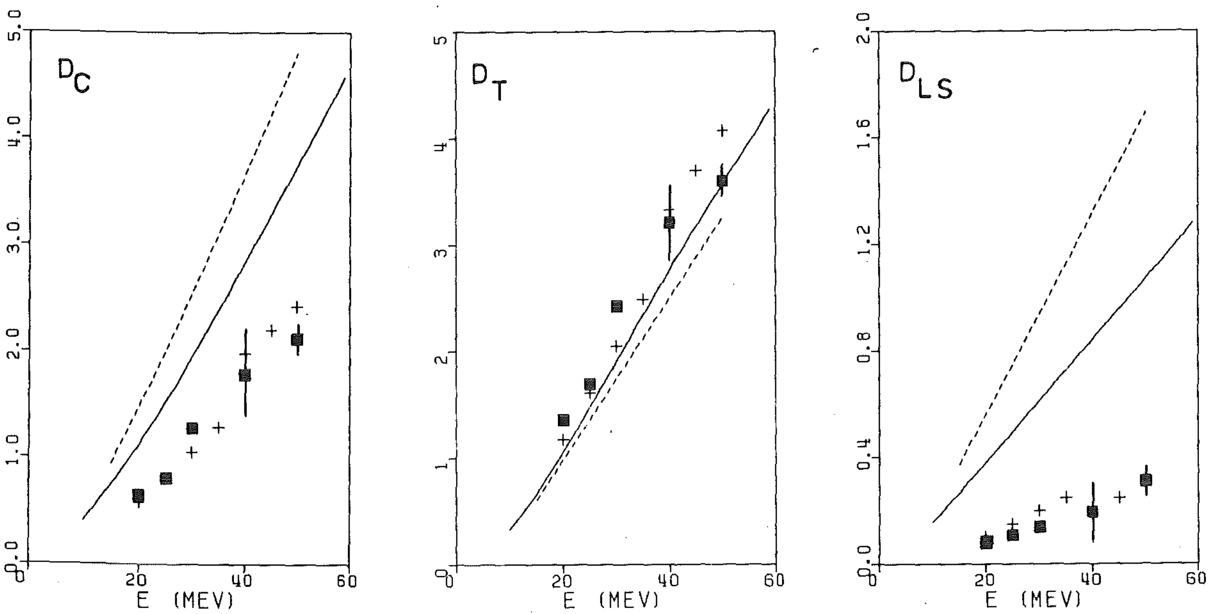

Fig. 2 Comparison of theoretical and experimental values of the combined ^{3}D-scattering phases. For meaning of symbols, see Fig.1.

energy range.

(1) K.Holinde and R.Machleidt, Nucl.Phys. A247 (1975) 495
R.Machleidt, private communication (1982)
(2) M.Lacombe, B.Loiseau, J.M.Richard, R.Vinh Mau, J.Cote, B.Pires and R.de Tourreil, Phys.Rev. C21 (1980) 861
(3) R.A.Arndt, R.H.Hackman and L.D.Roper, Phys.Rev. C15 (1977) 1021
R.A.Arndt, private communication (1984)
(4) P.Signell, in The (n,p) Reaction and the Nucleon-Nucleon Force (Plenum Press, N.Y. 1980) p.1
(5) D.Bugg, J.Phys.G: Nucl.Phys. 6 (1980) 1329
(6) J.Wilczynski, F.P.Brady, P.Doll, W.Heeringa, J.C.Hiebert, H.O.Klages and P.Plischke, Nucl. Phys. A425 (1984) 458
(7) J.Wilczynski, Ph.D. thesis, Karlsruhe (1984)
(8) W.Haeberli, private communication (1983)
(9) L.Heller and M.Sher, Phys.Rev. 182 (1969) 1031

1.2.3 MULTIPLE SCATTERING AND FINITE GEOMETRY CORRECTIONS TO n-d ANALYZING POWER DATA

P.Doll, K.Hofmann, H.O.Klages, W.Nitz

A measurement of the analyzing power of the n-d scattering has been done using the continuous energy polarized neutron beam at the Karlsruhe cyclotron. The collimated neutron beam from POLKA was scattered on a sample consisting of a glas-cell of 3" x 3" Ø filled with deuterated NE 213 liquid scintillator. Angular distributions of the scattered neutrons were measured from 39^{o} - 153^{o} c.m. The pulse shape properties of the sample material were excellent. This enables us to cut off the inelastic scattering of neutrons on carbon and/or deuterons, evaluating only elastic scattering events (recoiled deuterons) in the off-line analysis.

Nevertheless the results have to be corrected for multiple scattering and finite geometry effects. This can be done using the structure of a program that has been developed recently for correcting results of the n-p analysing power with a NE 213 liquid scintillator as scattering sample (1). This program simulates the way of a neutron in the inner range of the scattering sample which has been detected later by a neutron detector outside.

As an input the programm needs the total cross sections for all considerable reactions in the scattering sample, tabulated in steps of 0.1 MeV from 0.1 MeV to 50 MeV, the light output function of the scintillator, and for all reactions the differential cross section and analyzing power tabulated in 1 MeV steps.

The deuterated NE 213 has a composition similar to normal NE 213 it includes deuterated naphthalene, but the solvent is deuterated benzene, not xylene which is not readily available in deuterated form. The D/C-ratio has been estimated to 0.97.

Due to the excellent pulse-shape properties mentioned before it is not necessary to consider all possible reactions. Only n-D elastic and n-^{12}C elastic and inelastic scattering have to be taken into account.

Using a Faddeev-code of Y.Koike (2) with the GRAZ II-potential as an input for the nucleon-nucleon interaction, we could produce the necessary input for the neutron-deuteron scattering. The calculated observables reproduce sufficiently the experimental data of the differential cross section (3) and the analyzing power (4). For other observables like depolarisation and the four rotational parameters no experimental data are available.

Total and elastic cross sections were taken from refs. (5) and (3). The elastic and inelastic scattering of neutrons from carbon has been calculated with an optical model code using potential parameters of J.R. Rapaport (6). The results have been compared with measurements (7).

Fig. 1 shows our measured data at 40 MeV and the corrected data for multiple scattering and finite geometry. In general, due to the low background in the measurements and the careful data reduction, the corrections

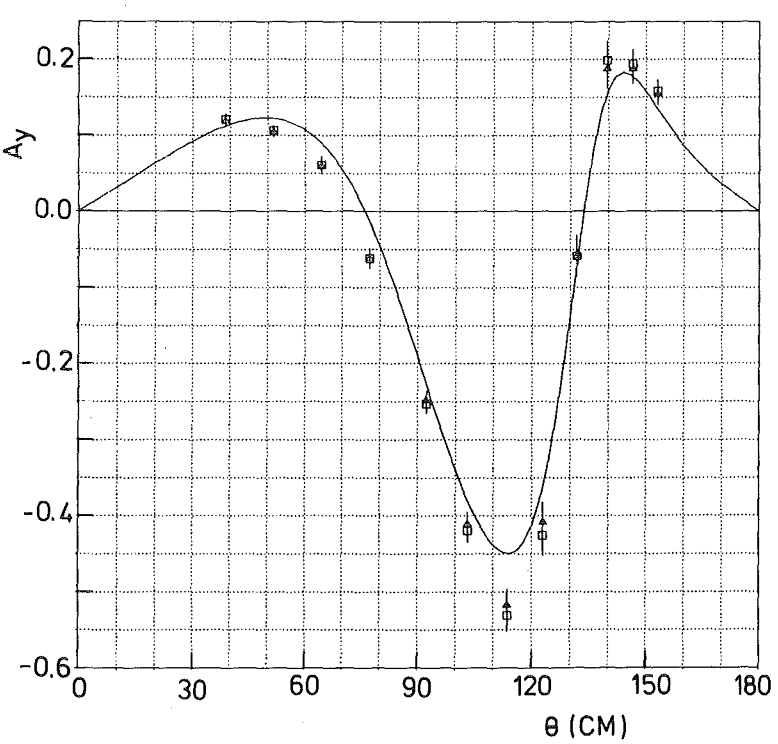

Fig. 1:
A_y for n-d elastic scattering at 40 MeV. Triangles are measured data, squares corrected data. See also text.

are small compared to the statistical errors. The solid curve shows a Faddeev calculation with the GRAZ II potential as nucleon-nucleon input.

(1) J.Hansmeyer, Diploma thesis, Karlsruhe (1983)
(2) Y.Koike, priv. communication (1983)
(3) P.Schwarz, H.O.Klages, P.Doll, B.Haesner, J.Wilczynski, B.Zeitnitz Nucl.Phys. A398 (1983) 1
(4) J.W.Watson, R.Garrett, F.P.Brady, D.H.Fitzgerald, J.L.Romero, J.L.Ulmann, C.J.Zanelli, J.D.Carlson, A.L.Sayle, T.S.Subramanian, Phys.Rev. C25, 5 (1982) 2214
H.Dobiasch, R.Fischer, B.Haesner, H.O.Klages, P.Schwarz, B.Zeitnitz Phys.Lett. 76B, 2 (1978)
P.Brady, P.Doll, E.Finckh, K.Hofmann, H.O.Klages, W.Nitz, J.Wilczynski, Verh. DPG (VI) 18 (1983) 977
(5) H.Bente, Diploma thesis, Karlsruhe (1979)
(6) J.R.Rapaport, Phys.Rep. 87, 2 (1982) 25
(7) E.Woye, Ph.D. thesis, Tübingen (1982)

1.2.4 FADDEEV CALCULATIONS OF ELASTIC n-d SCATTERING OBSERVABLES

K.Hofmann, H.O.Klages, Y.Koike*, W.Nitz

By means of the Faddeev method of coupled integral equations the nonrelativistic 3-nucleon problem can be treated in so-called "exact" calculations. In most cases (1) separable nucleon-nucleon potentials are used as two-body input. The Coulomb interaction cannot be included in the calculations and is handled approximatively if p-d observables are determined.

For a direct and meaningful comparison precise data on n-d observables are needed. Several measurements of this kind have been carried out by us recently (2,3) and more data will be analyzed in the near future.

A three-nucleon code (4) based upon the AGS form of the Faddeev equations has been installed at the KfK computer. It enables us to calculate n-d observables for elastic scattering using various two-nucleon potentials as input. The calculations can be done in the whole energy range covered by our experiments, up to 50 MeV. The potentials used up to now are of separable type, mainly the GRAZ II potential (5) and, in addition, potentials constructed by Doleschall (6).

We compared our data for the differential cross section and the analyzing power of the elastic n-d scattering to the results of the calcu-

*RCNP Osaka, Japan

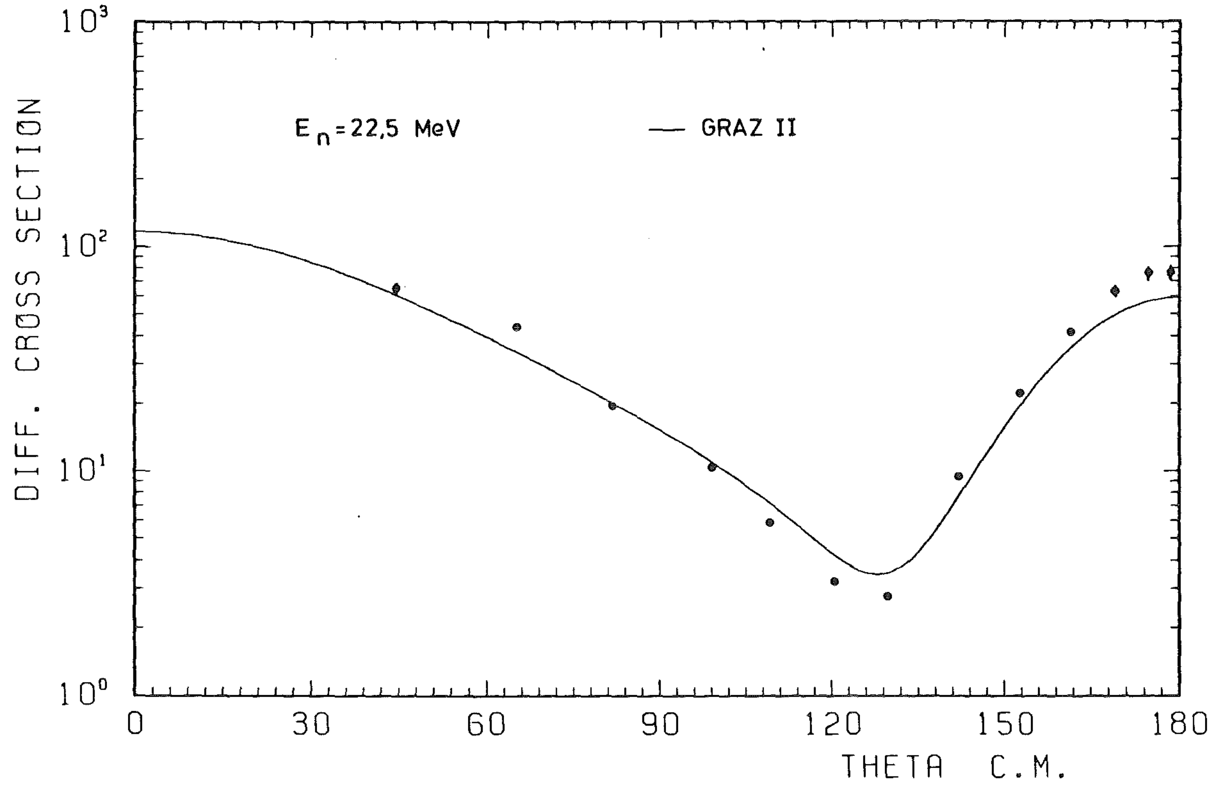

Fig. 1: Differential cross section result for the elastic nd scattering (E_n = 22.5 MeV). Solid line: result of a Faddeev calculation with the GRAZ II potential.

lations. In general, the GRAZ II potential gives the better description of the experimental values. However, as can be seen in Fig. 1 the differential cross section measured at backward angles is not reproduced by the Faddeev calculations. This problem is discussed in contr. 1.2.5 of this report.

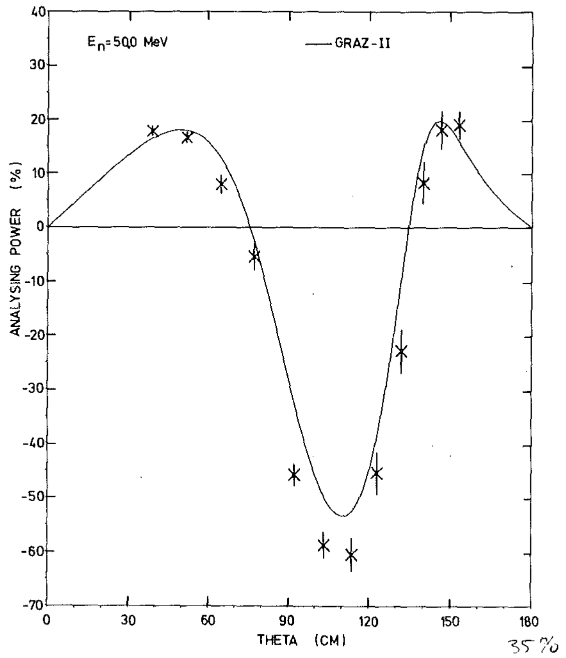

Fig. 2
Analyzing power of $\vec{n}d$ scattering at 50 MeV and the result of the Faddeev calculation with the GRAZ II potential.

Fig. 2 shows the $\vec{n}$-d analyzing power at 50 MeV. The results of the calculations using the GRAZ II potential are in good agreement with our raw data (see contr. 1.2.3).

Presently the installation of the refined nucleon-nucleon potential "PEST" by the Graz group (7) into the code is beeing done. This separable potential simulates the on-shell and off-shell behaviour of the PARIS potential and should lead to even more realistic results also for the inelastic channel. The inclusion of breakup calculations in the code is in preparation.

(1) J.A.Tjon, Nucl.Phys. A353 (1981) p.47c
(2) P.Schwarz, H.O.Klages, P.Doll, B.Haesner, J.Wilczynski, B.Zeitnitz and J.Kecskemeti, Nucl.Phys. A398 (1983) 1
(3) P.Brady, P.Doll, E.Finckh, K.Hofmann, H.O.Klages, W.Nitz and J.Wilczynski, DPG (VI) 18 (1983) 977
(4) Y.Koike, private communication (1983)
(5) L.Mathelitsch, W.Plessas and W.Schweiger, Phys.Rev. C26 (1982), 65
(6) F.D.Conell, G.G.Ohlsen, R.E.Brown, R.A.Hardekopf, N.Jarmie and P.Doleschall, Phys.Rev. C23 (1981), 960
(7) J.Haidenbauer and W.Plessas, UNIGRAZ UTP 02184 (1984)

1.2.5 MEASUREMENT OF $d\sigma/d\Omega$ FOR ELASTIC n-d SCATTERING AT BACKWARD ANGLES

P.Doll, G.Fink, R.Garrett, W.Heeringa, K.Hofmann, H.O.Klages and H.Krupp

The three-nucleon problem has been investigated both experimentally and theoretically in great detail. Precision data exist especially for the p-d system (1). For the n-d system, where exact Faddeev calculations can be performed, differential cross sections and analyzing power distributions have been measured, but the data base above 20 MeV is very small. As can be seen in contr. 1.2.4 to this report the agreement of the data with the Faddeev calculations is satisfactory.

The only discrepancies remain at far backward angles, where the calculations are always smaller than the experimental results. Whether this is due to an unadequate nucleon-nucleon input for the calculations or to unresolved problems in the experimental data has to be checked.

Therefore, we measured the n-d elastic scattering cross section at backward angles with a technique different from the method used by Schwarz et al. (2). We employed the telescope technique for the charged recoil particles from a thin deuterated polyethylene foil. The n-d scattering was

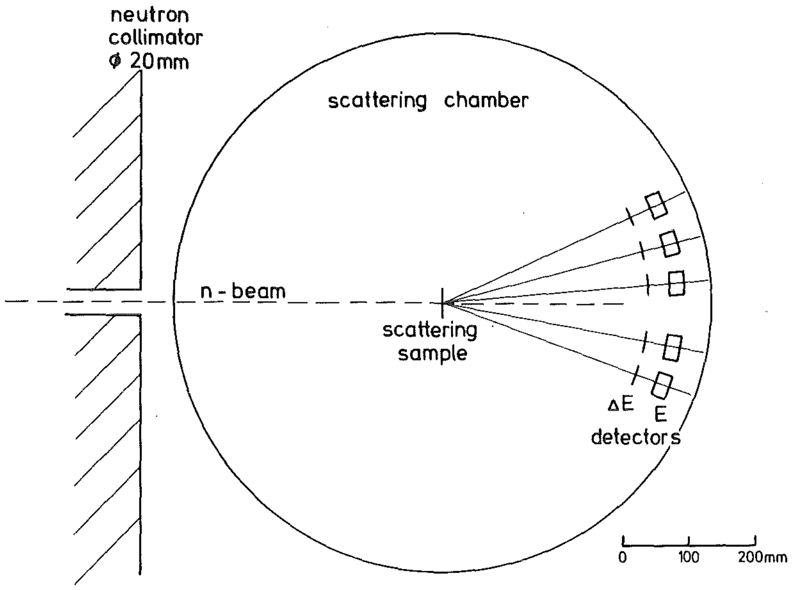

Fig. 1: Schematic view of the experimental set-up.

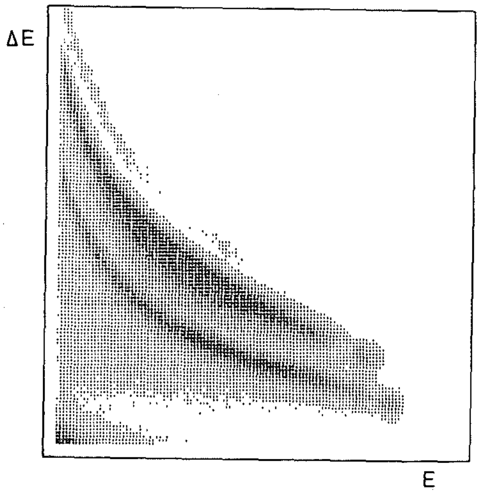

Fig. 2:
Energy loss vz. energy for nd scattering on a deuterated polyethylene foil.

measured relative to the n-p scattering from a polyethylene foil of similar thickness.

We used the continuous energy neutron beam at POLKA (3) and took data in the energy range from 19 to 50 MeV simultaneously. The angular range covered was 5^{o} to 25^{o} in the lab. system corresponding to $\theta_{c.m.}$ = 130^{o} - 170^{o} for the scattered neutrons. The experimental setup is shown in Fig. 1.

The incident neutron flux is monitored by a proton telescope system (4). Five identical detection systems are used in an evacuated scattering chamber for the n-d scattering experiment, each consisting of a 500 μ Si ΔE-detector and a 1" NE102 E-detector.

Multiparameter data acquisition was performed to separate off-line elastic scattering events from reaction products with carbon.

The data are presently beeing analyzed. The statistical accuracy achieved is far better than in previous experiments in this energy range (2,5). Fig. 2 shows a data sample during the off-line analysis.

(1) W.Grübler, Nucl.Phys. A353 (1981), 31c

(2) P.Schwarz, H.O.Klages, P.Doll, B.Haesner, J.Wilczynski, B.Zeitnitz and J.Kecskemeti, Nucl.Phys. A398 (1983), p.1

(3) H.O.Klages, H.Dobiasch, P.Doll, H.Krupp, M.Oexner, P.Plischke, B.Zeitnitz, F.P.Brady and J.C.Hiebert, NIM 219 (1984), p.269

(4) P.Doll, F.P.Brady, E.Finckh, H.O.Klages, J.Wilczynski, internal report (Jan. 1984)

(5) F.P.Brady, W.B.Broste, J.C.Wang, J.L.Romero and P.Martens, Phys.Rev. C9 (1974) 1784

1.2.6 MEASUREMENT OF THE ANALYSING POWER OF THE ELASTIC n-^{3}He SCATTERING AT LOW ENERGIES

G.M.Hale*, W.Heeringa, K.Hofmann, P.Jany, H.O.Klages, H.Krupp and Chr.Maier

In the framework of systematic investigations of the four-nucleon system using the n+^{3}He entrance channel (1,2,3) the analysing power of the elastic n-^{3}He scattering has been measured in the energy range from 0.95 to 2 MeV.

The polarised neutrons were produced by the T(p,n)^{3}He reaction using the pulsed proton beam at the Karlsruhe Van-de-Graaff accelerator. The polarisation of the neutrons was determined to an accuracy of ~ 1% by a two-dimensional interpolation of recently measured precise analysing power (4,5) and polarisation (6) data for the source reaction.

The polarised neutrons passed a superconducting solenoid which was used to reverse the spin-direction every ten minutes and a boron-paraffine collimator which formed a narrow, rectangular shaped beam. A liquid ^{3}He scintillation detector (7) which had been improved for the detection of low pulse heights served as scattering sample (Fig. 1). The scattered neutrons were detected by 6 pairs of neutron detectors at scattering angles from 50^0 to 160^0 (CM). Multiparameter data acquisition and off-line analysis were performed.

*Theor.Div., Los Alamos Nat.Lab., USA

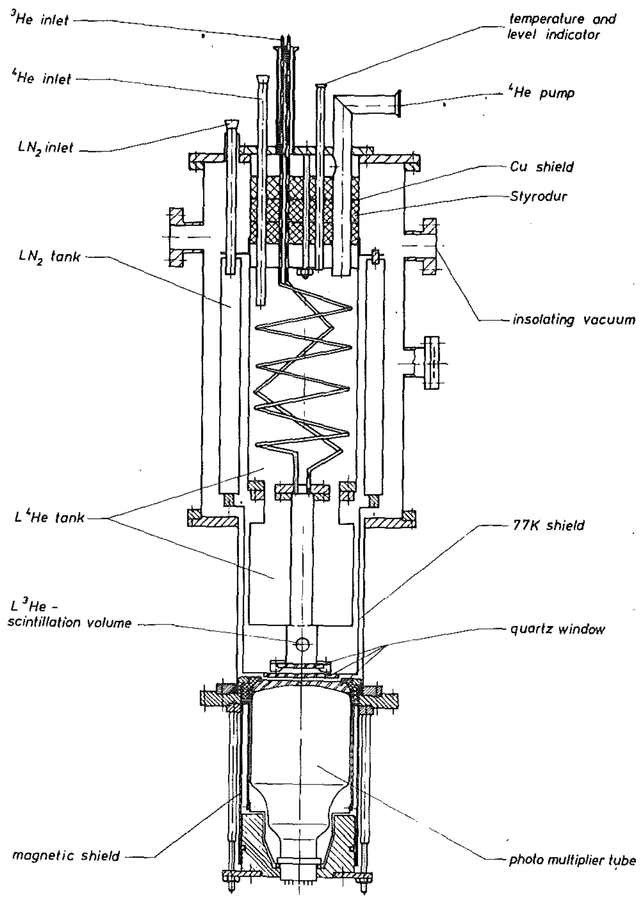

Fig. 1
Liquid ^{3}He-scintillation sample with optimised light collection for the detection of low recoil energies.

The angular distributions for A_y were obtained with low background and improved statistical accuracy compared to previous data (8,9,10). In the energy region from 0.9 to 1.5 MeV the analysing power was measured for the first time.

The data have to be corrected for multiple scattering and finite geometry effects. These effects are expected to shift the measured A_y data by 2 - 4%. The final results will be compared to R-matrix calculations. An

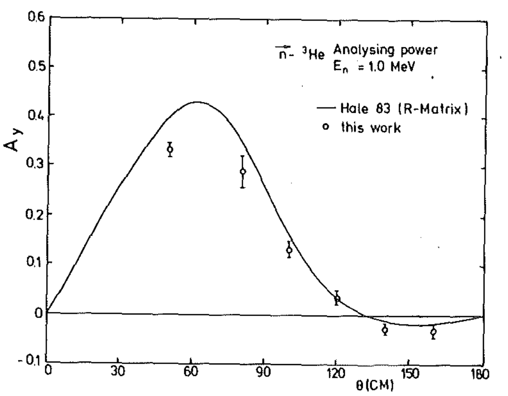

Fig. 2
Preliminary uncorrected A_y data for 1.0 MeV neutron energy (data points) and R-matrix calculations (solid line). The error bars show the statistical errors.

interesting systematic difference seems to be present between these calculations and the measured A_y distributions which are at all energies lower in the maximum A_y value. An example is shown in Fig. 2.

(1) H.Dobiasch, Ph.D. thesis, Karlsruhe (1979)
(2) B.Haesner, Ph.D. thesis, Karlsruhe (1982)
(3) B.Haesner, W.Heeringa, H.O.Klages, H.Dobiasch, G.Schmalz, P.Schwarz, J.Wilczynski, B.Zeitnitz and B.Kaeppeler, Phys.Rev. C28 (1983) 995
(4) Sr.M.A.Doyle, H.W.Clark, L.J.Dries, J.L.Regner, T.R.Donoghue and G.M.Hale, Nucl. Phys. A371 (1981) 225
(5) T.R.Donoghue, priv. communication
(6) W.Tornow, R.C.Byrd, P.W.Lisowski, R.L.Walter and T.R.Donoghue, Nucl.Phys. A371 (1981) 235
(7) R. van Staa, J.Reher and B.Zeitnitz, Nucl.Instr.Meth. 136 (1976) 61
(8) J.D.Seagrave, L.Cranberg and J.E.Simmons, Phys.Rev. 109 (1960) 1981
(9) L.Drigo, G.Tornielli and G.Zannoni, Lett.Nuo.Cim. 18 (1977) 306
(10) L.Drigo and G.Tornielli, Ann.d.Phys. 39 (1982) 408

1.2.7 FINAL RESULTS OF THE n-^{3}HELIUM ANALYZING POWER UP TO 50 MeV AND PHASE SHIFT ANALYSIS

H.O.Klages, H.Krupp, Chr.Maier, J.Wilczynski

At the Karlsruhe polarized neutron facility POLKA a measurement of the $\vec{n}$-^{3}He analyzing power A_y in the energy range from 16 MeV to 50 MeV was performed. A liquid-^{3}He scintillation detector served as scattering sample. Neutrons were detected at 14 angles from 38^o to 158^o (CM) at a distance of 1 m from the sample.

These data had to be corrected for multiple scattering and finite geometry effects. Therefore, the Monte Carlo code "PMS", which simulates the scattering of spin 1/2 - on spin 0 - particles was changed. The new code, called "PMS3", is able to calculate the scattering of spin 1/2 - on spin 1/2 - particles, like the n-^{3}He scattering. "PMS3" needs as input slowly varying phase shifts of the n-^{3}He system up to an energy of 50 MeV. Until now only phase shifts up to 22 MeV have been published. So a new phase shift analysis in the energy range from 16 MeV to 50 MeV was attempted. As input data the uncorrected A_y results of this work, total cross sections (1), and differential cross sections (2) were used. The solution of the phase shift analysis is not unique, because there are too many parameters and not enough data points. Therefore, two conditions were introduced: the phase shifts have to be smooth with energy and have to describe the data

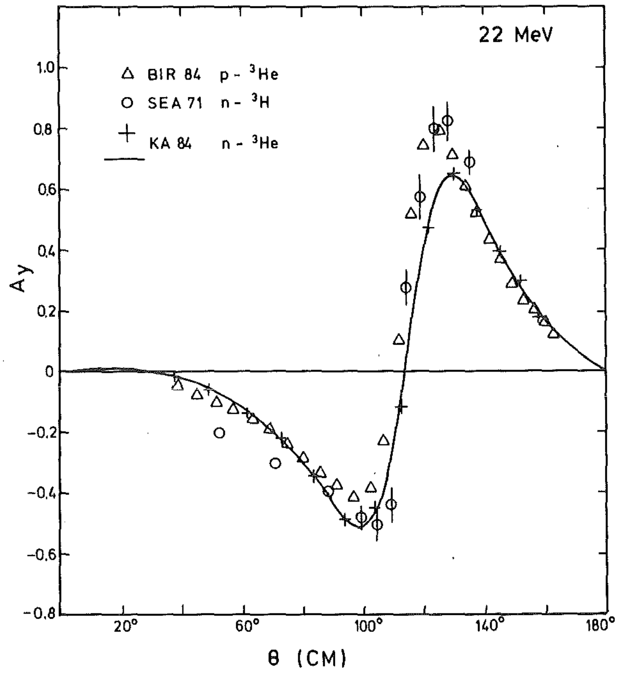

Fig.1:
Comparison of A_y values in the A=4 system at 22 MeV.

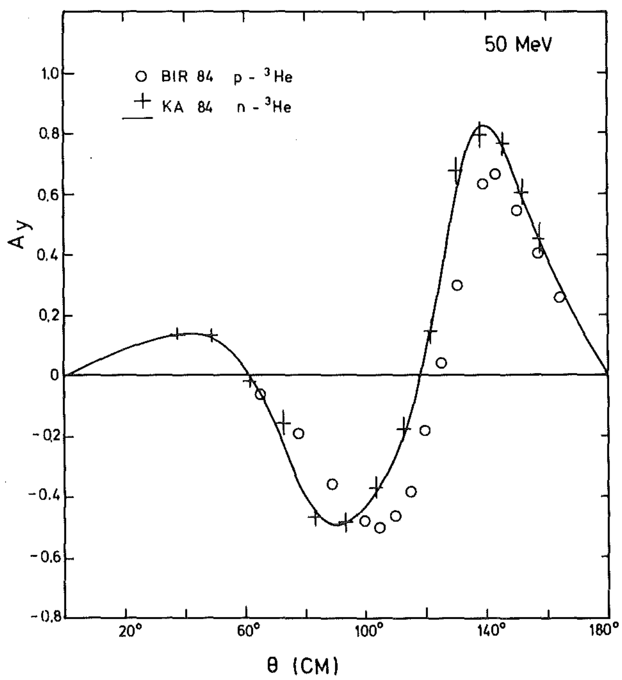

Fig.2:
Comparison of A_y values in the A=4 system at 50 MeV.

points. We calculated the real part of the phase shifts, the absorption parameters and the mixing parameters up to L = 3. With the new phase shifts as input in "PMS3" our A_y data were corrected. The corrections are in general small compared to the statistical errors.

The final results can be compared with other A_y data in the ^4He-system. Whereas at 22 MeV the data of Dobiasch (3) are in good agreement with our results, the angular distribution of Busse et al. (4) shows a different shape. The comparison with other A_y data in the A = 4 system is also possible. Fig. 1 shows the A_y data of the n-^{3}He scattering, of the p-^{3}He (5) and the n-T scattering (6) at 22 MeV. The curve is calculated by our new phase shifts. Fig. 2 shows the angular distributions of the analyzing power of the n-^{3}He and the p-^{3}He scattering at 50 MeV.

(1) B.Haesner, W.Heeringa, H.O.Klages, H.Dobiasch, G.Schmalz, P.Schwarz, J.Wilcznyski and B.Zeitnitz, Phys.Rev.C28 (1983) 995

(2) B.Haesner, KfK report 3395 (1982)

(3) H.Dobiasch, Ph.D. thesis, Karlsruhe (1979)

(4) W.Busse, B.Efken, D.Hilscher, and J.A.Scheer, Nucl.Phys. A187 (1972) 21

(5) J.Birchall, W.T.H. van Oers, J.W.Watson, H.E.Conzett, R.M.Larimer, B.Leemann, E.J.Stephenson, and R.E.Brown, Phys.Rev. C29 (1984) 2009

(6) J.D.Seagrave et al., Pol. Phen. in Nucl. Reactions, (Univ. Wisc. Press, Madison, 1971) p.477

1.2.8 THE CAPTURE WIDTH OF THE 1.15 keV s-WAVE NEUTRON RESONANCE IN ^{56}Fe

K. Wisshak, F. Corvi[+], and C. Bastian[+]

The neutron resonance at 1.15 keV in ^{56}Fe is by far the most important resonance in structural materials of reactors. It contributes about 35 % to the total capture rate in iron in a typical fast core. The experimental values for their resonance area are quite discrepant. An evaluation of transmission experiments (1) gave a consistent result of $A_\gamma = g\Gamma_n\Gamma_\gamma/\Gamma = 56$ meV, while recent capture experiments (2,3) yielded $A_\gamma = 67$ meV. This 20 % discrepancy is far outside the quoted experimental uncertainties and much larger than the accuracy requested for this resonance. In the capture experiments C_6D_6 or C_6F_6 detectors and the pulse height weighting technique was used. There was some ground for suspicion that this method may fail for resonances with very hard capture gamma-ray spectra. Therefore the present collaboration was started and in the present experiments Moxon Rae detectors served for the detection of capture gamma-rays. Thus the systematic uncertainties of the results are completely independent from previous measurements.

The experiment was performed at the 150 MeV Geel Linac at a flight path of 28.4 m. Capture events were registrated from three Moxon Rae detectors with graphite, bismuth graphite and bismuth converters, respectively. Normalization was performed via the 4.91 eV resonance in gold applying the black resonance technique. Sample and reference sample (0.5 mm ^{56}Fe enriched to 99.87 % and 50 μ gold) were positioned simultaneously in the neutron beam. The flux shape was determined by means of a ^{10}B ionization chamber. Two runs were carried out locating the detectors at 90° and 120° with respect to the beam axis. The data as measured with different converter materials have been corrected according to the respective detector efficiency. The final results are compiled in Table I. Within the quoted uncertainties they are consistent

Table I Results for the Resonance Area of the 1.15 keV Resonance in ^{56}Fe

Run	Convertermaterial	$A_\gamma = g\Gamma_n\Gamma_\gamma/\Gamma$ (meV)	A_γ weighted average (meV)
I	Bi	61.4	
I (120°)	Bi + C	66.9	63.5 ± 3.0
I	C	62.9	
II	Bi	60.6	
II (90°)	Bi + C	66.6	62.4 ± 2.9
II	C	61.2	

with the other recent capture measurements. Thus the discrepancy between capture and transmission experiments has been increased.

(1) F.G. Perey, Report to the NEANDC Meeting Tokai-Mura March 1984
(2) F. Corvi, A. Brusegan, R. Buyl, and G. Rohr, Proc. of a Consultants Meeting on Nuclear Data for Structural Materials Vienna 2-4 November, 1983
(3) R.C. Macklin, Nucl. Sci. Eng. 83, 309 (1983)
+ C.B.N.M. Euratom Geel, Belgien

1.2.9 COLD FRAGMENTATION OF ^{240}Pu

C. Schmitt[+], A. Gnessous[++], J.P. Bocquet, H.-G. Clerc[+], R. Brissot[+++], D. Engelhardt, H.R. Faust[+++], F. Gönnenwein[+++], M. Mutterer[+], H. Niefenecker[++], J. Pannicke[+++], Ch. Ristori[++], J.P. Theobald[+]

Previous experiments of the Lohengrin-Collaboration studying fission yields at different fission product kinetic energies for thermal-neutron induced fission of ^{239}Pu (1) by using the Lohengrin mass separator showed that it would be interesting to study cold fragmentation of the nucleus ^{240}Pu. This experiment was performed in 1984, using a new position sensitive ionization chamber covering a large part of the focal plane of the on-line mass separator Lohengrin at the ILL. A rough survey of the experimental data, for which analysis is under way, suggests that cold fragmentation of ^{240}Pu is comparable to that of ^{236}U previously measured at Lohengrin with lower statistics (2).

(1) C. Schmitt, A. Gnessous, J.P. Bocquet, H.-G. Clerc, R. Brissot, D. Engelhardt, H.R. Faust, F. Gönnenwein, M. Mutterer, H. Niefenecker, J. Pannicke, Ch. Ristori, J.P. Theobald, Technical Report IKDA 84/2, (1984) in print by Nuclear Physics

(2) U. Quade, Doctoral Thesis, University of Munich (1983)

+ Institut für Kernphysik, TH Darmstadt
++ Centre d'Études Nucléaires - DRF, Grenoble
+++ Institut Laue-Langevin, Grenoble

1.2.10 MASS AND ENERGY YIELDS IN FISSION OF ^{239}Np

M. Afgard[+], G. Barreau[++], R. Brissot[+++], M. Djedara[++], M. Done[++], D. Engelhardt, H. Faust[+++], F. Gönnenwein[+++], B. Leroux[++], M. Mutterer[++++], C. Sicre[++], J.B. Theobald[++++]

This experiment was performed in June 1984 by double neutron capture on ^{237}Np at the Lohengrin facility in a collaboration with groups from Grenoble and Bordeaux, using a position sensitive ionization chamber in the focal plane of the mass separator. The data contain a complete set of fission yields of the light group at different fission product kinetic energies for thermal-neutron induced fission of ^{239}Np and they contain also information on cold fragmentation of the nucleus ^{239}Np.

+ Centre d' Études Nucleâires, Algar
++ Centré d' Études Nucleâires, Bordeaux
+++ Institut Laue-Langevin, Grenoble
++++ Institut für Kernphysik, TH Darmstadt

1.3 NUCLEAR REACTIONS BY CHARGED PARTICLES

1.3.1 ISOTOPIC AND ISOTONIC DIFFERENCES BETWEEN ALPHA PARTICLE OPTICAL POTENTIALS AND NUCLEAR DENSITIES OF $1f_{7/2}$ NUCLEI

H.J. Gils, H. Rebel, E. Friedman+, Phys. Rev. C29 (1984) 1295

The elastic scattering of 104 MeV α particles by $^{40,42,43,44,48}Ca$, ^{50}Ti, ^{51}V, and ^{52}Cr has been analyzed by phenomenological and semimicroscopic optical potentials in order to get information on isotopic and isotonic differences of the α particle optical potentials and of nuclear matter densities. The phenomenological optical potentials based on a Fourier-Bessel description of the real part reveal different behaviour in size and shape for the isotonic chain as compared to the isotopic chain. Odd-even effects are also indicated to be different for isotones and isotopes. The semimicroscopic analyses use a single-folding model with a density-dependent effective αN interaction including a realistic local density approximation. The calculated potentials are fully consistent with the phenomenological ones. Isotopic and isotonic differences of the nuclear matter densities obtained from the folding model in general show a similar behavior as the optical potential differences. The results on matter densities are compared to other investigations.

+ The Racah Institute of Physics, The Hebrew University of Jerusalem

1.3.2 NEUTRON DENSITY DISTRIBUTIONS FROM COMBINED ANALYSIS OF PIONIC ATOMS AND ELASTIC SCATTERING OF α PARTICLES

H.J. Gils and E. Friedman+

Information on the size and radial shape of the distribution of neutrons or total matter in nuclei suffers from the dependence on the interaction model needed for the analysis of any type of experiments involving strongly interacting probes. In addition to the uncertainties introduced by the usual approximation of the interaction process in terms of a microscopically generated effective ("optical") probe-nucleus potential most of the models contain some characteristic parameters which are not a priori given and which cannot always reliably be determined from independent sources. With regard to these problems it may be interesting to perform combined analyses of different experiments where it is expected to reduce the model dependence of the results in particular that part due to parameter ambiguities.

Combined analyses may in particular be promising if the experiments chosen probe rather different quantities of the nucleon distribution. Experiments on the elastic scattering of protons and α particles have been shown (1) to be sensitive to the radial shape of the nuclear density. As an example, Fig. 1 shows the neutron distribution of ^{42}Ca as obtained from analysis of 104 MeV α-particle scattering where the traditional functional form has been replaced by the more bias-free ("model-independent") Fourier-Bessel series (FB) (2).

On the other hand, measurements of strong interaction level shifts ε and widths Γ in pionic atoms provide only two experimental numbers for each nucleus, thus making it impossible to fit parameters of a Fourier-Bessel series. However, these experiments determine integral quantities of the neutron distribution like the root mean square (rms) radius r_n quite precisely as soon as the correct values of the π-N-interaction parameters (3) are known. This is demonstrated in Fig. 2.

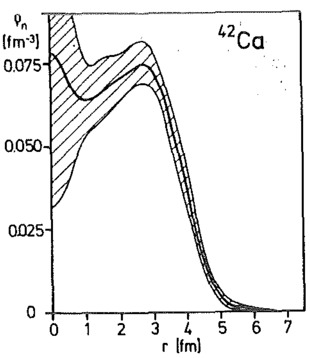

Fig. 1

Neutron density distribution of ^{42}Ca obtained from analysis of elastic α particle scattering

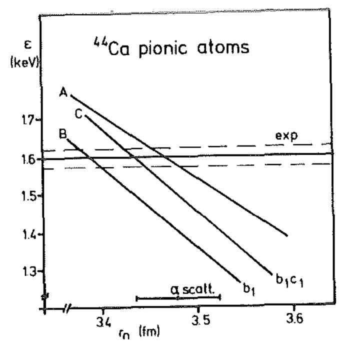

Fig. 2

Calculated values of ε in ^{44}Ca as a function of r_n, compared with experiment. The curves A, B, and C correspond to different parameter sets of the π-N interaction potential (3)

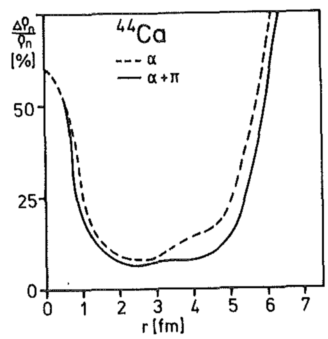

Fig. 3

Relative errors of the neutron density distribution of ^{44}Ca as obtained from elastic α particle scattering (dashed) and from combined analysis with pionic atoms (solid line)

In combined analyses of pionic atoms and elastic scattering of α particles which we performed for the isotopes $^{40,42,44,48}Ca$ the ambiguities due to interaction parameters are completely removed. Moreover, the two different types of experiments are fully consistent with each other and the errors of the extracted quantities of the neutron density distribution are slightly smaller than from independent analyses, as shown in Fig. 3. The corresponding values of r_n are $r_n = 3.475 \pm 0.042$ fm (α) and $r_n = 3.469 \pm 0.029$ fm (α + π), respectively. The results are encouraging for combined analyses of other experiments like elastic scattering of protons and pionic atoms.

(1) E. Friedman, H.J. Gils, H. Rebel, Phys. Rev. C 24 (1982) 1551
(2) H.J. Gils, H. Rebel, E. Friedman, Phys. Rev. C 29 (1984) 1295
(3) C.J. Batty, E. Friedman, A. Gal, Nucl. Phys. A402 (1983) 411

+ The Racah Institute of Physics, The Hebrew University of Jerusalem, Israel

1.3.3 THE DENSITY DEPENDENCE OF THE EFFECITVE ALPHA-NUCLEON FORCE AND ISOSCALAR TRANSITION RATES OF NUCLEI

D.K. Srivastava+, H. Rebel, Z. Phys. A - Atoms and Nuclei 316 (1984) 225

Effects of the density-dependence of the α-particle-bound nucleon effective interaction on single-folding models of inelastic α-particle scattering are studied, in particular in view of corrections of the isoscalar transitions rates extracted by implicit folding procedures. The l-dependent corrections factors C_l are calculated and tabulated for applications.

+ On leave from the Variable Energy Cyclotron Centre, Calcutta, India

1.3.4 ISOSCALAR TRANSITION RATES OF sd-SHELL NUCLEI USING A MODIFIED IMPLICIT FOLDING PROCEDURE

D.K. Srivastava+ and H. Rebel, KfK-Report 3708

Elastic and inelastic scattering data for 104 MeV alpha-particles from $^{20,22}Ne$, $^{24,26}Mg$, ^{28}Si and ^{32}S have been analysed in a coupled channels approach assuming a Woods-Saxon and a Woods-Saxon squared shape for the real potential. The isoscalar transition rates for the $\Delta L = 2$ and $\Delta L = 4$ transitions are evaluated using the implicit folding procedures.

+ On leave from Variable Energy Cyclotron Centre, Calcutta

1.3.5 DYNAMIC DENSITY DEPENDENCE OF THE ALPHA-NUCLEON FORCE IN FOLDING MODELS OF INELASTIC SCATTERING OF ALPHA-PARTICLES

D.K. Srivastava+ and H. Rebel, J. Phys. G: Nucl. Phys. 10 (1984) L127; KfK-Report 3735 (1984)

The importance of a dynamic density dependence of the α-particle-bound nucleon force is demonstrated by deformed folding model analyses of elastic and inelastic scattering of 104 MeV α-particles from ^{50}Ti and ^{52}Cr. Various approximations are discussed and technical details are given.

+ On leave from Variable Energy Cyclotron Centre, Calcutta

1.3.6 EXCITATION OF COLLECTIVE NUCLEAR STATES BY ALPHA-PARTICLE SCATTERING

H. Rebel, D.K. Srivastava+ and H.J. Gils

The interpretation of α-particle scattering on the basis of folding models has been considerably successful for the understanding of the α-particle-nucleus interaction potentials in terms of the ground-state nucleon density distribution and of transition densities of inelastic excitations. A density-independent effective interaction V_{eff} (as derived by the analysis of the forward-angle scattering from ^{40}Ca, e.g.), though providing a good description of the differential cross sections in the diffraction region, is unable to describe the cross sections at larger scattering angles. Additionally, it does not reproduce the values of the volume integrals J_V of the phenomenologically observed potentials (determined by rather model-independent methods). The (real) phenomenological potentials do not follow the folding relation $J_V/J_{Veff} = A$, with J_{Veff} being the volume integral of V_{eff}. These features strongly indicate a density dependence of the effective interaction. The description of elastic scattering has been significantly improved by an additional saturation factor

$$g(\rho) = 1 - \gamma\rho^{2/3}(r) \qquad (\gamma = 1.9 \text{ fm}^2) \tag{1}$$

in

$$V_{eff}(\vec{r}_\alpha,\vec{r}) = V_{DI}(\vec{r}_\alpha,\vec{r})g(\rho) \tag{2}$$

Applying such a density-*dependent* force to inelastic excitation replaces the transition potential of a $(0^+ \to J_f = L)$ transition, e.g.

$$\langle J_f = L||U||J_i = 0\rangle = -i^L(2L+1)^{-1/2}\, \beta_L^m c_o \int \frac{\partial\rho}{\partial r} V_L(r_\alpha,r)r^2 dr + \text{ second order terms} \tag{3a}$$

by

$$\langle J_f = L||U||J_i = 0\rangle = -i^L(2L+1)^{-1/2}\, \beta_L^m c_o \int \frac{\partial\rho}{\partial r} g(\rho)V_L^{DI}(r_\alpha,r)r^2 dr + \text{ second order terms} \tag{3b}$$

with β_L^m the "deformation" parameter of the deformed density $\rho(r)$ and V_L the L th multipole component of the density-independent part of V_{eff}.

We have shown (1) that the density dependence is not restricted to the monopole part $\rho_{L=0}(r)$ of the deformed density, but follows dynamic changes of $\rho(\vec{r})$. As the inclusion of the density dependence can be considered as a replacement of $\rho(\vec{r})$ in the folding integral by an effective density

$$\rho_{eff}(\vec{r}) = \rho(\vec{\theta})(1 - \gamma\rho^{2/3}(\vec{r})) \tag{4}$$

the dynamic density dependence factor is derived from the expansion of the effective density which gives for a first order excitation

$$\tilde{g}(\rho) = 1 - \frac{5}{3}\gamma\rho_{L=0}^{2/3}(r) \tag{5}$$

different from $g(\rho)$ by a the factor of 5/3.

The suspiciously small transition rates found previously in explicit single as well as in double folding analyses (2,3), even with extremely good fits to the data, are a consequence of ignoring the dynamic density dependence of inelastic transitions. When including it, any necessity of a "renormalization" of the transition rates naturally disappears.

There is now an impressive agreement in the results of implicit (MIFP) and explicit (DDF) folding procedures (with density dependent forces). The examples given in Tab. 1 demonstrate not only the questionable quality

^{26}Mg	E_x(MeV)	B(EL) (e^2fm^{2L})	$^{26}Mg(\alpha,\alpha')$		B(IS)/B(EL)	$(M_n/M_p)^2$
			th[a]	exp(BP)	exp(MIFP)	th[a]
$0^+-2_1^+$	1.81	301±13	0.81	1.00±(0.14)	0.85±(0.08)	0.64
$0^+-2_2^+$	2.94	9±2	2.99	6.00±(1.2)	3.70±(0.5)	2.45

a B.A. Brown and B.H. Wildenthal (Phys. Rev. C21, 2107 1980)

Giant Resonance Excitation in ^{90}Zr by (α,α') Scattering[b]

	G_L(BP)(s.p.u)	G_L(IFP)(s.p.u)	G_L(MIFP)(s.p.u)	G_L(DDF)(s.p.u)
L=2(GQR)	5.7	15.3	13.1	13.2
(E_x=14.0 MeV)				
S_x (%)	35	94	80	81
L=3(LEOR)	10.7	43.2	32.5	30.0
(E_x=7.5(MeV)				
S_x (%)	13	53	40	38

b Experimental data from Fuchs et al. (1984)

Tab. 1 Examples of isoscalar rates deduced by different procedures from experimental (α,α') cross sections

of the obsolete Bernstein procedure (BP) and the importance of the density dependence, but also the internal consistency of the improved procedures. This has to be required for obtaining meaningful and relevant results which can be furtheron discussed in terms of differences in neutron- and proton matrix elements and compared to π^+/π^- scattering results.

(1) D.K. Srivastava and H. Rebel, Journal Phys. G: Nucl. Phys. 10 (1984) L 127

(2) R. Pesl, H.J. Gils, H. Rebel, E. Friedman, J. Buschmann, H. Klewe-Nebenius and S. Zagromski Z. Phys. A313 (1983) 111

(3) A.M. Kobos, B.A. Brown, R. Lindsay and G.R. Satchler Nucl. Phys. A (submitted)

+ On leave from Variable Energy Cyclotron Centre, Calcutta, India

1.3.7 ANALYSIS OF ELASTIC AND INELASTIC SCATTERING OF 172.5 MeV ALPHA-PARTICLES FROM Ni-ISOTOPES

J. Albiński, H. Rebel and A. Budzanowski+

It is known that the radial shape of the real part of the α-particle-nucleus optical potential as deduced from elastic scattering is well approximated by a squared Woods-Saxon form (WS-2) rather than by the traditional Woods-Saxon form (WS). In contrast for a *deformed* optical potential including excitations of collective nuclear states the radial shape is not so well studied. There arises the question to which extent the experimental cross sections for inelastic scattering are sensitive to the detailed radial shape, and how pre-chosen forms acting as constraints in the analysis do affect the values of the transition rates extracted from the data. We considered these questions by an analysis of elastic and inelastic α-particle cross sections measured at E_α = 172.5 MeV for low-lying states of $^{58,60,62,64}Ni$ (1). The data extend to fairly large angles beyond the diffraction region and should be sensitive to the radial form of the interaction potential. The analysis based on a coupled channel procedure parametrizes the transition matrix elements in terms of an anharmonic vibrational model of second order

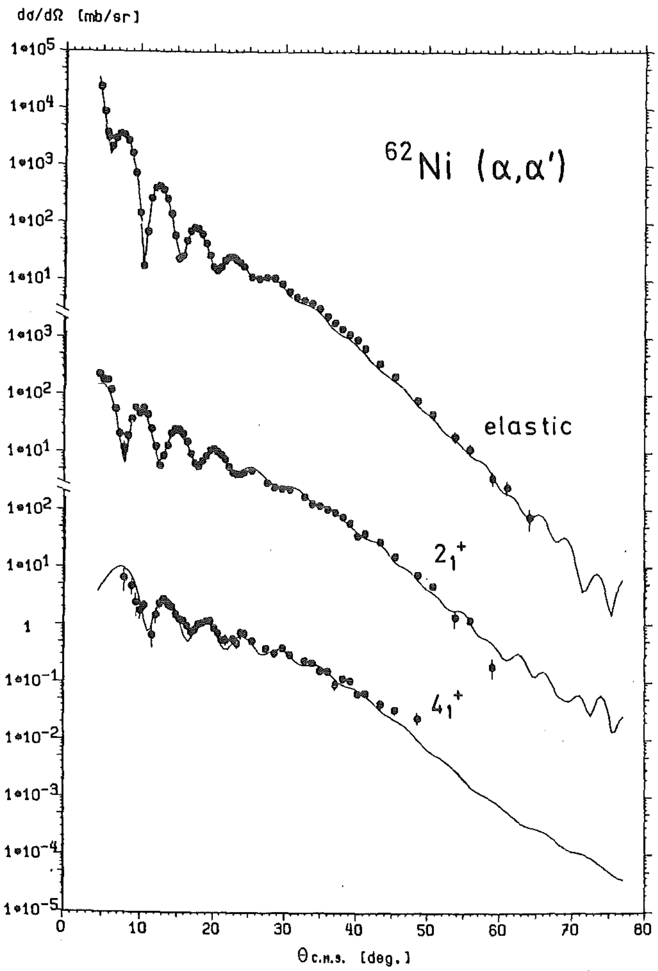

Fig. 1
$^{62}Ni(\alpha,\alpha')^{62}Ni$: Experimental cross sections and results of coupled channel calculations

This model provides a large flexibility and removes some model dependence of the results to a large extent. The transition potentials are calculated with both radial formfactors (WS and WS-2), and the deformation and potential parameters are determined by fits to the experimental data. Fig. 1 displays an example demonstrating the good agreement between experimental and theoretical cross sections. The 4_1^+ cross sections show a significant contribution of direct hexadecapole excitation.

However, within the limits of the experimental accuracy of the data, no significant preference for one of the radial form factors has been found, though the elastic cross section alone prefers the WS-2 form. It might be that different radial form factors are required for the diagonal and transition potentials, somewhat obscured in our analysis by the use of a common form factor for both. The values of the transition rates are found to be insensitive to such details. Tab. 1 presents the isoscalar transitions rates extracted by a modified implicit folding procedure (2). The values are compared to results of electromagnetic excitation.

I^π, Ex	WS-2 formfactor GI(s.p.u.)	WS formfactor GI(s.p.u.)	ELM values
^{58}Ni, 2^+,1.454	10.7	10.3	11.0 ± 1.0
4^+,2.459	2.8	3.3	3.5 ± 1.1
2^+,3.265	1.8	1.8	2.4 ± 0.2
3^-,4.475	12.3	12.1	16.0 ± 3.0
^{62}Ni, 2^+,1.172	12.5	12.3	12.0 ± 1.0
4^+,2.336	4.9	5.6	3.0 ± 0.3
2^+,3.270	1.1	1.0	---
3^-,3.757	13.7	13.8	13.0 ± 1.0
^{64}Ni, 2^+,1.344	10.3	10.3	8.6 ± 0.5
4^+,2.605	1.6	1.7	---
2^+,3.270	0.9	0.8	---
3^-,3.560	13.0	14.1	---
2^+,4.600	1.0	0.8	---

Tab. 1 Isoscalar and electromagnetic transition rates in Ni-Isotopes

(1) A. Budzanowski, J. Albiński, C. Alderliesten, J. Bojowald, H. Dabrowski, W. Oelert, Z. Rogalska, P. Turek and S. Wiktor in KfK-Report 2830 (1979) and to be published
(2) D.K. Srivastava and H. Rebel, Z. Physik A 316 (1984) 225

+ Institute of Nuclear Physics, Cracow and Hahn-Meitner-Institut für Kernforschung, Berlin

1.3.8 LOCAL DENSITY APPROXIMATION IN EFFECTIVE DENSITY-DEPENDENT αN-INTERACTIONS

H.J. Gils, Z. Phys. A - Atoms and Nuclei 317 (1984) 65

Different forms of a local density approximation (LDA) in effective density-dependent αN-interactions are compared in single-folding optical model analyses of elastic α particle scattering by $^{40,42,44,48}Ca$ at E_α = 104 MeV and by ^{40}Ca at E_α = 140 MeV. It is shown that the form of the LDA considerably influences the results on folded optical potentials. A variable form of the LDA is suggested and discussed which includes previous forms as limiting cases. The new form leads to better fits to the data and to full consistency with the best available "model-independent" optical potentials.

1.3.9 PROJECTILE BREAK UP ASSOCIATED WITH GAMMA RAY FROM INTERACTIONS OF THE NON-SPECTATOR FRAGMENT WITH THE NUCLEUS

M. Albińska[+], J. Albiński[++], J. Buschmann, H.J. Gils, H. Klewe-Nebenius, H. Rebel, S. Zagromski

The break up reaction is characterized by a broad and pronounced peak in the energy spectrum of the ejectiles at an energy which corresponds approximately to the beam-velocity. Experimental studies of the correlation of two projectile fragments following the break up reaction and theoretical predictions on the basis of the DWBA break up theory (1) suggest that there is a dominant reaction channel where only one projectile fragment is emitted without any interaction with the target (except elastically) while the other interacts nonelastically with the target nucleus. As a major fraction of the inelastic break up reaction the break up-fusion process is expected with absorption of the non-spectator fragment and decay of the excited system from pre-equilibrium and equilibrium stages. The process is highly related to in-complete fusion or "massive" transfer processes which lead to γ-ray emission in final stages of the decay and can be studied by particle - γ - coincidence measurements.

In order to clarify the relative importance of the break up - fusion process in ^{6}Li break up reactions at E_{Li} = 156 MeV we measured charged particle spectra from ^{6}Li induced reactions on ^{208}Pb in coincidence with discrete γ-rays from heavy residual nuclei. A careful evaluation of these data and assuming isotropic γ-emissions (since the γ-emission was only observed perpendicular to the projectile beam) leads to exclusive cross sections of charged particle emission. Fig. 1 compares a result for coincident emission of break up α-particles (centered in the energy spectra around the beam velocity energy) with the inclusive spectrum observed at the same emission angle.

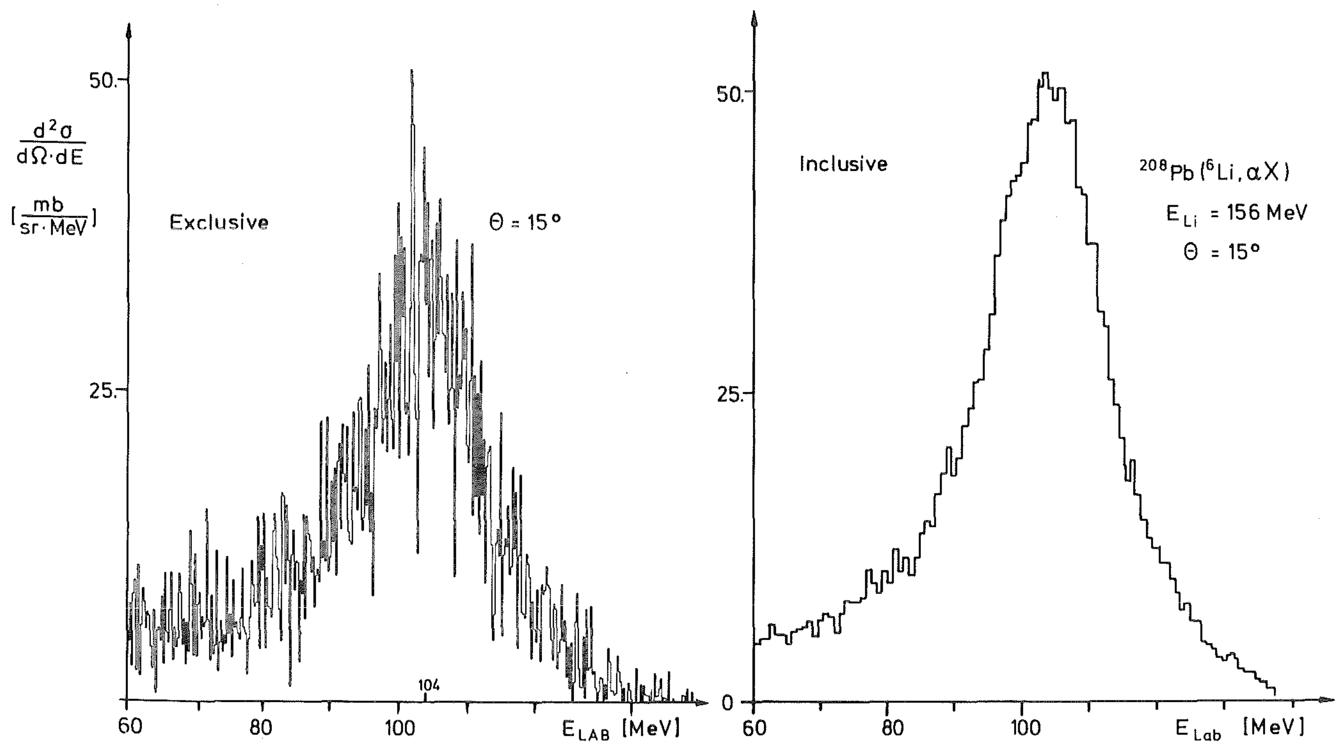

Fig. 1 Differential cross sections for emission of α-particles from the ^{6}Li induced reactions with ^{208}Pb at E_{Li} = 156 MeV

Actually the coincident cross section comprises more than 50% of the inclusive cross section, and when taking into account additionally the decay by a fission mode, one has to conclude that for a heavy target nucleus the absorptive break up exhausts the total inelastic break up cross section as predicted by theoretical calculations. The result is in contast to our findings in previous experiments (2) with a light target (^{40}Ca) where an unexpectedly small cross section for charged particle emission coincident with γ-rays from target-like evaporation residua is found. This may tentatively be ascribed to dominant contributions of direct reactions like transfer and knock-out by the non-spectator particle, not signalled by γ-ray emission of target-like products.

(1) B. Neumann, H. Rebel, H.J. Gils, R. Planeta, J. Buschmann, H. Klewe-Nebenius, S. Zagromski, R. Shyam and H. Machner
Nucl. Phys. A 382 (1982) 296

(2) R. Planeta, H. Klewe-Nebenius, B. Neumann, J. Buschmann, H.J. Gils, H. Rebel, S. Zagromski, L. Freindl, K. Grotowski
KfK 3642 (1983)

\+ On leave from Technological University, Cracow, Poland

++ On leave from Institute of Nuclear Physics, Cracow, Poland

1.3.10 THE OPTICAL POTENTIAL FOR ^{6}Li + ^{6}Li ELASTIC SCATTERING AT 156 MeV

S. Micek[+], Z. Majka[+], H. Rebel, H.J. Gils, H. Klewe-Nebenius[++]

Previous studies of elastic scattering of 156 MeV ^{6}Li projectiles from nuclei revealed cluster structure effects originating from the projectile and from both the projectile and the target nucleus (1). The question to which extent such effects may be evident in a scattering system of highly clusterized nuclear particles leads us to study elastic scattering of ^{6}Li from ^{6}Li in order to explore the radial shape and the microscopic structure of the interaction potential. The experimental differential cross sections have been analyzed on the basis of a double-folding cluster model (DFC). This approach generates the real part of the optical potential from d-α, α-α, and d-d interactions and internal cluster wave functions of ^{6}Li. Such a potential describes the experimental data as well as phenomenological potentials or the usual double-folding model with a density-dependent effective NN interaction. In order to fit the data, the strength of the semimicroscopic potentials had to be readjusted (by a factor N = 1.17 for the DFC potential). Fig. 1 displays the experimental and theoretical cross sections. The imaginary part of the optical potential is of the phenomenological Woods-Saxon form and a weak spin-orbit term is included.

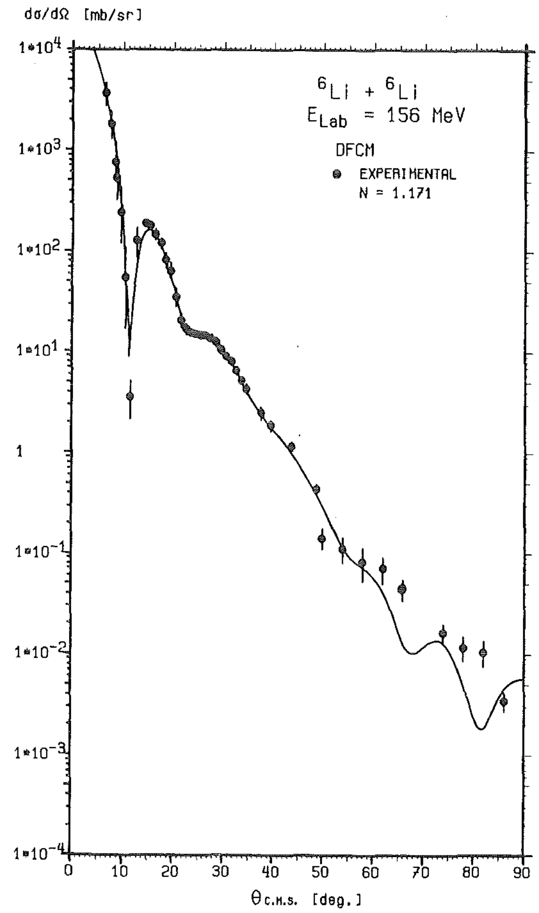

Fig. 1

Optical model description of 156 MeV ^{6}Li scattering by ^{6}Li using a double folding cluster potential (DFC) for the real part of the interaction potential

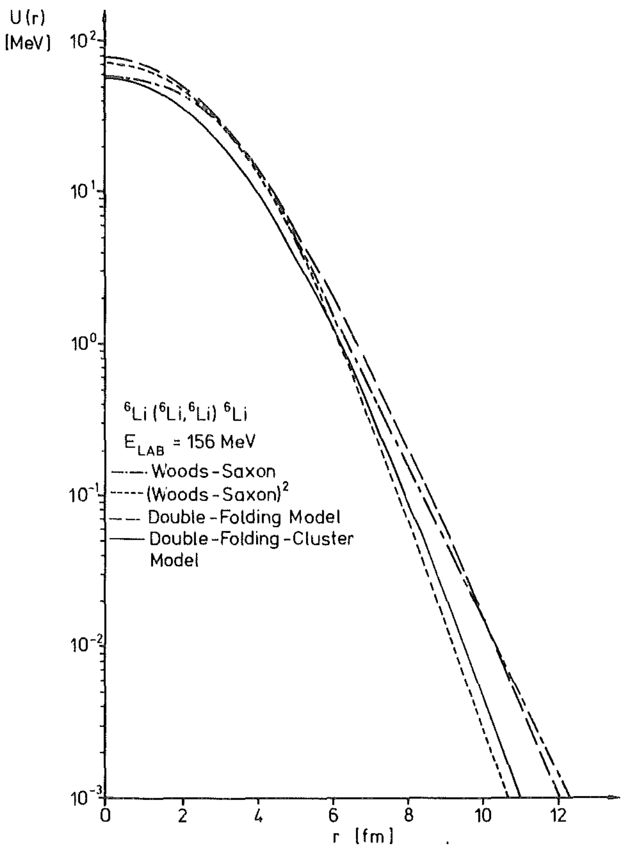

Fig. 2

Shapes of the real part of the ^{6}Li + ^{6}Li optical potential resulting from the best fits using different radial form factors

Fig. 2 compares the shapes of the real potential resulting from the analyses using different radial form factors. They agree very well in the range of r = 3 - 5.5 fm (-the semimicroscopic potentials after renormalization of the strengths-), which is obviously the radial part most sensitiveley determined by the data.

(1) Z. Majka, H.J. Gils, H. Rebel, Phys. Rev. C 25 (1982) 2996

+ Jagellonian University, Cracow, Poland
++ IRCH des Kernforschungszentrums Karlsruhe

1.3.11 INELASTIC SCATTERING OF 156 MeV ^{6}Li-PARTICLES FROM LOW LYING STATES AND GIANT RESONANCES OF ^{24}Mg AND ^{90}Zr

B. Mühldorfer[+], W. Eyrich[+], A. Hofmann[+], H. Rebel, U.Scheib[+], H. Schlösser[+] and M. Tresp[+]

The main advantage of using ^{6}Li scattering for the investigation of giant resonances (GR) is the relative low background in this reaction at higher excitation energies due to the low binding energy of this projectile. In the preceding annual report we presented first measurements on ^{24}Mg, ^{90}Zr and ^{208}Pb. In the meantime we completed the measurements on ^{24}Mg and ^{90}Zr and analyzed the data especially the GR region with the conventional macroscopic DWBA.

The spectrum of Fig. 1 obtained at θ_{lab} = 10° for ^{24}Mg shows beside the strongly excited low lying states the two parts of the GQR around 18.5 and 24.5 MeV excitation energy. In the lower part the angular distributions of the first excited state at E_x = 1.37 MeV and the GQR region are displayed. The angular distribution for the GQR region is rather flat which can be a hint for the additional excitation of higher multipolarities L ≠ 2 in this energy region. The deduced percentages of the energy weighted E 2 sumrule agree within the errors with those from α-scattering experiments.

In Fig. 2 on the left side the angular distributions for the low lying states of ^{90}Zr at E_x = 2.18 and 2.73 MeV are displayed. The experimental data are well reproduced by DWBA-calculations using a slightly modified potential from α-scattering analyses. The angular distributions of the GR's of ^{90}Zr are also reproduced quite well by DWBA-calculations using the same potential. The deduced values for the sumrule strenghts are in fair agreement with the results of α-scattering experiments. It should be mentioned however, that in this energy region from (α, α'n)-measurements (1) there is known also strength with higher multipolarities. In conclusion, our analysis shows within the relative large errors of GR-analysis in single hadron scattering experiments, mainly due to uncertainties in the background subtraction and the contribution of different multipolarities that ^{6}Li- and α-scattering give comparable results for the extracted strength. It has to be proved however, that more sophisticated analyses like e.g. folding model procedures give similar results.

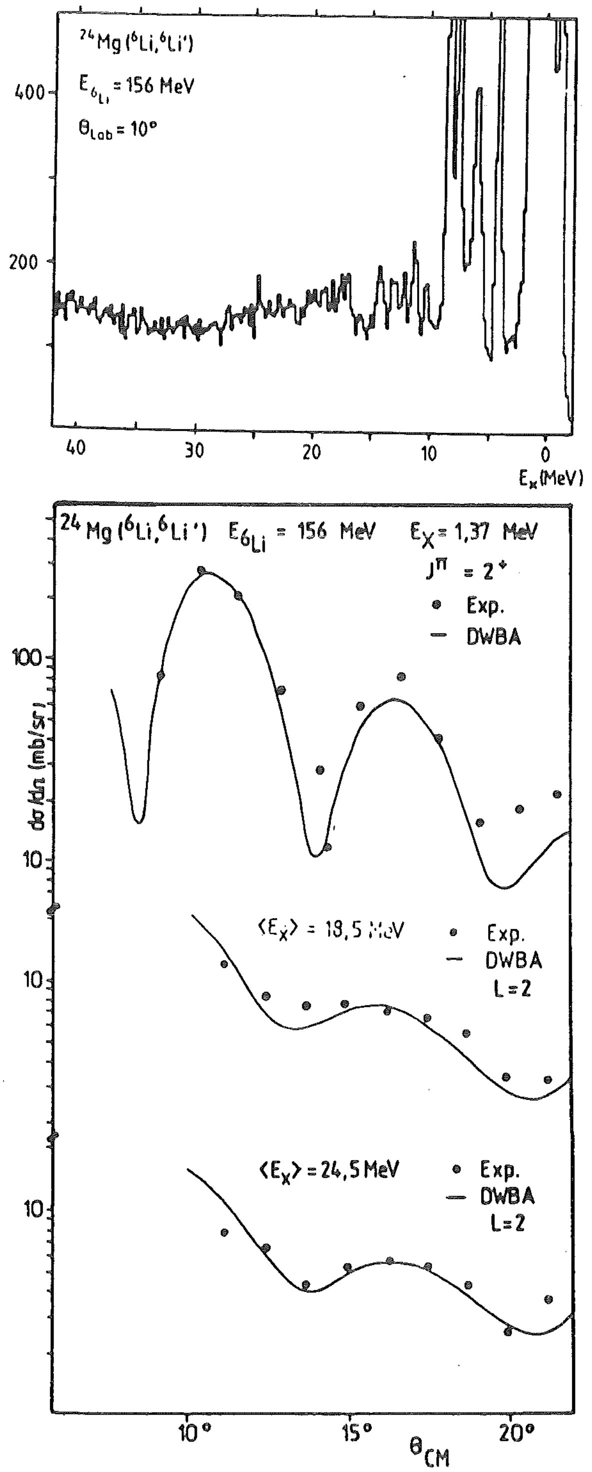

Fig. 1 ^{6}Li-scattering spectrum on ^{24}Mg (upper part) and angular distributions of the first excited state and the E2 - GR region.

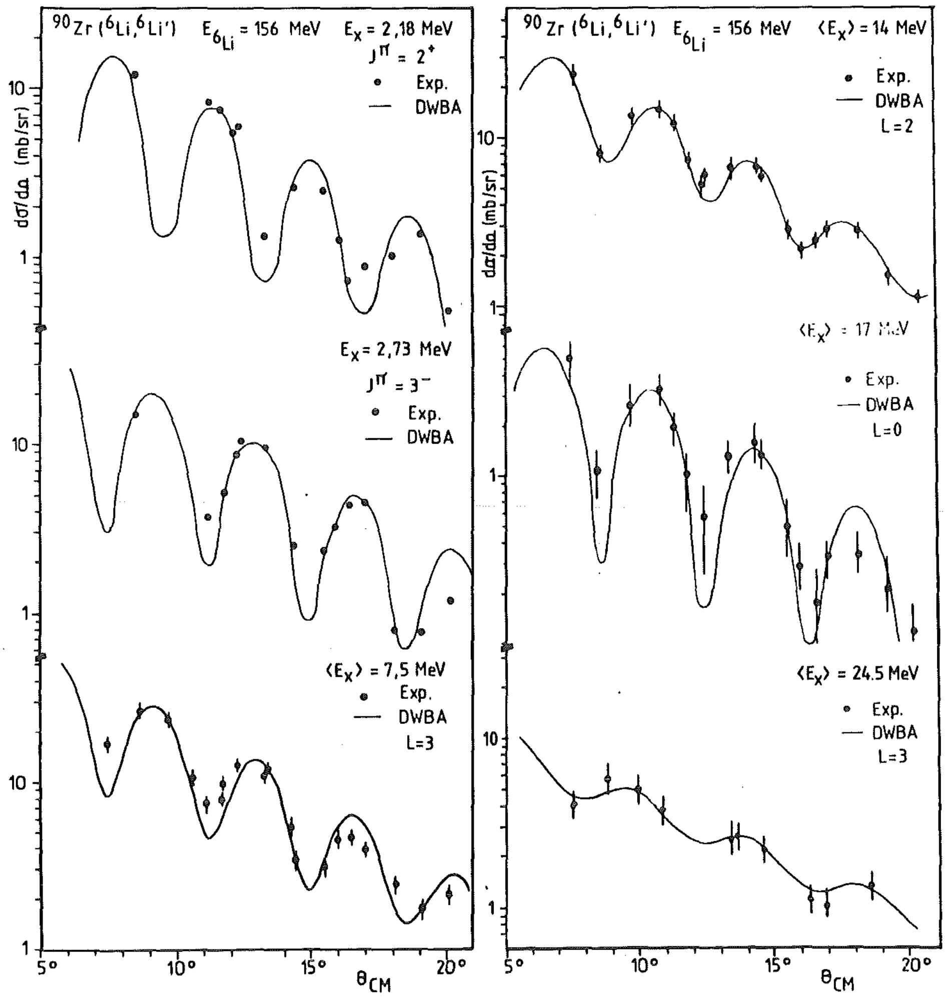

Fig. 2 Angular distributions of the E0, E2 and E3 GR's in ^{90}Zr from ^{6}Li-scattering

(1) K. Fuchs et al., to be published

\+ Physikalisches Institut, Universität Erlangen-Nürnberg

1.3.12 FIRST RESULTS OF THE DECAY OF THE GIANT MONOPOLE RESONANCE REGION IN ^{90}Zr FROM A (^{6}Li, ^{6}Li'n) COINCIDENCE EXPERIMENT

B. Mühldorfer+, W. Eyrich+, A. Hofmann+, H. Rebel, U. Scheib+ and H. Schlösser+

In the preceding annual report we presented the results of our (α,α'n) coincidence experiment concerning the decay of the giant monopole resonance region in ^{90}Zr. From the excess of fast neutrons in the decay spectrum, a direct decay component of 10-15% was extracted.

In order to get more detailed information about the decay of the GMR and the underlying background, we started a (^{6}Li, ^{6}Li'n) coincidence experiment.

One of the reasons to choose ^{6}Li-particles is the very different background behaviour of ^{6}Li-scattering as compared to α-scattering, due to the strong break-up channel of the ^{6}Li-particles.

In Fig.1 the spectra of the decay neutrons from the center of the GMR in ^{90}Zr, measured in a maximum of the resonant strength excited by ^{6}Li- and α-particles are compared. Assuming a pure statistical decay the n-spectra should show an evaporation shape (dashed line). The significant deviations at neutron energies $E_n \geq 4$ MeV in both spectra correspond to a direct decay of the GMR into low lying hole states of the residual nucleus ^{89}Zr. The excess in the n-energy region between $E_n = 3$ and $E_n = 4$ MeV should mainly be referred to a preequilibrium-decay into special 1phonon-1 hole states in ^{89}Zr as discussed in ref. 1 for a similar experiment on ^{208}Pb. The larger excess in the

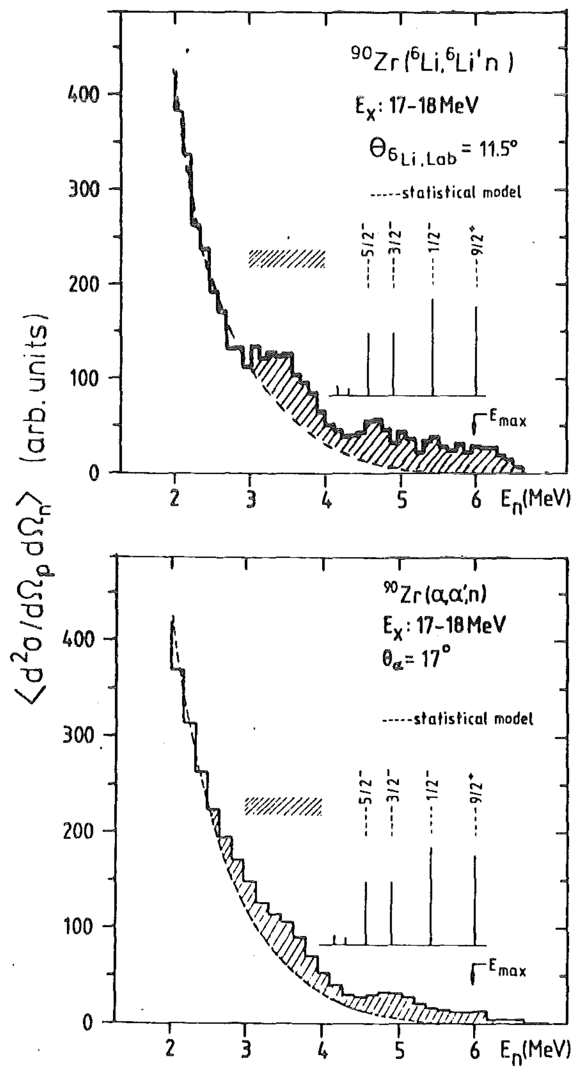

Fig. 1
n-decay spectrum from the GMR-region in ^{90}Zr from (α,α'n)-measurements (upper part) and (^{6}Li, ^{6}Li'n)-experiments (lower part)

spectrum of the (^{6}Li, $^{6}Li'n$) experiment in comparison to the ($\alpha,\alpha'n$)-spectrum is due to the smaller background, excited in the ^{6}Li-reaction confirming the results of our ($\alpha,\alpha'n$) experiments yielding nearly a pure statistical decay of the continuum. (1,2)

(1) W. Eyrich, K. Fuchs, A. Hofmann, U. Scheib, H. Rebel, Phys. Rev. C. 29 (1984) 418

(2) K. Fuchs et al., to be published

+ Physikalisches Institut, Universität Erlangen-Nürnberg

1.3.13 ß-γ ANGULAR CORRELATIONS IN THE ISOSPIN-TRIPLETT A=28

U. Scheib[+], W. Eyrich[+], H. Forkel[+], G. Gottschalk[+] and A. Hofmann[+]

The ß-decay of the isospin-triplett system A=28 is suitable to study small terms in the decay matrix elements. We looked especially for second class matrix elements, which should be observable in precise ß-γ angular correlation measurements.

Since the decay of ^{28}Al and ^{28}P into the first excited state of ^{28}Si is an allowed Gamow-Teller Transition, one would expect an isotropic angular correlation. However, forbidden matrix elements and induced matrix elements lead to a small anisotropy. This asymmetry can be calculated from shell-model wave-functions under the assumption that CVC is valid and no second class currents exist. By combining the results of both transitions the major part of the forbidden elements cancels and the comparison with the experimental results is nearly model independent.

The $ß^{+}$-decay of ^{28}P has been investigated at the Karlsruhe isochronous cyclotron. Because of the short half-life of only 268 ms we constructed a fast target handling system. Details of the experimental setup are described in ref. (1). The measurement of the mirror decay of ^{28}Al has been performed at the Erlangen tandem accelerator with the same experimental equipment.

The data are taken in list-mode to be independent of possible gain shifts in the detectors or in the coincidence electronics. The data-evaluation and the determination of the counting rates has been done on a PDP 11/23 by computer-programs with automatic integration routines to diminish systematic errors. The extracted experimental asymmetries for different energy regions of the ß-decay have to be corrected for accidental coincidences, the finite size of the detectors and for an apparative asymmetry caused mainly by the finite beamspot.

In Fig. 1 and 2 the final experimental results for both transitions are shown. The asymmetry of the angular correlation is expected to be energy-dependent in the form

$$\varepsilon(E) = a_{\beta\gamma}\, p^2 \;/\; E(1+b_{\beta\gamma}\, E)$$

In both figures best fits for $a_{\beta\gamma}$ and $b_{\beta\gamma}$ on the experimental data are shown. In the figures also theoretical calculations are displayed. These calculations are based on one-body-transition densities from shell model calculations (2). They do not include second class currents and are done up to second rank tensor matrix elements. One higher rank element could contribute in the high energy region of the β^+-decay. This contribution, however, is expected to be small.

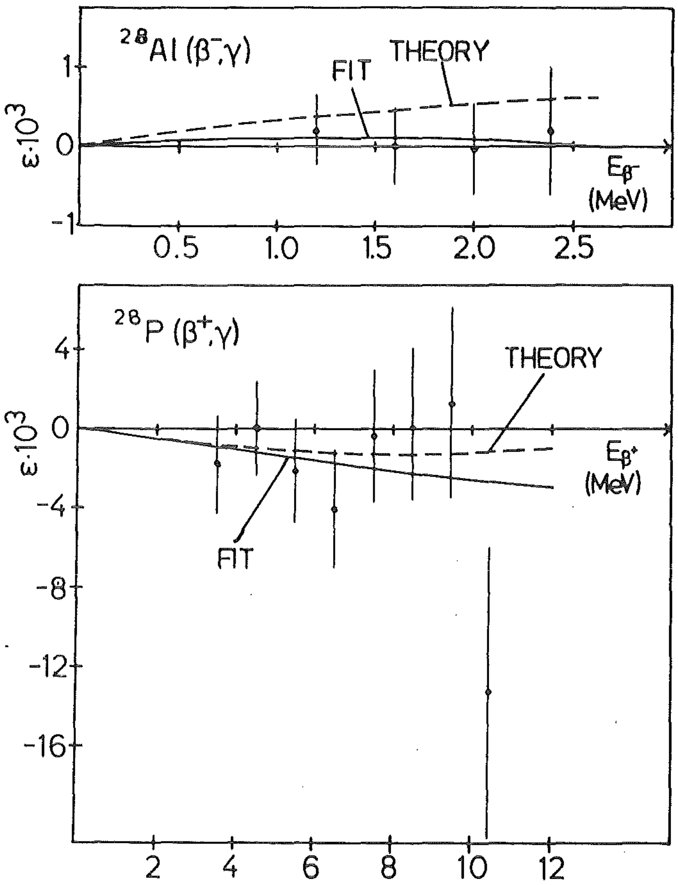

Fig. 1
Experimental and theoretical symmetries of the β-γ angular correlation of the decay of ^{28}Al (upper part) and ^{28}P (lower part).

The comparison of the theoretical and experimental results show no significant deviation, so second class currents are not necessary to describe the angular correlation of the mirror decay in the A=28 system. Calculation to deduce an upper limit for the second class current contribution are in progress.

We have profited from enlightening discussions with Dr. H. Behrens and his permanent interest in the present study.

(1) U. Scheib et al., Annual Report on Nuclear Physics Activities 1982/83, KfK 3621, p.55

(2) B.A. Brown and B.H. Wildenthal , to be published. We are very grateful to B.A. Brown and B.H. Wildenthal for the calculation of the special densities we needed for the comparison with our experiment.

1.3.14 DIRECT DECAY COMPONENT OF THE GIANT-MONOPOLE-RESONANCE REGION IN ^{208}Pb

W. Eyrich[+], K. Fuchs[+], A. Hofmann[+], U. Scheib[+], and H. Steuer[+],
Phys. Rev. C 29 (1984) 418
H. Rebel

The n-decay of the giant-monopole-resonance region in ^{208}Pb has been studied in an $(\alpha,\alpha'n)$ coincidence experiment at E_α = 104 MeV. From the fast-neutron emission corresponding to the decay into the low lying single hole states in ^{207}Pb a direct decay component of ∿ 15 % was estimated for the resonant strength. In addition, evidence for a preequilibrium decay was found.

+ Physikalisches Institut der Universität Erlangen-Nürnberg

1.4 NUCLEAR THEORY

1.4.1 THE CLUSTER MODEL WITH BREATHING CLUSTERS: DYNAMICAL DISTORTION EFFECTS IN ^{6}Li

R. Beck, F. Dickmann and A.T. Kruppa[+], (1)

Distortion effects in an assembly of clusters are studied by using a trial wave function in which - in addition to the intercluster separations - also the size parameters of individual clusters appear as generator coordinates. An application to the nucleus ^{6}Li which is described as a bound alpha + deuteron system shows that these new degrees of freedom which may be related to compressional vibrations are indeed important. We find that the deuteron cluster is compressed whereas the size and the compressibility of the alpha cluster are unchanged with respect to the free case.

(1) dito, submitted to Phys. Rev. C
+ Institute of Nuclear Research, Debrecen, Hungary

1.4.2 QUASIELASTIC CLUSTER KNOCK-OUT REACTIONS AND THE MICROSCOPIC CLUSTER MODEL

R. Beck, F. Dickmann and R.G. Lovas[+]

The spectroscopic information on the cluster structure of light nuclei obtainable from quasielastic cluster knock-out reactions is examined in the plane wave impulse approximation. The result shows that, because of the Pauli principle, the quantities (e.g. the fragmentation amplitude and the spectroscopic factor) extracted from experiment do not represent probabilities (e.g. the Fourier transform of the wave function related to the intercluster relative motion and the amount of clustering). A microscopic cluster model of ^{6}Li which explicitely makes allowance for an α + d and ^{5}Li + p clusterization, is used to examine the α + d structure of this nucleus. The model predicts the spectroscopic amplitude (amount of clustering) 1.04 (0.97) and 1.01 (0.94) for the ground and first excited state, respectively, and a fragmentation amplitude in good agreement with recent experimental data extracted from 590 MeV $^{6}Li(p,pd)\alpha$ and 700 MeV $^{6}Li(\alpha, 2\alpha)d$ experiments.

+ Institute of Nuclear Research, Debrecen, Hungary

2. LASER SPECTROSCOPY

2.0.1 NUCLEAR CHARGE RADII DIFFERENCES AND ELECTROMAGNETIC MOMENTS OF STABLE AND RADIOACTIVE Sn ISOTOPES FROM HIGH-RESOLUTION ATOMIC BEAM LASER SPECTROMETRY

M. Anselment, A. Hanser, J. Hoeffgen, S. Göring, G. Meisel, H. Rebel, G. Schatz

In the course of systematic studies of charge radius variations for long chains of isotopes, the element tin was investigated. The main interest arises from the fact that it has a magic proton number (Z = 50). The experiments preliminarily reported (1) have been improved in accuracy and extended to unstable isotopes. Our results are in global agreement with droplet model predictions, but show in detail some structure which originates from interesting nuclear structure effects.

The experimental method applied was laser induced fluorescence. Small samples of tin isotopes (50 pg or more) were evaporated in a vacuum to form a collimated beam of free atoms which were irradiated by the frequency doubled output of a cw dye laser. The absorption resonance from the $5p^2\ ^3P_0$ ground state into the $5p6s\ ^3P_1$ exited state at λ = 286,3 nm was observed by detecting the fluorescence light at 380,1 nm that is emitted when the excited atoms decay into the $5p^2\ ^1D_2$ state. The resonance was monitored while the laser frequency was tuned over the range of interest. To reach the high temperature of 2000 K required to evaporate the tin samples completely, an electron bombardment heater of special design was built.

For accurate control of the laser frequency and in order to make efficient use of the samples available the sideband method as described in (2) was used with some refinements.

Fig. 1 displays the results of the isotope measurements in terms of nuclear charge radius variations. Fig. 2 is a differential plot which reveals the differences from droplet-model predictions and shows a remarkable structure, in particular at the subshell closure at N=64. $\delta\langle r^2\rangle$ values were calculated (3) using the Hartree-Fock-Bogolyubov approach with the Skyrme effective interaction. Some details of the $\langle r^2\rangle$ dependence on the neutron number are fairly well reproduced, others, however, are not; altogether the theoretical understanding of the experimental results is not yet satisfactory.

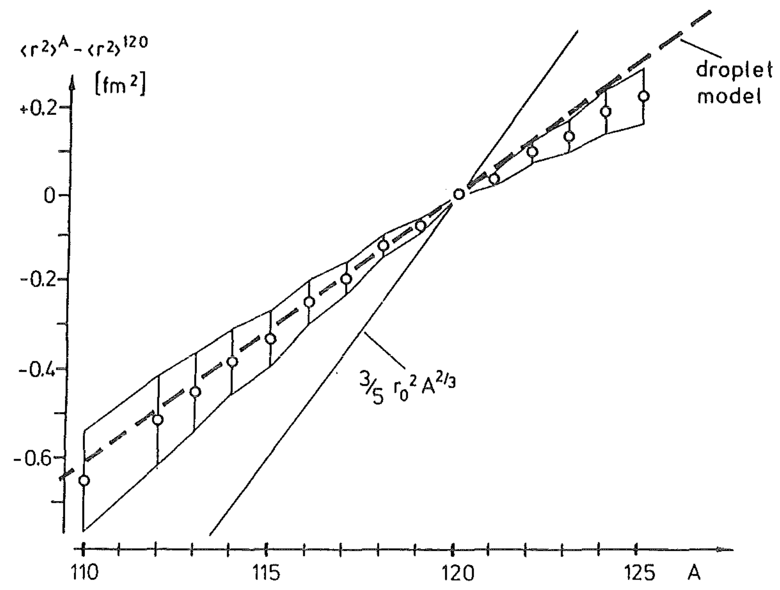

Fig.1 The nuclear charge radius for tin isotopes as function of mass number. The error band results from the uncertainty of electron shell parameters required to determine $\delta\langle r^2\rangle$ from the isotope shift. For comparison the liquid drop model curve with r_o = 1.2 fm and droplet model results are given.

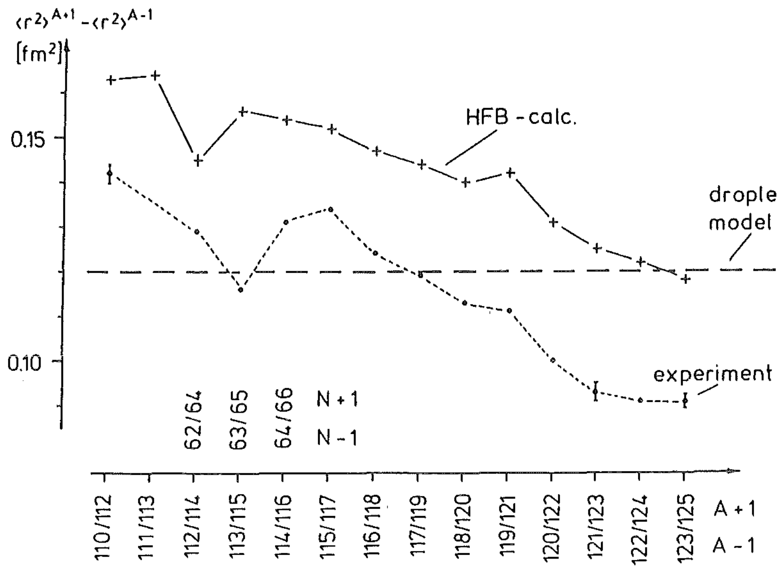

Fig.2 Differences of charge radii between second neighbours. The error bars are the bare experimental uncertainties. The results of droplet model (dashed curve) and Hartree-Fock-Bogolyubov (crosses) calculations (3) are also given.

(1) M. Anselment, A. Hanser, J. Hoeffgen, S. Göring, G. Meisel, H. Rebel, G. Schatz, KfK-Report 3621 (1983) 67
(2) M. Anselment, S. Chongkum, H. Hoeffgen, G. Meisel, KfK-Report 3621 (1983) 65
(3) J. Dobaczewski, H. Flocard, J. Treiner, Nucl. Phys. A 422 (1984) 103

2.0.2 LASER-OPTOGALVANIC EXPERIMENTS

W. Liewehr, K. Kälber, K. Bekk, G. Meisel, H. Rebel

Optogalvanic laserspectroscopy is based on the optogalvanic effect which is the change of the electrical impedance of a gas discharge caused by optical excitation of atoms or ions in the discharge. For spectroscopic studies of long-lived radioactive nuclides or for refractory elements optogalvanic spectroscopy with a closed discharge cell has some advantages. We have studied this method in detail, mainly to find out how well it is suited to study long lived radioactive α-emitters like Am. Fig. 1 gives a set-up used for Doppler limited observation. Its main part is a liquid-nitrogen cooled hollow-cathode lamp as discharge. The atoms of interest are deposited onto the surface of the cathode bore; during operation of the lamp they are sputtered from the wall. As they diffuse into the discharge they take part

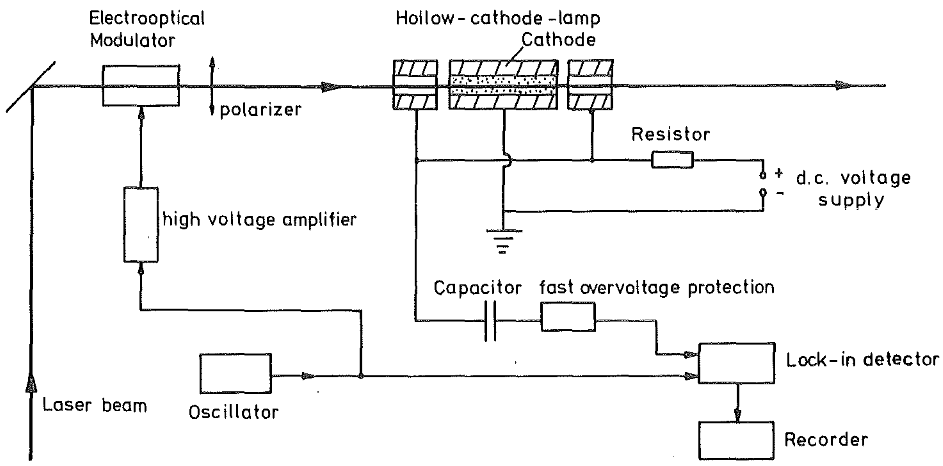

Fig.1 Set-up for Doppler-limited optogalvanic spectroscopy

in it. When they reach the laser beam that crosses the discharge they cause an optogalvanic effect if the laser is tuned into resonance with a transition of the atoms in question.

Fig. 2 shows a measured spectrum of the $4f^7 6s^2\ ^8S_{7/2} \rightarrow 4f^7 6s6p\ ^8P_{9/2}$ (λ = 601,8 nm) transition in stable EuI, which was used to study the method. For this experiment 8 μg of each isotope were vapor deposited under vacuum onto an aluminum foil. The foil was shaped to form a tubular inset to be used in the cathode bore as its "active layer". The cw laser power used was about 30 mW.

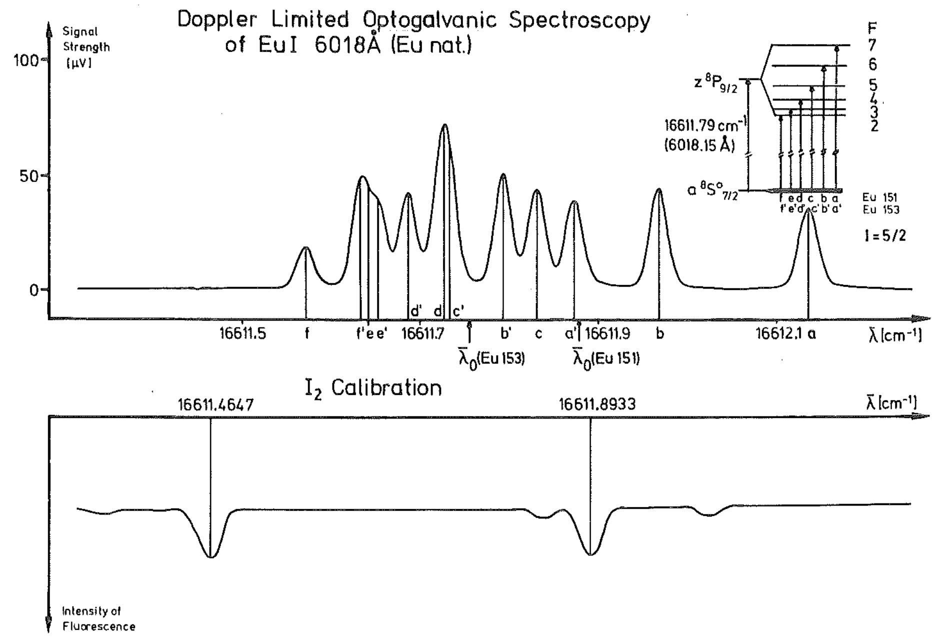

Fig.2 Single-mode-spectrum of the Eu-I-line 601,81 nm

2.0.3 FINE- AND HYPERFINE STRUCTURE ANALYSIS OF THE ODD CONFIGURATIONS IN THE LEAD ATOM

J. Dembczyński+ and H. Rebel, Z. Phys. A - Atoms and Nuclei 315, 137 - 144 (1984) and KfK-Report 3606

The fine- and hyperfine structure (hfs) analysis, on the basis of available experimental data, for the configuration $6s^2 6p6d + 6s^2 6p7s + 6s^2 6p8s$ in PbI has been performed. The Slater integrals, spin-orbit parameters and the effective hfs one-electron parameters have been determined. We find an off-diagonal core-polarization effect in the 6p6d+6p7s - space. Using the calculated radial parameters, the values of the quadrupole moment for stable and radioactive Pb-nuclei have been determined from measured B-factors of the 6p7s $^3P_1$ state. In addition, a repulsion effect on the hfs sublevels with the same quantum number F has been investigated.

\+ On leave from the Institute of Physics, Poznan-Technical University Poznan, Poland

2.0.4 PERTURBATION OF THE CONFIGURATIONS $5s^25pn's$ AND $5s^25pn''d$ BY THE CONFIGURATION $5s5p^3$ IN THE SPECTRUM Sn I

J. Dembczyński[+] and H. Rebel

A fine structure analysis for the system $5s^25pn's$ (n' = 6 to 11) + $5s^25pn''d$ (n'' = 5 to 12) + $5s5p^3$ is performed on the basis of available experimental data. The Slater integrals and spin-orbit parameters are determined. For the Slater integrals associated with the higher configurations we find a relation of the type

$$R^k(a,b)/R^k(c,d) = [n^*(c)n^*(d)/(n^*(a)\ n^*(b))]^{3/2},$$

where a,b,c,d denote a two-electron configuration nln'l', and the n*(nln'l') are effective quantum numbers. The configuration $5s5p^3$ is shown to influence strongly the odd spectrum SnI. On the basis of the theoretical results new spectroscopic assignments of the atomic levels involved are given in some cases.

(1) Physica C (in press) - KfK-Report 3703

\+ On leave from Institue of Physics,Poznan-Technical University Poznan, Poland

2.0.5 NUCLEAR QUADRUPOLE MOMENT AND B FACTOR OF THE 5p6s $^3P_1$ LEVEL IN Sn I

J. Dembczyński+, H. Rebel

There are current laserspectroscopic activities of measuring atomic hyperfine structure splitting (hfs) in stable and radioactive Sn isotopes with the aspect of nuclear structure investigations for long isotopic chains. The interpretation of the values of the hfs constants in terms of nuclear quantities (electromagnetic moments) requires the knowledge of the atomic structure ingredients either from a calibration by otherwise known nuclear moments or from reliable results of atomic structure calculations.

In a previous paper (1) we have analysed the fine-structure of the odd configurations in the level spectrum of Sn I. The resulting values of the electronic parameters and of the intermediate coupling eigenvector amplitudes can be used for the analysis of the hfs in Sn I.

Following Sandars and Beck the B-constant of the $5s^2$ 5p6s $^3P_1$ level is written in the intermediate-coupling approximation by

$$B(5p6s\ ^3P_1) = -0.050776\ b^{02}_{5p} + 0.010438\ b^{11}_{5p} \qquad (1)$$

In absence of configuration interaction the effective hfs-one-electron parameters $b^{\kappa k}_{nl}$ (MHz) are related to the quadrupole moment Q(barn) by

$$b^{\kappa k}_{nl} = 234.974\ \langle r^{-3}\rangle^{\kappa k}_{nl}\ Q \qquad (2)$$

with $\langle r^{-3}\ {}^{\kappa k}_{nl}\rangle$ given in a.u. and κk = 02,11 for the p-electron.

Relativistic calculations performed by Lindgren and Rosén (2) provide the ratio

$$b^{11}_{5p}/b^{02}_{5p} = \langle r^{-3}\rangle^{11}_{5p}\ /\ \langle r^{-3}\rangle^{02}_{5p} = -\ 0.226 \qquad (3)$$

which is an average value of the results of three different ab initio theoretical calculations.

Proceeding further similarly to ref. 3 we can write

$$\frac{\langle r^{-3}\rangle^{02}_{5p}\ (5p6s\ conf.)}{\langle r^{-3}\rangle^{02}_{5p}\ (5p^2\ conf.)} = \frac{\zeta_{5p}\ (5p6s\ conf.)}{\zeta_{5p}\ (5p_2\ conf.)}$$

with ζ_{nl} denoting the parameters of the spin-orbit interaction. Their values related to the ground state configuration $5s^2\ 5p^2$ are

$$\langle r^{-3}\rangle^{02}_{5p}\ (5p^2\ \text{conf.}) = 8.456\ \text{a.u.}$$

$$\zeta_{5p}\ (5p^2\ \text{conf.}) = 2229\ \text{cm}^{-1}$$

Adopting the value

$$\zeta_{5p}\ (5p6s\ \text{conf.}) = 2687\ (20)\ \text{cm}^{-1}$$

from ref. 3 we have

$$\langle r^{-3}\rangle^{02}_{5p}\ (5p6s\ \text{conf.}) = 10.2\ (6)\ \text{a.u.} \qquad (4)$$

and find

$$B(5p6s;\ ^3P_1) = -\ 127.3\ (7.7)\ Q$$

or

$$Q = -\ 0.0078\ (5) * B(5p6s;\ ^3P_1)$$

with B in MHz and Q in barn. The error reflects the uncertainty in the parameter values entering into this relation.

(1) J. Dembczyński, H. Rebel: Physica C (1984) accepted for publication
(2) I. Lindgren, A. Rosén: Case Stud. Atom. Phys. 4, 250 (1974)
(3) J. Dembczyński, H. Rebel: Z. Phys. A - Atoms and Nuclei 315, 137 (1984)

2.0.6 A WAVELENGTH METER FOR LASER LIGHT

A. Steiger, G. Meisel

The interferometric wavemeter as described in the preceeding report (1) was completed and put into operation. It is used to set a tunable dye laser to a desired frequency and to determine atomic frequencies that are induced as the laser is scanned across the resonances of atoms. A monochromator and three plane parallel Fabry-Perot interferometers with graded thicknesses are used in the system (2,3). The output interferometric patterns are continuously recorded by linear photodiode arrays and fed to a microcomputer to calculate the actual laser frequency.

The electronic part required some changes to make it less susceptible to electromagnetic interference. A major problem was the implementation of the NOVA computer and its software as well as the connection to the main computer. A complete reorganization of the total on-line computer system was necessary to match the different building blocks.

The software prepared to run the instrument includes an interferometer pattern recognition program and numerous features to display and output the results. One output is generated nearly every second. This period is mainly due to the speed of the Basic software used. As far as the photodiode arrays and their associated electronics are concerned, 20 outputs per second are possible.

The experience gained so far in use shows that the optical part works according to the design specifications. Due to the high finesse (F=40) of the high resolution etalon with widest mirror spacing, laser frequency changes as small as 10 MHz can be identified. Thus is enables one to determine e.g. atomic hyperfine features with this resolution on a short-term basis. Since it was also calibrated using a normal-frequency HeNe-laser and a dye laser that was tuned to electronic transitions in molecular iodine with well known optical frequencies, wavelengths can be determined with an overall accuracy of $\pm$ 50 MHz. This high long-term reproducibility results from the special design of the high resolution etalon, which was made of a Zerodur glass-ceramic spacer with lowest thermal expansion to which the mirrors are contacted. Thus the material problems of solid etalons, i.e. the change of the refractive index and of the length with temperature as well as their dispersion, are eliminated and the associated systematic errors are avoided. Furthermore this etalon was put into a vacuum container to eliminate the influence of air density fluctuations. The limiting factor for the long-term accuracy is the mechanical misalignment caused by ambient temperature variations; their control would improve the performance of the instrument even further.

(1) A. Steiger, G. Meisel, KfK-Report 3621 (1983) 69
(2) A. Fischer, R. Kullmer, W. Demtröder, Opt. Comm. 39 (1981) 277
(3) R.L. Byer, J. Paul, M.D. Duncan, Laser Spectroscopy III (Springer, Heidelberg 1977) p. 414

3. NEUTRINOPHYSICS

KARMEN Collaboration

G. Drexlin, T.A. Gabriel, H.Gemmeke, G. Giorginis, A. Grimm,
H. Hucker, L. Husson, S. Kiontke, J. Kleinfeller, R. Maschuw,
M. Momayezi, K.H. Ottmann, P. Plischke, F. Raupp, E. Remane,
M. Reuscher, F.K. Schmidt, R. Schulz, G. Spohrer, J. Wochele,
W. Grandegger, R. Gumbsheimer, B. Zeitnitz
Kernforschungszentrum Karlsruhe, IK 1 and University of Karlsruhe

E. Finckh, W. Kretschmer, K. Stauber, D. Vötisch
University of Erlangen

N.E. Booth
Oxford University

J.A. Edgington, G. Marinos
Queen Mary College, London

The Karlsruhe Rutherford Medium Energy Neutrino experiment KARMEN denotes a programme of neutrino physics to be performed at the pulsed Spallation Neutron Source SNS of the Rutherford Appleton Laboratories (RAL).

The physics aims, properties of the ν-source etc. have been described earlier (1,2,3). The main purpose is to contribute to the questions of neutrino oscillations, neutrino nuclear physics and neutrino electron scattering. With the result of the Bugey reactor disappearance experiment $\nu_e \rightarrow x$ (4) the problem of possible neutrino oscillations has gained new impact. Refined sensitivity studies of our ν-oscillation programme have been carried out and will be discussed below. Meanwhile the works on the neutrino facility itself, the detector design, prototype development, the electronic system etc. have been proceeded.

3.0.1 STATUS OF THE PROJECT

The neutrino facility

The experiments will be carried out in a massive neutrino blockhouse with inner dimensions of 10 m x 4 m x 7 m located at about 17 m from the SNS target station (detector position). It has 2 m thick iron walls and an iron roof with a thickness of 3 m. Continuously cast iron slabs with 180 mm thickness are mounted around a rigid box steelwork structure anchored in a 1.2 m thick concrete plinth.

The site is prepared for erection of the neutrino bunker as well as for a 600 tonnes sliding door for access to the bunker. A 25 t crane has been installed and the works for a neutrino hall extension have been finished. The first steel slabs have arrived at RAL site and erection of the blockhouse has started. All mechanics work is expected to be ready until May 1985 when assembly of the KARMEN 1 detector is scheduled to start.

Detector design

The KARMEN detector (Fig. 1) uses 60 000 l of mineral oil based liquid scintillator for observation of neutrino induced reactions with ^{12}C and ^{1}H nuclei of the organic material. Very thin totally reflecting double lucite layers are assembled to provide a structure of 512 optically separated modules (180 mm x 174 mm x 3500 mm) viewed by two 3" phototubes on both ends each. These modules are surrounded by an inner veto of half the module thickness to achieve optimum fiducial volume. The double walled tank is inserted into an inner passive iron shielding of 180 mm thickness which simultaneously provides adequate mechanical strength. An active scintillator veto outside the inner passive shield will be used to reduce background of neutrals mainly originating from the passive shielding by cosmics bremsstrahlung. To move the detector an air pad support system will be used.

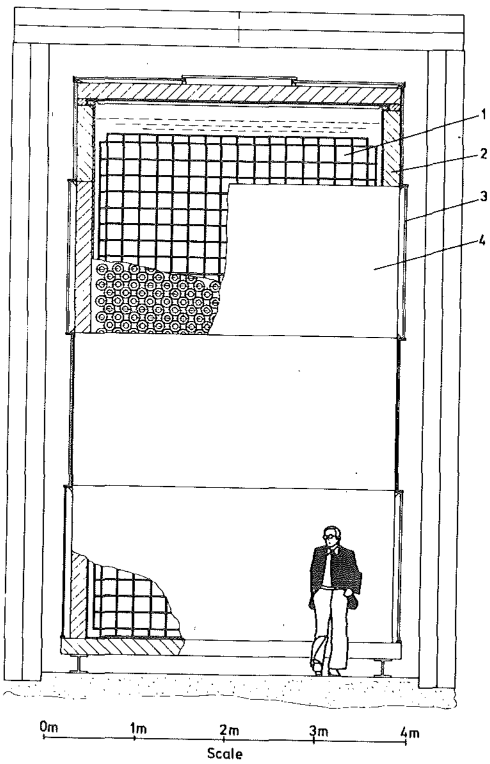

Fig. 1:
The KARMEN 50 t liquid scintillation detector.
1: 512 totally reflecting optical modules
2: inner passive shielding
3 and 4: active anticounter

Thorough investigations of various scintillators have been carried out concerning light output and light attenuation as well as compatibility with and resistivity of various materials, bondings etc.. The method of fabrication of totally reflecting double lucite layers has been worked out and production will start soon. The same holds for the phototube housing and optical coupling to the scintillator.

Meanwhile 2300 phototubes of the type Philips XP 3462 with incorporated voltage divider have been ordered. These are 3" eight stage fast tubes with a gain of 10^6, rise time < 3nsec and single photo-electron resolution P/V > 2. A test and selection facility has been built at RAL to check the specifications of each tube with respect to gain, rise time, linearity and resolution. Delivery and testing of the tubes has started.

Electronics

The design of the electronics system has now been worked out in detail. The heart of the system the "asterix" board which finally holds all energy and timing information for 4 out of 512 modules is now ready to be tested as prototype. A large amount of electronic components has already been bought; manufacturing of the different devices will start soon. The same is true for programme development for the data acquisition system with LSI 11/23 and VAX 750.

In 1985 sufficient electronics will be available to be run and tested with a prototype III detector.

Prototype developments

Prototyping of the KARMEN 1 detector will proceed in three stages: Prototype I (see issue 1982/83) has shown the feasibility of the optical segmentation method for a large volume liquid scintillator. Prototype II (Fig. 2) consists already of 9 modules but with reduced length (175 mm). It was built to investigate position dependent time-, spatial- and energy resolution as well as module intercorrelations in detail. This detector with position sensitive multiwire chambers on top and bottom has taken cosmic data for more than three months. Evaluation of the data is still going on.

A prototype III detector is now under construction at KfK. It will be identical to the main detector in any respect except the overall number of modules. In particular the optical segmentation, the scintillator and the phototubes are finally destinated to be used in the main detector at a

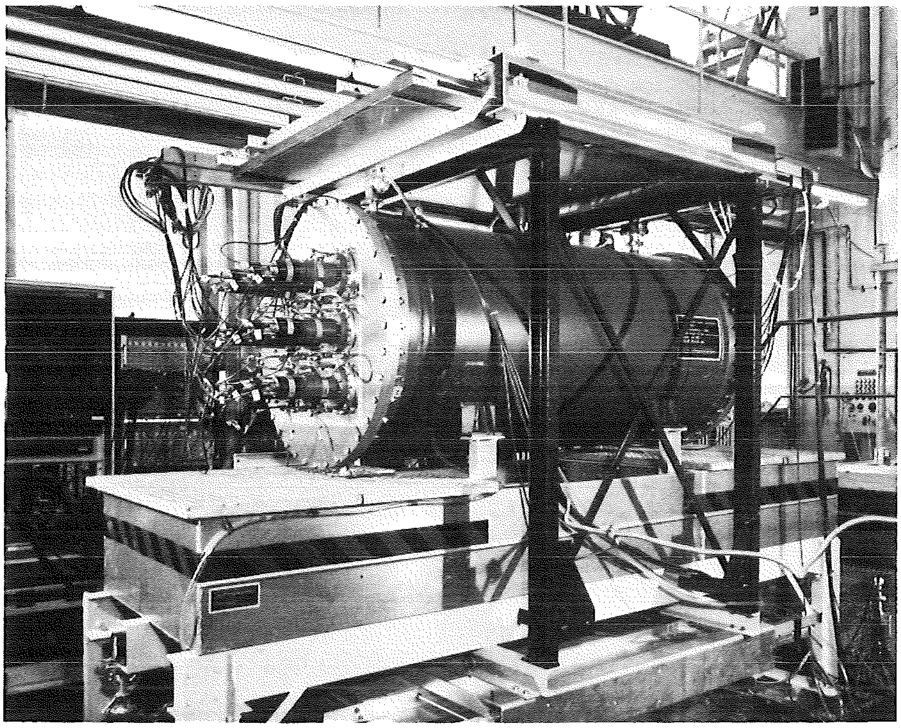

Fig. 2: Prototpye II liquid scintillation detector

later stage. Prototype III is a 8000 l tank containing 35 modules (180 mm x 174 mm x 3500 mm) surrounded by 24 inner veto modules. 188 phototubes will look into the scintillator tank. Large scintillator paddel counters are used as cosmics trigger or to simulate the active anticounter.

The purpose of this detector is to finally test all the mechanics, electronics and also the physics properties of a large scale detector of this type already during the phase of assembly of the actual detector at RAL. The detector may also be used to study background problems in the neutrino bunker during the "first day" neutrino beam period in 1985.

(1) R.Maschuw, B.Zeitnitz, KfK 3362 (Jun.1982).
(2) R.Maschuw, Proc. 3rd LAMPF II Workshop, July 1983 LA-9933-C-Vol I, 405-418
(3) B.Zeitnitz, Low Energy Neutrinophysics at High Intensity Pulsed Proton Accelerators, Reports on Nuclear and Particle Physics, 1984,in print
(4) J.F.Cavenignac, A.Hoummada, D.H.Koang, B.Vignon, Y.Declais, H.de Kerret, H.Pessard, J.M.Themard, Report of Laboratoire dAnnecy le Vieux de Physique des Particules, LAPP-EXP-84-03

3.0.2 NEUTRINO OSCILLATION SENSITIVITIES FOR THE KARMEN EXPERIMENT

If lepton number is not absolutely conserved and the neutrinos have a finite mass, then the physical neutrinos may be composed from different neutrino mass eigenstates. This could lead to the occurence of ν-oscillations. The probability that in a pure beam of muon neutrinos ν_μ, e.g. electron neutrinos ν_e may appear is

$$P(\nu_\mu \rightarrow \nu_e) = \sin^2 2\theta \sin^2 \left(\frac{1.27\ \Delta m^2\ L}{E_\nu}\right); \qquad (1)$$

For a given mixing of the neutrino mass eigenstates with m_1 and m_2 defined by the mixing angle θ this probability depends on $\Delta m^2 = m_2^2 - m_1^2$ expressed in eV^2, on the neutrino energy (in MeV), and on the distance from the source L in metres.

The SNS produces ν_μ, ν_e and $\bar{\nu}_\mu$ neutrinos with equal intensities but different time and energy distributions. ν_μ come from π^+ decay essentially during the beam on time (two 100 ns bursts with a gap of 230 ns and a repetition rate of 50 Hz) (1). ν_e and $\bar{\nu}_\mu$ timing is given by the μ^+ lifetime of 2.2 μs; their energies are distributed between 0 and 53 MeV while the ν_μ component is monoenergetic with $E_{\nu_\mu} = 29.79$ MeV.

For the measurement of $\nu_\mu \rightarrow \nu_e$ oscillations, we will detect electrons from the inverse ß-decay: $\nu_e + {}^{12}C \rightarrow e^- + {}^{12}N + Q$ with $Q = -17.3$ MeV. The ^{12}N nucleus undergoes β^+ decay with a lifetime of 11 ms and a β^+ end energy of 16.3 MeV. This gives an excellent event signature practically eliminating all background: an electron within the ν_e production time of about 5 μs must be followed by a delayed positron coincidence at the <u>same</u> location within the detector.

We compare the count rate N_1 during "beam on" time T_1 to the rate N_2 during T_2 = 0.5 to 5μs after the start of the beam. During T_1, ν_μ are produced with a small contamination of ν_e. After 500 ns the ν_μ component has dropped to zero. $\nu_\mu \rightarrow \nu_e$ oscillation would increase N_1 while $\nu_e \rightarrow x$ would decrease N_2. The appearance experiment related to N1 is expected to be much more sensitive than ν_e disappearance. We will evaluate $R = N_1/N_2$ thus eliminating absolute flux and cross section normalizations. ν_e neutrinos from $\nu_\mu \rightarrow \nu_e$ oscillation are monoenergetic. Applying an energy window of a few MeV around $E_{\beta^-} = E\nu_\mu + Q = 12.5$ MeV reduces the source ν_e component during T_1 to 1% of ν_μ. Applied to N_2, too, it further reduces energy dependent normalization errors. During one year of full beam intensity (1 fby) at the SNS, 7 (84) events from original ν_e within E_{ν_e} = 25 to 32 MeV

(0 to 53 MeV) are expected for N_1 and 110 (1285) events for N_2. If all ν_μ events oscillated to ν_e, N_1 = 653 events with E_{ν_e} = 29.79 MeV would be measured.

The sensitivity for $\nu_\mu \rightarrow \nu_e$ oscillation has been calculated for 2 fby of measurement with the KARMEN 1 detector. Statistics play the dominant role in determining the 90% confidence limits shown in Fig. 2a. All combinations of Δm^2 and $\sin^2 2\Theta$ to the left and below the curve cannot be distinguished from the "no oscillation" case.

As there are no $\bar{\nu}_e$ in the primary beam of the SNS the appearance of $\bar{\nu}_e$ will be strong evidence for the oscillation $\bar{\nu}_\mu \rightarrow \bar{\nu}_e$.

The selective reaction is

$$\bar{\nu}_e + p \rightarrow e^+ + n \qquad (2)$$

The signature of this reaction is very distinct:

- A positron is detected within the time window of 0.5 to 5 μsec after the beam pulse carrying nearly the whole energy of the neutrino. Fig. 1 shows the calculated energy spectrum of the positron. The mean energy is E_{e^+} = 42 MeV.

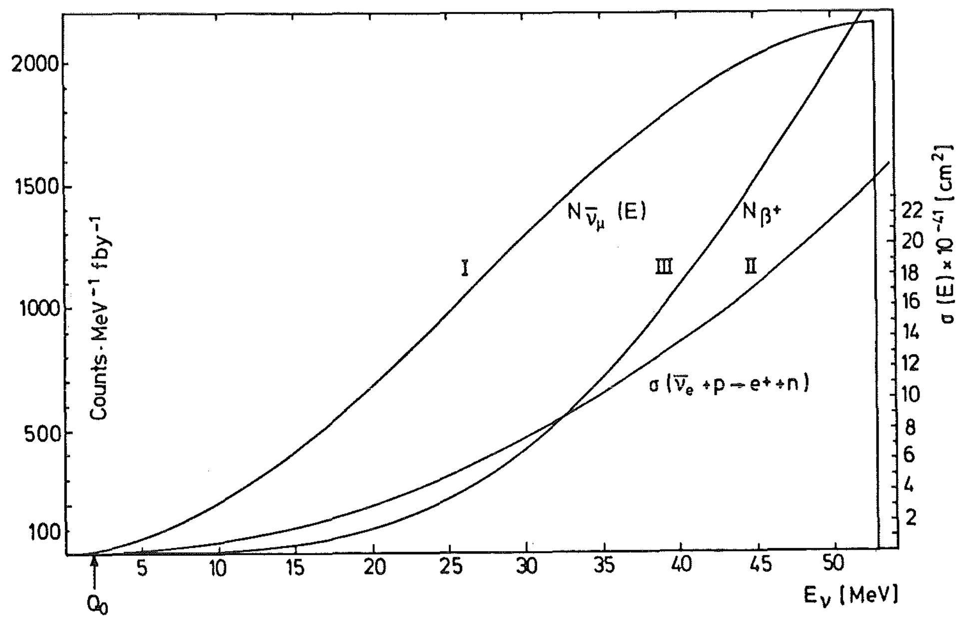

Fig. 1: I. Energy distribution of $\bar{\nu}_\mu$ from the SNS (relative units)

II. Cross section for $\bar{\nu}_e + p \rightarrow e^+ + n$ (scale on the right)

III. Energy distribution of $\bar{\nu}_e + p \rightarrow e^+ + n$ assuming oscillation probability P = 1 for $\bar{\nu}_\mu \rightarrow \bar{\nu}_e$

- Using Gadolinium within the scintillator the neutron may, after moderation inside the detector volume, be absorbed by the Gd. γ-rays of a total energy of about 9 MeV will then be emitted by the Gd and should appear within a volume of about 1 m^3 around the detection point of the positron within a time window of about 200 μsec.

The sensitivity for our experiment has been calculated assuming for the neutron efficiency ε = 30% with an uncertainty of ± 5% and estimating the $\bar{\nu}_e$ background from the source to .1% ± .02%. The statistical errors for 2 fby of measurement still exceed these systematic ones, even though the systematic errors are more important in this case compared to the $\nu_\mu \to \nu_e$ oscillation. The result of a realistic sensitivity calculation is shown in Fig. 2b.

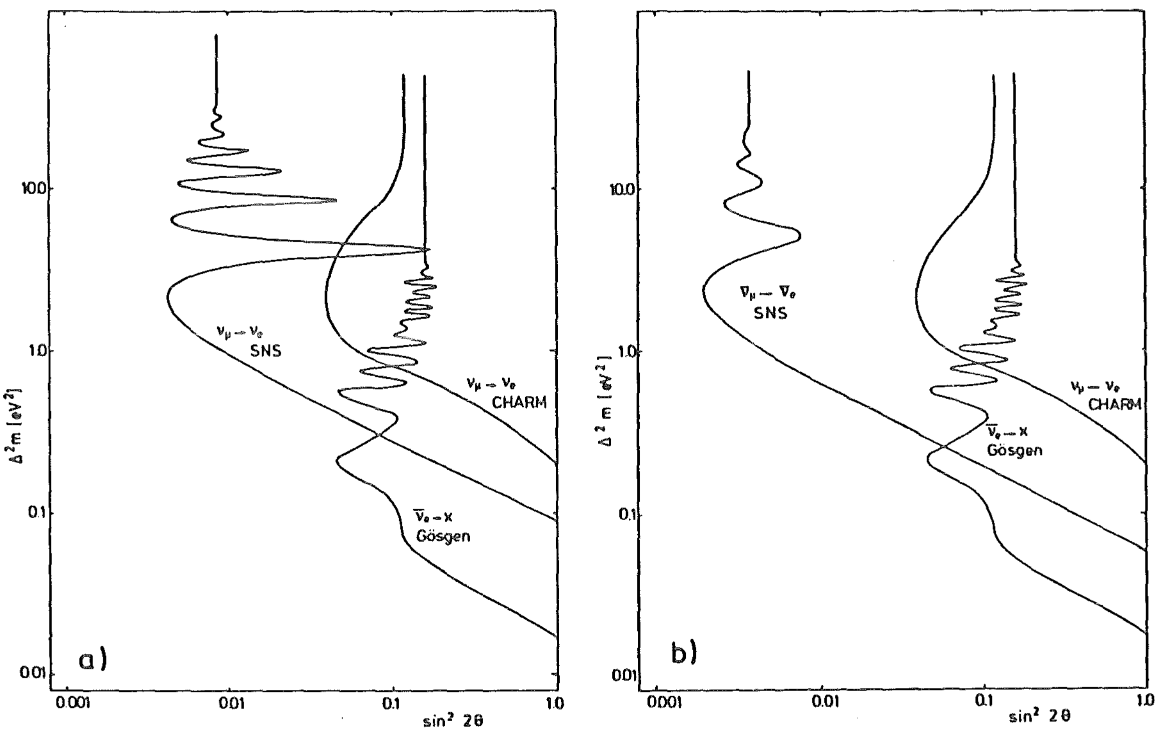

Fig. 2: Experimental sensitivities for oscillation (0% C.L.)

a. $\nu_\mu \to \nu_e$: Appearance sensitivity of KARMEN for two full beam years at the SNS.

b. $\bar{\nu}_\mu \to \bar{\nu}_e$: Appearance sensitivity of KARMEN for two full beam years at the SNS.

(1) R.Maschuw, B.Zeitnitz, Research Proposal for Neutrinophysics at SNS, KfK 3362 (1982)
(2) K.Gabathuler et al., Phys.Lett. 138B, 449 (1984)
(3) F.Bergsma et al., Phys.Lett. 142, 103 (1984).

3.0.3 INVESTIGATIONS ON LIQUID SCINTILLATORS FOR LARGE VOLUME DETECTORS

For active large volume detectors like the KARMEN 1 neutrino detector price performance considerations often lead to the use of liquid scintillator rather than any plastics. Those liquids on the other hand need containment, light guidance and adequate optical coupling to phototubes. Thus not only the physical properties of light output and light attenuation but also compatibility with other materials are of importance. We therefore concentrated on mineral oil based scintillators from aliphatic hydrocarbons with only 25 to 30% aromatics content. Compared to purely aromatic scintillators these are much less agressive and in particular compatible with acrylic material. In addition they are also less hazardeous concerning flame point and toxicity. For different scintillators of this type - three commercial ones and two composed by ourselves - we have measured the light output and light attenuation to find the optimum scintillator for our 50 t neutrinodetector. The attenuation length is defined as the distance of 1/e decrease of the intensity and is strongly geometry dependent. For the various scintillators it was measured with a quartz pipe of 40 mm diameter and 1 m length coupled to a 2" phototube. Position dependent light output was then deduced from the compton edge of a ^{60}Co source at different distances from the phototube. The light output at 175 cm which is half the length of our neutrino detector module was taken as figure of merit for comparison of the different scintillators.

The results are listed in table 1. The light output is given in per

Table 1: Properties of various liquid scintillators

Scintillator	light output I_0 % anthrazene	attenuation length λ (cm)	figure of merit $g=I_0 \exp -(175/\lambda)$
NE 235 H*	55	264	0.283
NE 235 C*	61	179	0.230
Zinsser R**	44	273	0.234
PMP 1	50	261	0.256
PMP 2	60	245	0.294

* Nuclear Enterprises, Scotland

** Zinsser Analytic GmbH., Frankfurt

cent anthrazene. The quoted attenuation lengths are those measured with the quartz pipe. PMP 1 and 2 are scintillators composed by ourselves from mineral or paraffin oil, respectively pseudocumene and a one component scintillator PMP developed at KfK (1).

From the figure of merit the scintillators NE 235 H and PMP 2 turn out to be the most appropriate for our purposes.

(1) H.Güsten, P.Schuster, W.Seitz, J.Phys.Chem. 82 (1978) 459

3.0.4 LIQUID ARGON TEST DETECTOR

Neutrino electron scattering is proposed to be measured at the SNS with a liquid argon time projection chamber (LATPC) as observation of these processes requires a tracking calorimeter with excellent energy as well as angular (spatial) resolution. (A different attempt of a Cerenkov drift chamber sandwich detector is under investigation at QMC London.) In a 20 1 LAr ionization test detector with 50 mm drift distance (see annual report 1982) the effect of electronegative impurities on the drift electrons in liquid argon has been studied. The collected ionization charge of 1 MeV conversion electrons from a ^{207}Bi source has been measured by varying the drift distance between 5 and 45 mm at a constant drift field (see Fig. 1). Attenuation lengths up to 100 cm have been achieved. As the test detector has no continuously operating purifaction system a decrease of the attenuation length has been observed over a three week measuring period as shown

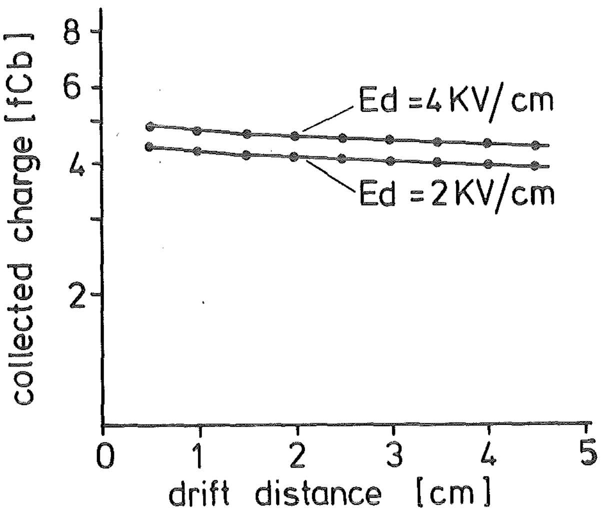

Fig. 1:
Drift space dependence of collected charge from 1 MeV conversion electrons of a ^{207}Bi source.

in Fig. 2. This corresponds to an impurity rate of approximately 3 ppb/day oxygen equivalent. The test detector will be upgraded to achieve drift paths of more than 100 mm as well as to demonstrate the time projection method with a segmented anode configuration.

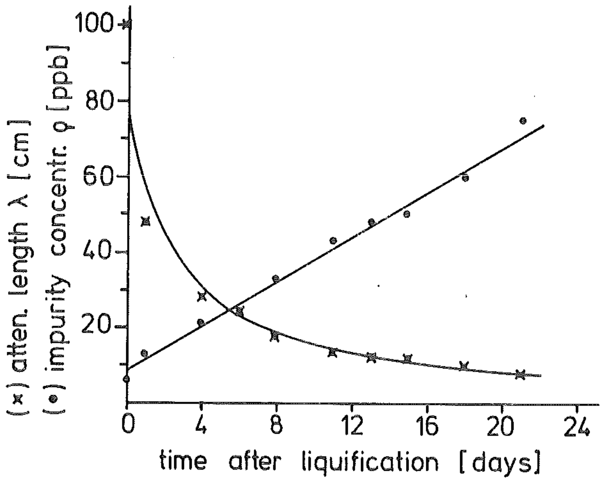

Fig. 2:
Variation of the attenuation length and impurity concentration with time in the test detector; solid lines from least square fits

4. INTERMEDIATE ENERGY PHYSICS

4.1 PION - NUCLEUS INTERACTION

4.1.1 COULOMB-NUCLEAR INTERFERENCE IN $\pi^{\pm}$p-SCATTERING AT 55 MeV

U. Wiedener, K. Göring, U. Klein, W. Kluge, H. Matthäy, M. Metzler, E. Pedroni[++], W. Fetscher[+], H.J. Gerber[+]

During the last year the experimental set-up to measure the elastic $\pi^{\pm}$p-scattering at forward angles (between 7.5^{o} and 27.5^{o}) has been assembled and successfully tested. Data have been taken during a four weeks run at the πM3 channel of SIN set to 140 MeV/c (corresponding to about 55 MeV actual scattering energy in the laboratory system).

The goal of the measurement (1) is the determination of the real part of the isospin even D^+ amplitude of pion-nucleon scattering as a function of the four-momentum transfer t, and the subsequent extrapolation of Re $D^+(t)$ to $t = 0$ (i.e. to the forward direction).

With a dispersion analysis the σ-term of πN-scattering will be obtained by a further extrapolation of the on-shell πN amplitude to the unphysical Chen-Dashen point ($t = m_{\pi}^2$, $\nu = 0$) (2). This value allows a comparison with predictions (3) of quantum chromodynamics (QCD). At present the "experimental" value and the QCD-value differ by a factor of about 2. We expect that our measurement of Re $D^+(t)$ at small t and at a low pion energy results in a more confident value of the σ-term due to a shorter extrapolation path to the Cheng-Dashen point.

The main components of our apparatus are (see Fig. 1):

i) The liquid hydrogen target.

In order to have a liquid hydrogen volume of well defined thickness, a target consisting of three cells is used. The inner cell contains liquid hydrogen, while the two outer cells are filled with hydrogen gas at the corresponding vapour pressure. The cells are separated from each other by 30 µm mylar foils. The diameter of the target is 150 mm. Two targets of 40 and 80 mm thickness have been used during the runs. The target is a closed loop system stabilised by a refrigerator-cryostat system. The background arising from the target cell is measured separately with the liquid hydrogen removed from the inner target cell.

ii) Six multi wire proportional chambers with single wire read-out. They allow to trace back the trajectories of the particles in the entrance and exit channels to the interaction point in order to select events from the target region only and to determine the scattering angle precisely.

iii) The range telescope. It consists of 20 plastic scintillator sheets (of 2, 3, 5, 10 mm thickness and of an area of 160 x 200 mm^2) to measure the range and the energy loss of the detected particles. The observed differential range distributions are similar for incident π^+ and π^-. The range telescope allows the elimination of the most significant background of muons arising from pion decay within the target region.

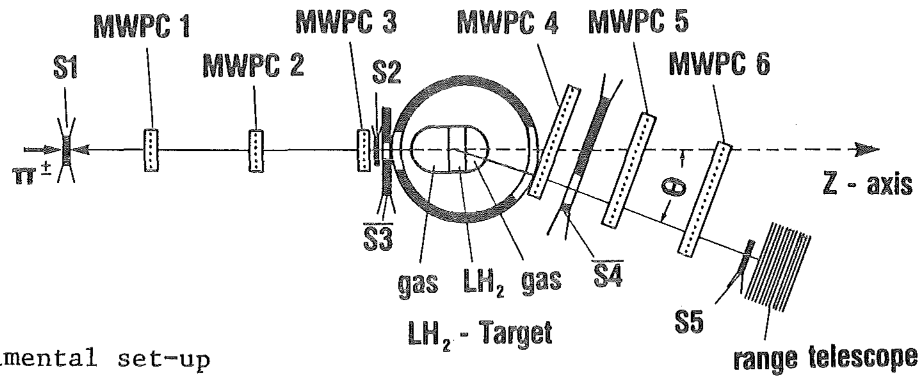

Fig. 1 Experimental set-up

The electronics has to provide control over the number and kind of particles in the entrance and exit channel. Incident pions are identified by the signal $(1 \cdot 2 \cdot RF_\pi)\ \bar{3}$, where RF_π denotes a coincidence with the RF of the cyclotron in such a way, that only pions are selected via their time relation to the RF.

The main experimental trigger $(1 \cdot 2 \cdot RF_\pi)\ \bar{3}\ \bar{4}\ 5$ defines a coincidence between an incident pion with a particle in the exit channel. For calibration purposes a sample of the incident beam has been recorded simultaneously. Particles in the exit channel are identified by their interaction (scattering or decay) point and by their energy losses and ranges in the range telescope.

It turned out that a substantial additional reduction of the muon background is possible through the registration of the decay sequences $\pi^+ \rightarrow \mu^+\nu$ and $\mu \rightarrow e\nu\nu$ following the stop of the parent particle in the range telescope. More than 90% of the positive pions have been identified within the range telescope by measuring the kinetic energy of 4.2 MeV of their decay muons in addition to the kinetic energy of the stopping π^+ using

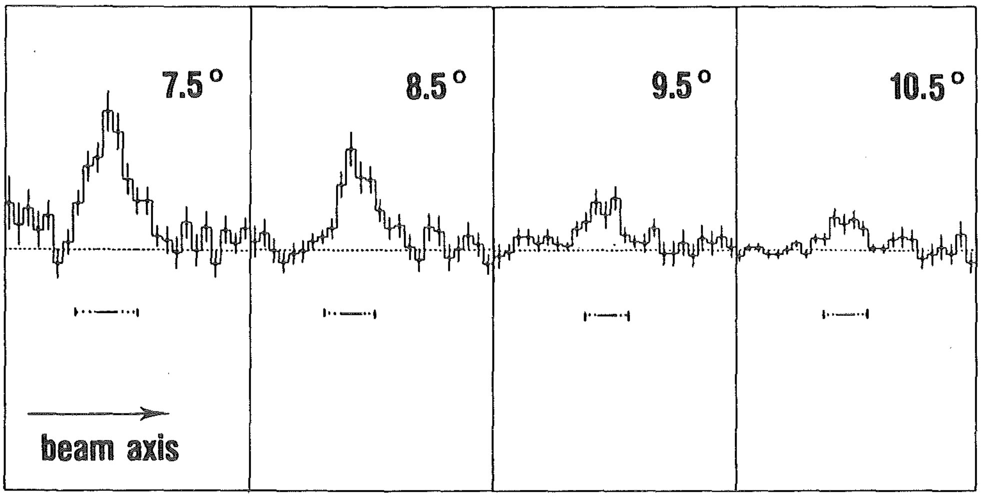

Fig. 2 π^+p scattering at 7.5^0, 8.5^0, 9.5^0, 10.5^0 (from left to right). These data have been obtained in a three hours' test run. The distribution of the coordinate of the interaction point along the incident beam axis is shown. The target position is indicated in full, dots represent the experimental resolution.

charge integrating ADC (within a time window of 100 ns). Negative stopped muons originating from the target region are identified within the range telescope by their minimum ionising decay electrons (within a 10 μs window). In total information from 55 ADC, 5 TDC, 2 coincidence registers and the addresses of firing wires from the read-out system of the wire chambers have been recorded on magnetic tape for each event. First preliminary results for π^+p scattering analysing the data of a three hours test run are shown in Fig. 2, where four distributions of the coordinate of the interaction point along the incident beam axis are presented. The background (obtained by empty target measurements) has been subtracted. The observed events thus represent pion scattering from liquid hydrogen. The data are normalised and indicate the rapid decrease of the π^+p cross-section with increasing angle.

In the four weeks run of June/July 1984 angular distributions between 7.5^0 and 27.5^0 have been measured with good statistics. Data evaluation is presently under way.

(1) Karlsruhe-SIN-ETHZ Collaboration, SIN proposal R-82-17, January 1983

(2) R. Koch, Z. Physik C15(1982)161

(3) J. Gasser, H. Leutwyler, Phys. Reports 87(1982)77

+ Institut für Mittelenergiephysik, ETH Zürich

++ Schweizerisches Institut für Nuklearforschung

4.1.2 MEASUREMENTS OF iT_{11} IN $\pi^+-\vec{d}$ ELASTIC SCATTERING AT FORWARD ANGLES

G.R. Smith, E.L. Mathie, E.T. Boschitz, C.R. Ottermann, S. Mango[+], J.A. Konter[+], M. Daum[+], M. Meyer[++], R. Olszewski[++], F. Vogler[++]

First results on the measurement of the analyzing power iT_{11} in $\pi\vec{d}$ elastic scattering using a vector polarized deuteron target and the SUSI pion spectrometer have been reported (1). Further measurements extended the data set to three further energies but again the few angles available for each energy made a systematic analysis difficult (2).

Then a new experimental set-up consisting of a six fold array of pion scintillation counter telescopes in coincidence with an array of six associated recoil deuteron scintillators and proton veto counters has been developped. Here the signature of a $\pi\vec{d}$ elastic scattering event was obtained from the time-of-flight difference between the deuteron and the pion signals. With this set-up an overall factor of more than 20 was gained in the efficiency of data acquisition with this experimental arrangement in comparison to the pion spectrometer at backward angles.

At forward scattering angles the kinetic energy of the deuterons decreases. Eventually, some of them are stopped already in the target and a coincidence measurement technique becomes less and less efficient. Thus, data in the angular range corresponding to 30^o to 100^o in the center of mass system were measured using the SUSI pion spectrometer and πM1 beam line. The Carbon and Oxygen ground states were always well separated from the $\pi\vec{d}$ elastic peask. However, at some angles small contributions from the inelastic states of these nuclei appeared in the region of $\pi\vec{d}$ elastic scattering. Therefore background measurements on normal (non-deuterated) butanol were taken at each angle. In this way the background due to the other (unpolarized) nuclei present in the polarized target was explicitly measured for later subtraction.

Adding the new forward angle data to the earlier data finally, a comprehensive set of data covering a wide range of angles at 12 bombarding energies has been recorded. Fig. 1 shows the angular distribution of iT_{11} between 134 and 325 MeV. As the incident pion energy is raised, the smooth, beel shaped angular distribution of iT_{11} develops a dip at forward angles (near 70 degrees) which becomes more and more pronounced at energies above 256 MeV. The maximum of about 3o% in the angular distribution of iT_{11} occurs near 100 degrees, where the differential cross section has a minimum.

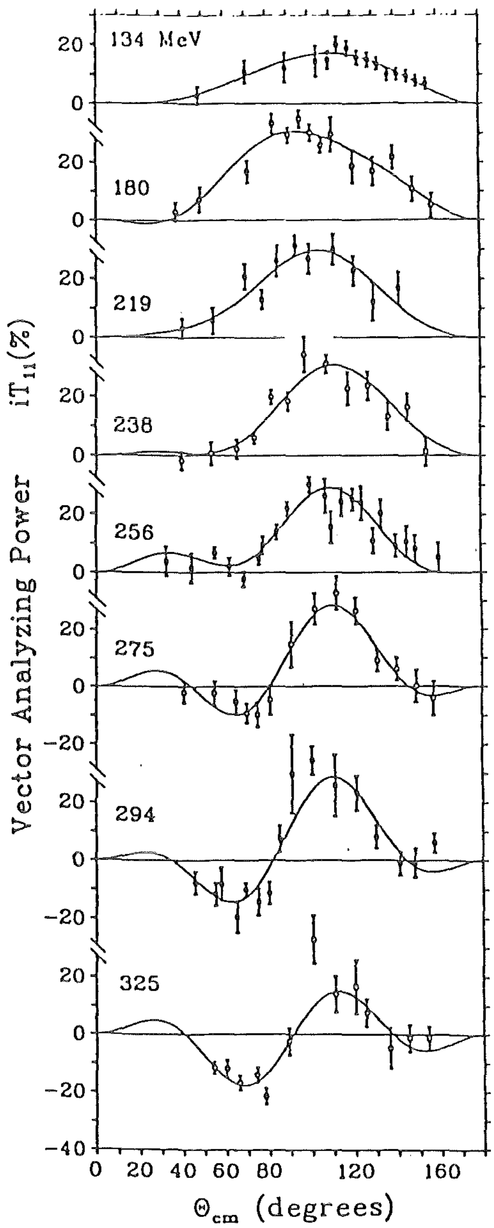

Fig 1

Values of the vector analizing power iT_{11} from $\pi\vec{d}$ elastic scattering versus the scattering angle in the center of mass system. As the energy is raised the smooth, bell shaped angular distribution of iT_{11} develops a dip at forward angles (near 70^{o}) which becomes more and more pronounced at energies above 256 MeV. The curves, drawn to guide the eyes, are fits using Legenndre polynomials.

The completeness of the data allows for the first time the study of the behaviour of iT_{11} with sufficient statistics, angles and energies to compare reliably with the theoretical predictions. There is good agreement among the various Faddeev predictions and with the data up to 180 MeV. At higher energies no published Faddeev prediction is able to describe the angular distribution of iT_{11}. The details of the experiment and the theoretical conclusions are discussed in two new publications (3), (4).

(1) J.Bolger et al., Phys. Rev. Lett. 46(1981)167
(2) J.Bolger et al., Phys. Rev. Lett. 48(1982)1667
(3) E.L. Mathie et al., Phys. Rev. C28(1983)2558
(4) G.R. Smith et al., Phys. Rev. C29(1984)2206

+ Schweizerisches Institut für Nuklearforschung
++ Universität Erlangen-Nürnberg

4.1.3 STUDY OF THE VECTOR ANALYZING POWER iT_{11} IN THE $\pi^+ - \vec{d} \rightarrow 2p$ REACTION

C.R. Ottermann, E.L. Mathie, E.T. Boschitz, G.R. Smith, W. Gyles, S. Mango[+], J.A. Konter[+], B. van den Brandt[+], R. Olszewski[++], R.R. Johnson[+++]

The $\pi^+ d \leftrightarrow 2p$ reaction is of fundamental importance for the understanding of nuclear theory at intermediate energies. Since the observed candidates for dibaryon resonances occur in the energy region where the NN collisions are highly inelastic, they may also appear in the pp $\leftrightarrow \pi^+ d$

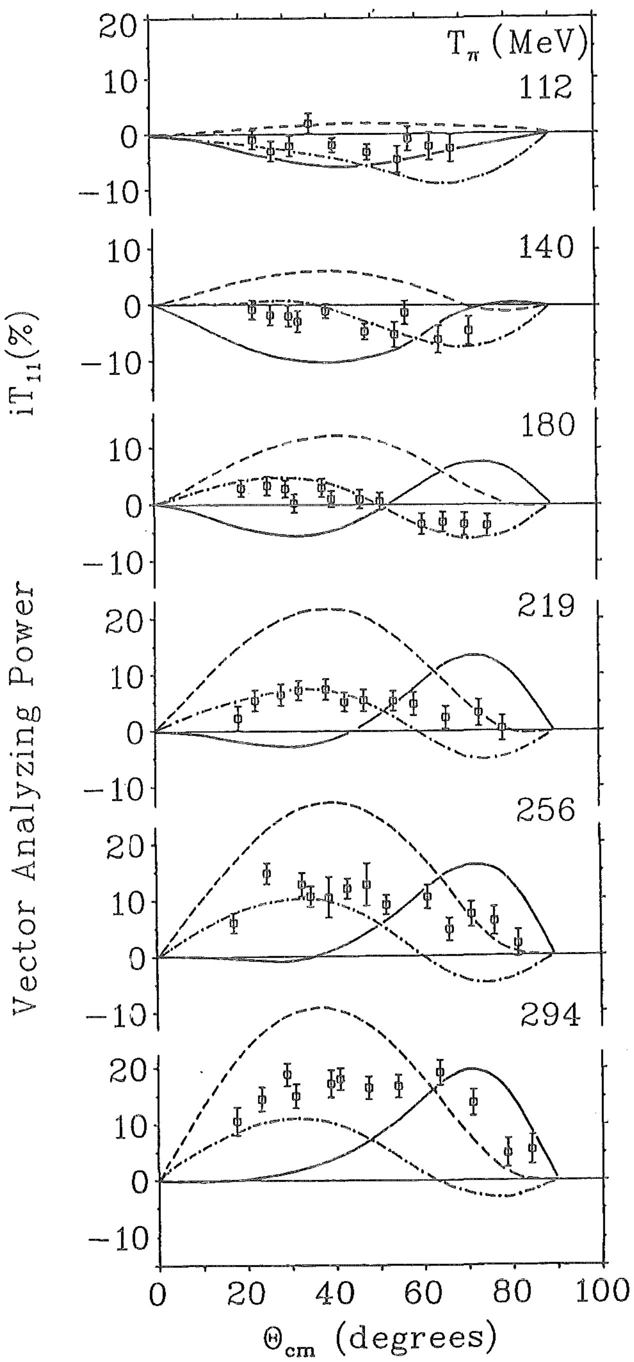

Fig. 1
The vector analizing power for the pion deuteron absorption reaction compared with theoretical predictions. The solid curve is from the two body predictions of Niskanen (4), the dashed curve is from three body calculations of Rinat et al. (3), the dot-dashed curve is from the corresponding calculations of the Lyon Group (2).

reaction. In this work the results of a new comprehensive set of measurements designed to accurately map out the bahaviour of the vector anlyzing power iT_{11} in the $\pi^+d \to 2p$ reaction with a TOF technique are reported. The data cover an average of twelve angles per energy, for seven incident energies between 112 and 325 MeV. The new data confirm very well the earlier ones (1) within the quoted normalization uncertainties. Not only is the angular distribution of iT_{11} in excellent agreement with the present results, but the energy dependence as explored earlier with an excitation function at 55^o c.m. is also verified. The data are shown in Fig. 1 together with theoretical predictions. The three body calculation of Fayard et al. (2) agree well with the data except at the two highest energies. The three body calculation of Rinat et al. (3) overestimate the vector analyzing power by almost a factor of two. The prediction of Niskanen (4) agree only at the lowest energy. This is not surprizing because at the higher energies the nonrelativistic nature of his calculation becomes a serious problem.

Preliminary amplitude analyses by Bugg (5) indicate the importance of this data set for fixing amplitudes which could not be determined otherwise.

(1) G.R. Smith, J. Bolger, E. Boschitz, E.L. Mathie, G. Proebstle, M. Meyer, F. Vogler, and S. Mango, Phys. Rev. C25(1982)3228
(2) C. Fayard, G.H. Lamot, and J.L. Perrot, private communication
(3) A.S. Rinat and Y. Starkand, Nucl. Phys. A397(1983)381 and A.S. Rinat, private communication
(4) J.A. Niskanen, private communication
(5) D. Bugg, private communication

+ Schweizerisches Institut für Nuklearforschung
++ Universität Erlangen-Nürnberg
+++ University of British Columbia, Vancouver, B.C., Canada

4.1.4 POLARISATION EFFECTS IN THE $\pi^+\vec{d} \to \pi^+ np$ REACTION

W. Gyles, E.L. Mathie, C. Ottermann, G.R. Smith, E.T. Boschitz, J.A. Konter[+], S. Mango[+], A. Matsuynama[+], R.R. Johnson[++], R. Olszewski[+++]

The various coupled reaction channels of the pion-deuteron system can in principle be calculated exactly using relativistic Faddeev equations. Discrepancies between the experiments and the theoretical predictions may then reveal effects due to quark degrees of freedom such as the presence of dibaryon resonances. The measurements of the cross sections and vector analysing power, iT_{11}, of the breakup channel is expected to be particularly sensitive to the presence of dibaryon resonances, since this is calculated

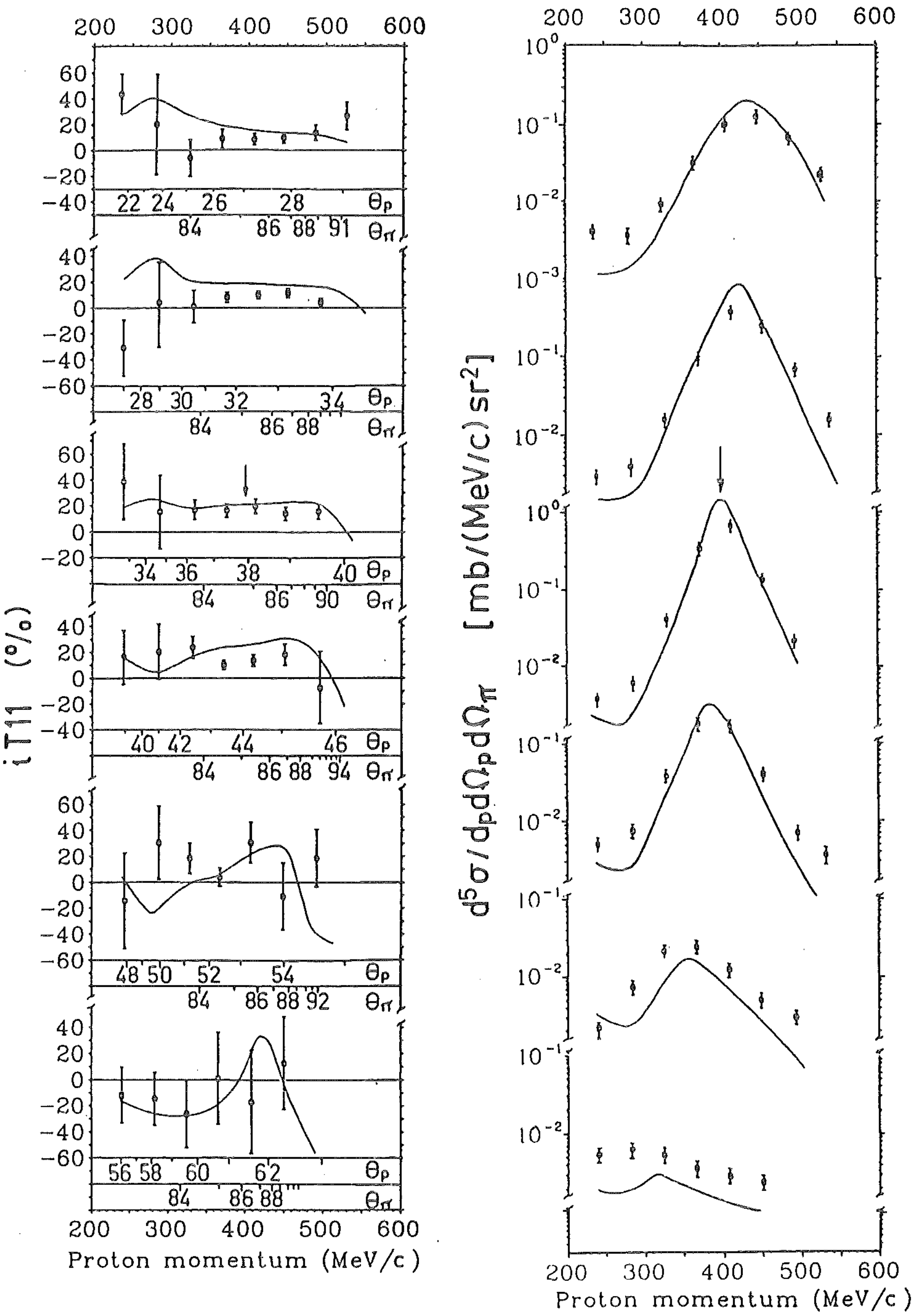

Fig. 1 Vector analysing power, iT_{11}, and corresponding differential cross section for various proton angles and a nominal pion angle of 85°. The actual scattering angles vary with proton momentum and are shown with the iT_{11} data; the cross sections are in the same sequence as the iT_{11}. The lines are theoretical predictions. The arrow indicates the positions corresponding to quasi free πp scattering.

(1),(2) to be the dominant decay channel.

In this kinemtatically complete experiment, 228 MeV pions were focussed onto a vector polarised deuterated-butanol target, with a polarisation of 0.20. The outgoing protons were detected in six scintillator telescopes on one side of the beamline and the outgoing pions in six telescopes on the other side between 50^{o} and 170^{o}. Coincidences were accepted between any proton telescope and any pion telescope, giving 36 proton/pion angle pairs. Six of these pairs were at the angles for free πp scattering. The remaining 30 angle pairs included proton angles up to 29^{o} away from the free πp kinematics. The energy of the protons was measured by the time of flight over the 1.3 m from the target. The target polarisation was reversed at regular intervals giving 12 pairs of polarised target runs. Meausrements of background were made with a target composed of solid CO_2 and carbon in correct proportion to simulate the background from butanol.

Only a sample of the large amount of data is shown in Fig. 1. It is compared with calculations by one of us (A.M.). The peaks of the cross secions correspond to the kinematics of the smallest pn relative momentum in the deuteron, where the impulse process dominates. The rather flat structure of the cross sections in the low momentum region in Fig. 1 reflects the onset of the pn final state interaction which enhances the cross section. The calculated results can reproduce the cross sections and analyzing powers fairly well in the region where the impulse process dominates. In the region of the quasi-free kinematics where the multiple scattering is more important, the agreement is not always as good, due to the relatively crude approximations for the multiple scatterings.

(1) W. Grein, K. Kubodera and M.P. Locher, Nucl. Phys. A356(1981)269
(2) I. Duck and E. Umland, Phys. Lett. 96B(1980)230

+ Schweizerisches Institut für Nuklearforschung
++ University of British Columbia, Vancouver, B.C., Canada
+++ Universität Erlangen-Nürnberg

4.1.5 DEVELOPMENTS FOR T_{20} MEASUREMENTS IN πd ELASTIC SCATTERING

E. Boschitz, W. Gyles, W. List, E.L. Mathie, C. Ottermann,
G.R. Smith, S. Mango[+], J.A. Konter[+], B. van den Brandt[+]

Recently, the tensor polarization t_{20} for πd elastic scattering has been measured by two groups: the ANL group at LAMPF and the ETH group at SIN. Both groups utilized a double scattering technique where the tensor polarization of the recoiling deuteron in the πd scattering reaction is determined from the cross section of the $^3He(d,p)^4He$ reaction at zero degrees. The ETH group (1) found a surprizingly rapid variation of t_{20} as a function of scattering angle and energy which might be a clear signal for an exotic resonance (some quark degree of freedom). Contrary to these results the ANL group (2) observed a rather smooth angular and energy dependence. It is extremely important to resolve this discrepancy by an independent experiment.

During the past year we have prepared such an experiment. Different from the ETH and the ANL group a tensor polarized deuteron target will be used in a single scattering experiment. The principle of the measurement is the following one:

The polarized cross section σ_{pol} for πd elastic scattering is in general:

$$\sigma_{pol} = \sigma_{unpol} \,(1+2\langle it_{11}\rangle\langle iT_{11}\rangle + \langle t_{20}\rangle\langle T_{20}\rangle + 2\,\langle t_{21}\rangle\langle T_{21}\rangle + 2\,\langle t_{22}\rangle\langle T_{22}\rangle)$$

where the observables with capital letters are the analyzing powers and the observables with small letters are the initial state polarizations. When the target magnetic field (quantization axis) is aligned with the incident beam direction all initial state polarizations except $\langle t_{20}\rangle$ are zero. This leads to the simplified expression for the relative cross sections:

$$\sigma_{pol} = \sigma_{unpol} \,(1 + \langle t_{20}\rangle\langle T_{20}\rangle)$$

σ_{pol} and σ_{unpol} are measured in a π-d coincidence set up (see Fig. 1) at 9 angles simultaneously. The tensor polarization of the deuteron target $T = \sqrt{2}\,\langle t_{20}\rangle$ is determined from the measured vectorpolarization P according to the approximate expression

$$T = 2 - \sqrt{4 - 3P^2}$$

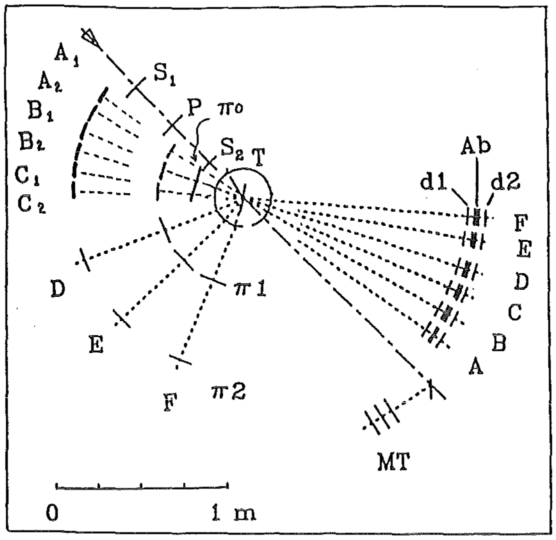

Fig. 1
Experimental set-up for the T_{20} measurements. P = beam profile chamber, S = scintillator, T = scattering target, π = pion detectors, Ab = absorber, MT = monitor telescope.

For P = 0.40 a tensor polarization T = 0.13 is obtained. To achieve a vector polarization of P = 0.40 is nontrivial. A special target had to be developped in collaboration with the polarized target group at SIN. This target consists of a new pair of superconducting Helmholtz coils with proper N_2 and He reservoirs. A dilution refrigerator has been manufactured by SHE in California. The target is presently being assembled for testing at SIN. The crucial target material, 6 and 8 fold deuterated propandiol with a Crome V complex added has been obtained from CERN. If a sufficiently high vector polarization is obtained, the entire experiment is ready for testing.

(1) W. Gruebler et al., Phys. Rev. Lett. 49(1982)444
(2) E. Ungricht et al., Phys. Rev. Lett. 52(1984)333

+ Schweizerisches Institut für Nuklearforschung

4.1.6 S-WAVE ABSORPTION OF STOPPED π^- ON ^{3}He

D. Gotta, S. Cierjacks, S. Ljungfelt, G. Schmidt, H. Ullrich, G. Backenstoss+, M. Izycki+, W. Kowald+, H.J. Weyer+

In previous work it has been found that pion absorption in ^{3}He proceeds to about 60% via pure quasifree absorption (1). The remaining part is populated about equally by the bound final state (dn) and the kinematical regions characteristic for NN final state interactions.

The quasifree process on isospin I = 0 pairs dominates the one on I = 1 pairs yielding a ratio

$$R = \frac{r(\pi^- pn \rightarrow nn)}{r(\pi^- pp \rightarrow pn)} = 8.8 \pm 2.0$$

Such an enhancement of absorption on I = 0 nucleon pairs has been qualitatively explained assuming the reaction proceeds from a $\ell_\pi = 1$ state through an ΔN intermediate state. However it is surprising that this mechanism known to be dominant in the Δ-resonance region should have such a strength at threshold. Several authors have tried to calculate the ratio R at rest using the rescattering model with off-shell π nucleon amplitudes (2) or nucleon-nucleon correlations (3). For ^3He calculations yielded (4) R = 3.

In order to investigate the experimental situation we have measured the 2 and 3 body final states in coincidence with a K-X-ray which identifies absorption from an atomic 1s state. The experiment was performed at the πE1 channel at SIN.

The X-rays were measured with 6 very thin NaI crastals located beneath a gasous ^3He-target cooled to 4K. The nucleons were detected by two time of flight counters of large solid angle (1). About 500 triple coincidences could be attributed separately to the reactions π^-(pn,nn), π^-(pp,pn) and π^-(pp,d).

Since the kinematics of the final states have been completely determined also here the identification of the quasifree 2N absorption on pn and pp pairs as well as processes with nn- and np final state interactions was possible.

The result for the quasifree absorption is

R_S = 11,6 ± 20%.

This value can be compared with theoretical predictions. In particular, we can exclude a significant influence of p wave absorption on the high R value at rest.

(1) D. Gotta, M. Dörr, W. Fetscher, G. Schmidt, H. Ullrich, G. Backenstoss, W. Kowald, I. Schwanner and H.-J. Weyer, Phys. Lett. 112B(1982)129
(2) F. Hachenberg and b.J. Pirner, Ann. Phys. (NY) 112(1978)401
(3) R. Shimizu, A. Faessler, Nucl. Phys. A333(1980)495
(4) Th. Schucan, Proc. 9. ICOHEPANS, Versailles 1981, p. 275, H. Nägeli, Thesis University Basel 1980.

+ Institute for Physics, University of Basel, Klingelbergstr. 82, 4056 Basel, Switzerland

4.1.7 ABSORPTION OF π^+ AND π^- IN FLIGHT ON ^3He

S. Cierjacks, S. Ljungfelt, U. Mankin, H. Ullrich, G. Backenstoss[+], M. Izycki[+], M. Steinacher[+], P. Weber[+], H.J. Weyer[+], M. Furić[++], T. Petković[++]

Elementary pion absorption processes have been studied in the past mainly by the $\pi d \rightleftarrows 2N$ reactions. Kinematically complete experiments on the 3N system of ^3He provide further extensions of such investigations:

i) On the influence of nuclear density for the absorption on isospin I = 0 nucleon pairs (comparison with absorption on the deuterium)

ii) On the absorption on I = 1 pairs

iii) On absorption mechanism involving 3 nucleons.

Starting with our first measurement at SIN with pions at rest (1), (2) pion absorption in ^3He has received considerable theoretical (3)-(6) and experimental (7)-(9) interest.

In order to study point i) the ratio

$$R(^3He) = \frac{d\sigma}{d\Omega}(\pi^+,pp) \ / \ \frac{d\sigma}{d\Omega}(\pi^-,np)$$

has been investigated at different angles and energies. The experimental results from our group can be compared with TRIUMF data at low energies and with LAMPF data at higher energies. While there is consistency at low energies (8) discrepancies at high energies (7) were indicated. Only very recent measurements made by both groups (9), (10) resolved this discrepancies and showed that the old LAMPF data were wrong by a factor of 3. An updated compilation of results is given in Fig. 1.

Further results concerning points i) to iii) are :

- There is no indication of a strong density effect.

- The ratio $\sigma_{\pi^+ \to pp}(^3He) \ / \ \sigma_{\pi^+ \to pp}(^2He) = 1.5$ is consistent with the number of I = 0 pairs in both nuclei.

- From absolute cross sections it could be derived that the large value of R originates from the suppression of the absorption on I = 1 pairs, whereas $\pi^+ pn \to pp$ agrees with the deuteron data. The main reason is assumed to stem from the intermediate ΔN channel $^5S_2$ which dominates the $\pi^+ \to pp$ reaction in ^3He as well as in ^2H. It is forbidden for $\pi^- \to np$ by selection rules.

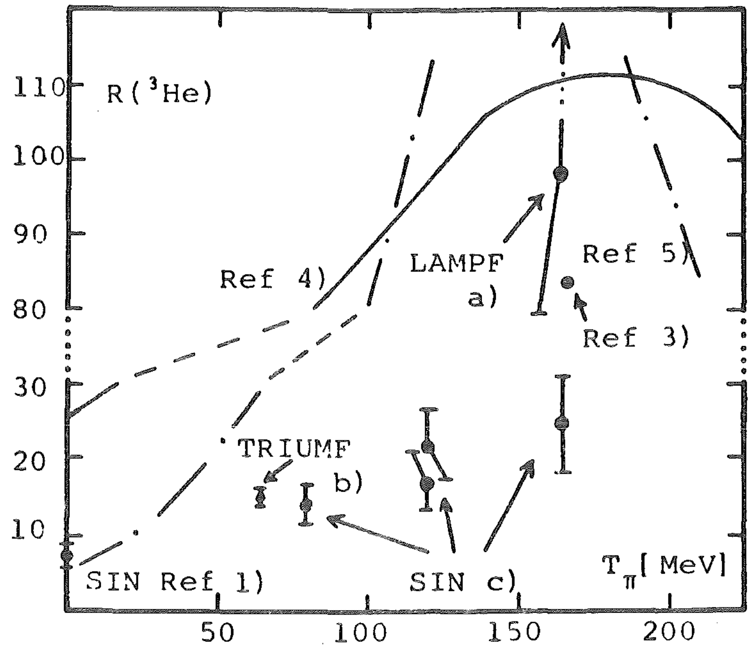

Fig. 1 Compilation of experimental and theoretical results on the isospin ratio R at different energies. Note the interruption of the ordinate between R = 30 and 80. a) Ref. 7, b) Ref. 8, c) Ref. 9.

- We found non-negligible contributions of final state interactions (FSI). Especially for the π^- absorption pronounced FSI peaks and significant (nd) cross sections could be established. In addition also non collinear three nucleon absorption has been observed. The different energy and angle dependences in the region of quasifree absorption and outside this region have been measured and are expected to be sensitive to different theoretical approaches.

(1) D. Gotta, M. Dörr, W. Fetscher, G. Schmidt, H. Ullrich, G. Backenstoss, W. Kowald, I. Schwanner and H.-J. Weyer; Phys. Lett. 112B(1982)129
(2) D. Gotta, Thesis University Karlsruhe 1981, Technical Report KfK-3226 (1981)
(3) T.-S. Lee and K. Ohta, Phys. Rev. Lett. 49(1982)1079
(4) H. Toki and H. Sarafian, Phys. Lett. 119B(1982)285
(5) R. Silbar and E. Piasetzky, LAMPF Preprint (1983)
(6) Th. Schucan, Proc. 9. ICOHEPANS, Versailles 1981, p. 275, H. Nägeli, Thesis University Basel 1980
(7) D. Ashery et al., Phys. Rev. Lett. 47(1981)895
(8) M. Moinester et al., Phys. Rev. Lett. 52(1984)1203
(9) G. Backenstoss, M. Izycki, M. Steinacher, P. Weber, H.-J. Weyer, K. von Weymarn, S. Cierjacks, S. Ljungfelt, U. Mankin, T. Petkovic, G. Schmidt, H. Ullrich and M. Furić, Phys. Lett. 137B(1984)329
(10) D. Ashery, private communication

+ Institut für Physik, Universität Basel
++ Faculty of Sciences, University of Zagreb

4.1.8 INVESTIGATION OF THE Δ-NUCLEAR SPIN DEPENDENCE BY MEANS OF $\pi - {}^{6}\vec{Li}$ AND $\pi - {}^{13}\vec{C}$ SCATTERING

E.T. Boschitz, S. Mango[+], E.L. Mathie, G. Smith, M. Thies[+]

There is a general consensus that the isobar-doorway model of pion nucleus scattering is a more satisfactory description in the region of the (3,3) resonance than the optical model approach. Yet, in order to account for the observed total and integrated elastic cross sections a strong energy dependence of the spreading potential was needed which was difficult to justify. Also, while reproducing the general behaviour of the elastic angular distributions of $\pi-{}^{4}He$, $\pi-{}^{12}C$ and $\pi-{}^{16}O$ scattering considerable discrepancies remained around the large angle minima of the cross section. These difficulties can be overcome by introducing a Δ-nucleus spin-orbit interaction with a similiar strength and the same sign as the nucleon-nucleus one (1). Although this ad-hoc addition of a Δ-spin-orbit term seems plausible,direct experimental information is needed. Such information could be obtained by means of scattering pions from polarized nuclear targets. We have looked into the possibilities of utilizing polarized ${}^{13}C$ and ${}^{6}Li$. ${}^{13}C$ can be polarized as a butanol-target (C_4H_1OH) where the four ${}^{12}C$ atoms are replaced by ${}^{13}C$. Test experiments have shown that the energy resolution of the SUSI spectrometer should be adequate for separate the

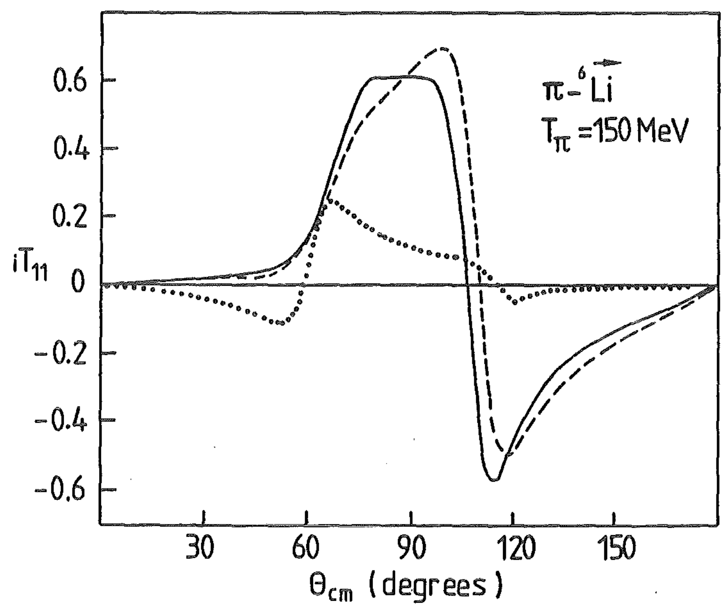

Fig. 1 Predictions of iT_{11} in $\pi\,{}^{6}\vec{Li}$ elastic scattering. Δ-hole calculation with (——) and without LS-term (---) and closure approximation (...).

π-^{13}C ground state from the π-^{16}O ground state, at least at larger angles. Unfortunately the π-^{13}C cross sections is falling rapidly, and longer runs have to be anticipated. A much better target from the experimental and theoretical point of view is ^{6}Li as ^{6}LiD. Experimentally the ground state could be well separated, the cross section is rather flat and the degree of vector polarization of ^{6}Li in the ^{6}LiD compound has been shown to be very high. (up to 60% with a frozen spin target). Theoretically, polarization effects are proportional to 1/A, A being the nuclear mass. A preliminary calculation (Fig. 1) shows the predicted vector analyzing power iT_{11} in the full Δ-hole model including L•S interaction (solid line), the same without L•S interaction (dashed line) and the closure approximation (dotted line). Clearly the vector analysing power is very sensitive to the details of the reaction dynamics. The use of a ^{6}LiD target is presently being studied at SIN.

(1) Y. Horikawa, M. Thies, F. Lenz, Nucl. Phys. A345(1980)386

\+ Schweizerisches Institut für Nuklearforschung

4.2 INTERACTIONS OF ANTIPROTONS AND PROTONS

4.2.1 FIRST RESULTS FROM ANTIPROTONIC X-RAY STUDIES AT LEAR

G. Büche, A.D. Hancock, H. Koch, Th. Köhler, A. Kreissl , H. Poth, U. Raich, D. Rohmann, Ch. Findeisen[+], L. Tauscher[+], A. Nilsson[++], S. Carius[++], M. Suffert[+++], S. Charalambus[++++], M. Chardalas[++++], S. Dedoussis[++++]

In collaboration with Basel, Stockholm, Strasbourg and Thessaloniki we have set up an experiment at LEAR (PS 176) to study the interaction an antiproton undergoes when it is stopped in a target. The experiment was performed in close cooperation with a group from the Technical University of Munich and from the University of Mississippi.

In the first beam time for this experiment at LEAR the following aspects were mainly studied:

i) the measurement of isotope effects caused by strong interaction in $\bar{p}$- $^{16}O/^{17}O/^{18}O$ in order to disentangle the $\bar{p}p$ from $\bar{p}n$ interaction.

ii) the determination of shift, widths and attenuation in the 4-3 transition in nuclei adjacent to oxygen.

iii) the measurements of the strong interaction effects in resolved fine structure components of the 8-7 transition of $\bar{p}$-^{138}Ba aiming at the determination of the L-S-dependence of the $\bar{p}$-nuclear force.

The experimental set-up consisted of six solid state detectors, a 3" x 3" and a 10^2 x 12" NAI and a liquid scintillator neutron counter. The energy range between a few keV and 1 GeV was covered allowing for the measurement of atomic X-rays, nuclear γ-rays and the spectrum of high energetic γ-rays associated with $\bar{p}$-annihilation. With the n-detector the spectra of neutrons emmitted after $\bar{p}$-absorption were measured via time-of-flight. The data were collected with a fast data acquisition system consisting of a front-end microprocessor linked to a PDP. A trigger was generated when an incoming antiproton was detected by a scintillator telescope and one of the neutral counters had fired. The corresponding time and energy of the neutral event was stored in a two dimensional array in the large memory of the microprocessor. The data were accumulated during one spill (1 hour) and then transferred to the PDP during the beam-off-time. The task of the PDP was also to control the target and moderator position and to monitor the various count rates. The data were transferred immediately after the spill end via the CERN computer comminication network to a LSI computer. There a rapid pre-analysis of the data was done after each spill.

In December 1983 and during April and May 1984 a total of about 35 h of 300 MeV/c antiproton beam time was allocated. Within this time the beam properties were studied and the settings were optimized. Finally data were collected for $\bar{p}$-^{16}O/^{17}O/^{18}O, $\bar{p}$-^{19}F, $\bar{p}$-^{14}N and $\bar{p}$-^{138}Ba. Moreover test measurements were performed on $\bar{p}$-^{208}Pb and $\bar{p}$-^{44}Ca.

In spite of the short beam time excellent data could be accumulated due to the high reliability of the complete set-up. Good statistics spectrum were obtained for the light nuclei. In $\bar{p}$-^{138}Ba, where the beam time was to short, the fine structure components of the 8-7 transition could, however, be resolved and for the first time direct evidence for strong L-S-effects in $\bar{p}$-nucleus interaction were found.

In general the spectra were clean and of low background. The average antiproton rate was around 4×10^4 s^{-1}. The $\bar{p}$-beam size at 300 MeV/c was less than 1 cm^2.

Fig. 1 shows the spectrum of $\bar{p}$-^{16}O. A large part of the X-rays cascade is observed. Note the excellent peak/background ratio. There are

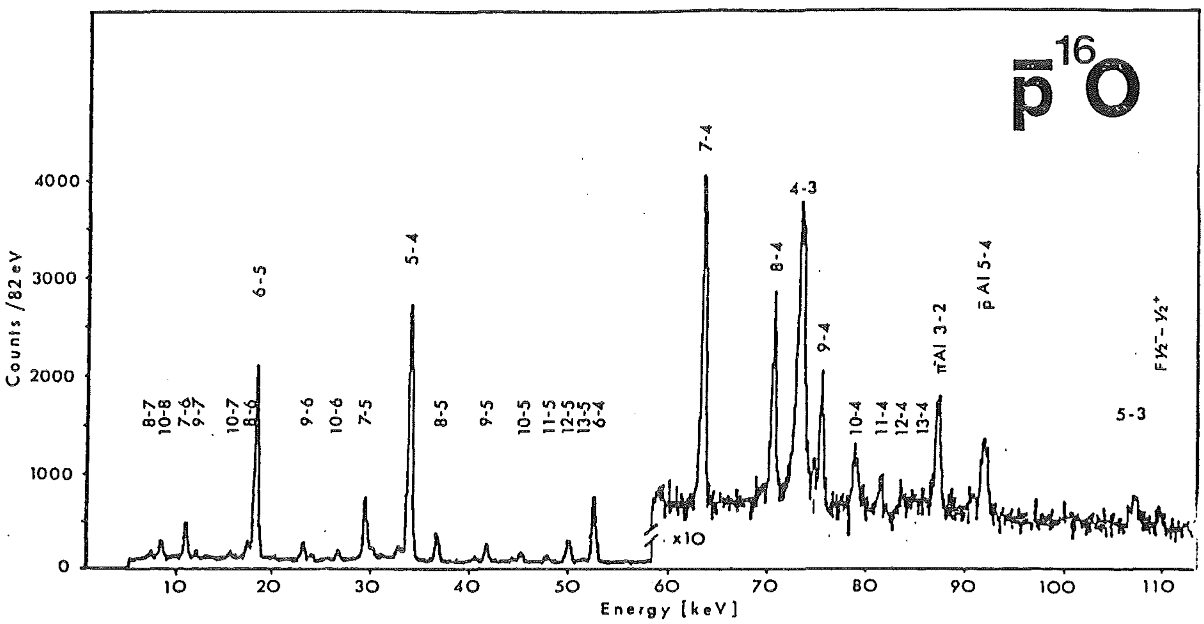

Fig. 1 X-ray spectrum from antiprotonic oxygen, corresponding to 1.8×10^8 antiproton stops in a water target.

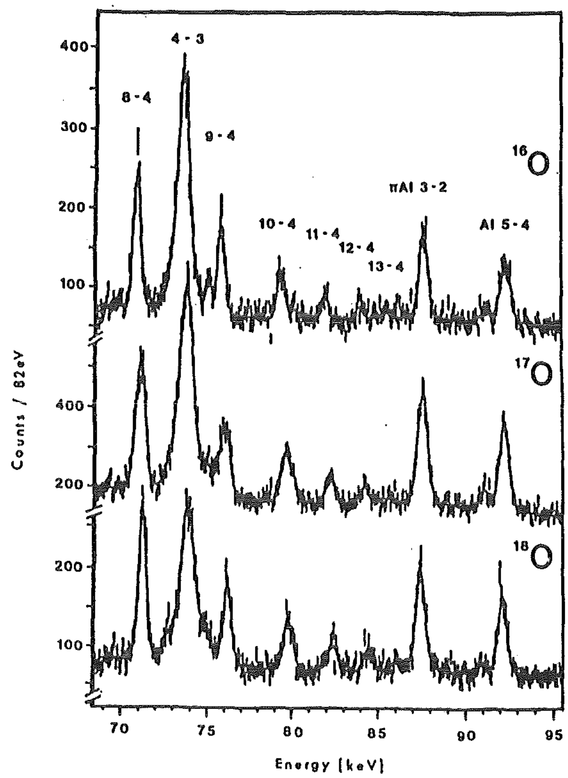

Fig.2
Comparison of the antiprotonic x-ray spectra for the three stable oxygen isotopes.

practically no background lines in the spectrum apart from pionic and antiprotonic aluminium origination from annihilation pions or antiprotons stopping in the target frame. The last observable X-ray transition in oxygen is the 4-3 line.

Isotope effects caused by strong interaction are clearly visible in Fig. 2. With respect to the unperturbed 8-4 transition the 4-3 line is attenuated and broadened going from ^{16}O to ^{18}O.

The strong interaction effects in the 4-3 transition were measured with good precision in nitrogen, the stable oxygen isotopes and in fluorine. The data evaluation is in progress. Tentative results from strong interaction effects are summarized in Table 1. As shown there, these effects

Table 1 Preliminary results of experiment PS 176

Target	Isotopical composition of the target	Total $\bar{p}$-rate x 10^8	Attenuated transition	Intensity	Shift (eV)	Width (eV)
H_2O	$^{16}O(99.9\%)$	1.8	4 - 3	4260(230)	-115(15)	495(45)
H_2O	$^{16}O(26\%)\ ^{17}O(42\%)\ ^{18}O(32\%)$	4.7	4 - 3	8250(350)*		
H_2O	$^{18}O(99\%)$	2.0	4 - 3	3530(270)	-210(20)	650(70)
NaF	F (natural)	6.5	4 - 3	10600(380)	-470(50)	1400(140)
$Ba(NO_3)_2$	$^{138}Ba(99\%)$	} 11.5	3 - 7	5000(300)		1300-1700
$Ba(NO_3)_2$	N (natural)		4 - 3	10400(140)		100(50)

* Contributions from all three isotopes

are measured with a precision of 10% or better. The isotope effect in the oxygen data are very pronounced. These tentative results were used to make a first analysis of $\bar{p}$-nucleus potential within the frame-work of an optical potential model. The results clearly indicate that a deep real and imaginary part of the optical potential is needed to explain the data. This is in agreement with $\bar{p}$-nucleus scattering data and rules out speculations that $\bar{p}$-atom data can also be explain by a shallow potential.

The recorded spectra contain a plethora of information on the $\bar{p}$-atomic cascade, the $\bar{p}$-absorption and the residual nuclei distribution which is presently analyzed. First indications show that in light nuclei the antiproton is predominantly absorbed on a single nucleon and the residual nucleus remains intact while in heavy nuclei a large number of nucleons are evaporated after $\bar{p}$-absorption.

Most recently (August 1984) new measurements were done with a 200 MeV/c $\bar{p}$-beam at LEAR in order to accumulate high statistics data on antiprotonic oxygen and lead. Compared to the 300 MeV/c beam the new spectra are still cleaner.

+ Institute for Physics, University of Basel, Klingelbergstr. 84, Basel, Switzerland
++ Research Institut for Physics, Stockholm, Sweden
+++ Centre de Recherches Nucléaires and Université Louis Pasteur, Strasbourg, France
++++ Department of Nuclear Physics, University of Thessalonik, Greece

4.2.2 CRITICAL ABSORPTION OF ANTIPROTONIC X-RAYS

B. Jödicke, G. Zach, G. Büche, H. Koch

The high flux of antiprotons from LEAR which became available recently enables us to measure energies and intensities of X-rays emitted from antiprotonic atoms with remarkably good statistics. This opens the possibility for studying strong interaction effects as well as electromagnetic corrections to the transition energies on new scales of accuracy. Using the method of critical absorption of quanta on a suitable K-edge, we intend to measure X-ray transition energies at least in a few cases with an accuracy of about 1 eV. The photoabsorption coefficient rises steeply within the region of a K-edge. Therefore the ratio of the intensities measured without and with the critical absorber determines the energy of the radiation. A list of cases has been worked out giving the energies of prominent lines of antiprotonic X-rays coinciding occasionally within ±10 eV with the energy of a K-edge. All stable isotopes have been scanned resulting in a number of roughly 50 cases.

In order to find the most sensitive among these cases, two major points have to be taken into account. The first point is the structure of the K-edge depending on Z, the electronic structure of the atomic shells and the chemical compound of the absorber material and which is given by the slope and smoothness of the absorption cross section. The second point is the structure of the X-ray emission line itself which is governed by the fine structure splitting, the number of various components $(n_i;\ l_i \leq n_i-1) \rightarrow (n_f;\ \leq n_f-1)$ and the related intensity ratios. The convolution of the two structures enables us to decide on cases suited for an energy measurement. Half dozen of them look promising and will be tested in the near future.

In addition to this work we extended the computer code PBAR (1). This code is able to solve the Dirac equation for a system of an antiprotonic atom containing additional terms that become relevant if an accuracy of the given size is aimed at. Effects from recoil correction, electron screening, vacuum polarization of finite size nuclei as well as from nuclear polarisability are added to the program. A few of these corrections are expected to contribute between 1 and 10 eV to the transition energies. Consequently, they are essential for the interpretation of X-ray spectra, if further effects from strong interactions, like spin effects or

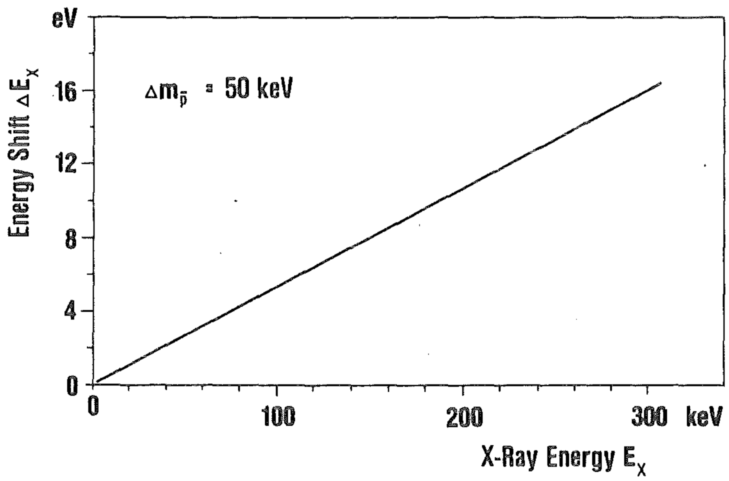

Fig. 1 The contribution ΔE_x to the energy E_x of an X-ray transition from an antiprotonic atom, if the mass of the antiproton is allowed to deviate from the proton mass by an amount of $\Delta m_{\bar{p}}$.

long range QCD effects are to be analyzed or if invariance principles are to be tested.

As an example to the last category, Fig. 1 shows the size of the energy shift which is introduced into the transition energy E_x if the mass of the antiproton $m_{\bar{p}}$ is allowed to deviate from the proton mass m_p by an amount of $\Delta m_{\bar{p}}$ = 50 keV. This figure corresponds to the actual uncertainty of the $m_{\bar{p}}$ value. A further example where the expected size of a possible long range QCD effect is discussed, is given in a separate contribution to this report.

(1) E. Borie and G.A. Rinker, Rev. Mod. Phys. 54(1982) 67;
E. Borie, Phys. Rev. A28(1983)555

4.2.3 POSSIBLE LONG RANGE QCD-EFFECTS IN ANTIPROTONIC ATOMS

K. Heitlinger, G. Büche, H. Koch

A formal analogy between quantum electrodynamics and quantum chromodynamics was used to claim for an exchange of 2 gluons between color singlets (hadrons) leading to long range strong interactions. Bounds on possible interactions of this kind are given in Ref. 1 together with a short review of the literature. Similar to the van der Waals potential in molecular physics such a strong interaction potential with long range could have the form

$$V_{1r} = \frac{\lambda}{r_o}\left(\frac{r_o}{R}\right)^N \quad \text{for } R \geq 1 \text{ fm} \qquad (1)$$

$$= \text{const} \qquad \text{otherwise}$$

where λ is a coupling constant and r_o = 1 fm is a length convention. If N = 6 Eq.(1) is identical with the van der Waals potential. The expression (1) is to be added to the 'usual' strong interaction potential which we used in the scattering length approximation

$$V_{st} = 4\pi \left(1 + \frac{2mp}{m_p + m_n}\right) a\, \rho(r) \qquad (2)$$

with $\rho(r)$ being the distribution of nucleons and a signifies the antiproton nucleon scattering length. The radial dependence of the potential $V_{st} + V_{1r}$ is shown in Fig. 1.

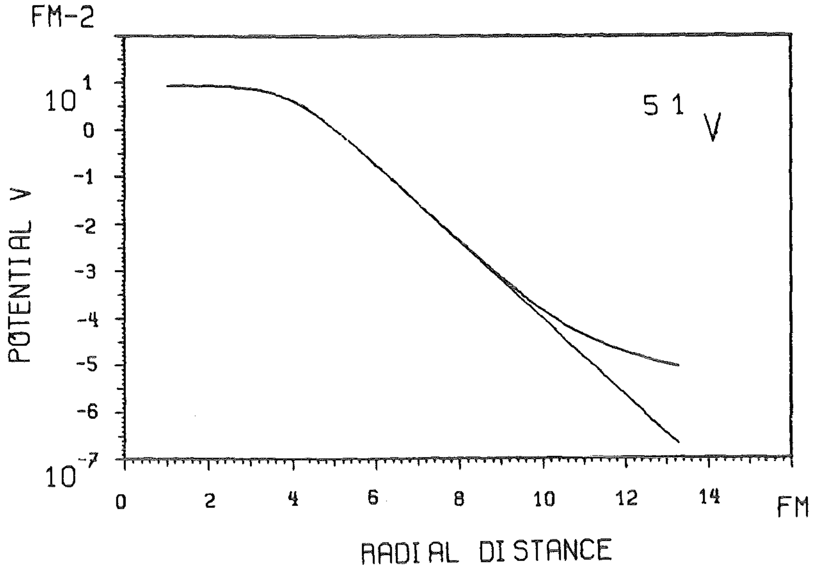

Fig. 1 The radial dependence of the strong interaction potential and the added long range interaction potential for ^{51}V.

We studied the size of this presumed effect on the energy levels of antiprotonic atoms leading to a shift of X-ray transition energies. Cases where V_{st} is small and where V_{lr} together with the Coulomb potential are the leading terms have been investigated. Quite a series of stable nuclei ranging from ^{11}B through ^{209}Bi was taken into account. For intermediate mass nuclei $20 \leq Z \leq 38$ and circular X-ray transitions effects of the order of 1 eV were found. Using the parameter values N = 6 and $\lambda = 0{,}1$ for the range and the strength of the potential, respectively, we were able to confirm the estimates of Fiorentini and Tripiccione (2). In addition to their results we found shifts of the order of 10 eV for several heavy nuclei. Shifts of this last magnitude are measurable using presently available detector techniques.

In a second part of this work the parameters N and λ were varied. It could be shown that extending the range of the potential by one order (N = 5) or rising its strength by one order of magnitude ($\lambda = 1.0$) enlarges the expected effect on the transition energies to at least 10 eV. As a conclusion of this study it seems possible to detect the existence and to estimate the size of the long range effects from a measurement on X-ray transitions emitted from antiprotonic atoms.

(1) G. Feinberg and J. Sucher, Phys. Rev. D20(1979)1717;
L. Bracci, G. Fiorentini and R. Tripiccione, Nucl. Phys. B217(1983) 215

(2) G. Fiorentini and R. Tripiccione, Pisa preprint IFUP Th 10/82

4.2.4 SEARCH FOR NARROW STATES IN THE $\bar{p}$-^{4}He-SYSTEM

L. Adiels[+], G. Backenstoss[++], P. Blüm, I. Bergström[+], K. Fransson[+], R. Guigas, H. Koch, A. Kerek[+], M. Meyer, P. Pavlopoulos[++], H. Poth, U. Raich, B. Richter, J. Repond, M. Suffert[+++], L. Tauscher[+], D. Tröster[+], and K. Zioutas[++++], Physics Letters 138B(1984)235

In the inclusive γ-spectrum of the reaction $(\bar{p}p)_{stop} \rightarrow \gamma X$ narrow structures have been observed, which can be tentatively attributed to Baryonium $(qq\bar{q}\bar{q})$ or Glue ball (ggg) states (1), (2). The experiment was performed with a 54-modular NaI-detector with high energy resolution and big solid angle. With the same apparatures the reaction $(\bar{p}\,^4He)_{stop} \rightarrow \gamma X$ was measured. The gross features of the spectrum originating from the Gamma-decay of neutral particles (π^0, η) of the annihilation process could be quantitatively understood by folding the γ-spectrum of the $\bar{p}p$-reaction with the Fermi-motion of the nucleons in ^{4}He, assuming absorption of the antiproton on only one nucleon (p or n) in ^{4}He. After the subtraction of this background (and a small additional background below 200 MeV) these narrow structures appeared in the spectrum as shown in Fig. 1. The structure around 50 MeV (2.7σ) seems to be too narrow in comparison with the experimental resolution and is therefore disregarded in the following discussion of the data. More interesting are the two peaks at 161.9 and 203 MeV γ-energy: (i) The energy difference of these peaks ($41.1^{+6.6}_{-5.0}$ MeV) corresponds to the case that the $\bar{p}N$-state corresponding to the 160 MeV γ-ray would be formed by the reaction $(\bar{p}\,^4He)_{stop} \rightarrow \bar{p}N + t(^3He)$, while the state corresponding to 200 MeV would be formed via $(\bar{p}\,^4He)_{stop} \rightarrow \bar{p}N + 3N$

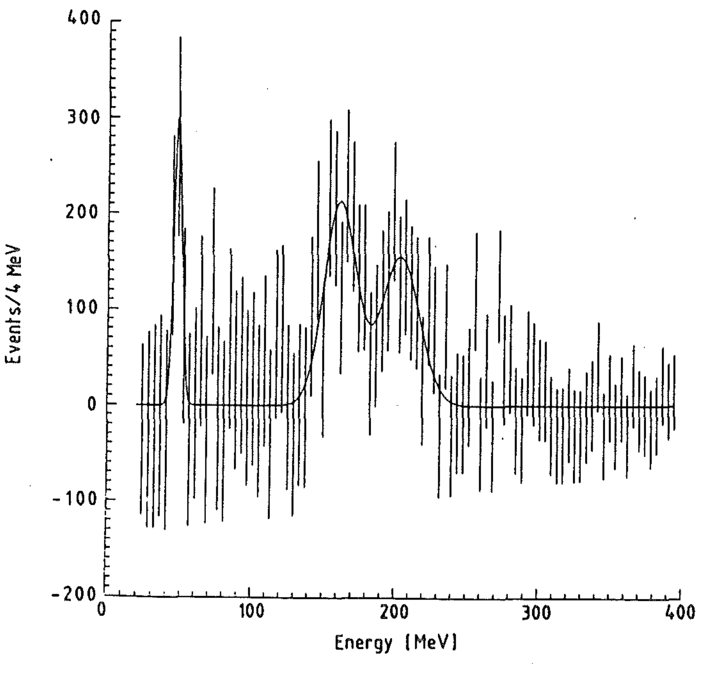

Fig. 1
Gamma spectrum of the reaction $(\bar{p}\,^4He)_{rest} \rightarrow \gamma + X$, background subtracted

(free). (ii) The yield of the γ-lines is about 1%, and thus a factor of three higher than in the p̄p-spectra. (iii) The energies of the lines (after correction for Fermi-motion) is about 5% apart from two γ-lines seen in the p̄p-spectrum, which could be still within the calibration error of both experiments.

The experiment shows that hight nuclear targets may be good candidates for the investigation of narrow states in the p̄N-system. The p̄n-channel which is now open might lead to higher yieldes of transitions and serves as a powerful mean to get information on the quantum number (e.g. isospin) of the states.

(1) B. Richter, Suche nach gebundenen Baryoniumzuständen und seltenen Annihilationskanälen mittels Gamma-Spektrometrie KfK-3441 (Februar 83)

(2) B. Richter et al., New Results in the Search for Narrow States in the p̄p-System below threshold, P.L. 126B(1983)284

+ Research Institute for Physics, Stockholm, Sweden
++ Institute for Physics, University of Basle, Switzerland
+++ Centre de recherches nucléaires and Université Louis Pasteur, Strasbourg, France
++++ Department of Nuclear Physics, University of Thessaloniki, Greece

4.2.5 THE ANALYZING POWER OF ELASTIC PROTON-PROTON SCATTERING AT 582 MeV

A. Berdoz[+], B. Favier[+], F. Foroughi[+], Ch. Weddigen, J. Phys. G9 (1983)L261

In a series of experiments (1), (2) the NESIKA collaboration (Neuchâtel-SIN-Karlsruhe) has developed an apparatus for precision two-body measurements installed at the PM1 beam line of SIN. This apparatus was used to perform measurements of theyanal zing power A_{yo} for elastic p-p scattering at 582 MeV. The experimental set-up (Fig. 1) was similar to that described in Ref. 2:

The polarization P = 0.4165 ± 0.0040 of the proton beam, incident on CH_2 and C targets for foreground and background measurements, respectively, was rotated in a superconducting solenoid to evaluate coincident counting rates $N_{R^\pm}$ and $N_{L^\pm}$ for protons scattered to the right (detectors PR_1 and PR_2) and to the left (detectors PL_1 and PL_2), for P up (+) and down (-). After background subtraction A_{yo} was deduced from the

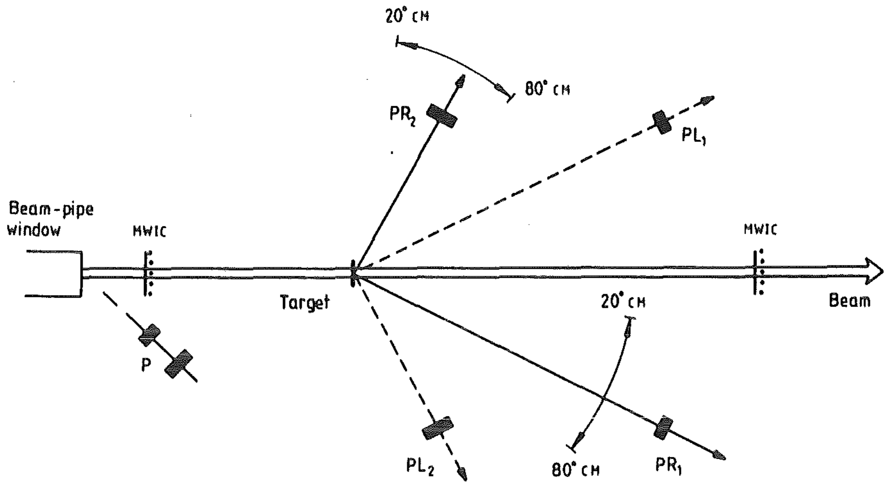

Fig. 1 Experimental set-up for the measurement of the analyzing power of p-p elastic scattering.

relation

$$A_{yo} = \frac{1}{P} \frac{\varepsilon-1}{\varepsilon+1}$$

where $\varepsilon = \{N_{L^+} \cdot N_{R^-})(N_{L^-} \cdot N_{R^+})\}^{1/2}$.

In Fig. 2 our results (solid dots) are compared with those of previous experiments (open symbols). The relative deviation of our results form the smooth curve fitting our data in Fig. 2 is shown in Fig. 3. The interpolated maximum value is $A_{yo}(38^{o})$ = + 0.5312 ± 0.0053 where the main

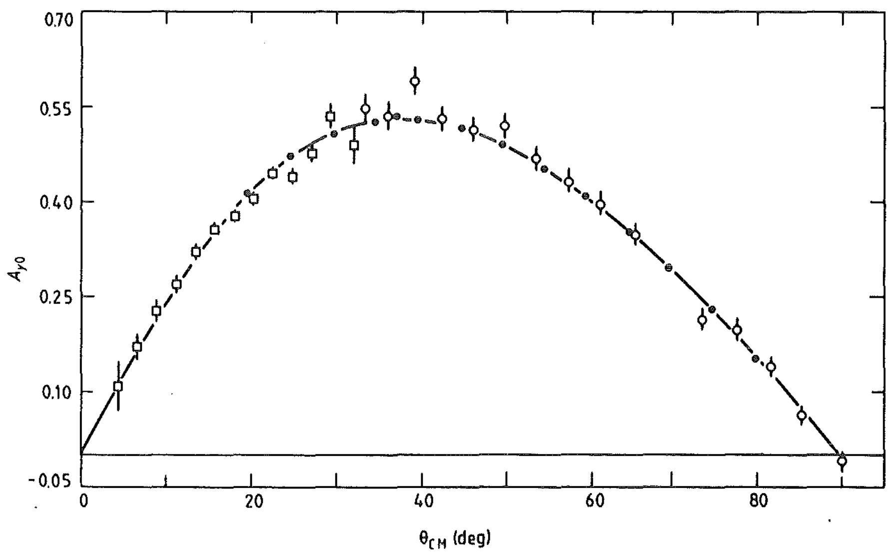

Fig. 2 Comparison of the NESIKA results (solid dots) for the analyzing power A_{yo} for p-p elastic scattering at 582 MeV with earlier data (3) at 578 MeV (circles) and (4) at 575 MeV (squares). The curve represents a Legendre polynomal fit to our data and serves to guide the eye.

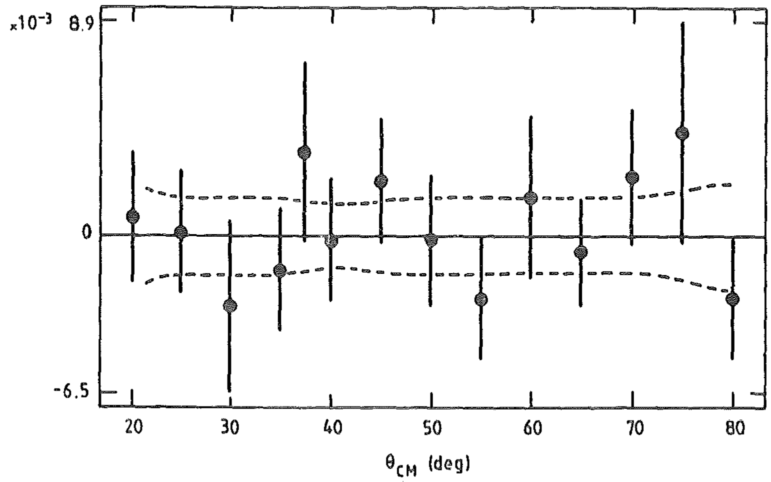

Fig. 3 Deviation of the NESIKA results from the fit in Fig. 2. The broken lines represent the error consider of the fit.

contribution to the error stems from the uncertainty of the beam polarisation P. Such precise data are needed for future phase-shift analyses in order to answer the still outstanding question of the existence of dibaryon resonances.

(1) P. Chatelain, B. Favier, F. Foroughi, J. Hoftizer, S. Jaccard, J. Piffaretti, P. Walden, and Ch. Weddigen, J. Phys. G8(1982)643
J. Hoftiezer, Ch. Weddigen, P. Chatelain, B. Favier, F. Foroughi, C. Nußbaum, J. Piffaretti, S. Jaccard, and P. Walden, Nucl. Phys. A402(1983)429
J. Hoftiezer, G.S. Mutchler, Ch. Weddigen, J.A. Konter, S. Mango, A. Berdoz, B. Favier, and F. Foroughi, Nucl. Phys. A412(1984)273

(2) A. Berdoz, B. Favier, F. Foroughi, J. Hoftiezer, G.S. Mutchler, and Ch. Weddigen, J. Phys. G8(1982)1363
J. Hoftiezer, Ch. Weddigen, P. Chatelain, B. Favier, F. Foroughi, and J. Piffaretti, Nucl. Phys. A412(1984)286

(3) D. Besset, H.Q. Do, B. Favier, R. Hausamann, E. Heer, R. Hess, C. Lechanoine-LeLuc, W.R. Leo, D. Rapin, D.W. Werren, and Ch. Weddigen, Nucl. Phys. A345(1980)435

(4) D. Besset, B. Favier, L.G. Greenians, R. Hess, C. Lechanoine, D.W. Werren, and Ch. Weddigen, Phys. Rev. D21(1980)580

+ Institut de Physique, Université de Neuchâtel, Switzerland

4.2.6 VALIDATION OF HETC MODEL CALCULATIONS FOR NEUTRON PRODUCTION

S. Cierjacks, Y. Hino, D. Filges[+], T.W. Armstrong[+], P. Cloth[+]

As part of a study to assess the accuracy of model predictions from theory the intranuclear-cascade-evaporation model in its version of HETC/KFA-1 has been used to calculate double differential neutron production cross sections from non-elastic 590 MeV proton collisions with elementary uranium, lead, tantalum, indium, niobium, iron aluminium and carbon targets. These model predictions have been compared with the systematic KfK measurements performed in recent years at the SIN cyclotron (1). A typical result is given in Fig. 1 which shows the comparison for uranium at a laboratory angle of 30^o. In general, the HETC predicts within 20% the measured cross sections in the evaporation region ($E_n \lesssim 15$ MeV) for target nuclei heavier than iron, while some larger differences occur for the lighter elements. A major deficiency of the present models involved in the HETC/KFA-1 code is the underestimation of high energy neutron production ($E_n \gtrsim 15$ MeV). The calculations yield cross sections which at ~100 MeV and 30^o are approximately a factor of 2-3 smaller than the measured ones. The underestimation of high energy neutrons further increases with increasing neutron energy and increasing emission angle. There are various possibilities for suitable model modifications which can, in principle, improve the agreement between measurement and calculations in the high energy and

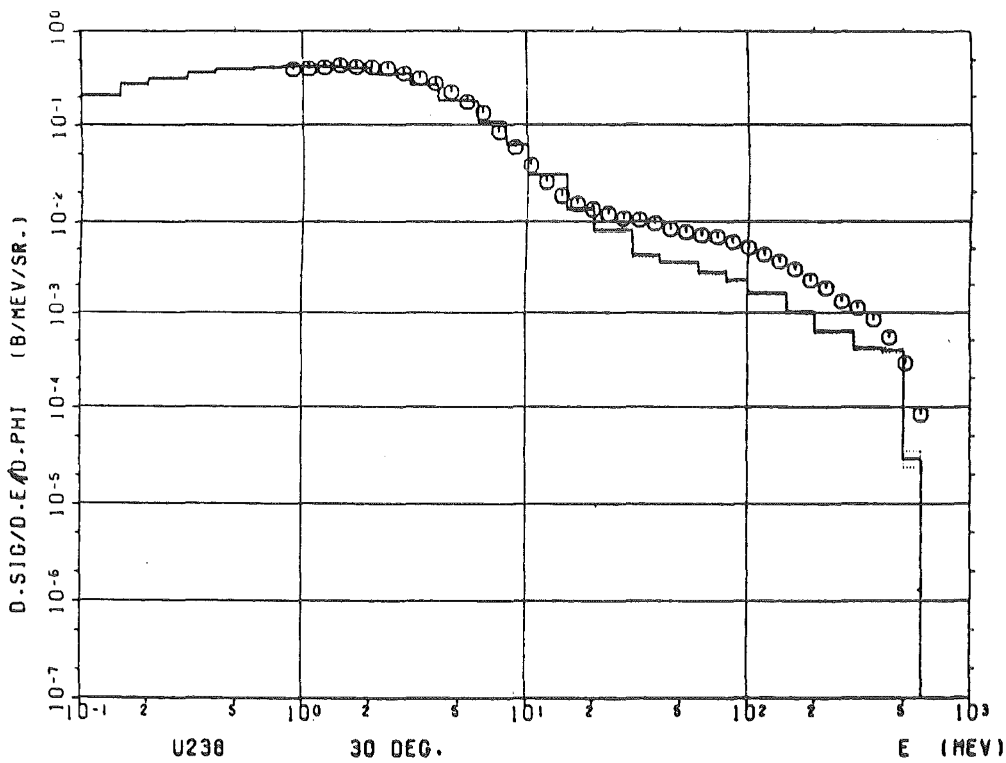

Fig. 1 Measured (⊙) and calculated (—) double differential 30^o neutron production cross sections for 590 MeV protons on uranium. It can be seen that the HETC/KFA-1 code predicts approximately the correct neutron production in the evaporation region ($E_n \lesssim 15$ MeV), whereas in the cascade region ($E_n \gtrsim 15$ MeV) there are systematic discrepancies.

and large angle range. The proper choice of modifications is presently under investigation.

A documentation of measured and calculated neutron production cross sections over the whole range of investigated targets and emission angles has been prepared for publication in a joint KfK/KFA report (2). In this report experimental and theoretical results are presented in tabulated and graphical form.

(1) S. Cierjacks, Y. Hino, S.D. Howe, F. Raupp and L. Buth, Conf. on Nucl. Data for Science and Technology, Antwerpen 1982 (D. Reidel Publ. Comp., Dordrecht, 1983) p. 383

(2) D. Filges, S. Cierjacks, Y. Hino, T.W. Armstrong and P. Cloth, Kernforschungszentrum Karlsruhe, KfK 3779, to be published

+ Institut für Reaktorentwicklung, Kernforschungsanlage Jülich

5. HIGH ENERGY PHYSICS

CELLO Collaboration

H.-J. Behrend, J. Bürger, L. Criegee, H. Fenner, G. Franke, J. Meyer, V. Schröder, H. Sindt, U. Timm, G.G. Winter, W. Zimmermann
Deutsches Elektronen-Synchrotron, DESY, Hamburg, Germany

P.J. Bussey, A.J. Campbell, J.B. Dainton, D. Hendry, J.M. Scarr, I.O. Skillicorn, K.M. Smith
University of Glasgow, United Kingdom

M. Poppe, H. Spitzer
II. Institut für Experimentalphysik, Universität Hamburg, Germany

O. Achterberg, G. D'Agostini, W.-D. Apel, J. Engler, G. Flügge, B. Forstbauer, D.C. Fries, W. Fues, K. Gamerdinger, Th. Henkes, G. Hopp, J. Knapp, M. Krüger, H. Küster, H. Müller, H. Randoll, K.H. Ranitzsch, G. Schmidt, H. Schneider
Kernforschungszentrum Karlsruhe and Universität Karlsruhe, Germany

W. de Boer, G. Buschhorn, G. Grindhammer, P. Grosse-Wiesmann, B. Gunderson, Ch. Kiesling, R. Kotthaus, H. Lierl, D. Lüers, H. Oberlack, P. Schacht
Max-Planck-Institut für Physik und Astrophysik, München, Germany

G. Bonneaud, P. Colas, A. Cordier, M. Davier, D. Fournier, J.F. Grivaz, J. Haissinski, V. Journé, F. Le Diberdier, U. Mallik, E. Ros, J.-J. Viellet
Laboratoire de l'Accélérateur Linéaire, Orsay, France

J.H. Field, R. George, M. Goldberg, O. Hamon, F. Kapusta, F. Kovacs, R. Pain, L. Poggioli, M. Rivoal
Laboratoire de Physique Nucléaire et Hautes Energies, Université de Paris, France

M. Gaspero, B. Stella
University of Rome, Italy

R. Aleksan, J. Bouchez, G. Carnesecchi, G. Cozzika, Y. Ducros, A. Gaidot, P. Jarry, Y. Lavagne, F. Ould Saada, J. Pamela, J.P. Pansart, F. Pierre
Centre d'Etudes Nucléaires, Saclay, France

G. Alexander, G. Bella, Y. Gnat, J. Grunhaus
Tel Aviv University, Israel

During the last year the High Energy Physics group of the IK 1 again concentrated on e^+e^- physics using the CELLO detector at the e^+e^- storage ring PETRA at DESY in Hamburg. The CELLO detector is a large spectrometer facility which was initially designed and built by three French groups from Orsay, Saclay and Paris and the German groups from KfK and Universität Karlsruhe, MPI München and DESY Hamburg. After an upgrading of the central tracking detector and the LAr calorimeter the CELLO detector moved back into the beam in August 1982. At the same time, five new groups from the former PLUTO group joined the CELLO collaboration. Since 1983 the detector has been operating smoothly up to the highest e^+e^- energies of 46.78 GeV which were ever reached. Most of this time until spring 1984 was used to search for the sixth (top) quark. Since summer data are collected at high energy around 44 GeV to search for rare processes. A possible candidate for such rare events had been found by the CELLO group in the course of the high energy scan at 43.45 GeV.

In 1983, a new inner detector - the stereo wire chamber SWC - was designed together with the newcoming groups. The SWC is under construction now and is scheduled to be ready in summer 1985.

The Karlsruhe group has several major responsibilities in the CELLO collaboration including

- CELLO spokesman (G. Flügge)
- CELLO analysis coordinator (W.-D. Apel)
- Liquid Argon (LAr) System (J. Engler)

The main activities of the Karlsruhe group during the last year included

- Maintenance of the LAr system and construction and testing of a new improved LAr trigger system
- Participation to the planning and construction of the SWC
- Process and analyse the CELLO data using the KfK computer centre. The physics topics concentrated on total cross section, test of QCD, and search for new particles.

5.1 HARDWARE ACTIVITIES

5.1.1 CELLO OPERATION

The CELLO detector operated smoothly and without major problems in

1983 and 1984. A contamination of the LAr system with 18 ppm of O_2 which occured in September 1983 could be cured in the winter shutdown 1983/84 by cleaning and partly replacing the argon. Since the electronic noise in the system could be largely reduced in summer 1983, the LAr calorimeter was sufficiently well operating even during the two months with contaiminated argon. A technician of the institute, permanently at Hamburg operates and supervises the LAr cryogenic and electronic system. In 1984 the electronic noise was low enough to trigger on single photons of 2.5 GeV energy. Together with a 'hole tagger' which fills the hole between the cylindrical and endcap calorimeter, this allows to search for hypothetical rare processes like production of supersymmetric electrons and photinos. This 'hole tagger' consists of two layers of scintillator with 2 cm of lead in between to detect electromagnetic showers. The installation was completed during the winter shutdown 83/84. This component is operational since beginning of 84 and is working well.

The momentum resolution of the central detector could be improved by using a cooler gas (50% argon and 50% ethane) and adding two layers of drift tubes near the beam pipe. The present momentum resolution is 1.3%·p (GeV) at high energies. A price, however, had to be paid for this improvement. The new gas mixture seems to be more sensitive to polymerization of the hydrocarbons under the influence of radiation than the old methane/argon mixture. We observe first signs of ageing in the two innermost drift chambers since the end of 1983.

5.1.2 THE STEREO WIRE CHAMBER (SWC)

For the above reason we have proposed in 1983 to rebuild our inner detector. The new design is presently under construction and will be ready in 1985. To meet the physics requirements at highest PETRA energies the new design was required to provide good pattern recognition and good momentum resolution over the largest possible solid angle for both annihilation and two-photon events. Good vertex resolution should be achieved. In addition, the amount of material in front of the photon detectors should be minimized also in forward direction to improve photon detection and allow electron tagging down to very small angles. This lead us to the following design criteria:

- high momentum resolution
- good vertex resolution

- good pattern recognition at high track densities
- large solid angle coverage
- thin endplates
- dE/dx option.

Given the high magnetic field of CELLO, possible choices were either a TPC or a drift chamber with small drift cells. We finally decided to build a standard drift chamber. A small hexagonal drift cell of 3 to 6 mm drift path will provide a simple and uniform time-space relationsship and a certain freedom in the choice of the gas. Pairs of staggered wires will resolve the left-right ambiguities locally. The chamber will have the option of being pressurized up to 3 bar for precise space resolution and a dE/dx option. A thin Be-beam pipe will ensure good vertex resolution.

The mechanical design of the chamber is shown in Fig. 1. Rigid spherical endplates with precision holes for the wire feed throughs are part of the pressure vessel. To obtain the best possible solid angle coverage the vertex detector and the Be-beam pipe have been integrated into the large wire chamber.

For good pattern recognition the chamber should contain as many layers of wires as could possibly be packed into the limited space from 7 to 70 cm radius between beam pipe and outer chamber wall. To provide precise z coordinates stereo wires are required.

In a standard drift chamber with stereo angle wires usually about half of the wire planes are parallel to the beam (0^0) and the other half is distributed at $\pm\ \alpha$ (stereo angle). In our configuration we have chosen a more symmetric solution with 18 planes at $-\alpha$ and 18 planes at $+\alpha$ (Stereo Wire Chamber, SWC). Such a configuration allows trackfinding in both views and has the additional advantage to

- provide better z resolution
- allow for maximum plane density (same hyperbolic sagging in all planes) and
- deliver the same curvature in both views provided the stereo angle α is constant in all planes.

In our design, a stereo angle of $\alpha = 2^0$ was chosen.

The situation in August 84 is the following: Tests of a small prototype chamber are performed with participation of the physicists from the institute in order to study several technicald details. For the final chamber most of the parts (endplates, wire feed-throughs, etc.) are delivered

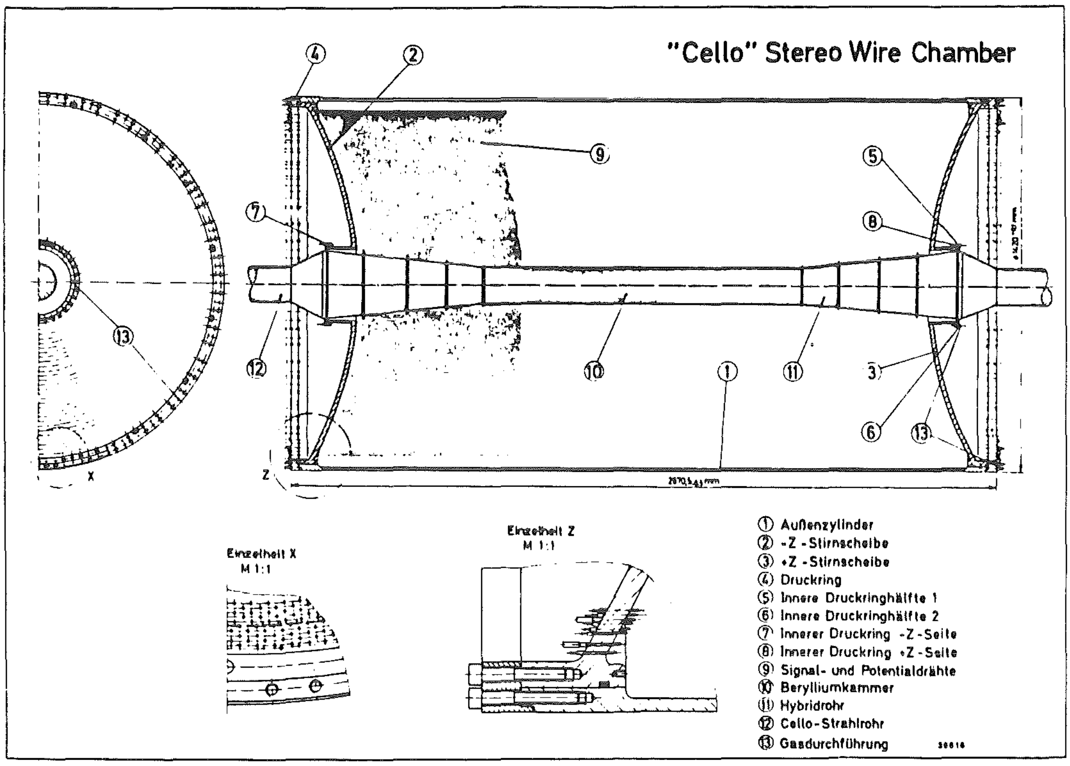

Fig. 1 The Stereo Wire Chamber (SWC). 1 = outer cylinder, 2 = -Z endplate, 3 = +Z endplate, 4 = pressure ring, 5 to 8 = inner pressure rings, 9 = signal and potential wires, 10 = beryllium pipe, 11 = hybrid cone, 12 = beam pipe, 13 = gas feed throughs.

and are actually being assembled at DESY. Stringing the wires is scheduled to begin 1st October. The institute participates with one technician, who will stay at Hamburg during the manufacturing period.

5.1.3 DEVELOPMENT IN THE INSTITUTE

The main activity lies in research and development of a calorimeter using room temperature liquids (1). A prototype modul with 15 mm Fe plates and using TMS (Tetramethylsilane) is under construction. The charge output as determined in a ionization chamber is shown in Fig. 1. A large purification system allowing to purify 50 ℓ/week is actually being assembled. In parallel, design work for a TMS hadron calorimeter using uranium as converter plates, material studies in a test ionization chamber and development of a new amplifier chain are under way. Other liquids like TMT (tetrame-

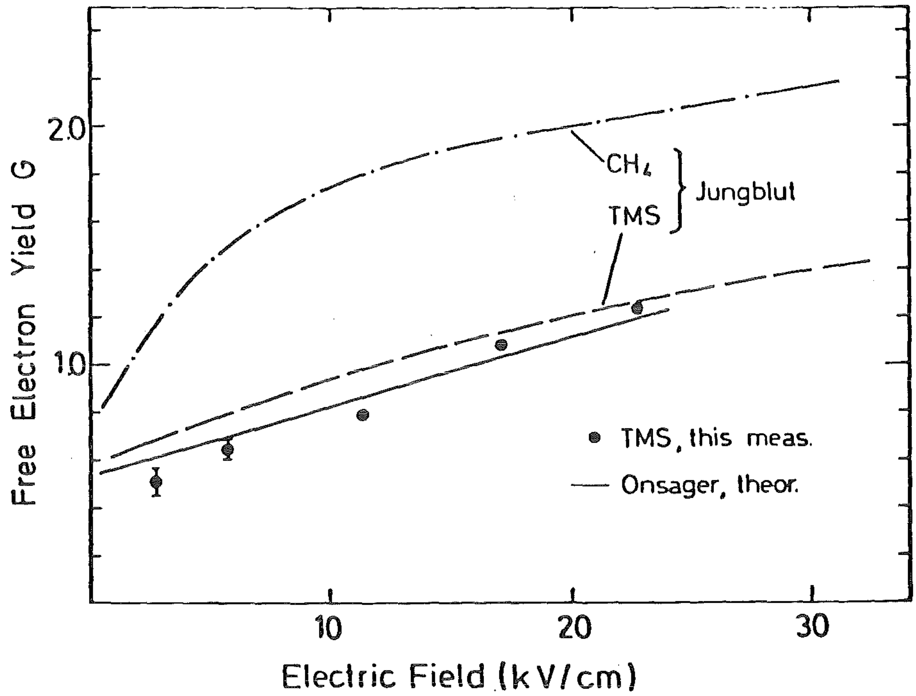

Fig. 1 The collected charge in an ionization chamber using Tetramethylsilane. G is the number of electrons per 100 eV deposited ionization charge. For comparison measurements of Jungbluth (Hahn-Meitner-Institut, Berlin) for methane and TMS.

thyltin) and TMAE (tetrakis-dimethylamino-ethylen) are under study.

(1) J. Engler and H. Keim, Nucl.Instr.Meth. 223 (1984) 47

5.2 ANALYSIS OF HADRONIC FINAL STATES AND TEST OF QCD

5.2.1 ON THE MODEL DEPENDENCE OF THE DETERMINATION OF THE STRONG COUPLING CONSTANT α_s

In a previous analysis of hadronic events obtained with the CELLO detector at PETRA we found that the determination of α_s using first order Monte Carlo calculations is model dependent (1).

It was claimed afterwards by other experiments (2,3), that this model dependence is reduced when including second order QCD calculations. We therefore started a detailed investigation on this question.

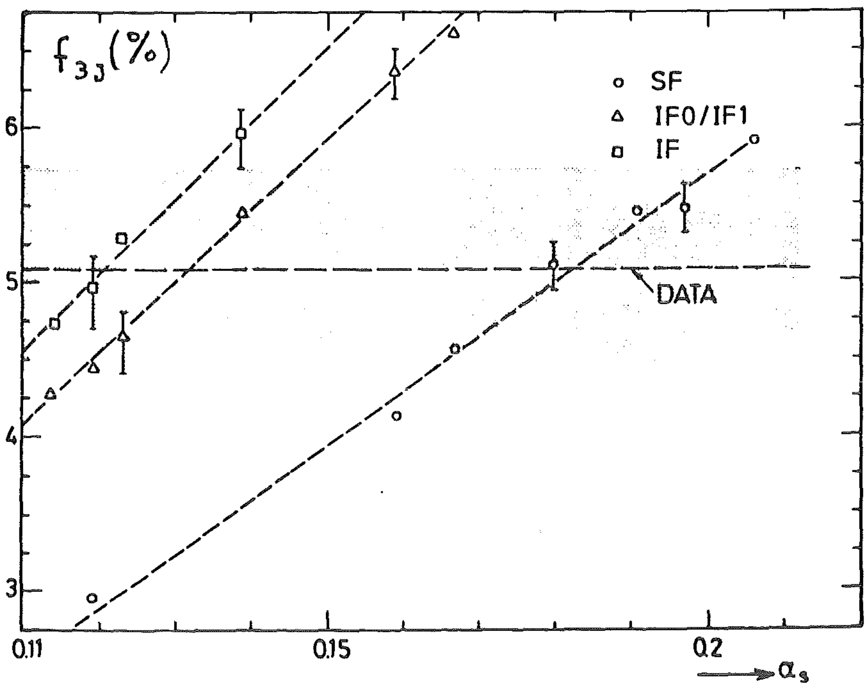

Fig. 1: Fraction of three cluster events as function of α_s for the two models and for different Energy-Momentum Conservation schemes (E.P.)

IFO: no E.P. conservation

IF1: Odorico E.P. conservation

IF: Hoyer E.P. conservation

SF: String Fragmentation

TABLE 1 Results from the shape analysis fits (second order QCD)

	Independent Fragmentation (IF)		String Fragmentation (SF)		SF/IF
	α_s	σ_q (MeV)	α_s	σ_q (MeV)	
Q-Plot & P_{Tout}	0.13 ±0.015	290 ±20	0.18 ±0.02	290 ±20	1.4
Thrust & Oblateness	0.13 ±0.015	300 ±20	0.19 ±0.02	300 ±20	1.5

We compared two different fragmentation models: String Fragmentation (SF: Lund-Sjöstrand) and Independent Fragmentation (IF: Ali, Hoyer) as described in (4). Two different methods for the determination of α_s were used:

a) Shape Analysis

The shape of hadronic events is mainly determined from the parton state, generated according to the formulae of perturbative QCD and their

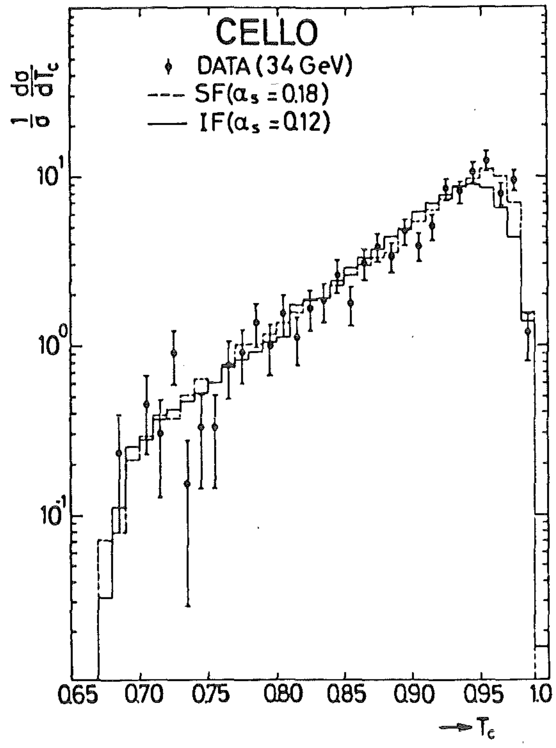

Fig. 2: Corrected Cluster Thrust from data compared with SF and IF. The corrections were independent of the fragmentation model.

TABLE 2: Results from the Cluster Analysis (second order QCD)

Model	SF	IF0	IF1	IF	SF/IF
α_s	0.18	0.13	0.13	0.12	1.5

subsequent fragmentation into hadrons. A fit of α_s and of the fragmentation model parameter σ_q was performed, in order to fit the shape of hadronic events. Therefore we choose pairs of distributions each one being particularly sensitive to one of the parameters.

Two combinations were tested: Q-Plot & $P_{T_{out}}$ and Thrust & Oblateness.

b) Cluster Analysis

Another determination of α_s has been made from events with three clusters and having a cluster thrust T_c smaller than 0.85. The three cluster events were selected with a cluster algorithm (5).

The error bars in Fig. 1 indicate the systematic errors coming from a variation in σ_q between 0.18 and 0.45 and variation in Y between 0.17 and 0.05. We also studied the influence of different Gluon-Fragmentation schemes. The difference between the two models is larger than the systematic error of 0.02. The shaded area gives the errors of data.

Conclusion:

The determination of α_s using Shape Analysis or Cluster Thrust is model dependent even in second order QCD.

(1) Annual Report on Nuclear Physics Activities, KfK 3621 (1983)
(2) MARK J Coll., B. Adeva et al., Phys.Rev.Lett. 50 (1983) 2051
(3) JADE Coll., W. Bartel et al., Phys.Lett. 119B (1982) 239
(4) T. Sjöstrand, Comp. Phys. Comm. 27 (1982) 243, ibid 28 (1983) 229
(5) CELLO Coll., H.-J. Behrend et al., Phys.Lett. 110B 3,4 (1981) 329

5.2.2 INCLUSIVE γ AND π^0 PRODUCTION IN e^+e^- ANNIHILATION AT 14, 22 AND 34 GeV c.m. ENERGY

We have measured the scale invariant inclusive photon and π^0 cross sections at W = 14, 22 and 34 GeV. A comparison with $\pi^\pm$ data shows no significant difference between neutral and charged pion production (1).

Comparing the integrated cross section in the x range $0.15 < x < 1.0$ we observe a considerable decrease from 14 GeV to 34 GeV with a statistical significance of 1.5 standard deviations. This is compatible with the expectations for scaling violations from QCD.

TABLE 1 Integrated inclusive cross section $\sigma = \int_{0.2}^{0.6} \frac{s}{\beta} \frac{d\sigma}{dx}$ for π^0 and $1/2\ (\pi^+ + \pi^-)$ (2)

W [GeV]	$\sigma\ (\pi^0)$ [μb GeV^2]	$\sigma(1/2(\pi^+ + \pi^-))$ [μb GeV^2]	$\frac{2\pi^0}{\pi^+ + \pi^-}$
14	0.204 ± 0.066	0.168 ± 0.021	1.21 ± 0.42
22	0.140 ± 0.055	0.146 ± 0.019	0.96 ± 0.40
34	0.137 ± 0.045	0.135 ± 0.016	1.01 ± 0.35

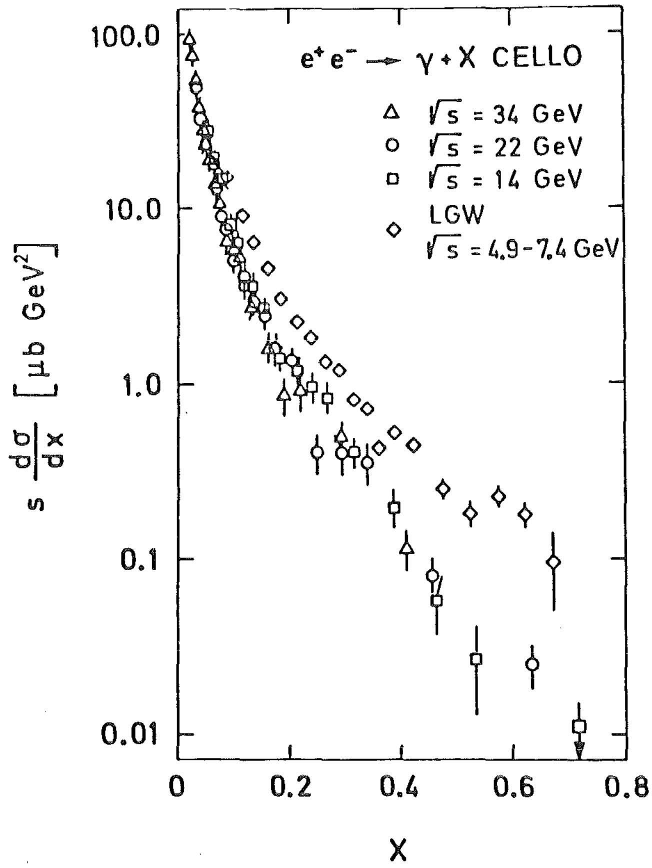

Fig. 1

Cross sections $s\,\frac{d\sigma}{dx}$ for inclusive photon production at W = 14, 22 and 34 GeV in comparison to data from SPEAR (3).

(1) TASSO Coll., R. Brandelik et al., Phys.Lett. 114B (1982) 66
MARK II Coll., J.F. Patrick et al., Phys.Rev.Lett. 49 (1982) 1232
TASSO Coll., R. Brandelik et al., Phys.Lett. 108B (1982) 71
TASSO Coll., R. Brandelik et al., Phys.Lett. 113B (1982) 98
(2) CELLO Collaboration, H.-J. Behrend et al., Z.f.Phys. C14 (1982) 189
(3) MARK I-LGW-Coll., D.L. Scharre et al., Phys.Rev.Lett. 41 (1978) 1005

5.3 SEARCH FOR NEW PARTICLES

5.3.1 SEARCH FOR NEW HEAVY QUARKS IN e^+e^- COLLISIONS UP TO 46.78 GeV C.M. ENERGY*

CELLO performed a measurement of the total e^+e^- annihilation cross section into multihadron final states up to a c.m. energy of 46.78 GeV, which is the highest energy reached in e^+e^- collisions so far.

Previous measurements (1,2) have shown that the ratio

* DESY 84-051, sumbitted to Phys.Lett. B

$R = \sigma(e^+e^- \rightarrow \text{hadrons})/\sigma_{point}$ is consistent with the quantum flavour dynamics (QFD) expectation for coloured u,d,s,c, and b quarks taking second order QCD and electroweak corrections into account. The main objective of this measurement was to search for the theoretically expected t quark of charge 2/3 e through the following signals:

- the existence of narrow resonances of $t\bar{t}$ bound states,
- an increase of R by approximately 4/3 above the $t\bar{t}$ production threshold,
- the occurence of events of large sphericity and aplanarity expected from decays of heavy hadrons containing the t quark, and
- the observation of leptons with high transverse momentum (p_T) with respect to the event axis initiated by the heavy flavour decays.

The data were taken at energies between 38.66 and 46.78 GeV in 1983 and 1984. A luminosity of 12.1 pb^{-1} was collected. The center of mass energy was varied in steps of 30 MeV. With a c.m. energy spread σ_W of about 37 MeV a continuous coverage of the following energy ranges was obtained:

$$38.66 < W < 38.78 \text{ GeV}$$
$$39.79 < W < 46.78 \text{ GeV}$$

The total number of multihadron events collected was 1998.

The trigger efficiency, detector acceptance, losses due to the cuts described, and radiative corrections (3) - dominated by hard photon radiation in the initial state - were determined by a Monte Carlo (MC) simulation of the experiment.

Multihadron events were generated using $q\bar{q}$ and $q\bar{q}g$ creation and fragmentation (4) (q = u,d,s,c,b).

The measured values of R as a function of W are shown in Figs. 1a) and b). Only statistical errors are shown. Systematic point to point variations are small compared to the statistical fluctuations. The data show neither a statistically significant narrow resonance nor an increase of R of the size expected for $t\bar{t}$ production.

To search for resonances much narrower than σ_W, the data was fitted by a Gaussian of width $\sigma_W = 2.2 \times 10^{-5}\ W^2/\text{GeV}$ taking into account radiative smearing (5) and a constant background. The integral over W of the hadronic cross section, σ_V, of a narrow $J^P = 1^-$ Breit Wigner resonance of mass M_V is given by:

$$\int \sigma_V(W)dW = \frac{6\pi^2}{M_V^2} \frac{\Gamma_{ee}\,\Gamma_{had}}{\Gamma_{tot}}$$

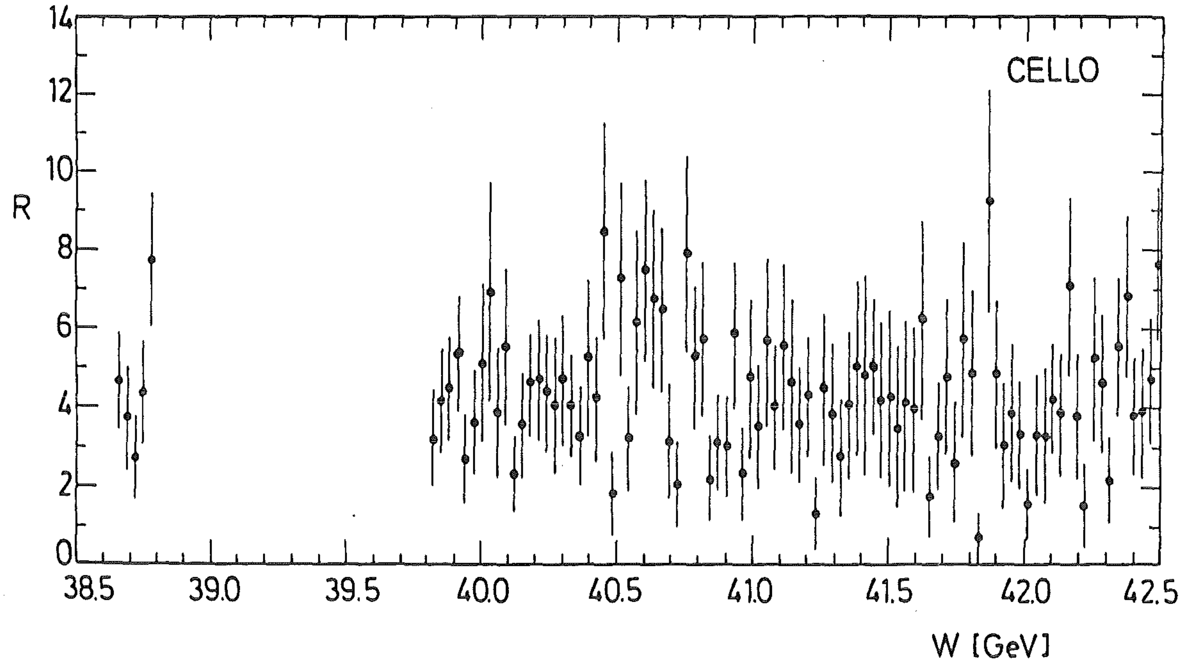

FIGURE 1a

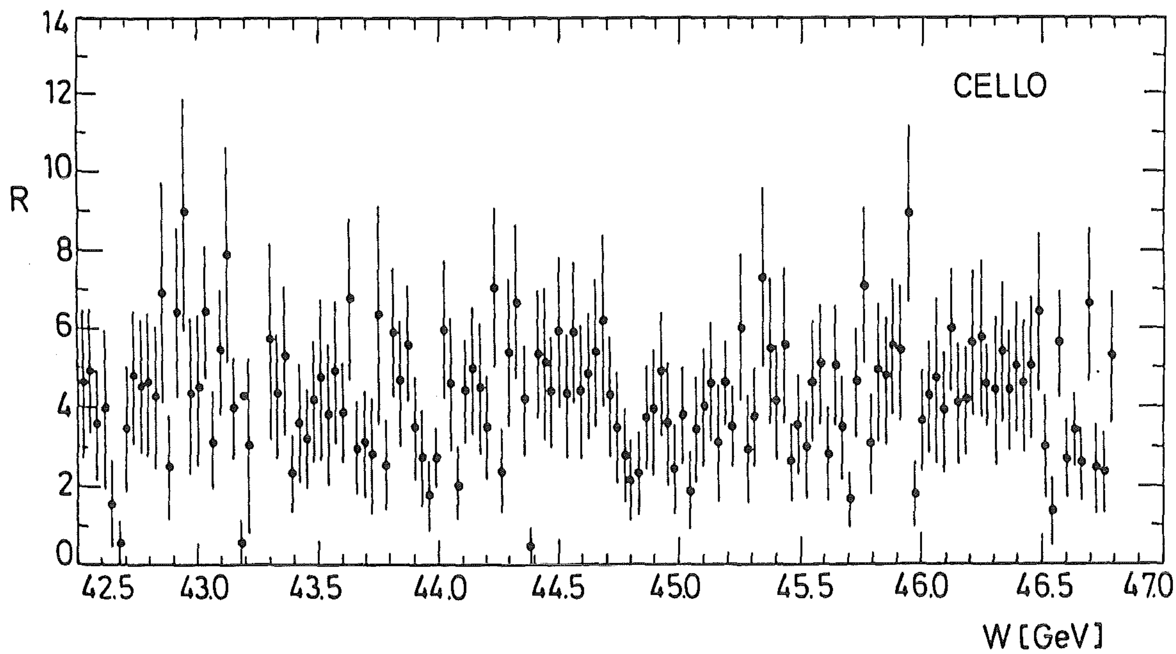

FIGURE 1b

Fig. 1: $R = \sigma(e^+e^- \rightarrow \text{hadrons})/\sigma_{point}$ vs c.m. energy W.
Only statistical errors are shown.

where Γ_{tot}, Γ_{ee}, and Γ_{had} are the total width and the partial decay widths into e^+e^- and hadrons respectively. The gaussian fit was found to be larggest for W = 42.94 GeV giving an upper limit of

$$B_{had} \cdot \Gamma_{ee} = \frac{\Gamma_{had}}{\Gamma_{tot}} \Gamma_{ee} < 2.9 \text{ keV}$$

at the 95% confidence level. For a quark of charge 2/3 e Γ_{ee} is expected to be between 4 and 5 keV (6). Assuming a hadronic branching fraction $\Gamma_{had}/\Gamma_{tot}$ of 0.8, our experimental upper limit on Γ_{ee} is well below a $t\bar{t}$ bound state in the covered mass range.

The average values of R for the energy scan is

$$R = 4.04 \pm 0.10 \text{ (statistical)} \pm 0.31 \text{ (systematic)}$$

Our estimate of the overall normalization uncertainty is dominated by the systematic errors of the MC simulation and the luminosity measurement.

The measured value is consistent with 4.01 expected for the five known quarks including second order QCD ($\alpha_s = 0.18$) (7) at $Q^2 = 1200$ GeV^2 in $\overline{MS}$-scheme) and electroweak ($\sin^2\theta_W = 0.22$) corrections. It strongly disfavours the existence of a t quark in or below our energy range, for which one expects R = 5.4 for the pointlike production of open top flavour.

Further evidence against the existence of a new heavy quark is obtained from an analysis of the aplanarity (8) distribution of multihadronic events. Fig. 2 shows the observed aplanarity A for the data from W = 45.7 to 46.78 GeV. The data are in good agreement with a Monte Carlo simulation involving the known 5 quarks and QCD corrections up to second order. Also shown in Fig. 2 is the MC simulation, if one adds the pointlike production of a new quark with a mass of 21 GeV an charge e_q with a change in R of 3 e_q^2.

As can be seen, the data above 45.7 GeV clearly rules out both charge possibilities of 1/3 e and 2/3 e. A limit on the threshold W_{th} for the continuum production of new flavours has been obtained by varying W_{th} up to the energy, where the MC prediction for the number of aplanar events ($A > 0.1$) for 6 quarks equals the 95% confidence level upper limit on the observed number of aplanar events above W_{th}.

Assuming a contribution to R above W_{th} of 3 e_q^2, we find that the continuum production of a new quark is ruled out at 95% confidence level below c.m. energies of 45.4 and 46.6 GeV for quark charges 1/3 e and 2/3 e, respectively.

The study of inclusive production of leptons with high transverse momentum (p_T) with respect to the event axis provides a sensitive test for the open production of a new heavy quark. Depending on the mass of the parent hadron, leptons resulting from the semileptonic decay dominate diffe-

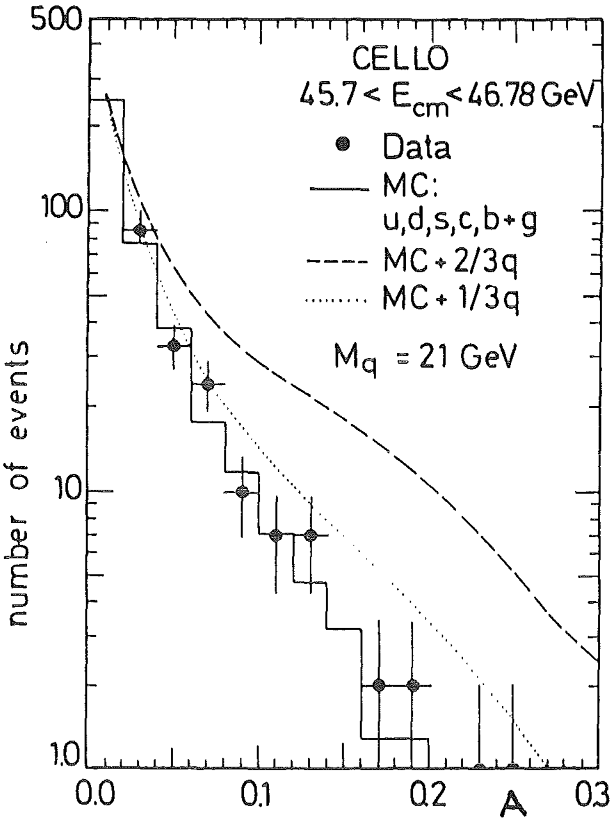

Fig.: 2
Distribution of events in aplanarity for data above c.m. energies of 45.7 GeV.
The solid line represents a MC simulation of $q\bar{q}$ and $q\bar{q}g$ production and fragmentation with q = u,d,s,c,b.
The dashed (dotted) line includes an additional quark with charge 2/2 (1/3) e and a mass of 21 GeV.

rent regions in the (p_T)-distribution: Whereas the u,d,s, and c quarks yield leptons with rather small p_T (typically p_T < 1.0 GeV/c), the region p_T > 1.0 GeV/c is dominated by the decay of hadrons containing a b-quark. Open pair production of a heavy quark carrying a new flavour (t,b') will result in an excess of leptons in this large p_T region.

CELLO makes uses of both the electron and muon channels.

To identify electrons all track measured in the inner detector have been extrapolated to the LAr calorimeter. Then we demand the longitudinal and lateral shower distributions to be compatible with a distribution as expected from a single electron. All cut-off parameters have been optimized with respect to π/e-separation by comparison with detailed MC simulations.

The electron identification efficiency increases from 49% at 1.5 GeV up to 73% at 4 GeV. In this energy range we obtain typically a π-misidentification probability of $3 \cdot 10^{-3}$.

To identify muons, space points reconstructed in the muon chambers outside our hadron filter of ~ 1 m of iron are associated with the charged particles recorded by the central detector and extrapolated to the chambers. The uncertainties due to the track reconstruction in the central detector, multiple Coulomb scattering in the hadronic filter and distortions of the extrapolation through the magnetic field are taken into account.

There are two different background sources: Random associations between tracks and background hits in the muon chambers, π/K-decay and hadron punch through. The hadron misidentification probability from π/K-decay and hadron punch through is typically $(5 \pm 1) \cdot 10^{-3}$ at 2 GeV and $(12 \pm 2) \cdot 10^{-3}$ at 7 GeV. As can be seen from Tables 1 and 2, the dominant lepton at high p_T sources is the semileptonic decay of the b quark which amounts to 56.4% in the electron case and to 31% in the muon case (not taking int account the cascade process $b \to c \to e, \mu$). The total number of electrons is expected to be 3.7 (1.7 for events with $T < 0.85$), that of muons to be 5.9. Applying the same cuts to the data we find 1 electron (0 for events with $T < 0.85$) and 5 muons (all in events with $T < 0.85$). These values are thus compatible with the MC expectations based on the pair production of 5 quarks including second order QCD effects.

For a standard value of the semileptonic branching ratio of 10% the production of a $Q = 2/3$ quark is excluded by our data up to a c.m. energy of 45.8 GeV (corresponding to a quark mass of 22.9 GeV) for the decay into both electrons and muons. Our present statistics does not allow a similar conclusion for a $Q = 1/3$ quark.

TABLE 1 Contributions to the electron yield in the region $p > 1.0$ GeV/c and $p_T > 1.0$ GeV/c expected in the 5-quark QCD model (4).

Source of electrons	Events	
Light quarks (u,d,s)		
Misidentified π/K's	0.27	7.3%
Converted γ's, π/K-decay	0.07	1.8%
Inelastic Compton effect	0.05	1.4%
Deep inelastic Scattering	0.14	3.7%
Heavy quarks (c,b)		
Misidentfied π/K's	0.21	5.7%
Converted γ's, π/K-decay	0.13	3.5%
$c \to e$, $b \to c \to e$	0.75	20.2%
$b \to e$	2.09	56.4%
Number of electron candidates expected		
Total	3.7	
In events with $T < 0.85$	1.7	

TABLE 2 Contributions to the muon yield in the region $p > 2.0$ GeV/c and $p_T > 2.0$ GeV/c expected in the 5-quark QCD model (4).

Source of muons	Events	
π/K-decay	0.8	14%
Hadron punch-through	1.2	20%
Random associations	1.6	27%
$c \to \mu$, $b \to c \to \mu$	0.5	8%
$b \to \mu$	1.8	31%
Total number of muon candidates expected	5.9	

In conclusion, the average value of R up to the highest c.m. energies obtained in e^+e^- annihilation - 46.78 GeV - is in good agreement with the QFD expectation for 5 coloured quarks.

The absence of narrow resonances in our data excludes the existence of a new quark with charge 2/3 e in the scanned energy range. A new quark with charge 2/3 e at lower masses is excluded by the average value of R. The sensitivity for new quarks can be enhanced by searching for aplanar final states. From the number of events with aplanarity > 0.1, we rule out at the 95% confidence level the pointlike continuum production of new flavours below 45.4 GeV/c for a quark charge of 1/3 e and below 46.6 GeV/c for a quark charge of 2/3 e. Furtheron the nonobservation of an excess of high p_T leptons rules out the charge 2/3 e quark up to W = 45.8 GeV.

(1) MARK J Coll., D.P. Barber et al., Phys.Rev.Lett 43 (1979), 901
PLUTO Coll., Ch. Berger et al., Phys.Lett. 81B (1979), 410
TASSO Coll., R. Brandelik et al., Phys.Lett. 83B (1979), 261
and Phys.Lett. 138B (1984), 441
JADE Coll., W. Bartel et al., Phys.Lett. 88B (1979), 171
and Phys.Lett. 100B (1981), 364
MARK J Coll., B. Adeva et al., MIT Technical Report Number 134 (1984)
A review of older data can be found e.g. in S. Yamada, Proc. 1983, Int. Symp. on Lepton and Photon Int. at High Energies, Cornell (1983)

(2) CELLO Coll., H.-J. Behrend et al., Proceedings Int. Conf. on High Energy Physics, Lisbon, July 9-15 (1981), 751

(3) G. Bonneaud and F. Martin, Nucl.Phys. B27 (1971), 381
F.A. Berends and G.J. Komen, Phys.Lett. 63B (1976), 432

(4) T. Sjöstrand, Computer Physics Comm. 27 (1982), 243
T. Sjöstrand, Computer Physics Comm. 28 (1983), 229
B. Anderson, G. Gustafson, T. Sjöstrand, Z.f.Phys. C6 (1980), 235
B. Anderson, G. Gustafson, T. Sjöstrand, Nucl.Phys. B197 (1982), 45
(5) J.D. Jackson and D.L. Scharre, Nucl.Instr.Meth. 128 (1975), 13
(6) D.R. Yennie, Phys.Rev.Lett. 34 (1975), 239
M. Kramer, H. Krasemann, and S. Ono, DESY 80/25 (1980)
W. Buchmüller and S.-H.H. Tye, Phys.Rev. D24 (1981), 132
(7) CELLO Coll., H.-J. Behrend et al., Phys.Lett. 138B (1984), 311
(8) The aplanarity A = 3/2 Q1, where Q1 is the smallest eigenvalue of the momentum tensor, proposed by J.D. Bjorken, S. Brodsky, Phys.Rev. D1 (1970), 1416

5.3.2 LIMITS ON SPIN 0 BOSONS IN e^+e^- ANNIHILATION UP TO 45.2 GeV C.M. ENERGY

The occurence of scalar or pseudoscalar spin 0 bosons is expected in models in which the weak gauge bosons are composite (1-5). The observation of an excess of radiative Z^0 decay was an experimental hint for their existence (6). We have studied the reactions

$$e^+e^- \rightarrow e^+e^- \qquad (1)$$

$$e^+e^- \rightarrow \gamma\gamma \qquad (2)$$

$$e^+e^- \rightarrow \mu^+\mu^- \qquad (3)$$

$$e^+e^- \rightarrow \tau^+\tau^- \qquad (4)$$

in the center-of-mass (c.m. = energy range from 39.8 to 45.2 GeV using the CELLO detector at PETRA. We have determined upper limits on the partial width for new spin 0 bosons within and above the energy range covered.

A spinless boson X contributes isotropic to the differential cross section $d\sigma/d\Omega$ of the four reactions. Due to interference effects between s- and t-channel exchange in reaction (1), it causes some additional modifications of $d\sigma/d\Omega_{ee}$ (5,7). If the boson mass lies within the energy range, a resonant effect should be seen in the cross section for the four reactions.

The fit to our data gives no evidence for contributions of such new particles up to the highest PETRA energies. Their existence is ruled out for all suggested models at the 95% confidence level for X masses below the Z^0 mass, if the radiative width Γ_r of the Z^0 is $>$ 20 MeV. The allowed boson masses (for lower Γ_r) and the limits on the coupling constant α_H are shown in Fig. 1.

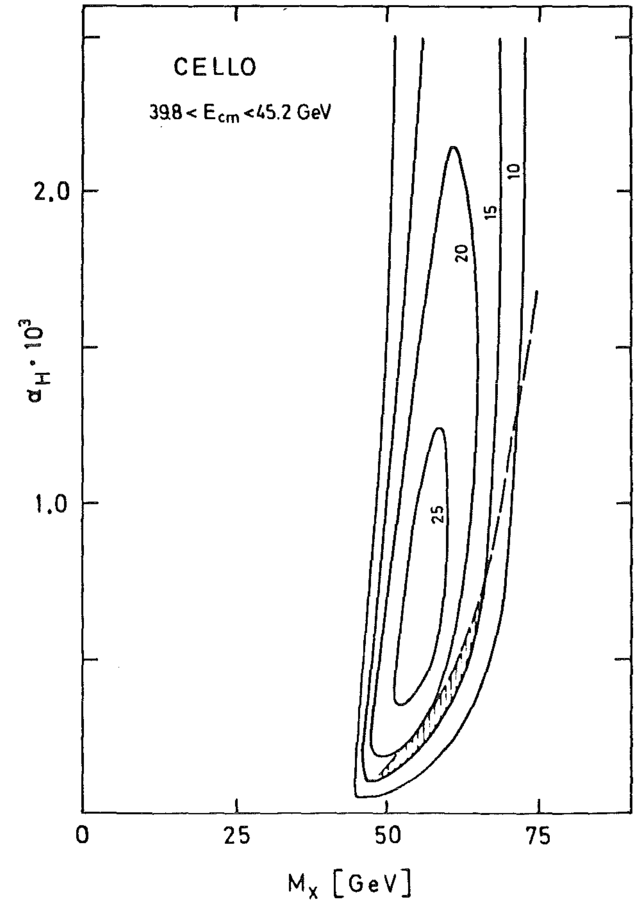

Fig. 1:
Limits of the 95% C.L. for the universal coupling constant α_H as a function of the mass M_X of the spinless boson from fits to the differential cross sections of $e^+e^- \rightarrow e^+e^-$ (dashed line) and $e^+e^- \rightarrow \gamma\gamma$ (solid contours for different values of the radiative width Γ_r of the Z^0. The numbers on the contours denote Γ_r in MeV). $\varepsilon = 1$ is assumed. The hatched area indicates the region allowed by the data for $\Gamma_r > 15$ MeV.

(1) R.D. Peccei, Preprint MPI-PAE/PTH 80/83 (1983), Phys.Lett. 136B (1984) 121
(2) U. Baur, H. Fritzsch and H. Faissner, Phys.Lett. 135B (1984) 313
(3) F.M. Renard, Preprint PM/83/11 (1983)
(4) F.W. Bopp et al., Preprint SI-83-23 (1983), SI-84-3 (1984)
(5) W. Hollik, B. Schrempp and F. Schrempp, DESY Report 81-011 (1984), to be published
(6) UA1-collaboration, G. Arnison et al., Phys.Lett. 135B (1984) 250
UA2-collaboration, P. Bagnaia et al., Phys.Lett. 129B (1983) 130
(7) D. Düsedau and R.D. Peccei, private communication
F.M. Renard, private communication

5.3.3 OBSERVATION OF A MULTIPARTICLE EVENT WITH 2 ISOLATED ENERGETIC MUONS IN e^+e^- INTERACTIONS*

High energy data between 43.2 and 45.2 GeV center of mass energy taken late in 1983 by the CELLO detector at PETRA (1) have been analysed to

* DESY Report 84-024, to be published in Phys.Lett. B

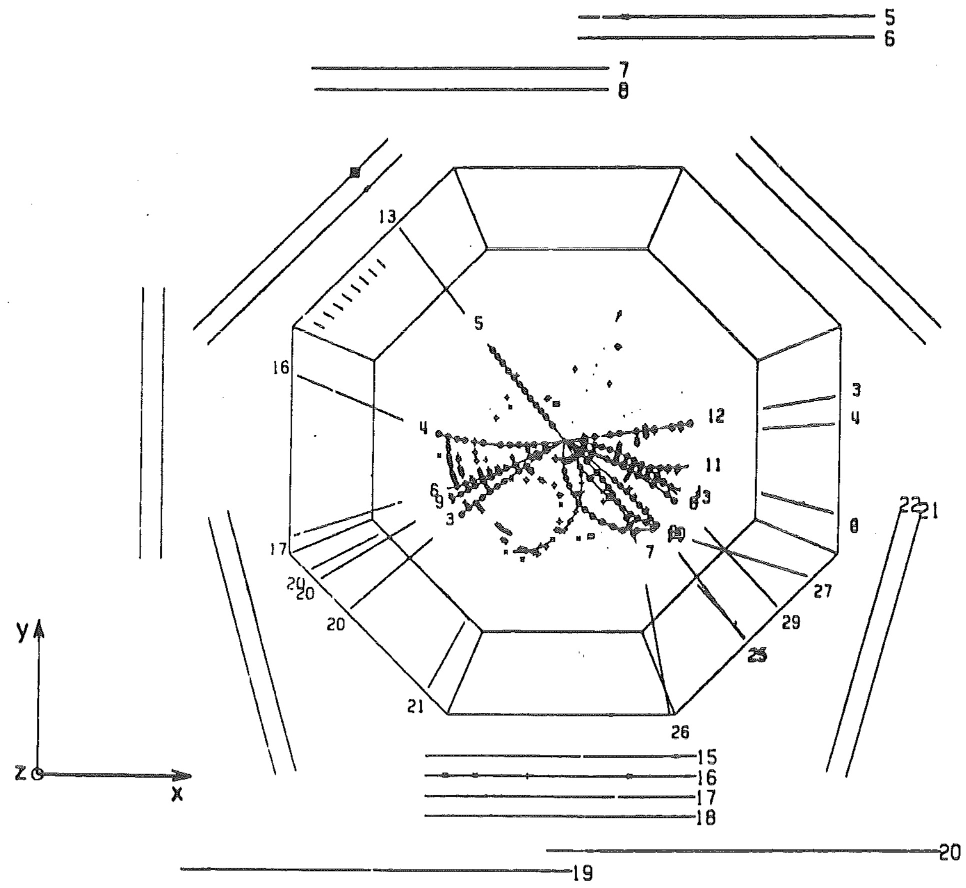

Fig. 1: Event view in the plane perpendicular to the beam axis. The coordinate system is indicated.

search for multihadronic events with isolated muons. The data correspond to an integrated luminosity of 3.9 pb^{-1}. Such events might indicate the production of new particles. This search has led to the finding of an unusual event where most of the center of mass energy is shared between the charged particles and two topologically isolated energetic muons.

A view of the event in the plane perpendicular to the beam axis is shown in Fig. 1. The event has a low aplanarity of A $\simeq$ 0.003 and has the structure of two subsystems each containing a high momentum muon back to back to a jet of hadrons. This structure is evident also from the nearly equal masses found when the jet an the muon are paired in this way. There is almost no additional energy detected in the calorimeter.

Sphericitiy and thrust values are respectively 0.36 and 0.86. Transverse momenta relative to the thrust axis are 7.2 GeV/c for the μ^+ is cos θ_{min} $\simeq$ 0.47 while the closest one to the μ^- is at cos θ_{min} $\simeq$ 0.97. Values for muon and jet momenta and μ-μ and μ-jet invariant masses are given in Table 1(a,b).

TABLE 1(a) Muon and jet four vectors

(GeV)	E	p_x	p_y	p_z	M
μ^+	11.0	-7.0	8.5	.5	.105
μ^-	12.6	11.0	1.3	-6.1	.105
jet 1	10.1	-7.4	-4.2	4.8	2.4
jet 2	9.1	6.7	-3.5	-2.0	4.7

TABLE 1(b): Invariant masses

Masses (GeV)	μ^+	μ^-	jet 1
jet 1	19.4 ± 1.3	9.5 ± .5	17.3 ± .3
jet 2	14.1 ± 1.0	22.2 ± 1.6	
μ^-	20.4 ± 1.1		

We have considered whether conventional sources of events with muon pairs could account for this event: for example muons from semi-leptonic decays of heavy quarks and meson decays in flight or punch-through and background in the muon chambers rendering fake muon signals.

We estimated these contibutions using the Lund (2) Monte Carlo event generator and considering in particular cos θ_{min}, the cosinus of the angle between the muon and the closest hadron. Table 2 shows the number of expected hadron faking 2 muons and (in brackets) the number of muons from the decay of b and e quarks as a function of cos θ_{min}.

The probability, that semileptonic decays of D or B mesons or punch through muons yield energetic isolated muons as seen in our event, is ac-

TABLE 2 Expected Number of Events from $e^+e^- \to q\bar{q}(g)$
Numbers are given for the expected number of isolated hadrons faking 2 muons, and for the semileptonic decay of b and c quarks in brackets

$p > 6$ GeV/c	$\cos\theta_{min} < .98$	$\cos\theta_{min} < .9$	$\cos\theta_{min} < .8$	$\cos\theta_{min} < .5$
$\cos\theta_{min} < .98$	$2.7\ 10^{-2}$ ($2.\ 10^{-2}$)			
$\cos\theta_{min} < .9$	$1.6\ 10^{-2}$ ($1.3\ 10^{-2}$)	$6.1\ 10^{-3}$ ($5.\ 10^{-3}$)		
$\cos\theta_{min} < .8$	$4.\ 10^{-3}$ ($2.5\ 10^{-3}$)	$1.8\ 10^{-3}$ ($1.6\ 10^{-3}$)	$< 8.\ 10^{-4}$ ($< 8.\ 10^{-4}$)	
$\cos\theta_{min} < .5$	$< 8.\ 10^{-4}$ ($< 8.\ 10^{-4}$)	$< 8.\ 10^{-4}$ ($< 8.\ 10^{-4}$)	$< 8.\ 10^{-4}$ ($< 8.\ 10^{-4}$)	$< 8.\ 10^{-4}$ ($< 8.\ 10^{-4}$)

cording to our estimates less than 10^{-3} (normalized to our integrated luminosity).

We have also estimated the probability of electromagnetic processes of order α^4 rendering a final state of 2 muons and 2 jets by using an approximation for the main contribution of the corresponding Feynman diagrams (Fig. 2) (3).

We have computed the expected number of events within our selection criteria for $\mu\mu$ and $q\bar{q}$ masses larger than 5 GeV/c^2. The results are given in Fig. 3. We find the probability to observe one event of this process with $\mu\mu$ and $q\bar{q}$ masses equal to or greater than the observed masses with less than $(3.2 \pm 1.0)\ 10^{-4}$.

Non-conventional dimuon sources are for example the production of new heavy quarks, of Higgs particles, of charged spin 1/2 new heavy leptons or of heavy neutrinos.

The production of new heavy quarks could give rise to muons with a large p_T with respect to the event thrust axis. However, the non-observation of a narrow resonance below 43.450 GeV and the absence of a step

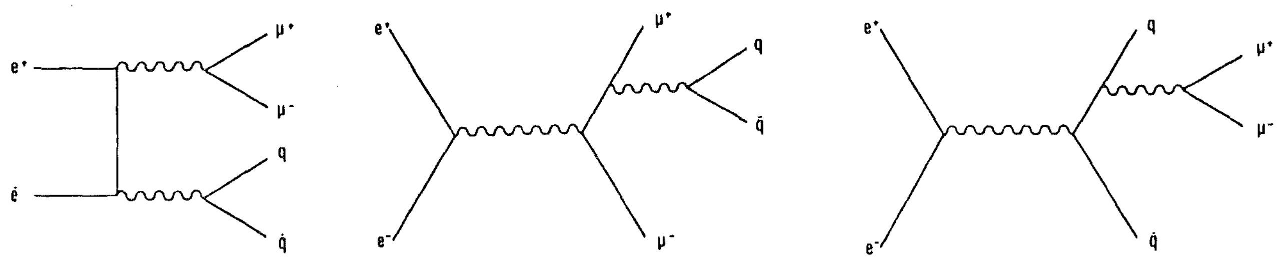

Fig. 2: Feynman graphs for $e^+e^- \rightarrow q\bar{q}\mu^+\mu^-$ for order α^4.

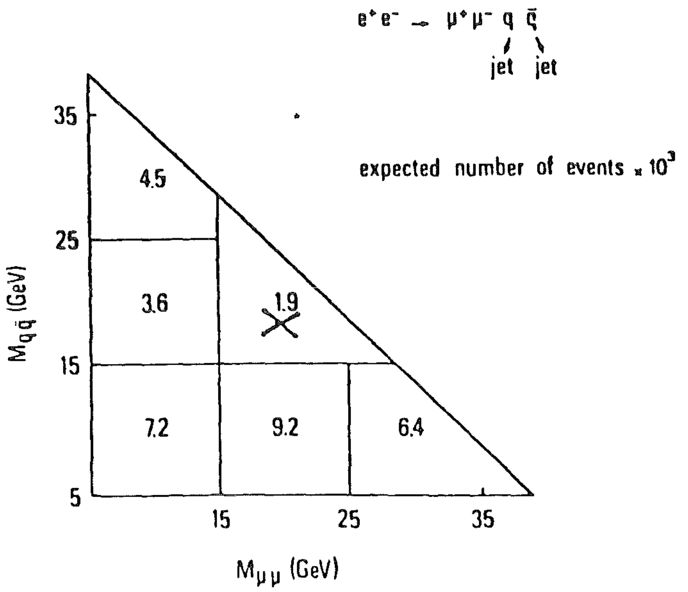

Fig. 3: Number of expected events ($\times\ 10^3$) for $e^+e^- \rightarrow q\bar{q}\ \mu^+\mu^-$ process within acceptance and selection criteria as a function of $\mu^+\mu^-$ and $q\bar{q}$ masses estimated from the diagrams in Fig. 2; indicated is the position of the event found.

(ΔR = 1.3) in the measurement of the R ratio at PETRA rule out the production of a charged 2/3 t quark.

For Higgs-like charged particles H^+H^-, the Higgs coupling constants are proportional to the mass of the fermions into which they decay. Thus ν_τ τ, $c\bar{s}$ and $c\bar{b}$ decays are favoured. In order to obtain at least one isolated muon, the decay of one of the Higgs particles into ν_τ τ can be invoked, however substantial energy should be missing in that case, and the energy of all charged particles excluding one of the muons should be less than the beam energy. Since this last condition is not fulfilled, this possibility can be rejected.

The cross section for the production of spin one half charged heavy leptons $L^\pm$ increases rapidly near threshold

$$\sigma(e^+e^- \rightarrow L^+L^-) = \frac{2\pi\alpha^2}{3s}\ \beta\ (3-\beta^2) \text{ with } \beta = \left[\ 1 - \frac{4M_L^2}{s}\right]^{1/2}$$

A sequential charged heavy lepton with a mass of 21.6 GeV/c ^{2} would lead to three expected events for BR($L^{\pm} \to \mu$ + neutrinos) $\simeq$ 0.1. Similar arguments as given in the previous paragraph rule out this possibility.

The pair production of a heavy muon close to threshold would explain the observed toplogy if the μ^* decays to μ + hadrons. However, about 30 such events for center of mass energies between 43.450 and 45.2 GeV and for a μ^* mass of 21.725 GeV/c ^{2} would be expected.

Pair production of a heavy neutrino has been estimated using

$$\sigma(e^+e^- \to \nu_H \bar{\nu}_H) = \frac{G^2}{96\pi} \frac{s\, M_Z{}^4}{(s-M_Z^2)^2} \beta\,(3+\beta^2)\ [1 - 4\sin^2\theta_W + 8\sin^4\theta_W]$$

with G the Fermi constant, M_Z the Z^0 mass and θ_W the Weinberg angle. For a 20 GeV/c ^{2} neutrino, the cross section is of the order of 0.3 pb (i.e. 1.2 events are expected).

The lifetime for a heavy neutrino can be expressed by

$$\tau_H = \tau_\mu \left(\frac{M_\mu}{M_H}\right)^5 BR(W^+ \to e\ \nu) \frac{1}{\sum_\ell |U_{\ell H}|^2}$$

where τ_μ is the μ lifetime, M_μ and M_H the μ and the ν_H masses, BR($W^+ \to e\,\nu$) the branching ratio of the virtual W to electron ($\simeq$ .1), and $U_{\ell H}$ the elements of the lepton mixing matrix. Since the common vertex of charged particles is close to the interaction point, we estimate the lifetime to be less than 10^{-10} s. A 20 GeV/c ^{2} neutrino would not severely constrain the mixing angles ($\Sigma |U_{\ell H}|^2 > 9.\ 10^{-9}$). But taking a V - A coupling, the mass recoiling against the muon should be peaked around $M_H/2$. The observed jet masses are substantially lower than this value.

We have also considered the possible production of a pair of spin 0 heavy muonic neutrinos as predicted by supersymmetric models. In this case, the rate would be small for a 20 GeV/c ^{2} neutrino, essentially because of the β^2 threshold behaviour (.12 event expected). It is also not clear that the observed event would fit naturally in the phenomenological framework describing the decay of these objects (4).

In summary, we have found one multihadronic event with two isolated energetic muons in which both the hadronic and dimuon masses are large. We expect of the order of 10^{-3} events of this kind from conventional sources.

(1) CELLO-Coll., H.-J. Behrend et al., Physica Scripta 23 (1981) 610
(2) B. Anderson, G. Gustafson, T. Sjöstrand, Phys.Lett. 98B (1980) 211

(3) R. Kleiss has since evaluated the α^4 QED cross section for $e^+e^- \rightarrow \mu^+\mu^-q\bar{q}$ for our configuration using all six contributing graphs and finds good agreement with our results.
R. Kleiss, preprint Institute Lorentz, Leiden (1984)

(4) R.M. Barnett et al., Phys.Rev.Lett. 51 (1983) 176

5.3.4 INVESTIGATION OF $e^+e^-e^+e^-$ AND $e^+e^-\mu^+\mu^-$ FINAL STATES IN e^+e^- INTERACTIONS

Electron-positron interactions going to the final states $e^+e^-e^+e^-$ and $e^+e^-\mu^+\mu^-$ have been looked for in the CELLO detector at PETRA.

Four lepton final states coming from e^+e^- interactions are examples of order α^4 QED processes. All available results so far have been produced in connection with 2-photon interactions where 2 electrons (no-tag) or 1 (single tag) are (is) undetected and go(es) at small angles with respect to the beam axis (1). In these kinematic regions, cross sections are dominated by the 2 multiperipheral processes (Fig. 1a,b).

Requiring that all leptons be emitted at large angle is of twofold interest. Firstly, in this domain, virtual bremsstrahlung processes (Fig. 1c) are expected to be dominant. Secondly, if high mass new particles decaying to leptons are being produced, an excess of events would appear above the QED prediction.

Complete calculations of all possible diagrams of order α^4 have been made recently by R. Kleiss (2). We have used these calculations introducing our acceptance cuts and our efficiencies in order to compute the expected number of events and distributions. Table 1 shows the results of the comparison between the observed number of events and the QED prediction.

We have observed 8 events where the four particles emerge at large angle ($> 23^0$) with respect to the beam axis. This number is consistent with the QED prediction of 6.3, although there is some indication of an experimental excess for events where large mass systems of zero leptonic charge are produced. One of those high mass events has a low aplanarity.

(1) M. Pohl in proceedings of photon-photon collisions, Aachen (1983), Ed. Ch. Berger
CELLO Coll., H.-J. Behrend et al., Phys.Lett. 126B (1983) 384
(see also 2 photon analysis of the PLUTO and MARK J Collaborations quoted there)

(2) R. Kleiss
Preprint Instituut-Lorentz, Leiden (1984)

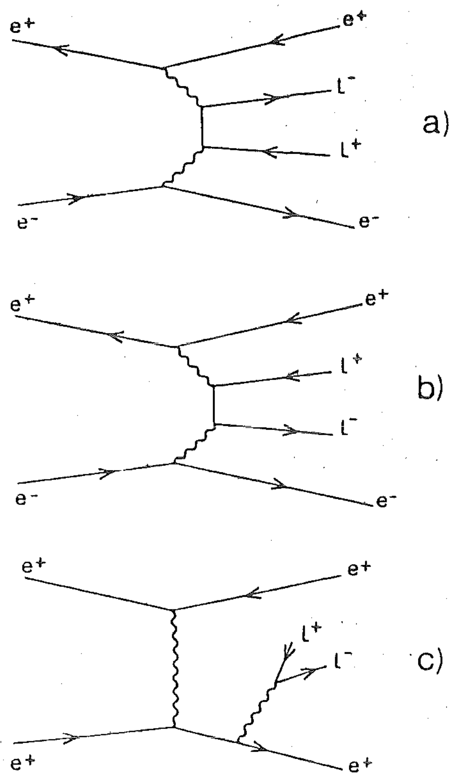

Fig. 1a) and 1b) Multiperipheral diagrams.
c) An example of virtual bremsstrahlung diagram.

TABLE 1

C.M. energy GeV	Integrated Luminosity (pb^{-1})	Process ($e = e^+e^-e^+e^-$, $\mu = e^+e^-\mu^+\mu^-$)	Expected number of events from QED	Observed number of events
42.5 (average)	8.95	μ	1.09	1
		e	1.16	1
34.0	7.7	μ	1.16	1
		e	1.11	2
22.0	2.5	μ	0.61	0
		e	0.49	1
14.0	1.0	μ	0.36	1
		e	0.29	1
TOTAL		μ	3.23	3
		e	3.05	5
		e+μ	6.28	8

5.3.5 SEARCH FOR SCALAR ELECTRONS AND NEUTRALINOS IN e^+e^- INTERACTIONS

Supersymmetry is a symmetry between fermions and bosons (1). The main feature of supersymmetric models is the prediction of a supersymmetric partner for each known particle whose spins differ by 1/2. Supersymmetry predicts the couplings of these new particles to be the same as for their ordinary partners. Since no supersymmetric particles have been observed yet, supersymmetry must be broken. The details of this symmetry breaking are unknown. Therefore there are essentially no predictions for the masses of the supersymmetric particles.

The supersymmetric partner of the electron, the scalar electron $\tilde{e}$, could be pair produced via photino exchange or annihilation into a virtual photon (2,3)

$$e^+e^- \rightarrow \tilde{e}^+\tilde{e}^- \qquad (1)$$

The $\tilde{e}$ is expected to decay immediately into an electron and a photino $\tilde{\gamma}$ being the spin 1/2 partner of the photon. The photinos escape the detector unobserved carrying away energy and momentum leading to a signature e^+e^- + missing energy. The cross section for $\tilde{e}$ pair production depends on the mass of the photino exchanged in the t channel.

In addition to the $\tilde{\gamma}$, supersymmetry predicts spin 1/2 partners of the vector bosons, the gauginos zino $\tilde{z}$ and wino $\tilde{w}$, and (at least) four spin 1/2 partners of the higgs mesons: the higgsinos $\tilde{h}_1^0$, $\tilde{h}_2^0$, $\tilde{h}^+$, and $\tilde{h}^-$. In general, the mass eigenstates of the two lowest lying uncoloured neutral supersymmetric fermions (neutralinos), $\tilde{\gamma}_1$, and $\tilde{\gamma}_2$, can be a mixture of $\tilde{\gamma}$, $\tilde{z}$, $\tilde{h}_1^0$, and $\tilde{h}_2^0$ (2). $\tilde{e}_1$ and $\tilde{e}_2$ could be produced in e^+e^- interactions via scalar electron exchange (4,5,6) (see Fig. 1a):

$$e^+e^- \rightarrow \tilde{\gamma}_1\tilde{\gamma}_2 \qquad (2)$$

The $\tilde{\gamma}_2$ is expected to decay into $e^+e^-\tilde{\gamma}_1$ (4,5,6) (see Fig. 1b) with a branching ratio sensitively depending on the mixing and on the whole mass spectrum of supersymmetric particles. The signature for this processes would be the same as for $\tilde{e}$ pair production, namely e^+e^- + missing energy carried away by the lightest neutralino $\tilde{\gamma}_1$.

This experiment has been performed using the CELLO detector at PETRA (7).

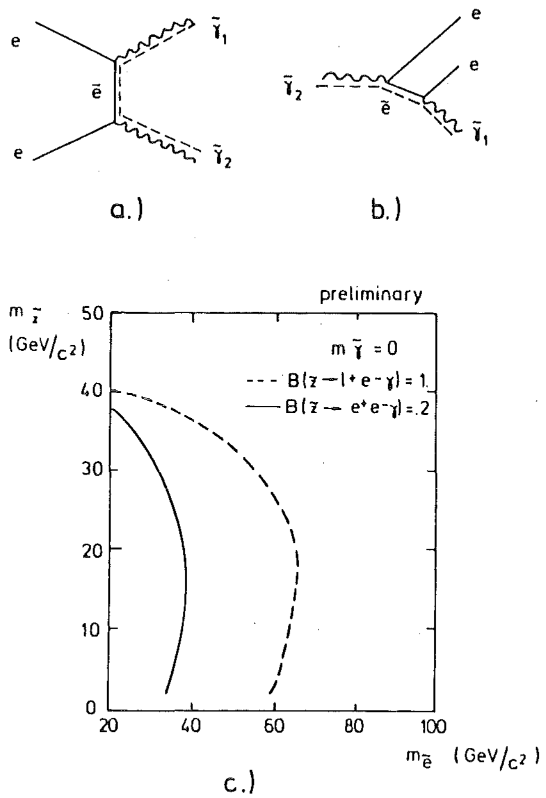

Fig. 1a Diagram for neutralino pair production

Fig. 1b Diagram for the decay of $\tilde{\gamma}_2 \rightarrow e^+e^-\tilde{\gamma}_1$

Fig. 1c 95% C.L. contours for lower limits of masses $m_{\tilde{Z}}$ and $m_{\tilde{e}}$ under the assumptions:

- $\tilde{\gamma}_1$ and $\tilde{\gamma}_2$ are pure $\tilde{\gamma}$ and $\tilde{Z}$ (no mixing)
- $m_{\tilde{\gamma}} = 0$
- $m_{\tilde{e},L} = m_{\tilde{e},R}$ ($m_{\tilde{e},L} \gg m_{\tilde{e},R}$ reduces the cross-section by a factor of ~ 2)
- $B(\tilde{\gamma}_2 \rightarrow e^+e^-\tilde{\gamma}_1) =$ 20% and 100% (see figure).

Triggers relevant for this analysis were

- one track candidate and at least 3 to 4 GeV (depending on the running period) energy deposition in one calorimeter module or
- an energy deposition of at least 4 to 5 GeV in two modules separated by at least 45^0 in the azimuth.

Calorimeter trigger efficiencies were determined from electrons from radiative Bhabha scattering triggered independently from the central calorimeter. The combined trigger efficiency for events of the type e^+e^- missing energy was found to be greater than 98%.

This analysis is based on 8.1 pb^{-1} of data collected at center of mass energies between 40.2 GeV and 44.9 GeV with $\sqrt{s}$ = 42.5 GeV. The following criteria were applied to select the data:

- two tracks in the inner detector within $|\cos\theta| < .85$ originating from the vertex
- acoplanarity of the two tracks between 30^0 and 170^0
- track momentum or energy of an associated shower $>$ 6 GeV for one track and $>$ 2.5 GeV for the other track
- both tracks must point into the fiducial volume of a calorimeter module to ensure a good particle identification

- polar angle of the missing momentum vector $|\cos\theta_{p\ miss}|$ is outside the range from .85 to .93 (i.e. the gap between the central and end cap calorimeter of CELLO).

Within 8.1 pb^{-1} of data no event was observed within these cuts.

To turn this result into a limit on the scalar electron mass $m_{\tilde{e}}$ and photino mass $m_{\tilde{\gamma}}$ we determined the expected number of events for various values of $m_{\tilde{e}}$ and $m_{\tilde{\gamma}}$ by generating Monte Carlo events using the differential cross section given by ref. 3 and subjecting them to a simple simulation of detector. Triggers were simulated using the measured efficiencies. Then the same cuts were applied as on the data. Fig. 2 shows the region of scalar electron and photino masses excluded at 95% C.L. by this experiment for both cases $m_{\tilde{e},L} = m_{\tilde{e},R}$ and $m_{\tilde{e},L} \gg m_{\tilde{e},R}$. For $m_{\tilde{\gamma}} = 0$ and $m_{\tilde{e},L} \gg m_{\tilde{e},R}$ the range

$$3.2 < m_{\tilde{e}} < 21.1 \text{ GeV}$$

is excluded at 95% C.L.

Since limits on neutralino masses depend on the mixing between the neutral supersymmetric fermions, the branching ratio of $\tilde{\gamma}_1$ into $e^+e^-\tilde{\gamma}_1$, and the mass splitting between $\tilde{e}_L$ and $\tilde{e}_R$ we prefer to quote an upper limit on the visible cross setion for reaction (2) within the cuts described above:

$$\sigma_{vis}(e^+e^- \to \tilde{\gamma}_1\tilde{\gamma}_2)\cdot B(\tilde{\gamma}_2 \to e^+e^-\tilde{\gamma}_1) < .35 \text{ pb} \quad 95\% \text{ C.L.}$$

at $\sqrt{s}$ = 42.5 GeV. For illustrative purposes Fig. 1c shows the 95% C.L., lower limits on zino and scalar electron masses corresponding to this cross section. The assumptions entering in the contour plot are summarized in the figure caption of Fig. 1c.

In conclusion, we have searched for the signature of acoplanar electron pair with missing energy at highest PETRA energies. No event of this type was observed. Hence we can set a limit on the scalar electron mass of

$$3.2 \text{ GeV} > m_{\tilde{e}} > 21.1 \text{ GeV} \qquad 95\% \text{ C.L.}$$

for $m_{\tilde{\gamma}} = 0$, $m_{\tilde{e},L} = \infty$. Limits on neutralino production have been discussed.

(1) Kr.A. Gol'fan, E.P. Likhtman, JETP Lett. 13 (1981) 323
J. Wess, B. Zumino, Nucl.Phys. B70 (1974) 39
P. Fayet, S. Ferrara, Phys.Rep. 322C (1977) 249

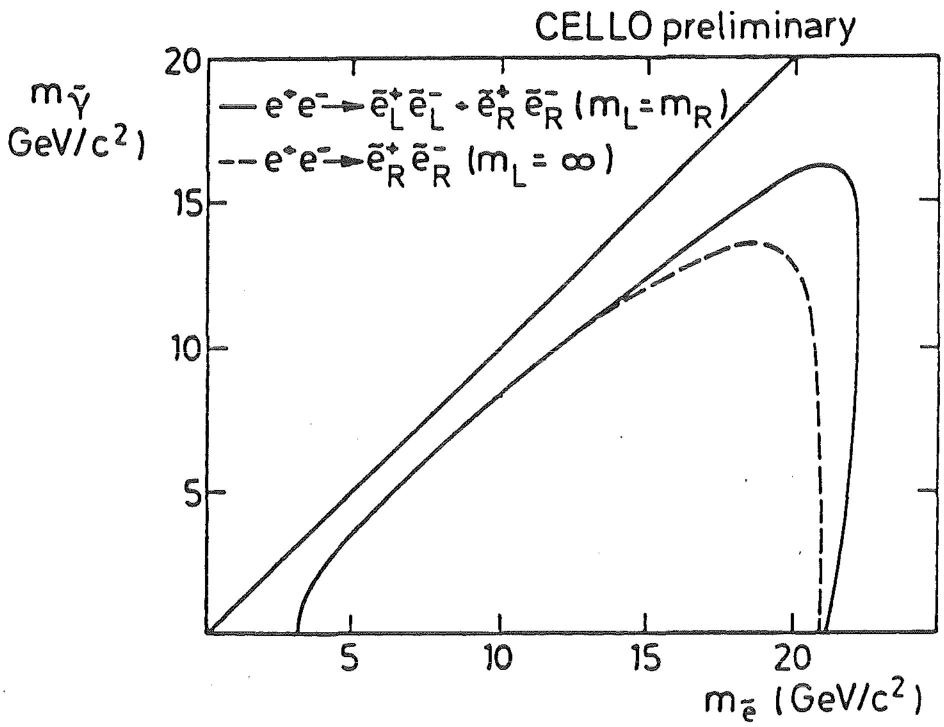

Fig. 2
95% C.L. contours indicating the range in $m_{\tilde{e}}$ and $m_{\tilde{\gamma}}$, where the area inside the contour is excluded, by this experiment.

(2) G. Farrar, P. Fayet, Phys.Lett. 89B (1980) 191
(3) M. Glück, E. Reya, Phys.Lett. 130B (1983) 423
(4) J. Ellis, J.M. Frère, J.S. Hagelin, G.L. Kane, S.T. Pectov, Phys.Lett. 132B (1983) 436
J.M. Frère, G.L. Kane, Nucl.Phys. B223 (1983) 331
(5) E. Reya, DO-TH 83/17 (1983)
(6) D.A. Discus, S. Nandi, W.W. Repko, X. Tata, Phys.Rev. D29 (1984) 1317
(7) H.J. Behrend et al., Phys.Scr. 23 (1981) 610

5.4 WEAK DECAYS

5.4.1 NEW DATA ON SEMIHADRONIC DECAYS OF THE τ LEPTON*

Branching ratios for the decay $\tau \rightarrow \nu$ + (n pions) with $n \geq 2$ have been evaluated from e^+e^- annihilation data, taken by the CELLO detector at PETRA for CMS energies of 14 and 22 GeV. The new data include all possible charge configurations of the pion system and, in particular, final states containing one or several neutral pions.

Topological branching ratios have been determined of both energies

* Z.f.Physik C23 (1984) 103

TABLE 1 Topological branching ratios. Errors given are statistical (first) and systematic (second).

	$\sqrt{s}$ = 14 [GeV]	$\sqrt{s}$ = 22 [GeV]
$\tau \to$ 1 prong + neutrals	0.852 ± .026 ± .013	0.851 ± .028 ± .013
$\tau \to$ 3 prong + neutrals	0.148 ± .020 ± .013	0.145 ± .022 ± .013
$\tau \to$ 5 prong + neutrals	0.01	0.01

separately and compared to a previous measurement of the same experiment at higher energies (1).

The values found are given in Table 1 and are in excellent agreement with other experiments (2).

The branching ratios were computed taking in account the correlated efficiencies in selecting the different decay channels. The efficiency matrix was obtained using Monte Carlo studies.

The corrected branching ratios for all channels measured in this experiment are given in Table 2 together with those for $\tau \to e\nu\nu$, $\mu\nu\nu$, $\pi\nu$ as measured previously (3).

TABLE 2 Measured τ branching ratios and predictions.

Decay channel	Experiment	Br(meas.) [%]	Pred. [%]
$\tau \to e\nu\nu$	ref. [2]	28.3 ± 2.4 ± 1.9	18.3
$\tau \to \mu\nu\nu$	ref. [2]	17.6 ± 2.6 ± 2.1	17.9
$\tau \to \rho\nu$	ref. [2] + this exp.	22.1 ± 1.9 ± 1.6	22.3
$\tau \to \pi\pi^0\nu$ (non res.)	this exp.	0.3 ± 0.1 ± 0.3	very small
$\tau \to \pi\pi\pi\pi^0\nu$	this exp.	6.2 ± 2.3 ± 1.7	6.6
$\tau \to \pi\pi^0\pi^0\pi^0\nu$	this exp.	3.0 ± 2.2 ± 1.5	1.1
$\tau \to \pi\nu$	ref. [2]	9.9 ± 1.7 ± 1.3	10.8
$\tau \to \pi\pi\pi\nu$	this exp.	9.7 ± 2.0 ± 1.3 }	upper limit 18.7 (15.4 $\pi\rho$)
$\tau \to \pi\pi^0\pi^0\nu$	this exp.	6.0 ± 3.0 ± 1.8 }	
$\tau \to \pi\pi\pi\pi\nu$ ref. [2]	this exp. .5	.9	0.9

The data are compared with predictions from CVC (even number of pions in final state) and current algebra (odd number of pions). They strongly support the standard coupling of the τ to the weak charged current (4).

(1) CELLO Coll., H.-J. Behrend et al., Phys.Lett. 114B (1982) 282
(2) MARK J Coll., B. Adeva et al., Phys.Rev.Lett. 48 (1982) 1701
D.P. Barber et al., Phys.Lett. 95B (1980) 159
JADE Coll., W. Bartel et al., Phys.Lett. 108B (1982) 140
Phys.Lett. 99B (1981) 281
CELLO Coll., H.-J. Behrend et al., Z.Phys. C16 (1983) 301
PLUTO Coll., Ch. Berger et al., Z.Phys. C7 (1981) 289
TASSO Coll., R. Brandelik et al., Phys.Lett. 117B (1982) 365
Phys.Lett. 110B (1980) 173
MAC Coll., E. Fernandez et al., Phys.Rev.Lett. 50 (1983) 11238
For a review see e.g. M. Davier Proceedings of the 21st Intern. Conf. on High Energy Physics, Paris (1982), p. c3-471
MARK II Coll., C.A. Blocker et al., Phys.Rev.Lett. 49 (1982) 1369
Phys.Lett. 109B (1982) 119
(3) CELLO Coll., H.-J. Behrend et al., Phys.Lett. 127B (1983) 270
(4) S.L. Glashow, Nucl.Phys. 22 (1961) 579
S. Weinberg, Phys.Rev.Lett. 19 (1967) 1264
A. Salam, Proc. of the 8th Nobel Symp. (Almqvist and Wiksell, Stockholm, 1968)

5.5 TWO PHOTON PHYSICS

5.5.1 PRODUCTION OF THE f_o (1270) MESON IN PHOTON-PHOTON COLLISIONS*

The production of the f_o in two photon collisions, with the subsequent decay $f_o \rightarrow \pi^+\pi^-$ has been observed in the CELLO detector at PETRA. The f_o peak was found to lie on a dipion continuum and to be shifted downwards in mass by $\simeq$ 50 MeV/c^2. The $\pi\pi$ mass spectrum from 0.8 to 1.5 GeV/c^2 was well fitted by the model of Mennessier using only a unitarised Born amplitude and helicity 2 f_o amplitude. The previously observed mass shift and distortion of the f_o peak are explained by strong interference between the Born and f_o amplitude. The only free parameter in the fit of the data to the model is the radiative width $\Gamma_{\gamma\gamma}(f_o)$. It was found that:

$$\Gamma_{\gamma\gamma}(f_o) = 2.5 \pm 0.1 \pm 0.5 \text{ keV}$$

where the first (second) quoted errors are statistical (systematic).

* Z.f.Physik C23 (1984) 223

5.5.2 MEASUREMENT OF THE REACTION $\gamma\gamma \rightarrow \pi^+\pi^+\pi^-\pi^-$ AT PETRA*

We have determined the cross section for $\gamma\gamma \rightarrow \pi^+\pi^+\pi^-\pi^-$ in a way free of assumptions about the relative contributions from $\rho^0\rho^0$, $\rho^0 2\pi$ and 4π (uncorrelated phase space). We find a sharp onset above threshold and a rather high cross section of about 200 nb around $W_{\gamma\gamma}$ = 1.5 GeV which consists to about 40% of $\rho^0\rho^0$ production with sizeable contributions from $\rho^0 2\pi$ and 4π (P.S.). The total cross section as well as the $\rho^0\rho^0$ content fall rather fast at higher c.m. energies. Attempts to explain this behaviour in terms of production of known resonances are not successful so far. The angular distributions do not show any significant structure pointing to resonance formation in the 4π-system. Only the ρ^0-meson is observed in the moment analysis. The decay distributions of the ρ^0 for forward produced rhos are fairly consistent with helicity conservation of the produced rhos in accordance with the VDM picture.

5.5.3 EVIDENCE FOR HARD SCATTERING IN UNTAGGED PHOTON-PHOTON COLLISIONS

We have studied the production of multihadronic events in untagged photon-photon scattering in e^+e^- interactions at 34 GeV center of mass energy, using an integrated luminosity of 7.9 pb^{-1}.

Inclusive $p_\perp$ distributions and a search for jet structure have been made. Events with at least two jets have been found and their p_T distributions are analysed. The Born term is not sufficient to explain the data.

* Z.f.Physik <u>C21</u> (1984) 205

6. DEVELOPMENTS AND APPLICATIONS

6.1. DETECTORS

6.1.1 SELF-ABSORPTION OF NEUTRON CAPTURE GAMMA-RAYS IN GOLD SAMPLES

K. Wisshak, G. Walter and F. Käppeler, Nucl. Instr. Meth. 219 (1984) 136

The self absorption of neutron capture gamma-rays in gold samples has been determined experimentally for two standard setups used in measurements of neutron capture cross sections. One makes use of an artificially collimated neutron beam and two C_6D_6 detectors, the other of kinematically collimated neutrons and three Moxon-Rae detectors. With a gold sample of 1 mm thickness correction factors up to 12 % were found for an actual neutron capture cross section measurement using the first setup while they are only 4 % for the second setup. The present data allow to determine the correction in an actual measurement with an accuracy of 0.5 - 1 %.

6.1.2 A GAS SCINTILLATION PROPORTIONAL COUNTER (GSPC) FOR DETECTION OF LOW ENERGY X-RAYS

R. Vogel, P. Blüm

The investigation of strong interaction effects in antiprotonic hydrogen/deuterium-atoms is only possible in isolated atomic systems. An efficient method to form isolated atoms is offered by the cyclotron trap (1); here low momentum antiprotons are trapped in a magnetic field of cyclotron character and showed down in low pressure gases (100 mbar). The characteristic X-ray energies affected by strong interaction are in the range of 2-12 keV. A new type of large area detector (GSPC) with good energy resolution and high efficiency in this energy range will be used. The geometrical size of the detector is limited by the bore hole of the magnet only. The active area is about 40 cm^2. The general set-up consists of a noble gas filled stainless steel cylinder, which is devided into three regions: convergion region, light producing region, and light detection region. The convergion region is defined by a 50 μm thick Be entrance

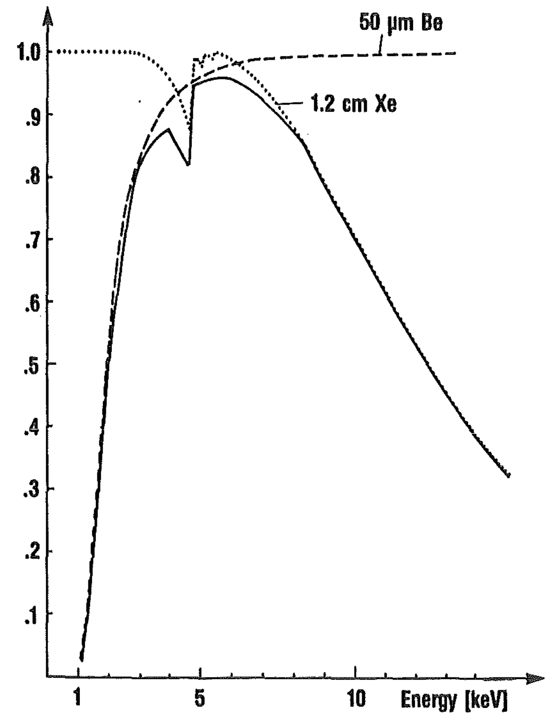

Fig. 1

Intrinsic efficiency of GSPC (———), conversion efficiency of 1.2 cm Xe (••••), and transmission of 50 µm Be (----).

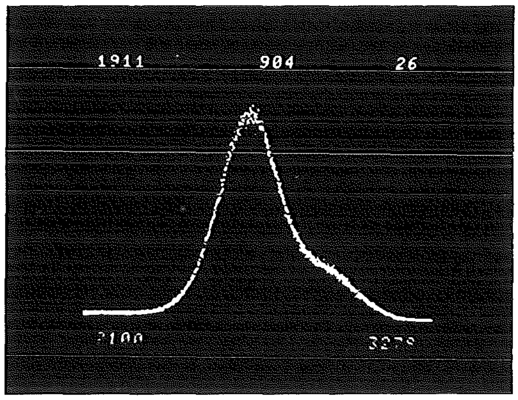

Fig. 2

Energy resolution at 5.898 keV: K_α(5.898 keV) and K_β(6.4 keV).

window and by a wire plane 12 mm apart. Thus a high intrinsic efficiency in this energy range could be achieved in a 1 atm Xe-gas, which is used as scintillation gas (Fig. 1). An electrical field of about 1500 V/cm guides the produced electrons towards the scintillation region, which is formed by a second wire plane at a distance of 7 mm. Here a high electrical field of about 4000 V/cm leads to a high emission of VuV light by the drifting electrons. The light detection system consist of a standard 2"-photomultiplier with an bialkali cathode and an uv-transmitting quartz window. For a good performance of the detector a high gas purity is essential. Therefore a continuous purification of the gas is necessary.

First tests of the detector with radioactive sources show a good linearity in the energy range of interest. An energy resolution of 8.9% at 5.898 keV (^{55}Fe-source) could be achieved (Fig. 2). Using the first light quanta produced in the conversion region we find a time resolution of 40 ns at 6.4 keV (^{57}Co-source) with respect to a fast plastic scintillator.

(1) P. Blüm, D. Gotta, R. Guigas, H. Koch, W. Kunold, M. Schneider, and L.M. Simons, CERN-Proposal PSCC/80-99/P27

6.1.3 A MULTIPLE TELESCOPE SYSTEM FOR NEUTRON INDUCED REACTIONS

P.Doll, G.Fink, R.Garrett, H.O.Klages

For detecting charged particles from neutron induced reactions by telescope technics it is necessary to have well defined target and geometry conditions especially when using a white neutron beam. We describe here a multiple telescope system operated in an evacuated scattering chamber. The vacuum is needed to avoid both neutron interaction with air and additional energy loss of the charged reaction products.

A steel chamber with an inner diameter of 80 cm and a height of 40 cm is used. Targets can be mounted on a target ladder either at the center of the chamber or in an evacuated box connected upstream to the chamber. The second position allows small angles ($\theta \geqslant 1.5^{o}$) and a long flight path ($\sim$ 100 cm) for the reaction products.

At present five telescope systems are operated in the chamber. The ΔE-detectors are 500 µm "passivated ion implanted" silicon detectors with an area of 12 x 42 mm, oriented vertically. These detectors have an energy resolution of about 20 keV for 5.5 MeV alpha particles. Fig. 1 shows the mounting of the ΔE detector and the housing of the E-plastic detector (NE 102 A, 22 x 25 x 53 mm^3). A curved light pipe going from a rectangular area 22 x 25 mm^2 to a circular area with 30 mm diameter guides the scintillation light to an XP 2061 phototube.

In any stage of assembling the E detector the light contact can be examined while leaving the side wall of the housing open. The voltage di-

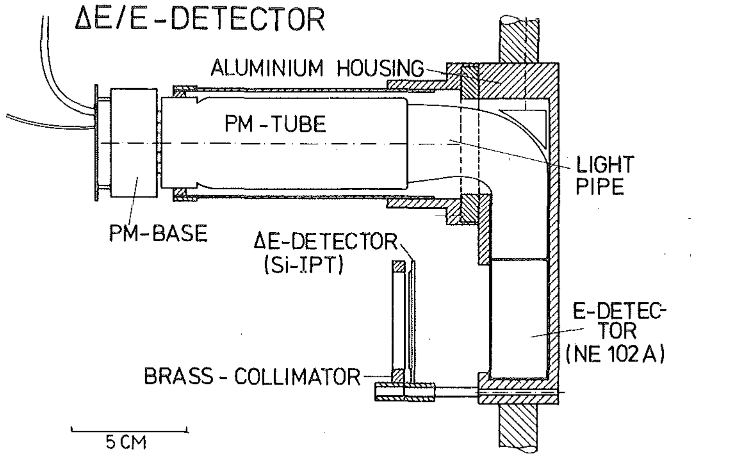

Fig. 1
Side-view of the ΔE-E telescope housing.

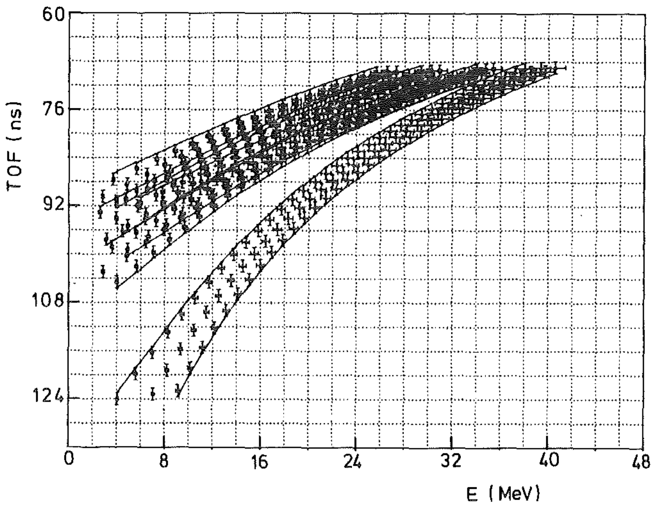

Fig. 2: Calculated TOF vs. E matrix at a detection angle of θ_L = 25^o, a 0.5 mm PE target and a 500 µm ΔE-silicon detector.

vider for the photo multiplier is operated in vacuum. The energy dissipation is less than 0.5 W and the voltage divider temperature was measured to rise about 5^o above the temperature of the chamber walls. The signal from the anode is used for both energy and timing information. Whereas it is very easy to discriminate protons from deuterons in the ΔE vs. E matrix, great problems with continuous neutron energies can occur in separating identical reaction products from different reactions, for example protons from $^1H(n,p)n$ and $^{12}C(n,p)^{12}B$ under special kinematic conditions, e.g. incident neutrons with energies > 30 MeV at $\theta_L > 30^o$.

Therefore, computer simulations were carried out for the three parameters measured in the experiment: the differential energy loss in the ΔE-detector, the total time-of-flight to the E detector, and the energy deposited in the E detector.

Fig.2 shows a calculated TOF vs. E matrix. The figure demonstrates that most of the broadening comes from the target thickness, less from the kinematics and the energy loss straggling.

The solid curves represent the boundaries for extreme energy loss situations. The lower band stems from the $^1H(n,p)n$ reaction whereas the other bands result from the $^{12}C(n,p)^{12}B$ reaction, leading to the ground state and first and second excited state.

6.1.4 FIRST RESULTS WITH MWPCs IN NEUTRON INDUCED REACTIONS

F.P.Brady, P.Doll, H.Krupp

Multiwire proportional chambers have been tested in the collimated neutron beam from POLKA. The neutron beam about 25 mm in diameter did hit a polyethylene target of 1 mm thickness. The scattered reaction products like protons and deuterons from reactions on hydrogen and carbon were detected by a detector system consisting of a plastic ΔE-detector, two MWPCs to measure the trajectories of the charged particles, and two plastic E-detectors covering an area of 15x30 cm^2 immediately behind the MWPCs. The set-up subtended an angular range from 11^o above the neutron beam to 22^o below, and from 9.2^o to 36^o to the left from the neutron beam in the laboratory system. Fig. 1 shows the set-up. The charged particles had to travel through air for 45 cm at most, causing low energy deuterons to be stopped.

The NE 102 A plastics were viewed by phototubes and their anode signals were fed directly into Camac ADCs. The chambers were operated with "magic" gas at normal pressure. The cathode signals went through delay lines, and into two fast amplifiers for each coordinate. They were processed by constant fraction discriminators whose threshold was set with a ^{55}Fe source, corresponding to an energy deposit of 5.9 keV in the chambers. The chambers anode signal provided an additional time and energy loss signal for the charged particles. All signals were fed into Camac and controlled

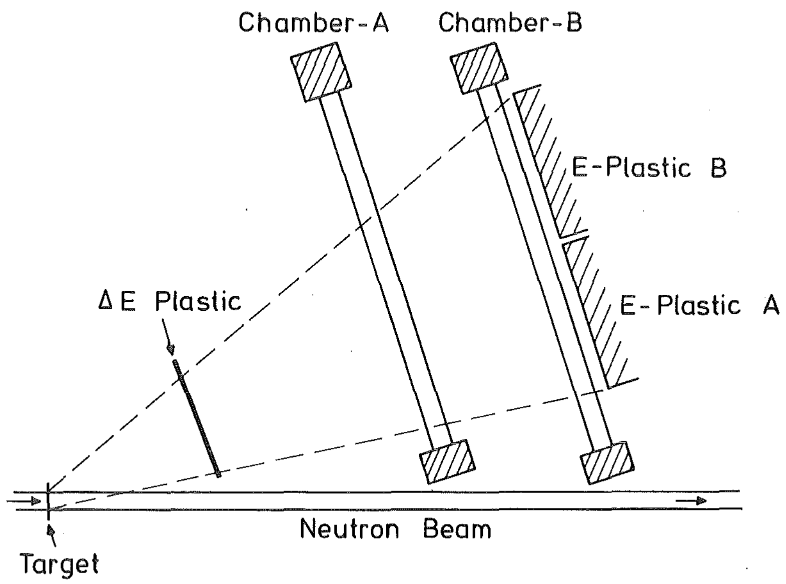

Fig. 1: Set-up of the multiwire chamber arrangement.

on-line by a data acquisition programm on a LSI 11/23 computer. A master coincidence between the E-plastic detector and the chambers defined the gate opening of the ADC and the start signal for the TDCs.

A preliminary data analysis was performed on the IBM computer, showing the properties of all position and energy parameters taken from the chambers. During the analysis circular cuts centered around the neutron beam axis are applied on the X,Y-position matrix from chamber B to allow for charged particles going in a well defined scattering angle interval. After this angle selection a ΔE-plastic versus E-plastic matrix provides a separation of protons from deuterons, however for all incident neutron energies.

Fig. 2 was obtained for scattering events with a laboratory angle of $15.4^{o} \pm 1^{o}$. Afterwards cuts in the time-of-flight spectrum define the incident neutron energy interval. A complete analysis has to be carried out in the near future, making use of all the parameters provided by the experiment, to obtain the angular distribution of n-p scattering in the full angular range subtended by the MWPCs.

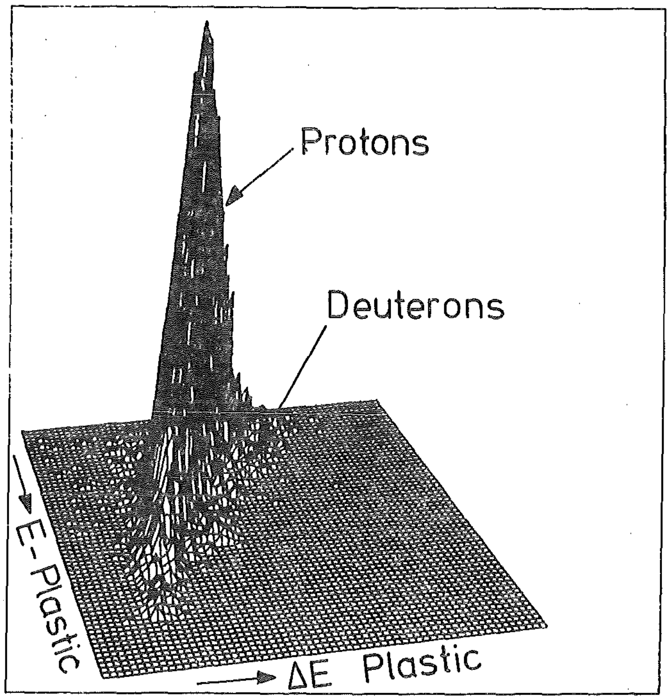

Fig.2:
ΔE versus E event matrix obtained with the plastic detectors, gated with an angular range of 15.4 ± 1^{0} in chamber B.

6.1.5 LARGE BARIUM FLUORIDE DETECTORS

K. Wisshak and F. Käppeler, (1)

Big BaF_2 crystals of 1 - 2 l volume and up to 15 cm thickness were investigated with respect to their application as gamma-ray detectors. In particular, we were interested in the light transmission in the UV region, and the energy and time resolution. We found that an energy resolution of ∿ 12 % (662 keV) and a time resolution of ∿ 0.4 ns (^{60}Co, 300 keV threshold) can be obtained simultaneously. For these features BaF_2 is superior to NaI or BGO in cases where good timing is essential. Gamma-rays and alpha particles can be clearly discriminated as for the latter the fast component does not show up in the scintillation light.

(1) dito, Nucl. Instr. Meth. (in print)

6.1.6 STATUS OF THE 4π BaF_2 DETECTOR FOR NEUTRON CAPTURE CROSS SECTION MEASUREMENTS

K. Wisshak, F. Käppeler, H. Müller, G. Rupp, J. Krisch+

For the geometry of the detector we chose a configuration with 42 elements (30 hexagons and 12 pentagons) forming a spherical shell of BaF_2 with an inner diameter of 20 cm and an outer diameter of 50 cm. The individual crystals as shown in Fig. 1 will be machined from cylindrical BaF_2 single crystals with 14 cm diameter and 15 cm thickness. The crystals have been or-

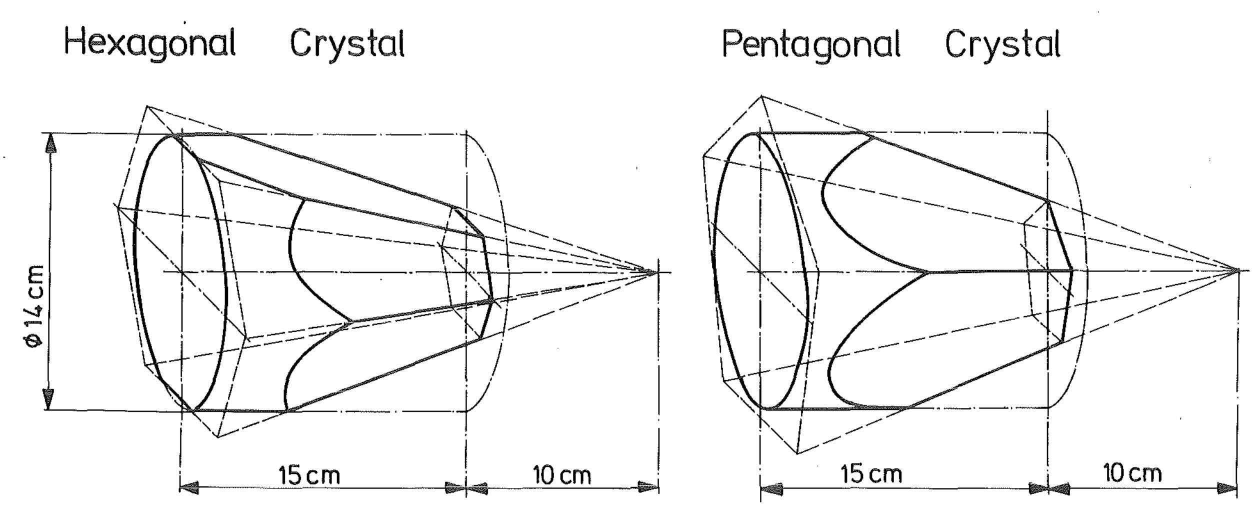

Fig.1 Shape of the two types of BaF_2 crystals.

dered from Fa. Dr. Karl Korth at Kiel and will be delivered between September 84 and December 85.

The mechanical support of the detector is designed according to the experience with the Heidelberg crystal ball detector. The individual crystals will be fixed in a spherical honeycomb structure with an outer diameter of 86 cm. In this way each element (crystal and photomultiplier) can be removed or mounted without disturbing the remaining detector. The grid structure will be made of aluminium while the mechanical support of the crystals inside the honeycomb structure will be made of fibre reinforced plastic material in order to reduce background due to capture of scattered neutrons.

Presently we are establishing the electronics for steering, control and adjustment of the detector parameters via CAMAC. This comprises high voltage power supply, constant fraction discriminator settings, multiplexers, delays etc.

A setup for testing the light transmission of the rough crystals at a wavelength of 220 and 310 nm has been completed. This will be used to verify the quality of the crystals prior to the mechanical shaping.

+ KfK IT-M

6.1.7 A PROGRAM FOR CALCULATING THE EFFICIENCY OF A 4π SCINTILLATION COUNTER

G. Schatz, J. Oehlschläger, (1)

A FORTRAN program is described which allows to calculate the efficiency of a 4π scintillation detector for γ-rays. The detector has the shape of a hollow sphere with the γ-ray source at the centre. The program calculates the distribution of the energy deposited in the scintillator for the materials bismuth germanate or barium fluoride.

(1) dito, KfK-report 3710 (1984)

6.1.8 MONTE CARLO CALCULATIONS FOR AN OPTIMIZED γ-DETECTOR IN THE ENERGY RANGE FROM 20 TO 1000 MeV

H. Koch, M. Kunze

About fifty percent of the annihilation products in the $\bar{p}p$-system are neutral particles (π^0,η,...) which decay into Gamms. Therefore, a complete understanding of the $\bar{p}p$-system is impossible without spectroscopy of neutral particles. Moreover, they play an important role in the search for exotic quark-states, like Baryonium ($qq\bar{q}\bar{q}$), which can be found in reactions like $\bar{p}p \rightarrow \pi^0 X$, ηX, γX.

It is obvious, that a good γ-spectrometer will be necessary for future LEAR experiments. Because of the low momenta of the decaying neutral particles (π^0,η,...) such a spectrometer has to span a nearly 4π solid angle. In addition, it must have good angular and energy resolution. In order to find an optimal solution for such a device a Monte-Carlo program was written which simulates the $\bar{p}p$-annihilation and the γ-detector surrounding a Hychron target. It takes into account:

- ball like geometry for γ-detector
- 62 annihilation channels with variable relative intensity
- target and beam spot of finite size
- variable angular resolution
- variable energy resolution
- reactions of secondary particles in the target
- variable energy threshold

First results have been obtained on the π^0-background suppression in the reaction $(\bar{p}p)_{stop} \rightarrow \gamma X$ and on the π^0-spectroscopy. E.g., a ball-like detector with 97% of the full solid angle, an energy resolution of

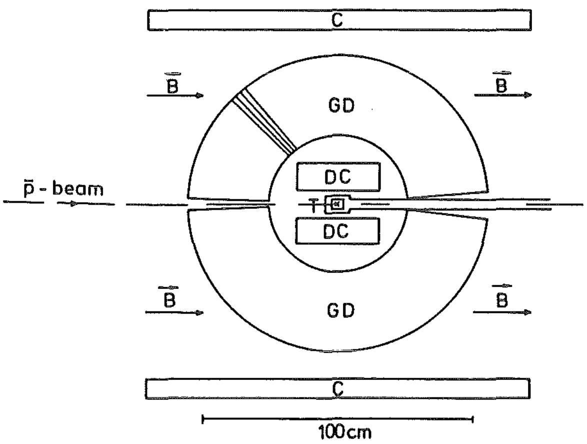

Fig. 1
Configuration of a detector array for a complete measurement of the $\bar{p}$ - Nucleon annihilation reactions. T = $H_2(D_2, {}^3He, {}^4He)$-target, DC = drift chamber of high spacial resolution (rotational geometry), GD = modular gamma detector (spherical geometry), C = coil (rotational geometry).

$\Delta E/E = 4\%/\sqrt{E(GeV)}$ and an angle resolution of 2^o supresses the π^o-background of an inclusive γ-spectrum by a factor of about 10 at E_γ = 200 MeV.

Presently, the programm is extended to take into account also the charged particles, which could be detected simultaneously with the neutrals in a detector array as given in Fig. 1. First tests of specific components of such a system are in preparation.

6.2 INSTRUMENTATION

6.2.1 FIRST EXPERIMENTAL EXPERIENCE WITH A CYCLOTRON TRAP

R. Abela[+], P. Blüm, D. Gotta, W. Kunold, D. Rohmann, U. Schneider, and L.M. Simons

Studying the formation of muonic atoms in low-Z gaseous materials a high negativ muon stop density is essential in dilute gases such as Ne or B_2H_6 (Diborane) (1). The density of the target is limited by the following consideration:

The observation of radiative transitions from the 2s level of muonic atoms requires a strong supression of competing processes such as Auger transitions, i.e. the refilling rate of the electron shells of the atom should be slow. Therefore the probability of collisions between the muonic atom and atoms of the rest gas during the life time of the 2s state should be small. This requirement can be met at a gas pressure of about 200-400 Torr.

In order to improve the available stop densities we developed a new method (cyclotron trap) to concentrate charged particles which makes use of the focusing properties of a suitably shaped magnetic field. The field is provided by a supraconducting split coil magnet which produces a field strength of about 4 Tesla in the central region. Particles with momenta up to 110 MeV/c can be accepted in the medium plane at a radius of 125 mm (injection point) and will then be decelerated due to the energy loss in the target gas and in additional degrader foils. The focusing properties of the cyclotron are used to compensate for displacements caused by Coulomb scattering in the target gas. In order to transport particles to the injection point, a beam momentum of typically 170 MeV/c for muons and pions is chosen. A degrading down to 110 MeV/c is then provided with a suitable shaped moderator.

First tests of the principle used were performed with α-particles from a collimated ^{241}Am source. The results confirmed the validity of the theoretical considerations (2).

Tests with particle beams have been performed at the πM3 channel at SIN with pions and muons. A movable scintillator rod of 5 mm diameter was used for radial scans inside the trap. The pions and muons have been classified according to the number of turns by time-of-flight and so the injection scheme would be optimized. Suitably placedadegr der foils provided a spatial separation of the beam from the moderator after the first turn. We observed for muons up to 60 turns in air at standard conditions

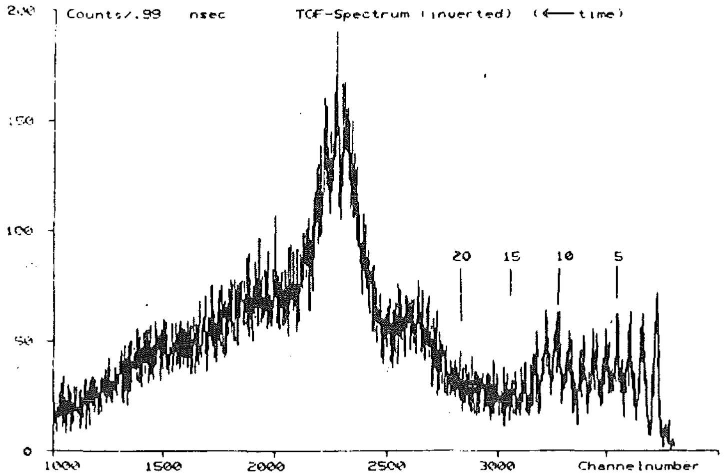

Fig. 1 Time-of-flight spectrum at radius r = 10 mm. The maximum intensity corresponds to 35 turns of the muons inside the trap. The side maxima belong to a class of muons with high betatron amplitudes.

which correspond to a deceleration time of about 200 ns. In Fig. 1 the time distribution at radius r = 10 mm is shown. The suitably degraded muons are seen as a broad maximum at 35 turn, whereas particles slowed down to momenta far below the injection momentum of 110 MeV/c are bend immediately toward the center of the trap producing the peaks belonging to turns 2-12. The side maxima (turns ~10,20,40,50) are caused by classes of incomplet degraded muons performing high betatron oscillations, which leads to processing roset orbits.

For muons two injection schemes have been tested:

In the first case, "beam muons" (i.e. muons from the pion decay in the vincinity of the production target) were directly injected and moderated. A stop density of $2 \times 10^4 \mu^-/g \cdot s$ at 100 μA proton intensity have been achieved. The stop distribution was measured by the detection of the nitrogen and oxygen X-rays of air from the central region of the trap (Fig. 2). By a radial scan with a 20 μm CH_2-foil and an axial scan with a 1 mm thick carbonsheet, the perturbation of the "air-spectrum" containing now carbon X-rays was detected and the stop distribution was derived. The stop volume has the shape of a rotational ellipsoid with a volume of 150 cm^3 (Table 1).

In a second series of experiments pions were injected and moderated

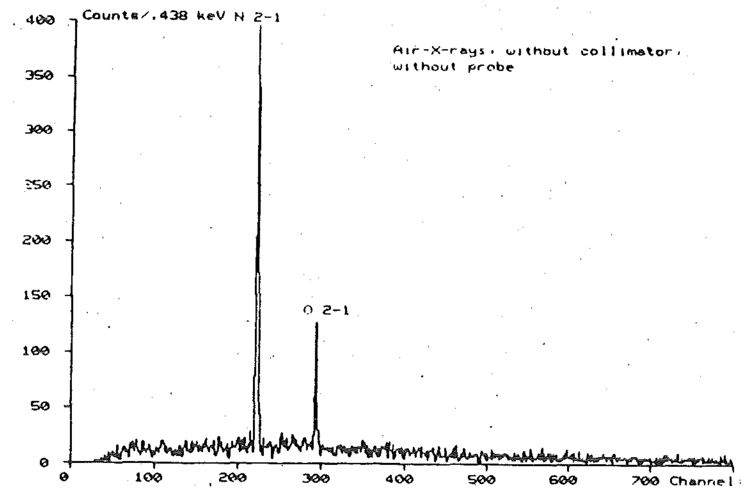

Fig. 2 Muonic nitrogen and oxygen X-rays from the neutral region of the trap measured with an intrinsic Ge-detector placed in the middle of one bore hole. No background lines of the surrounding materials are observed.

to about 80 MeV/c. These pions decayed in flight inside the trap and led to a radially much more extended stop distribution. By collimating the X-rays from muonic N and O to a central region with $r \leq 30$ mm a stop density of $5 \times 10^4 \mu^-/g \cdot s$ at 100 μA proton current could be measured.

These numbers may be compared with the stop density of $10^5 \mu^-/g \cdot s$ which can be achieved at the dedicated μE1 channel.

	SIN πM3 170 → 110 MeV/c air 1000 mbar	LEAR 309 → 110 MeV/c ^{4}He 375 mbar
particle	μ^-	$\bar{p}$
beam intensity	1 (700 s^{-1})	1 ($1.2 \cdot 10^4$ s^{-1})
injection window (r=120–130mm)	0.22	0.40
1. orbit	0.11	~ 0.20
2. orbit	0.08	~ 0.19
3. orbit	0.07	~ 0.15
stopped	0.05	~ 0.15
stop volume	150 cm^3	< 200 cm^3
stop density	$2 \cdot 10^4/g \cdot s$	$2 \cdot 10^5/g \cdot s$

Table 1 Intensities at various steps of the deceleration process and stop densities. The beam intensity is normalized to 1 (rates in brackets).

The goal at LEAR are the measurement of the Lyman-, Balmer- and Paschen series of antiprotonic hydrogen, deuterium and tritium (3). Due to the Stark effect the K_α-transition is strongly suppressed. From the shift and width of this transition the elementary complex scattering length of the $p\bar{p}$-system can be derived immediately. However the yield of about 10^{-3} requires high stop densities at pressures below 1 atm. To prove the existence of a concentrated stop distribution for antiprotons in the trap, measurements of $\bar{p}\,{}^4$He X-ray spectra at 600 and 375 mbar were performed. The incoming $\bar{p}$ of 309 MeV/c momentum, which entered the stopping chamber through a 100 μm Al-window, were slowed down to 110 MeV/c by a 13 mm thick Be-moderator placed at the injection radius of 125 mm. The fine adjustment was made by a turnable 1 mm thick CH_2-foil in front of the moderator. The percentage of injected $\bar{p}$ was measured with a 1 mm thick plastic scintillator of 1 x 1 cm^2 area. The radial dependence of the revolutions inside the stopping chamber was detected by the movable plastic scintillator rod via time of flight (revolution time ~ 20 ns). From the intensities of the revolutions it was derived that all $\bar{p}$ reaching the third orbit stop in a volume less than 200 cm^3 in the center of the stopping chamber. The X-ray were measured by a 30 mm^2 Sili detector (energy resolution in beam ΔE = 215 eV at 5.9 KeV) placed in one bore hole of the magnet at a distance of 16 cm from the center of the trap. The window thicknesses were 8 μm Be for the Sili detector and 12.5 μm Be for the stopping chamber. Table 1 shows the development of the beam intensity at various steps of the

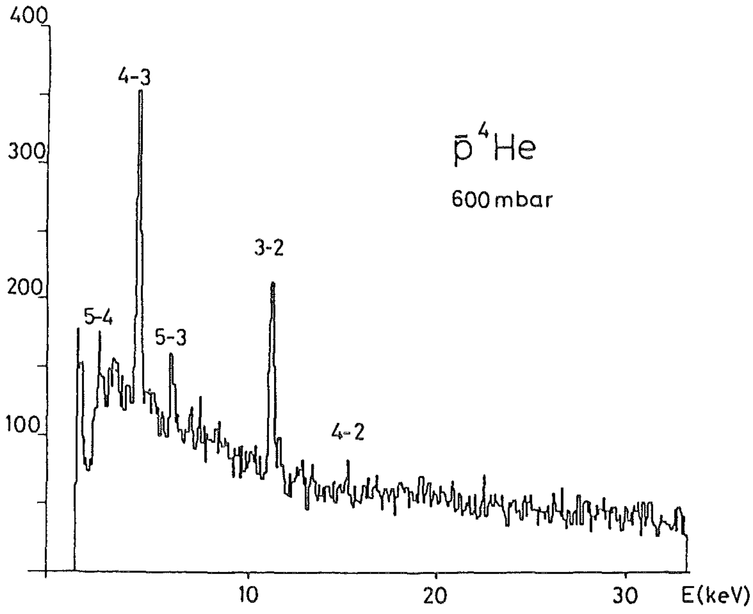

Fig. 3 $\bar{p}\,{}^4$He spectrum at 600 mbar. The measuring time was 3.5 h with $3.6 \cdot 10^8$ incoming $\bar{p}$. No background lines of the material of the stopping chamber are observed.

deceleration process in ^{4}He at 375 mbar. The losses are mainly caused by annihilation in Be inflight and the range straggling of about 25% in the moderator. This reduction of intensity will decrease drastically using the new 200 MeV/c beam at LEAR (moderator thickness 1 mm Be) which can be accepted in connection with a magnetic shiedling of the stray field. Fig. 3 shows the $\bar{p}\,^4$He spectrum measured in 3.5h which corresponds to 3.7 x 10^8 incoming antiprotons. No background lines are seen according to the concentrated stop distribution. From this spectrum the ratio of annihilation to X-ray emission from the 3d level was determined to be $\Gamma_{ann}/\Gamma_{rad}$ = 2.6 ± 0.5 resolving the discrepancy of two former experiments.(4).

(1) P. Blüm, E. Borie, D. Gotta, R. Guigas, H. Koch, W. Kunold, M. Schneider and L.M. Simons; SIN proposal R-81-02.1(1981)
(2) Annual Report on Nuclear Activities 1982/83; KfK 3621(1983)165-169
(3) P. Blüm, D. Gotta, R. Guigas, H. Koch, W. Kunold, M. Schneider and L.M. Simons; Proposal PS175 CERN/PSCC/S27(1980)
(4) E.G. Auld, J.M. Bailey, G.A. Beer, B. Dreher, H. Drumm, K. Erdmann, U. Gastaldi, E. Klempt, K. Merle, K.Neubecker, C. Sabev, H. Schwenk, U.H. Walther, R.D. Wendling, B.L. White and W.R. Wodrich, Phys. Lett. 77B(1978)454
H. Poth, R. Abela, G. Backenstoss, P. Blüm, W. Fetscher, R. Hagelberg, M. Izycki, H. Koch, A. Nilsson, P. Pavlopoulos, L.M. Simons and L. Tauscher, Phys. Lett. 76B(1978)523

+ Schweizerisches Institut für Nuklearforschung (SIN)

6.2.2 MODIFICATIONS OF THE BRUTE-FORCE POLARIZED PROTON TARGET

W. Heeringa and H. Skacel

For the measurement of the scattering of polarized neutrons by the polarized protons in our brute-force polarized TiH_2-target, it is necessary to measure also the scattering of polarized neutrons by a Ti dummy target. The count rate of the neutrons scattered by protons is in principle determined by subtracting the count rate of the Ti-dummy from the count rate of the TiH_2-target.

Up to now the exchange of targets was carried out by warming up the cryostat and opening it. This procedure takes many days, which appears to be too long with regard to the stability of the neutron detectors, the electronics and the cyclotron beam properties. We, therefore, have designed a construction, which enables to change the target without opening the cryostat.

The principle is shown in fig. 1. The TiH_2- and Ti-targets are mounted closely above each other on the copper rod to the mixing chamber of the dilution refrigerator. A target change is accomplished by raising or lowering the complete cryostat insert (of which the dilution unit forms the lower part) with regard to the magnet and the neutron beam.

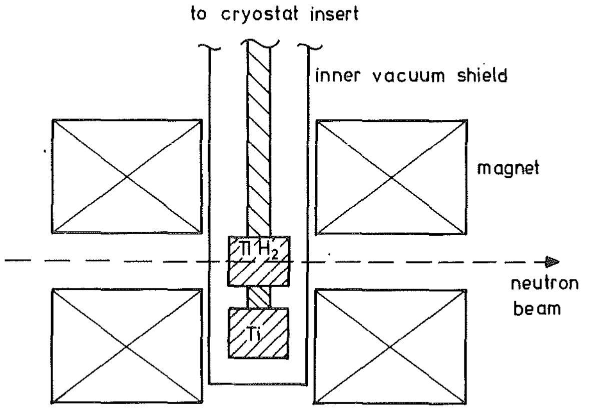

Fig. 1 Mounting of the targets

The vertical movement is initiated by a turning wheel (worm wheel) at the top of the cryostat, which has a screw-thread connection at its inner diameter to the upper flange of the insert. The worm wheel is driven by a worm gear mounted onto the shaft of an electromotor. The construction is shown in fig. 2. The worm wheel is supported by ball bearings on top and below. The

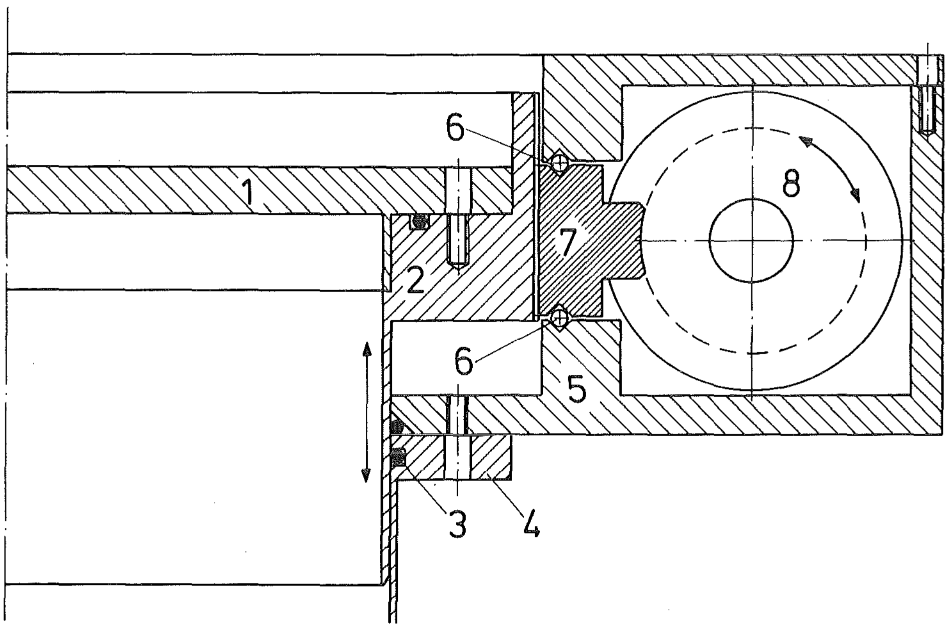

Fig. 2 Construction for the vertical target movement.
1. Top flange of cryostat insert, 2. top flange support ring with screwthread at its outside. 3. sliding o-ring seal, 4. upper flange of cryostat, 5. worm wheel support, 6. ball bearings, 7. worm wheel with screwthread at its inside, 8. worm gear drive

helium space, in which the insert is situated, is closed by a sliding o-ring seal.

The vertical displacement is about 35 mm, which will be completed in about 1 hour. The limiting factor is the heat from eddy currents, originating by the movement of the targets and the copper rod in the field of the polarizing magnet. The eddy current heating is largest in the copper rod, because of the high conductivity of copper and because the field gradient is largest at the rod. Calculations show that a heat load of some tenths of a microwatt can be expected when the target change is carried out in 1 hour. This is well tolerable by the dilution refrigerator and should have no measureable effect on the proton polarization.

6.2.3 A MINI STORAGE RING FOR INCREASING THE INTENSITY OF NEUTRON TIME OF FLIGHT EXPERIMENTS AT THE VAN DE GRAAFF

G. Schatz

Neutrons for time-of-flight measurements at the Van de Graaff accelerator are presently produced in the following way: The dc proton current from the ion source is swept across a diaphragm in the terminal, and only bunches of 10 to 20 nsec length are accelerated to full energy. These bunches are then compressed to approximately 1 nsec at the position of the neutron producing target by a Mobley system. Typical pulse repetition rates are near 1 MHz, so only few percent of the ion source current are used for neutron production although the Van de Graaff is capable to accelerate the full dc beam.

In this contribution it is proposed to instal a miniature storage ring between Van de Graaff and Mobley buncher in the same way as a similar system at the Indiana cyclotron (1). The system would be operated as follows: The dc beam from the Van de Graaff is injected into the ring by stripping (cf. Fig. 1). This requires that either H_2^+ ions at twice the voltage or H^- ions are accelerated. This increases the phase space density of the particles. After accumulating a number of turns a bunch of protons 10 to 20 nsec long is extracted from the ring by a pulsed deflector followed by a static one. This bunch extraction is repeated at the pulse repetition frequency while continuing to fill the ring steadily. If the magnet configuration is designed isochronous the azimuth current distribution is stable between extracting pulses and it is possible to systematically shift the azimuth of the extracted bunch for maximum intensity. For the required proton energies (1 to 4 MeV) and reasonable guide fields the ring would store at least ten bunches on its circumference.

The maximum intensity gain which can be achieved is the inverse of the duty factor of the present mode of operation and is of order 50 to 100. To what extent this limit can be approached will depend on the increase of the phase space density of particles because the efficiency of the Mobley buncher drops with increasing energy spread and beam emittance. The main limiting factors are:

1. Space charge
2. Energy loss and angular straggling induced by the stripper which the particles have to pass each turn.

In addition losses will occur during extraction by the finite rise and fall time of the deflecting pulse, e.g.

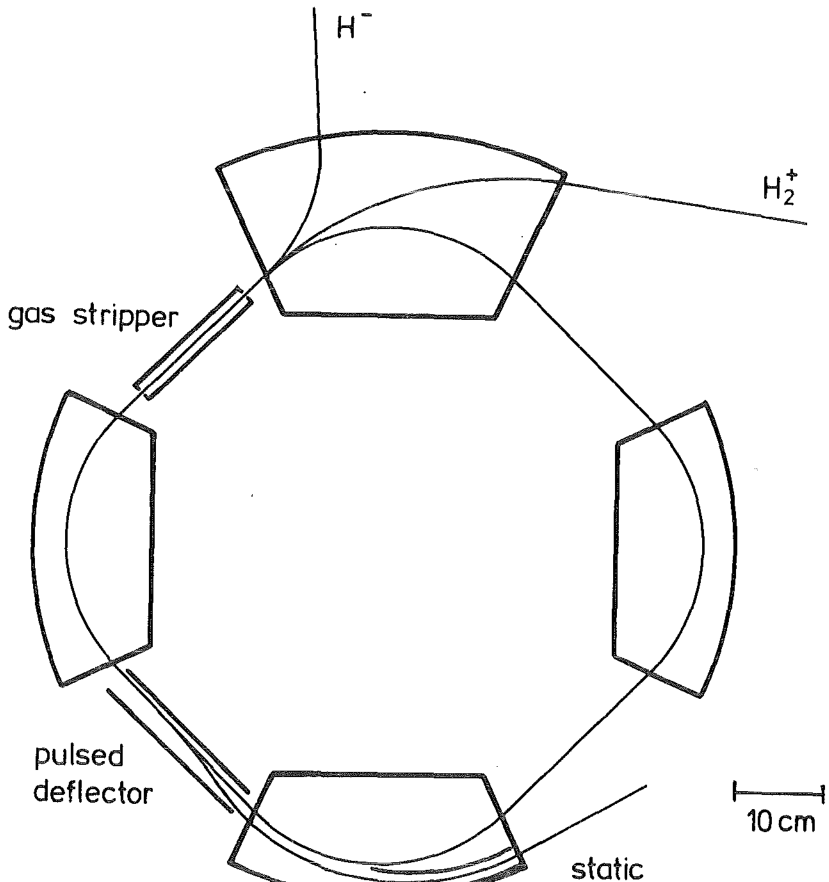

Fig. 1 A possible lay-out of the proposed mini storage ring.
The scale refers to a (homogeneous) field of 1 T inside the magnets and 2 MeV protons.

Multiple scattering and energy loss in the stripper are determined by its composition and its thickness which is determined by the stripping cross section. Based on measured cross sections (2) the required thickness is estimated to 0.5 to 1 μg/cm² at 2 MeV. This leads to insignificant energy loss and phase space dilution for a typical design. The influence of space charge is under study. The pulsed deflector and its power supply appear non-trivial but feasible.

(1) R. Pollock, private communication
(2) K.D. Groenveld, private communication

6.2.4 A FAST SAMPLE CHANGING SYSTEM FOR ACTIVATION MEASUREMENTS

G. Walter, G. Rupp, S. Schmitt, H. Beer

In order to improve the experimental facilities for the activation measurements of neutron capture cross sections, a fast sample changing system has been constructed. This set-up allows for the determination of Maxwellian average capture cross sections of nuclei where the product nucleus may have a half-life as short as one second.

The facility consists of a pressure driven sample changer being able to move from the irradiation position to the position of counting in about 750 ms and the necessary electronic control circuits. For counting of γ-rays a shielded large volume Ge(Li)-detector is used. Time intervalls from 1 to 999 seconds can be selected and up to 9999 cycles be preset. Some first test runs under experimental conditions proved the rated specifications.

6.2.5 STATUS OF THE MAGNETIC SPECTROGRAPH "LITTLE JOHN"

H.J. Gils, J. Buschmann, H. Jelitto, M. Heinz, H. Rebel, H. Schlösser[+] and S. Zagromski

The magnetic spectrograph "Little John" has been brought into operation together with the focal plane detection system (1,2) in four short beam periods serving for test purposes. The tests aimed mainly at the investigation of detector properties under realistic conditions at the cyclotron beam as described in the subsequent contribution.

In addition, the function and reliability of various components of the spectrograph have been studied and improved, if necessary. The experiences collected so far can be summarized as follows:

- Vacuum system: The vacuum system is now completely equipped. The hardware and the computer control (3) works reliably. The design goal of a pressure of 10^{-6} mbar is reached.
- Magnet system: For a precise setting of the magnets a ramping procedure has been used by which the magnetic fields can reproducibly be set within the accuracy of the focal plane detector. The installation of an NMR probe for the dipole magnet is in preparation. The programming of the computer control for the magnet system is delayed due to the implementation of a new control computer.
- Acceptance slits, target handling etc.: The manual control of the acceptance slits is working, its computer control program is presently developped. The target sluice with movable rod and target holder is under construction. Due to similar hardware (stepping motors, digitizers etc.) the manual and computer control of the target system will be identical to the control of the acceptance slits.
- Faraday cups: Different Faraday cups for small angle and zero degree measurements including repellers for exo-electrons have been constructed and partly tested. Small angle measurements down to $\Theta_{Lab} = 3°$ have been performed.
- Ion optical properties: The study of the ion optical properties of the spectrograph was concentrated on the focusing and imaging of elastically scattered particles. Using different methods (2) separating the intrinsic position resolution of the FP detector from the ion optically given spot size of the elastically scattered particles a minimum value of 1.1 mm has been obtained for the latter being 50% larger than the design value. At least part of this increased spot size has been shown to be due to unstabilities of the cyclotron beam which will be reduced by an additional entrance slit for the beam monochromator limiting the accepted angular coordinates of the beam phase space.

(1) S. Zagromski, unpublished results (1980)
(2) S. Zagromski, J. Buschmann, H.J. Gils, H. Jelitto, H. Rebel, H. Schlösser, contr. 6.2.6
(3) D. Manger, KfK 3702 B (1983)

+ Physikalisches Institut der Universität Erlangen-Nürnberg

6.2.6 ON-BEAM TESTS OF THE FOCAL PLANE DETECTOR OF THE MAGNETIC SPECTROGRAPH "LITTLE JOHN"

S. Zagromski, J. Buschmann, H.J. Gils, H. Jelitto, H. Rebel, H. Schlösser[+]

After various studies of the properties of the focal plane (FP) detection system using radioactive sources (1) the detector has been operated at the cyclotron beam in the high dispersion FP position (2) of "Little John". The main aims of these tests were to study the horizontal position resolution of the two position sensitive proportional counters and the particle identification of the ΔE (ionization chamber) and E (plastic scintillator) detector using high energy deuterons (52 MeV), α particles (104 MeV), and ^{6}Li ions (156 MeV) elastically scattered from a target. Furthermore, the background situation in the experimental hall was studied.

- Position resolution: The intrinsic position resolution of the position sensitive detectors were measured with two slits (1 mm width) in front of the detectors in order to eliminate the unknown spot size of the beam of elastically scattered particles. After unfolding the width of the slits a position resolution of 1.1 mm was observed being slightly worse than obtained with radioactive sources.
- Particle identification: The identification of the nuclear charge number of a detected particle using the ΔE and E signals has been verified for d, α, and ^{6}Li particles. However, the energy calibration curve of the plastic

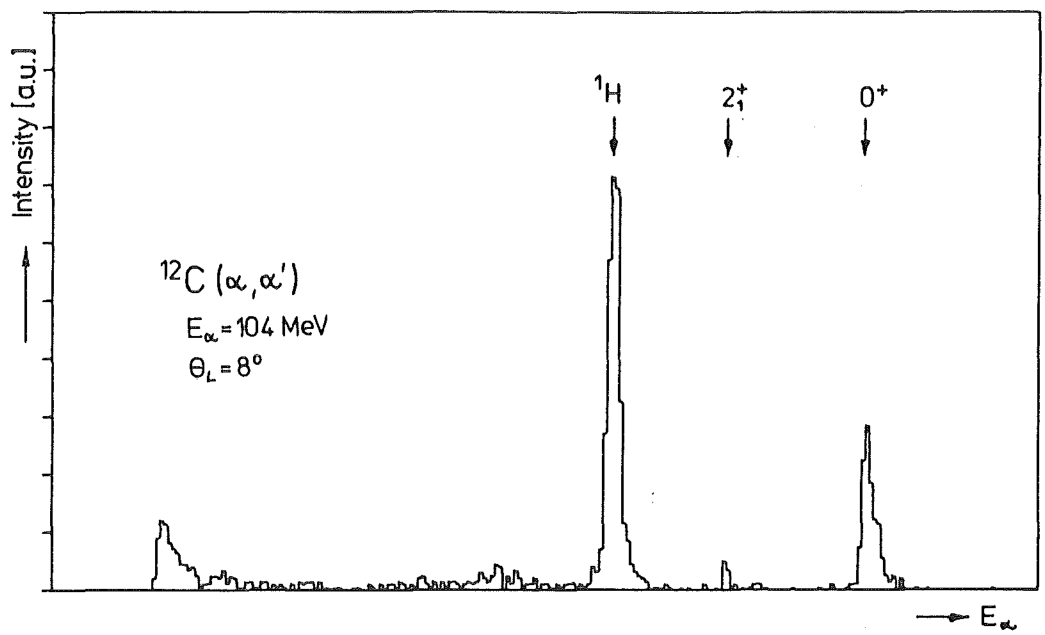

Fig. 1 Position spectrum from the first position sensitive detector for ^{12}C(α, α')

scintillator depends strongly on the detected particles. For a good resolution of different atomic masses the additional use of the time-of-flight signal is necessary.

- Background: The extremely high background observed in the single spectra of the different detector components is suppressed by a two stage coincidence. Further studies of background suppression using a faster coincidence is foreseen.

As an example of the present status of the detection system Fig. 1 shows a position spectrum of α particles scattered from a Carbon target at $\Theta_{Lab} = 8°$.

(1) S. Zagromski, M. Heinz KfK 3621 (1983) contr. 6.2.6
(2) H.J. Gils, KfK 3280 (1982) contr. 2.6.4

+ Physikalisches Institut der Universität Erlangen-Nürnberg

6.2.7 AN ACTIVE SYSTEM FOR SUPPRESSION OF SLIT SCATTERING

H. Schlösser+, W. Eyrich+, A. Hofmann+, and H. Rebel

The scattering of hadrons at small angles is a sensitive tool for the investigation of highly excited states in nuclei, especially of giant resonances. In practice, however, this method is limited mainly by the experimental background, which increases rapidly with decreasing scattering angles. A large part of the experimental background is caused by small angle scattering of particles on beam defining elements and even a very careful beam preparation is not sufficient to suppress this effect in a satisfactory way in all cases. A time-of-flight method to reduce the small angle scattering background is described in ref. 1. Another method is the use of active beam defining elements.

In the following such an active system will be described for the use on the Karlsruhe Isochronous Cyclotron to improve the set up for small angle scattering experiments. Fig. 1 shows the design of one of the four elements which will be installed in a crossed arrangement at the entrance of the scattering chamber of the magnetspectrograph "Little John".

The particles that will be scattered at the slit-element (SL) under small angles and hit the plastic scintillator (SC) give a veto signal in a photomultiplier (PM), which is connected with the scintillator via a plastic lightguide (LL). The scintillator juts out typically half a millimeter, depending on the actual experimental set up. The relative position between scintillator and slit element can be varied therefore in steps of 1/100 mm with the nut (M). The whole system (SC + LL) can be moved 40 mm with a drive motor (MOT) perpendicular to the beam-axis as shown in fig. 1. Since the system can pass the geometrical middle of the beamline, the arrangement can, in addition, be used for a beamscan in cases of low intensity beams.

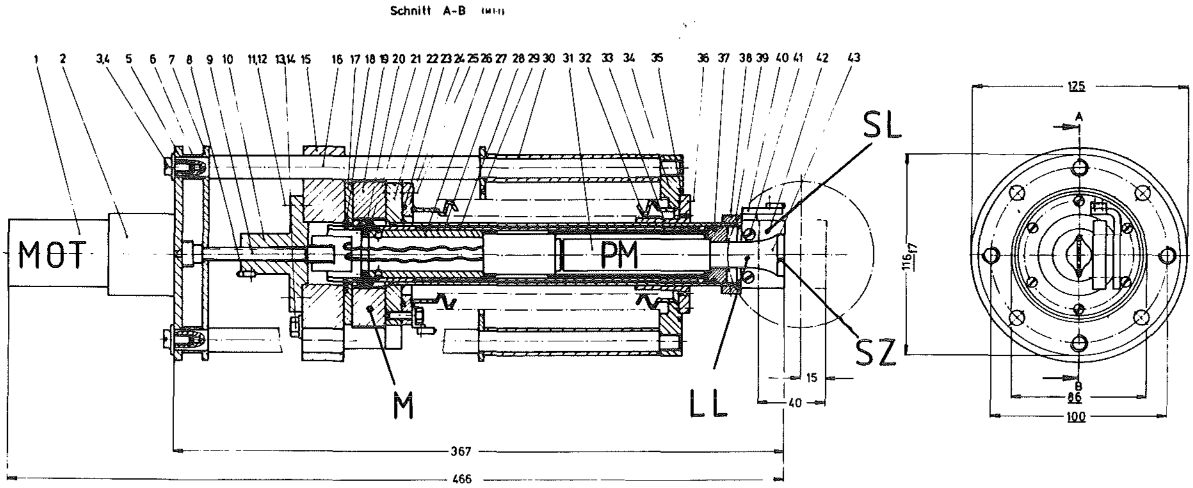

Fig. 1 Design of one active slit element

The system described was tested at the Erlangen tandem accelerator with a 9 MeV proton beam. To show the effectiveness we placed a surface barrier detector in a reduced beam (angular acceptance about 0 - 1.5 degrees) and cut one half of the proton beam with the slit element. The obtained slit

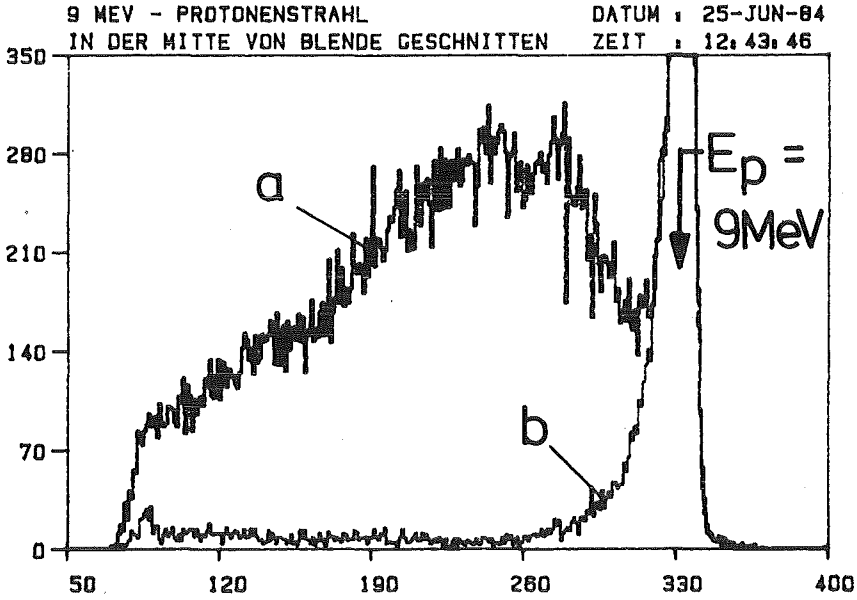

Fig. 2 Spectrum from slit scattering obtained with a surface barrier detector
curve a: without veto-signal
curve b: with veto-signal

scattering spectrum shown in fig. 2 (curve a) is strongly suppressed by use of the veto signal from the active slit element (curve b). One can estimate the suppression for the scattered events to be about 95%.

(1) W. Eyrich, H. Hassold, A. Hofmann, B. Mühldorfer, U. Scheib, H. Rebel Phys. Rev. C 24, 2720 (1981)

+ Physikalisches Institut der Universität Erlangen-Nürnberg

6.2.8 AN ON-LINE-DATA-EVALUATION-PROGRAM FOR THE MAGNETIC SPECTROGRAPH "LITTLE JOHN"

H. Schlösser[+], H.J. Gils

The characteristic quantities of a nuclear reaction product passing through the magnetic spectrograph "Little John" are detected by the focal plane (FP) detector (1) connected to a multidimensional data acquisition system. These quantities, like the atomic charge state Q, the atomic mass number M, the nuclear charge number Z, and the kinetic energy of the particle can not directly be deduced from the channel number of the projected single ADC-spectra. Further calculations are necessary to extract the relevant physical information which is important to be known during the experiment for the control of its correct running. For this purpose an on-line-data-evaluation-program (RUNEXP) is being developped.

The incoming data are splitted into two different CAMAC-dataways for two computers. One of them transfers all the data event by event on magnetic tape. The other one, at present an LSI-11/23 computer with 30 M-byte winchester-floppy-combination, accepts a part of these data and the program "RUNEXP" evaluates the interesting spectra. "RUNEXP" is a segmented FORTRAN IV program running with RT-11 operating system and optimized to use the whole dynamic memory of 256 k-byte. The RT-11 system and the program-code need 64 k-byte, the rest is used to store data as 16 bit integer values. Hence, 96 k-words for storage could be used. The memory could be devided into 96 single parts. Each part ("experiment") corresponds to a special combination of the ADC-data in the event-word. This event-word (max. 30 numbers) is constructed from incoming ADC-data (max. 20) and from spectrometer specific calculations with the ADC-data (max. 10). An "experiment" is a one- or two-dimensional spectrum, on which software windows (max. 8) can be set to look for several coincidence requirements.

It is intended to do the evaluation of the event-word, the incrementation into the memory, and the look for coincidence-conditions in a "background" program so that further service functions of the program (integration, calibration, datafit, etc.) can be used in parallel without stopping the data calculation.

Fig. 1 shows as an example for the display and the service functions of the program a hard-copy from the console-terminal after an integration in a two-dimensional spectrum. The displayed "integral" value is the content of all points located in the shown box. Fig. 2 shows the projection of this two-di-

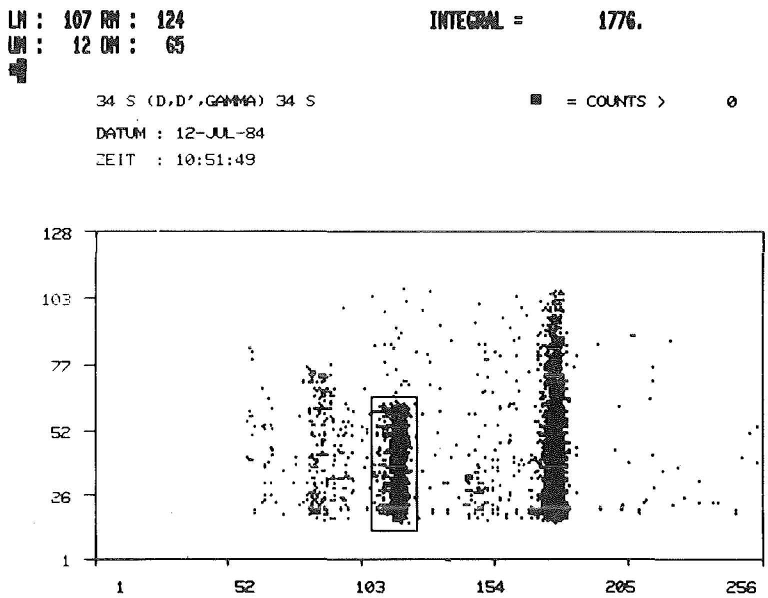

Fig. 1 Example for a two-dimensional spectrum display with integration function.

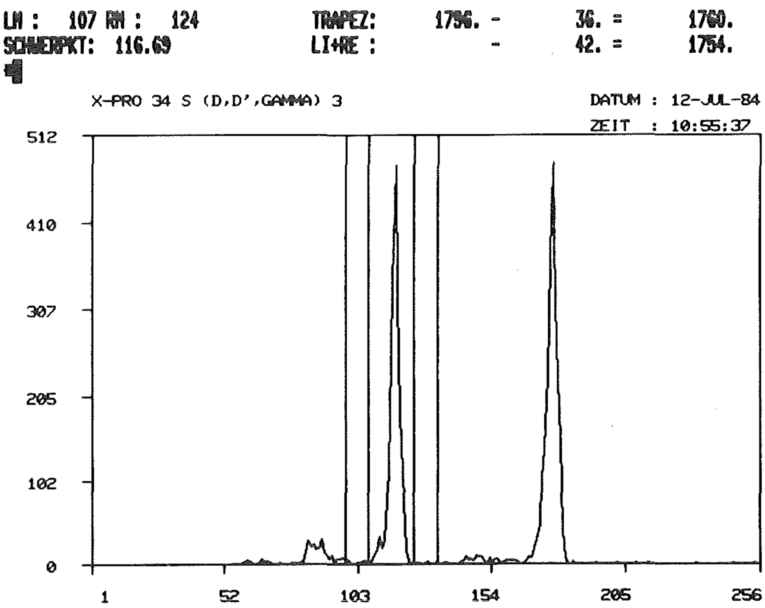

Fig. 2 X-projection from fig. 1

mensional spectrum on the x-axis. In these one-dimensional spectra the integration function also calculates the peak center and subtracts the background in two different ways (either in using the counts per channel of left and right margin to construct a trapezoid or in using the half integration interval left and right). Since users may have special demands the structure of the program is chosen to allow an easy implementation of additional functions.

(1) S. Zagromski, unpublished results (1980)
S. Zagromski, J. Buschmann, H.J. Gils, H. Jelitto, H. Rebel, H. Schlösser contr. 6.2.6

+ Physikalisches Institut der Universität Erlangen-Nürnberg

6.2.9 A MASS SPECTROMETER FOR FISSION FRAGMENTS BASED ON TIME-OF-FLIGHT AND ENERGY MEASUREMENTS

R. Brissot[+], P. Geltenbort[+], F. Gönnenwein[+], A. Oed[+], P. Perrin[+], E. Aker, D. Engelhardt, Nucl. Instr. and Meth. 219(1984)569

The fission fragment spectrometer "Cosi fan Tutte", previously set up by a collaboration of Tübingen University, ILL, Grenoble and Karlsruhe, was tested with fragments from the $^{235}U(n,f)$ reaction on an external thermal neutron beam at the ILL, Grenoble. The fragments being emitted from a thin fissile source on a thin backing after neutron capture by the target nucleus are detected by time-of-flight systems and ionization chambers. The time resolution achieved is 100 ps. The ionization chambers have the electric field arranged parallel to the particle trajectory, and with isobutane as the counting gas, the intrinsic energy resolution for fragments with $m \gtrsim 100$ amu is typically 400 KeV. In the light group of fission fragments, all masses are resolved individually with a mass resolving power $m/\delta m = 170$ for $m = 95$.

The velocity and kinetic energy data yield the final masses of fission fragments after prompt neutron evaporation. If the number of boil-off neutrons is low, coincidence measurements of both fragments allow the determination of the initial masses, as shown by E. Aker performing Monte Carlo calculations recently. In an approved experimental proposal we intend to investigate in 1984 the reaction $^{249}Cf(n,f)$ with the spectrometer described above.

+ Institut Laue-Langevin, Grenoble

6.2.10 STATUS OF THE LOW ENERGY PION SPECTROMETER PROJECT

H. Matthäy, K. Göring, A. Höhne, K. Kärcher, W. Kluge, M. Metzler,
D. Babic[+], D. George[+], M. Humbel[+], D. Renker[+]

The magnetic spectrometer LEPS (Low Energy Pion Spectromer), a more detailed description of which has been given elsewhere (1), will be used for the study of low energy pion scattering at SIN. It consists basically of two dipoles in a splitpole configuration preceeded by a quadrupole triplet. The function of the triplet is to reimage the target spot of the dispersed beam at an intermediate focus in front of the splitpole where low pressure multiwire proportional chambers will be placed. The detector at the intermediate focus will allow the simultaneous determination of the scattering angle and of the primary momentum of the incident pions. This particular design has the advantage that LEPS can be operated even at the maximum flux to be expected with the new Injector II.

During the last year the mechanical assembly of the spectrometer has been completed except for the splitpole vacuum chamber, and detailed field measurements have been carried out. The results of these measurements have been found to be in good agreement with the design specifications. As an example Fig. 1 shows for the central quadrupole Q_2 of the triplet the variations of the field gradient (Fig. 1a) and of the effective length (Fig. 1b), relative to the values tabulated in the figure as a function

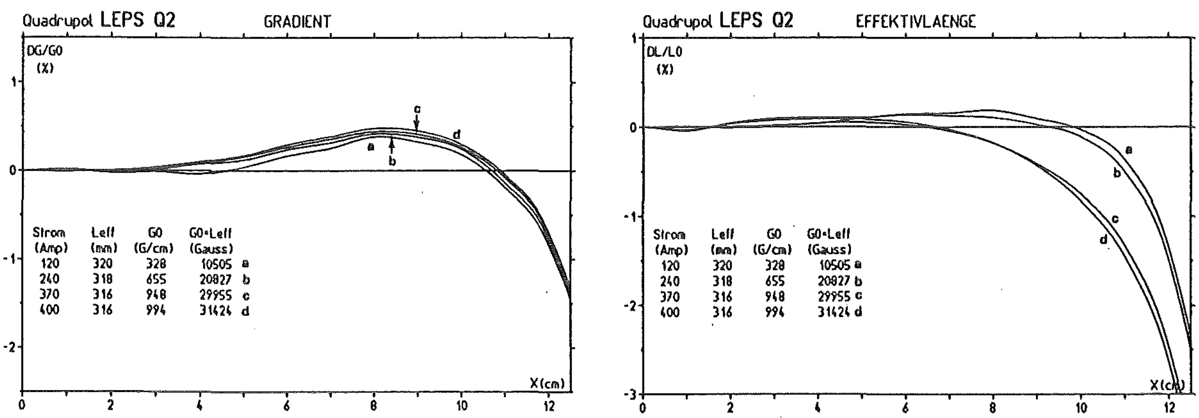

a) b)

Fig. 1 Field measurements with the central quadrupole Q_2. a: Deviation of the field gradient (in Gauss/cm) from the values G_o indicated in the figure as a function of the distance x from the symmetry axis (measured in the medium plane), for four currents. b: The corresponding deviation of the effective length from the values L_{eff} as given in the figure.

of the distance x from the symmetry axis (measured within the median plane) for 4 currents. A scale for these deviations is set by the aperture radius r = 80 mm. The results for the effective length have to be compared with the design value L_{eff} = 320 mm.

For the splitpole a set of field maps has been taken as well in the median plane as in planes with distances of ± 2.5 cm from the median plane covering most of the gap region (the gap width of both dipoles is d = 10 cm) crossed by the particle tracks. The field settings ranged from 0.4 through 1.4 T. Fig. 2a shows a field map for 1.35 T in the region of constant field corresponding to a central nominal momentum of p_o = 202.4 MeV/c. For an easier orientation also the contours of the two dipoles and the position of the cylindric spacers defining the gap width have been drawn. From these field maps all parameters which are required as input for the code RAYTRACE (2), i.e. position angle and curvature radii of the effective field boundaries and the fringe field coefficients have been redetermined.

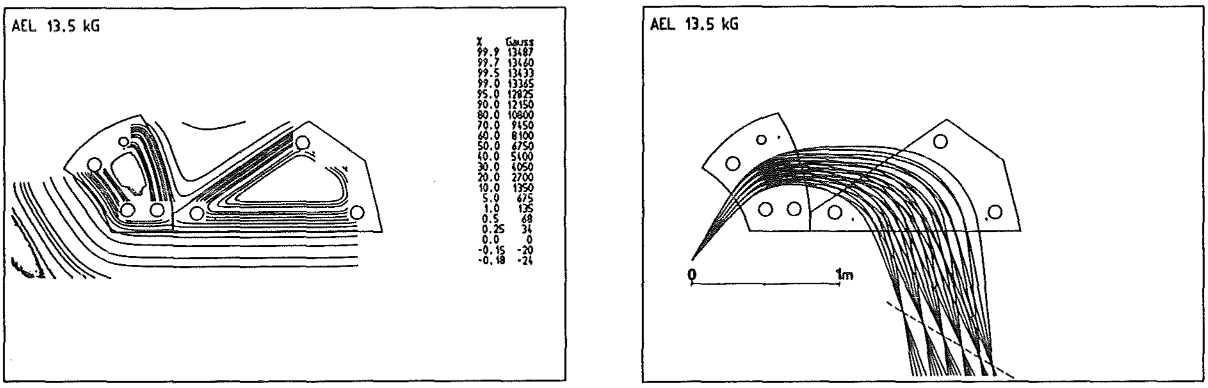

a) b)

Fig. 2 a: Field map in the medium plane of the splitpole for 1.35 T. b: Particle tracks calculated by means of the code GOCART. The position of the focal plane detector is indicated by a dashed line.

The observed deviations from the original design parameters are small and do not affect the inherent resolution of the spectrometer. As an additional check the code GOKART (3) developed at SIN has been used to calculate different rays in the median plane of the splitpole. In contrast to RAYTRACE GOKART uses only the measured field configuration and does not need any parametrisation of the field.

Fig. 2b displays the tracks of particles calculated by GOKART, which start with different momenta at the intermediate focus into the direction of the central ray and with angles of ± 50 mrad and ± 100 mrad relative to the latter. The six ray bundles to be seen on the exit side correspond to

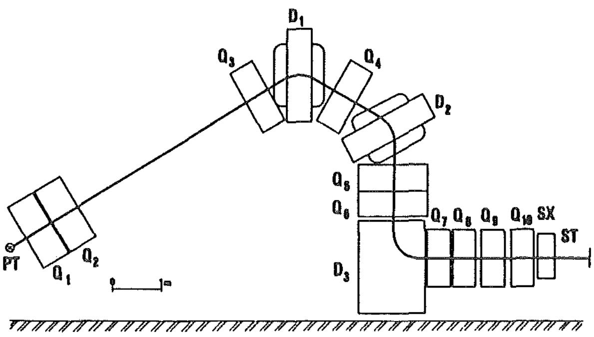

a)

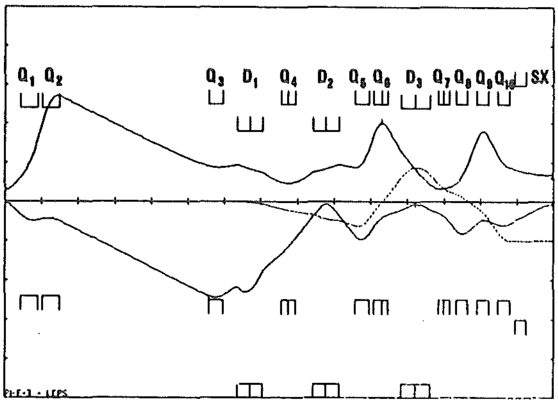

b)

Fig. 3 The modified πE3 beam for LEPS. a: Schematic lay-out (Q_1 - Q_{10} = quadrupoles, D_1 - D_3 = dipoles, SX = sextupole, PT = pion production target, ST = scattering target).
b: The upper curve represents the enveloppe for the nondispersive coordinate y, starting at the π-production target with $\Delta y_i = \pm 15$ mm and $\Delta\phi_i = \pm 60$ mrad. The lower curve represents the envelope for the dispersive coordinate x, starting with $\Delta x_i = \pm 1.5$ mm and $\Delta\theta_i = \pm 40$ mrad. In addition the dispersion trajectory for $\Delta p/p = 1\%$ is shown (dashed curve). The vertical axis is divided in units of 5 cm, the horizontal axis in units of 1 m.

the central momentum p_o and momenta differing from p_o by $\pm$ 7.5, $\pm$ 15, and + 20%, respectively.

Considerable efforts have been paid to the design of the modified pion channel πE3 for LEPS, which is depicted schematically in Fig. 3a. The ion-optical calculations, results of which are shown in Fig. 3b, the design of a new compact 90^o bending magnet (D_3), and the lay-out of the experimental area including supports, shieldings etc. have been completed. The beam spot at the target position will have a dispersion of 5 cm/(% of $\Delta p/p$), a size of 10 cm in the dispersive and of 4-5 cm in the nondispersive direction (see Fig. 3b). Sextupole components, i.e. the curvatures of the dipoles D_1-D_3 and the field strength of the sextupole S at the end of the channel have been adjusted to minimise the most dominant second order terms. Monte Carlo calculations with a modified RAYTRACE code including 1000 rays have shown that a momentum resolution of $< 10^{-3}$ can be expected.

(1) SIN Jahresbericht 1982, (SIN 1983) JB23
Annual Report on Nuclear Physics Activities 1982/83, Technical Report KfK 3621(1983)174

(2) H. Enge, S. Kowalski: Code RAYTRACE, Internal MIT-Report (1968)

(3) S. Adam, M. Humbel: Code GOKART(SIN 1984)

+ Schweitzerisches Institut für Nuklearforschung, Villigen

6.3 ACCELERATORS

6.3.1 OPERATION OF THE ISOCHRONOUS CYCLOTRON

F. Schulz, H. Schweickert

During the period of report the machine has been in full operation (see Table I,II). Since the compact cyclotron has taken over more or less all the commercial activities (isotope production, irradiation of machine parts) the machine operation has become smoother and much more efficient to run for nuclear physics experiments. The beam times for the injected particles ($^{6}Li^{3+}$, d↑) have been scheduled to be at least two weeks long. As expected this has led not only to higher available beam currents (up to 75 nA of extracted d↑) but also to a better beam quality.

Cyclotron Operational	With internal Ion Sources		With external Ion Sources		Total	
For Experiments	3404 h	75.5%	2754 h*	79.7%	6158 h	77.3%
Beam Development Testing new Components Developments for Isotope Production	412 h	9.1%	204 h	5.9%	616 h	7.7%
Total Time of Operation with the Beam on Targets	3816 h	84.6%	2958 h	85.6%	6774 h	85.0%
Scheduled shut-down for maintenance, Repair and Installation	172 h	3.8%	156 h	4.5%	328 h	5.0%
Unscheduled shut-down	525 h	11.6%	342 h	9.9%	867 h	10.0%
Total Shift Time	4513 h	100.0%	3456 h	100.0%	7969 h**	100.0%

* Polarized Deuteron 2032 h; $^{6}Li^{3+}$-Ion (156 MeV) 722 h

** The real time of 8760 h is achieved by adding a total 33 days shut down 24.12.83 - 13.2.84

Table I Statistics of the cyclotron from July 83 to June 1984

The main developments at the machine are:

- In december 1983 an atomic source was ordered from SECTEC (in Geneva). The source is specified to give a beam current of 50 μA within the phase acceptance of the cyclotron. When this sourve goes into operation in

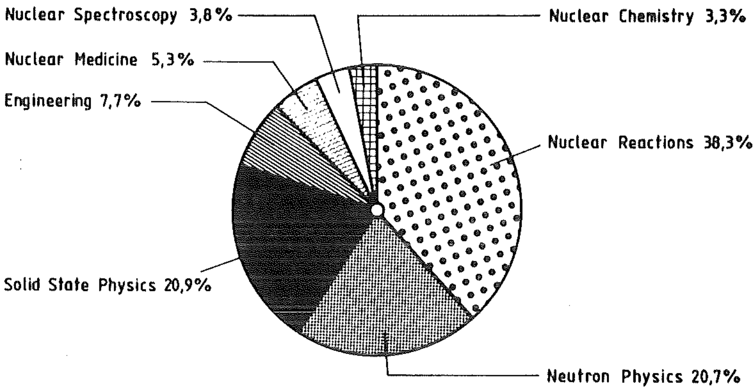

KfK-Karlsruhe Users

Institut für Kernphysik I	1277.33 h	20.74%
Institut für Kernphysik III	1060.58 h	17.22%
Institut für Radiochemie	180.50 h	2.93%
Labor für Isotopentechnik	46.42 h	0.75%
Institut für Heiße Chemie	19.75 h	0.32%
Institut für Nukleare Festkörper-Physik	14.83 h	0.24%
Technologie Transfer	0.83 h	0.01%
Hauptabteilung Ingenieurtechnik	0.50 h	0.01%
	2600.74 h	42.22%

External Users

Max-Planck-Institut für Kernphysik Heidelberg	831.08 h	13.45%
Universität Erlangen	623.50 h	10.12%
Freie Universität Berlin	556.33 h	9.03%
Techn. Universität München	477.17 h	7.75%
Universität Münster	230.25 h	3.74%
Universität des Saarlandes	49.92 h	0.81%
Universität Mainz	40.00 h	0.65%
Universität Bonn	20.75 h	0.34%
Technische Hochschule Darmstadt	12.03 h	0.20%
Universität Konstanz	9.25 h	0.15%
Universität Ulm	2.42 h	0.04%
	2852.75 h	46.32%

Aktivierung von Maschinenteilen	435.34 h	7.07%
Commercial Iodine-123-Production	147.75 h	2.40%
Commercial Rb-81-Production	122.08 h	1.98%
	705.17 h	11.46%
	6158.66 h	100.00%

Table II Statistics of the cyclotron from July 1983 to June 1984 early 1985 we expect to extract beam currents in the range of 1-2 μA. The first results of the special ECR-type ion source for the production of $^{6}Li^{3+}$, the other particle of interest for our machine, are looking very promising (see also report on ion source developments).

- In December 83 the new 100 kW amplifier, with a frequency range of 20-40 MHz, was deliviered and installed by the firm ZARAT (Warshaw). The amplifier tests on a 50 Ω waterload were satisfactorily finished by January 84 (see figure 1), but the available time for the first scheduled coupling to the cyclotron by February 84 had become too short. This is now planned for August 1984.

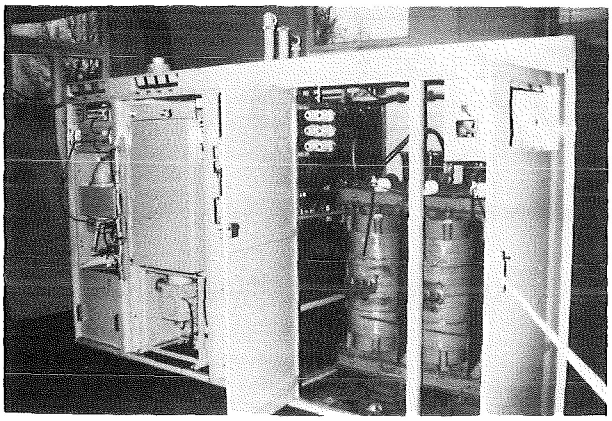

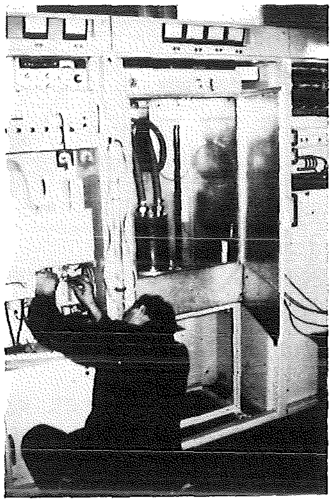

Fig. 1 The new 100 kW rf-amplifier installed outside the cyclotron vault. In the background is the 50 Ω transmission line to the cyclotron.

6.3.2 STATUS OF THE KARLSRUHE CP42H⁻ CYCLOTRON (KAZ)

J. Möllenbeck, H. Schweickert

In October 1983 the compact cyclotron $CP42H^-$ took over the isotope production from KIZ and by January 84 the irradiation of machine parts. For a new cyclotron the machine operates rather reliably, in fact the production has failed only once because of vacuum problems. In the last year we reported on a 0.37^{o} misalignment of the side-extracted beam. Since then the reason was found to be a shorting in one of the pancakes of the upper main coils. This could be compensated by an appropriate external shorting of one of the lower panackes.

In the spring of 1984 the extension of the KAZ-building was started for the so-called dual-beam target area. As seen from figures 2, in this new irradiation room the two beams (α-particles from KIZ, protons from KAZ) can be concentrated onto one target. It is planned to start the study of fusion wall materials in the mid of 1985.

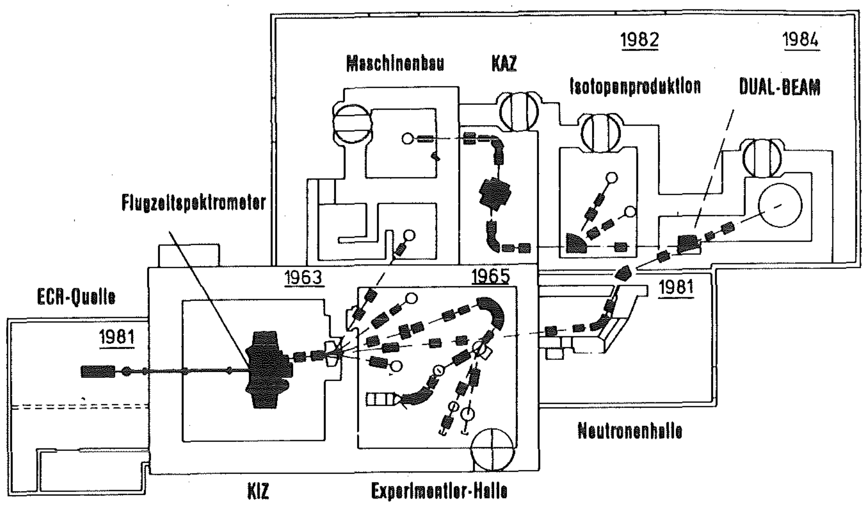

Fig. 2 Plan view of KIZ and KAZ including the building extension for the dual-beam set up.

6.3.3 COMPUTER CONTROL FOR THE BEAMLINES OF THE KARLSRUHE COMPACT CYCLOTRON

J. Bialy, H. Heinzmann, W.R. Kappel, B. Kögel, G. Rudolph, H. Schweickert, T.J. Thouw

The main features of this control system (1), which has shown to be very reliable since October 1983, are:

- Switch to a backup computer system within minutes.
- Comfortable and easy operation via touchpanels.
- Detailed and comprehensive warning/guiding message,
- Fast response to multiple operator action through separate touchpanel action and priority controlled tasks.
- Seven levels of sensitivity for the variable assignment potentiometer knobs.
- Many touchpanel controlled beam diagnostic elements.
- Extensive hard and software interlocks.
- Live update of all beamline parameters, in the form of block diagrams

and text on colour TV.

- Editor type "message system" for all groups.
- Flexible table driver, multitasking software written in Fortran.
- Easy to change off-line tables, database entries and warning/guiding message.

The hardware configuration shown in figure 1 consists mainly of two identical control console, a parallel Camac branch, two serial branches together with two NOVA 4 computers with peripherals, part of which is used by both NOVA's.

One console is in the compact cyclotron building, while the second is in the control room of the "big" Karlsruhe cyclotron.

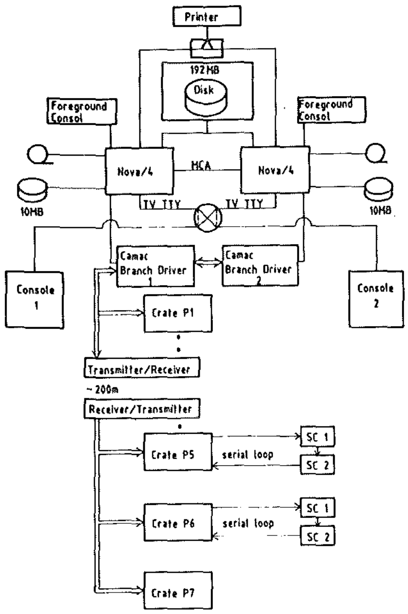

Fig. 1 Hardware configuration of the control system.

Fig. 2 Control consol.

All actions are initiated by touching a touchpanel field or, in special cases, by entering pre-defined commands at the Dasher keyboard. The touchpanels are used for all digital and beamdiagnostic actions, further to multiplex beam currents measurement on current display, to attach the magnet power supplies or vario TV control to the knobs, and for messages to all the groups.

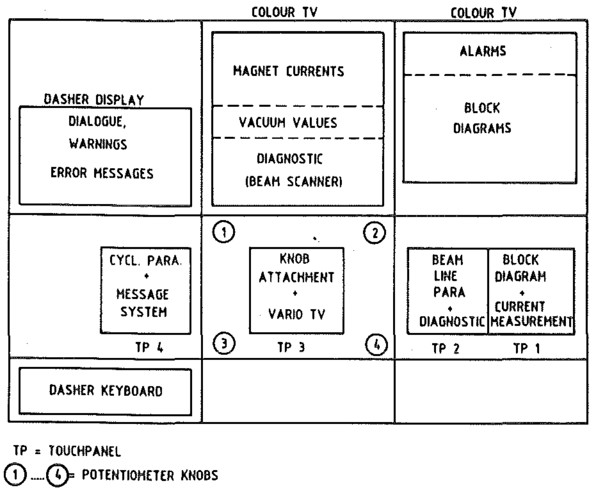

Fig. 3 Schematic view of the control console.

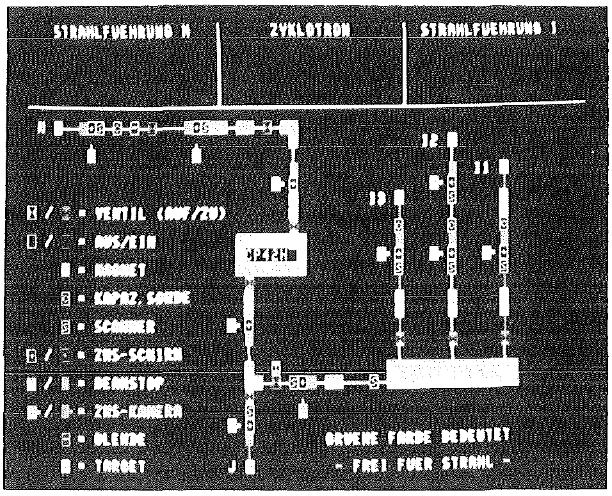

Fig. 4 Block diagram of all beamline parameter on the color display.

The control program (CP) written in assembler and Fortran, controls and supervises the environment. Basically the CP consists of two parts: the "consol management" running in the background and the "database management" in the foreground.

(1) J. Bialy, H. Heinzmann, W.R. Kappel, B. Kögel, H. Schweickert, G. Rudolph, T.J. Thouw
10th International Conference on Cyclotrons, East Lansing, USA 1984

6.3.4 ION SOURCE DEVELOPMENTS

V. Bechtold, H.P. Ehret, R. Ernst, L. Friedrich, J. Kaltenbaek, F. Schulz, L. Wiss, P. Ziegler

The external Penning and Lambshift sources are both still in operation. With the Lambshift source an extracted beam, from the cyclotron, of 52 MeV polarized deuterons with a maximum current of 76 nA has been achieved.

At the end of 1983 a polarized atomic source was ordered, and a special ECR-Li ion source built in order to obtain substantially higher intensities of both particle types, than are available at present.

Further improvements of HISKA (1), the heavy ion source for highly charged light ions, failed because of the rapid increase in the boil-off rate of the superconducting coils, which have been subsequently shipped back to the manufacturer. It is planned to reassemble the source at the end of this year. Meanwhile the charge state analyzing system of HISKA could be used for the development of LISKA, which is the small one stage ECR source designed for operation with Li vapour (figure 1). The permanent hexapole magnet is outside the vacuum chamber, which has to be heated to 350^{o}C and therefore requires metals sealings. For initial start up, the extraction system can be removed to achieve better pumping. During operation the vapour pressure is controlled by the wall temperature, and the Li vapour fed in by an oven. Special care has to be taken to protect the microwave window from the Li vapour. In an initial test run of 50 hours a current of about 3 μA of Li^{+++} was achieved after the Wienfilter (figure 2). The atomic beam source (PASKA) (figure 3) for polarized deuterons is planned to be installed at the beginning of 1985. An intensity of 60 μA is guaranteed within an emittance of 500 mm mrad at 10 keV. Cooling of the dissociator nozzle by liquid nitrogen is provided. Four hexapole magnets are used for optimum matching of the atomic beam to the ionizer, and the pumping is done by turbo and cryopumps. The source is vertically mounted with 90^{o} electrostatic deflection delivering a transverse polarized horizontal beam for injection into the cyclotron.

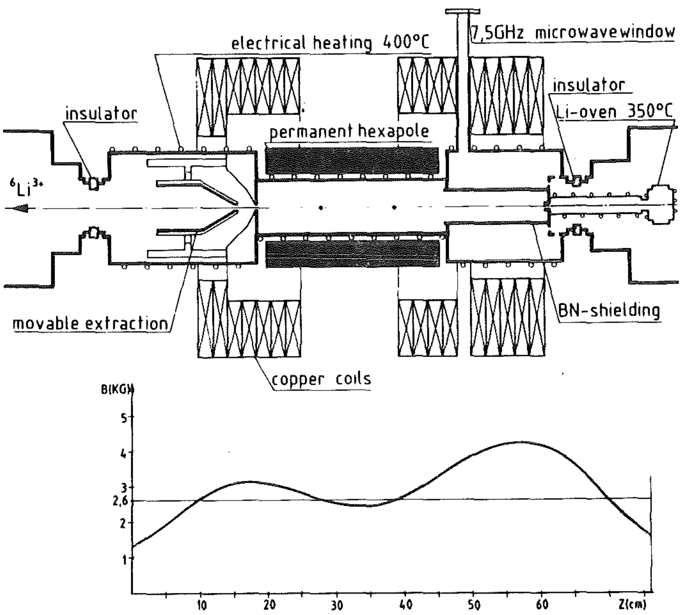

Fig. 1 A schematic layout of the Li-source LISKA. The measured field distribution anlong the axis is shown below.

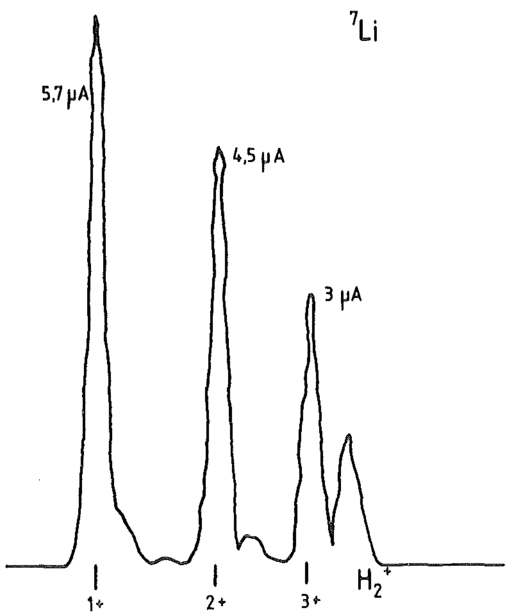

Fig. 2 Charge state distribution of ^{7}Li ions from LISKA

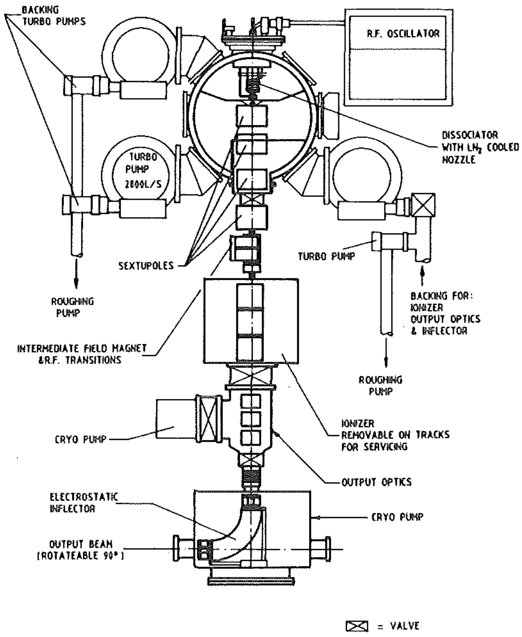

Fig. 3 Schematic layout of the polarized source PASKA

(1) V. Bechtold, L. Friedrich, F. Schulz
10th International Conference on Cyclotrons, East Lansing, USA 1984

6.3.5 MODIFICATION OF THE KARLSRUHE ISOCHRONOUS CYCLOTRON TO AN ENERGY VARIABLE MACHINE

H.P. Ehret, J. Schwabe, H. Schweickert, G. Starzewski+,
W. Wierba+

The modification of KIZ (1) to a K = 40 - 80 (Protons) and K = 50-130 (Z/A = 0.45-0.66) machine has been further studied. In the meantime it could be deduced from a number of beam dynamics calculations (2) that the proposed exchange of the pole face and the RF-system is feasable. At the moment the foreseen time schedule for this project is as following:

1. Replacing of the existing D-system in early 1986 and putting the machine into operation within 3 months. This will result in a more flexible machine in the 3rd harmonic mode giving us the possibility to accelerate not only completely stripped light ions (see Table I), and also energy variability.

Ion	Energy range (MeV/N)	Frequency range (MHz)
	16 - 30	25 - 34 (h = 3)
$\frac{e}{m} = \frac{1}{2}$	16 - 30	25 - 34 (h = 3)
$^{3}He^{2+}$	17 - 30	25 - 34 (h = 3)
$^{7}Li^{3+}$ ($^{7}Be^{3+}$)	19 - 26	27 - 32 (h = 3)
$^{12}C^{5+}$	17 - 25	25 - 34 (h = 3)
$^{14}N^{6+}$	18 - 26	26 - 32 (h = 3)
$^{20}Ne^{8+}$	16 - 23	25 - 30 (h = 3)

Table I Additional ions at KIZ by only replacing the resonatorsystem.

2. Replacing the straight sectors by spiraled ones in late 87 giving us, after about 6 month shut down, mainly the high energy protons (up to 80 MeV).

Therefore the main activities in the last months were concentrated on the designing of the new D-system. The rf-system consists of 3 separate resonators, each one of which is excited by an induction loop. The matching to the 50 Ω coaxial transmission line coming from one common power amplifier (100 kW, 24-40 MHz) via a high power splitter, is achieved by rotating the coupling loop. The coupling loop will be horizontal for 40 MHz and has to be rotated by 68° to match the 24 MHz. The geometry of the resonators inside the magnetic field is taken over from the existing machine. The final part of the outer conductor including the surrounding vacuum chamber has to be changed (figure 1). The tuning of the resonators is achieved by two vertical moving panels. To cover the frequency range of 24-40 MHz the calculated panel distance, Δd = 1-20 cm has to be realized. In a 1:3 model the calculations could be justified. The power consumption of the 3 resonators for the maximum frequency of 40 MHz will be:

losses in the resonator	70 kW
losses in the feeders	6 kW
losses in the power splitter	5 kW
losses in the 180° phase shifter for 2nd harmonic operation	3 kW
	84 kW

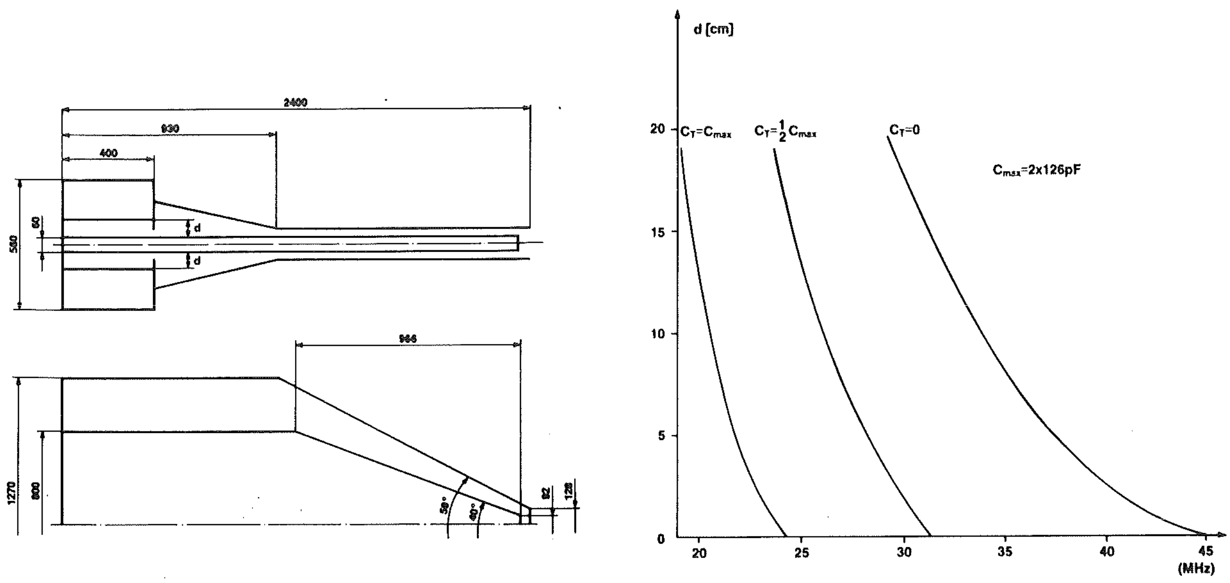

Fig. 1 Prinicple of the modified D-system. The tuning of the resonator is achieved by two vertical moving panels. For fine tuning an additional adjustable capacity is foresee. The shown tuning diagrams are measured values from the 3:1 model.

(1) J. Schwabe, H. Schweickert
Annual Report on Nuclear Physics Activities
KfK 3621 (1983) 183

(2) H.P. Ehret, J. Schwabe, H. Schweickert, G. Starzewski, W. Wierba
10th International Conference on Cyclotrons, East Lansing, USA 1984

+ Institute of Nuclear Physics, Krakow, Poland

6.3.6 PRODUCTION OF ISOTOPES FOR MEDICAL APPLICATION

K.H. Assmus, V. Bechtold, H. Dohrmann, D. Erbe, E. Foßhag, A. Hanser, N. Kernert, W. Maier, J.W. Peters, U. Sahm, H. Schweickert, S. Sheikh, S. Uhlemann

At the end of 1983 the routine production of radioactive isotopes for medical diagnostics was moved from the isochronous cyclotron (KIZ) to the new compact cyclotron (KAZ). Because the demand for beam time at KIZ for basic nuclear physics was so high, only a short test period at KAZ was possible for optimization of the beam-quality and target set-up. The following is the status in more detail:

^{123}I

Once again last year, the production of ^{123}I was the most important part of the isotope production program. In total, 750 batches, representing 43 Ci total activity, were produced. Most of the ^{123}I production is now sent to radiopharmaceutical companies for labelling purpose.

Due to the fact that major parts of the tellurium dioxide target at KAZ are fully compatible with the older KIZ target, there were no serious problems to switch the routine production.

$^{81}Rb/^{81m}Kr$ Generator

Besides 255 generators, which were sent to the hospitals directly an additonal 16 generators were produced for the production of mass-separated pure ^{81}Rb, which is used for basic nuclear medical research.

The production target at KAZ is shown in figure 1. To assure production reliability, two identical targets have been installed. A microprocessor based remote-control was installed for the automatic replacement of the target entrance foil, as well as the interchange of the target in use, in case of more several problems.

The installation of the specially designed hot cell for ^{81}Rb distribution and quality control will be finished in 84. This, together with the use of 70 % enriched krypton, will highly increase production capacity.

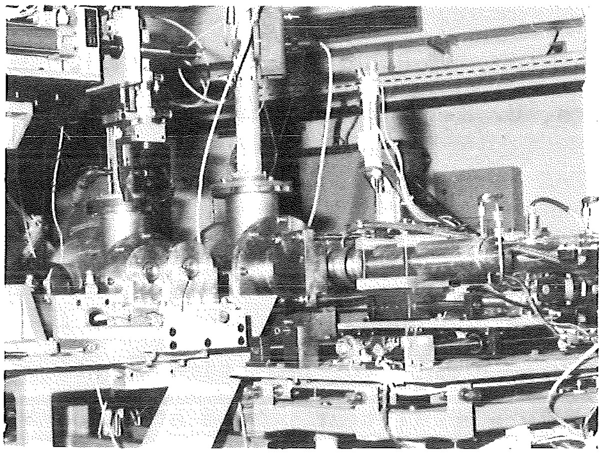

Fig. 1 ^{81}Rb production target at the compact cyclotron.

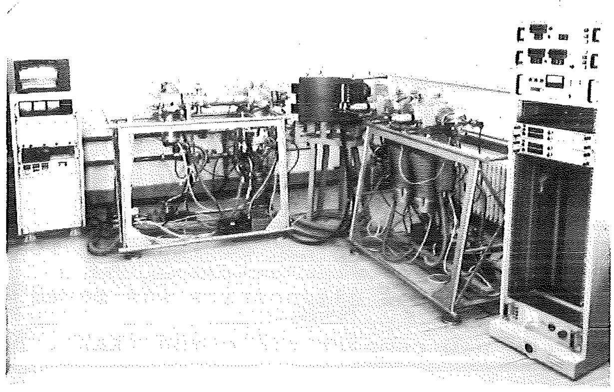

Fig. 2 90° Mass separator for the production of ultra pure iodine 123.

Ultra pure medical isotopes

Two 90° mass-separators have been installed (see figure 2) to produce routinely ultra pure iodine-123 and rubidium-81 for medical injection purposes. The main developments have been the special ion sources. For iodine a special ECR-type ion source and for rubidium a surface ionization source are used.

^{201}Tl

The irradiation and transportation system for the ^{201}Tl target has been finished and tested. Some minor changes are still necessary to improve the beam diagnostic capabilities. These will be finished by the end of 1984.

6.3.7 A NEW IRRADIATION SET-UP FOR MACHINE PARTS

P. Fehsenfeld, B.Gegenheimer, P.Herrmann, R.Pfeifer, R.Dreßen

Radionuclide technique for wear measurements developed at KfK has been used with a demand steadily increasing in industry and engineering research laboratories. To ensure the supply to the users of this technique with activated engine parts a new efficient irradiation facility is being erected at the Karlsruhe Compact Cyclotron. After a period of intensive testing the first stage of this computer controlled system for high quality series activation of engine components was put into operation in Januar 1984. The three-dimensional cross-slide arrangement in front of the head of beam line from the cyclotron (s.fig. below) enables to position machine components up to one ton weight in the incident beam with an accuracy of 0.02 mm. Increase in the guide bearing plays of the positioning unit, caused by wear, can be corrected without disassembly. So the original precision of the arrangement is maintained. The exact position of the engine parts in the incident beam is controlled by adjusting lasers.

The irradiation facility will be completed in 1986 to a capacity of 250 activated engine parts per year and can be extended at low costs to produce 700 parts per year. At that time up to 100 machine parts can be activated in one batch.

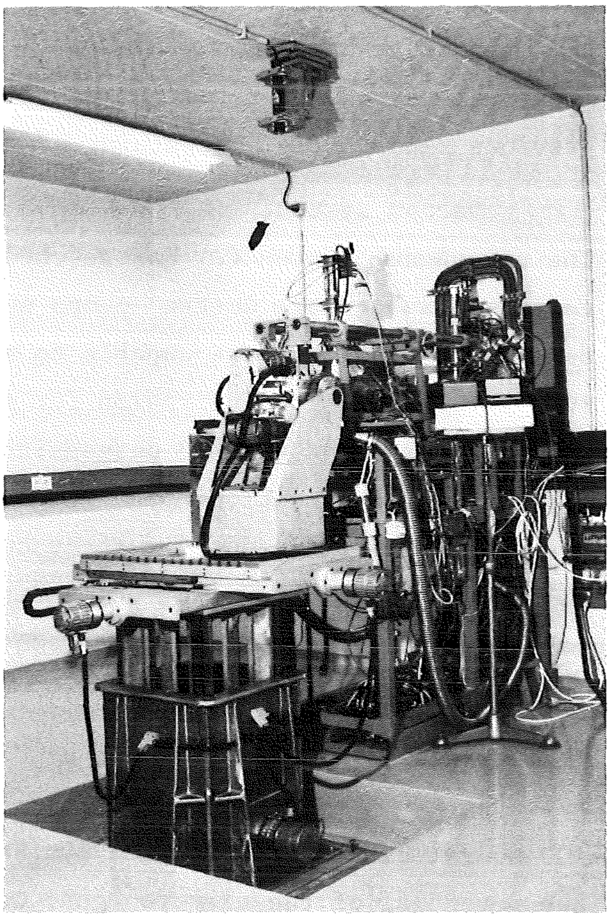

Fig.
Irradiation set-up for machine parts at Karlsruhe Compact Cyclotron (first stage). The computer controlled three-dimensional cross-slide system (fig. foreground) in front of the head of beam line enables to position machine components up to 1 t weight in the incident beam with an accuracy of 0.02 mm.

6.3.8 PROGRESS OF WORK ON THE ELECTRON COOLER FOR LEAR

M. Girardini[+], C. Habfast, H. Haseroth[+], C. Hill[+], L. Hütten, H. Poth, J.L. Vallet[+] and A. Wolf[++]

The Low Energy Antiproton Ring (LEAR) at CERN is in operation since summer 1983. It supplies about 16 experiments with antiprotons in the momentum range between 200 and 1500 MeV/c. The antiprotons are produced by the CERN Proton Synchrotron, stacked in the Antiproton Accumulator and injected into LEAR at 600 MeV/c. Prior to deceleration and during DC-extraction stochastic cooling is used to reduce beam dimensions.

At low momentum electron cooling will be used to facilitate further deceleration and the operation of an internal target. An electron beam of the same velocity is fractionally overlapped with the stored particles. Momentum spread and emittance of the circulating beam are cooled by repeated Coulomb interaction.

The electron cooler of the Initial Cooling Experiment (ICE) was adapted for use in LEAR in a KfK-CERN collaboration. The separate test of the components have been finished in summer 1984. The stages of the modifications and improvements of the ICE equipment were described in previous reports (1). The status of the work is as follows:

Vacuum system:
The new vacuum system (2) has reached the design vacuum of less than 10^{-11} Torr. Non Evaporable Getter pumps were installed and their performance determined (3). They are capable to maintain a pressure of less than 10^{-10} Torr in the cooling region for more than 20 hours with a gas flow equivalent to that from an outgassing hot thermocathode. The process for activation and conditioning has been optimized. Three hours after conditioning the pressure in the vacuum system passes $2 \cdot 10^{-11}$ Torr while it has been $1 \cdot 10^{-6}$ Torr during conditioning. The pumps have a saturation capacity of 1 Torr liter between cousecutive conditioning.

Control system:
The new control system has been used in connection with test beam measurements. It has been under operation with electron beam for about 100 hours. Part of the control system is installed in a Favaday cage at the potential of the electron gun. Communication is established by fiber optic links and television. The computer controlled value setting and

reading is completely independent from the analog control system which allows value to be set by fiber optics links and read-out by television. Both system can be used as a stand-alone control of the electron cooler. Neither faults nor neccessity of further improvements have been found. Computer control uses a menu-oriented FORTRAN program.

Test beam measurements:
The electron gun and the collecter of the ICE electron cooler connected by a short drifttube were subassembled for test measurements. Stable operation at 30 kV with a beam current of 800 mA and at 17 kV with 1200 mA has been reached so far. The collection efficiency is > 98% of the current and > 94% of the power. Parameter tables for computer controlled operation were taken. To maintain stable operation, slight modifications of the collector were necessary.

After the construction of correction coils for homogenification of the magnetic field (4) and final test beam measurements the installtion of all parts in the guiding magnet takes place in autumn 1984. Work has been started on non-destructive beam diagnostics and the construction of a 100 kV-gun. The collector will be further improved.

(1) Annual Report 1982/83, Technical Report KfK-3621(1983)187; L. Hütten et al., Proc. of the Workshop on Physics at LEAR with Low Energy Cooled Antiprotons, edts. U. Gastaldi and R. Klapisch (Plenum Publishing Corporation, 1984)

(2) L. Hütten et al., Das Ultrahochvakuumsystem der Elektronen-Kühlanlage für LEAR, Technical Report KfK-3816(1984)

(3) M. Girardini, Pompe modulaire à getter non evaporables; characteristiques et vitesses de pompages, PS/ML/Note 83-10(1983)

(4) A. Wolf et al., Magnetic field measurements in the electron cooling device for LEAR, Technical Report KfK-3718(1984)

+ CERN, PS Division, Geneva

++ now at CERN, EP Division, Geneva

6.3.9 STUDIES ON A HIGH INTENSITY PROTON ACCELERATOR

P. Blüm, H. Koch, G. Schaffer

Since several years European Medium Energy physicists agree on the usefulness of a facility for their special purposes. The interest concentrates on a proton machine with about 30 GeV energy and a high flux (≈ 100 μA). First studies for such a device were started at SIN, resulting in the scheme of a rapid cycling synchrotron feed by the 600 MeV SIN machine as injector. Since the very successful workshop on the "Future of Medium Energy Physics in Europe" in Freiburg (1) it became clear that also a great number of German physicists support such a project. It was felt that already at this very early stage of the project German phyicists should participate in the discussion of the technical details of the machine. Since then regular meetings take place at SIN and Karlsruhe. It was agreead that the expertise of the Karlsruhe physicists sould be helpful in the following items:

- Injection/extraction schemes via very fast kicker magnets. (This question is vital for the ligh cycling rate as envisaged).

- Studies of Ferrites for the fast tuning of the carities during the acceleration cycle.

- Design of low energy, very pure $K^{\pm}$-beams.

The work on these problems started recently is in progress. Different injection/extraction systems are compared and their costs are discussed in terms of the beam energies. A critical point of the design is the high HF-power to be installed around the ring. A good solution to this problem may be gas-cooled ferrite resonators, which are under study. With the programm "Transport" (2) studies on a 500 MeV/c low energy Kaon-beam were started. Particular emphasis was given to a design with an achromatic intermediate focus (3) which allows for high K^{-}-rates (about 2×10^{5}/sec) and simultaneously for a π/K-ratio which might be a factor of ten less than in previous beams.

(1) Proceedings of the "Workshop on the Future of Medium Energy Physics", Freiburg, 10-13. April 1984, to be published (Editors: H. Koch, F. Scheck)

(2) K.L. Brown et al., CERN-Yellow-Report 76-13 (1976)

(3) P. Birien, Proceedings of the International Conference on Hypernuclear and Kaon Physics, Heidelberg 1982, p. 371, (Editor: B. Povh)

6.4 APPLICATIONS

6.4.1 LOCAL MATRIX THICKNESS DETERMINATION IN SCANNED MICRO-PIXE BY PROTON BACKSCATTERING

D. Heck and E. Rokita[+], Nucl. Instr. Meth. 231 (1984) 259

Scanned micro-PIXE of microtome slices cut from medical tissue samples reveals local X-ray intensities of trace elements. These X-ray intensities vary locally due to the thickness variations of the slices. To eliminate this dependence, the mass distribution across the specimen slice must be known. We determine the thickness by simultaneous measurement of the elastically backscattered protons (Rutherford Back-Scattering), as proposed by Russell. A linear dependence of the RBS yield from the target thickness is only guaranteed if the scattering cross sections of the matrix constituents are free of resonances within the energy interval which the protons pass through by the slowing down. This holds for the main constituents of organic matter C, N and O at proton energies of 3 MeV, when the RBS detector is mounted in 135° (for kinematic reasons H does not contribute to the RBS count rate). For these three elements the cross sections are nearly constant from E_p = 3 MeV down to 2.7 MeV. This limits the target thickness to ∿ 2 mg cm^{-2}, which is much thicker than the microtome slices of ∿ 8 μm which we used. The calibration of the mass determination is performed with a homogeneous plastic foil. The different elemental compositions of this foil and of organic tissue are taken into account by an 8 % correction. Examples for mass corrected trace element distributions are given.

+ Institute of Physics, Jagellonian-University, Cracow, Poland

6.4.2 APPLICATION OF THE KARLSRUHE PROTON MICROPROBE TO MEDICAL SAMPLES

D. Heck and E. Rokita[+], Nucl. Instr. Meth. 231 (1984) 606

The Karlsruhe nuclear microprobe was used in the investigation of healthy and malign tissue of animals and men. Target preparation tests showed that cryofixation of the tissue before cutting with a microtome and succeeding lyophilization of the slices gave reliable results. The slices were mounted on backing foils of Formvar the thickness of which varied between 30 and 50 μg/cm². For irradiation we tested various patterns generated by the 3 MeV proton beam by sweeping in one or two dimensions. Most of the data were collected in line-scan mode, where 256 equidistant irradiation dots of 3x10 μm² formed a line of 750 μm length at beam currents of 250 pA. The target thickness was determined simultaneously by proton elastic scattering in all cases.

Radial concentration profiles of degenerated human arteries (atherosclerosis) showed a remarkable increase of Ca, partly correlated with local maxima of the Zn content, when compared with non-degenerated capillaries. Microtome cuts across a Morris Hepatoma 7777 cancer grown in a rat leg were investigated to correlate the concentration shifts of some trace elements in malign tissue with single cells.

+ Institute of Physics, Jagellonian-University, Cracow, Poland

6.4.3 NUCLEAR MICROPROBE ANALYSIS AT KARLSRUHE

D. Heck, Journal de Physique, 45 (1984) C2-245

Charged particle reactions are used in the Karlsruhe nuclear microprobe for the analysis of light elements. (d,p) reactions are performed to determine the content of carbon and nitrogen in metallic and nonmetallic bulk material specimens. Elements with $Z \geq 13$ are identified by means of particle induced X-ray emission (PIXE) in concentrations down to the ppm range. This method is best suited for detection of trace elements in organic matter.

6.4.4 TRACE ELEMENT DISTRIBUTIONS IN HUMAN LIVER

D. Heck, A. Ochs[+], C. Kratt[++], and K.P. Maier[+]

Small pieces of human liver, which were taken routinely during cholecystectomies, are snap-frozen and cut with a microtome. The 5 μm thick slices

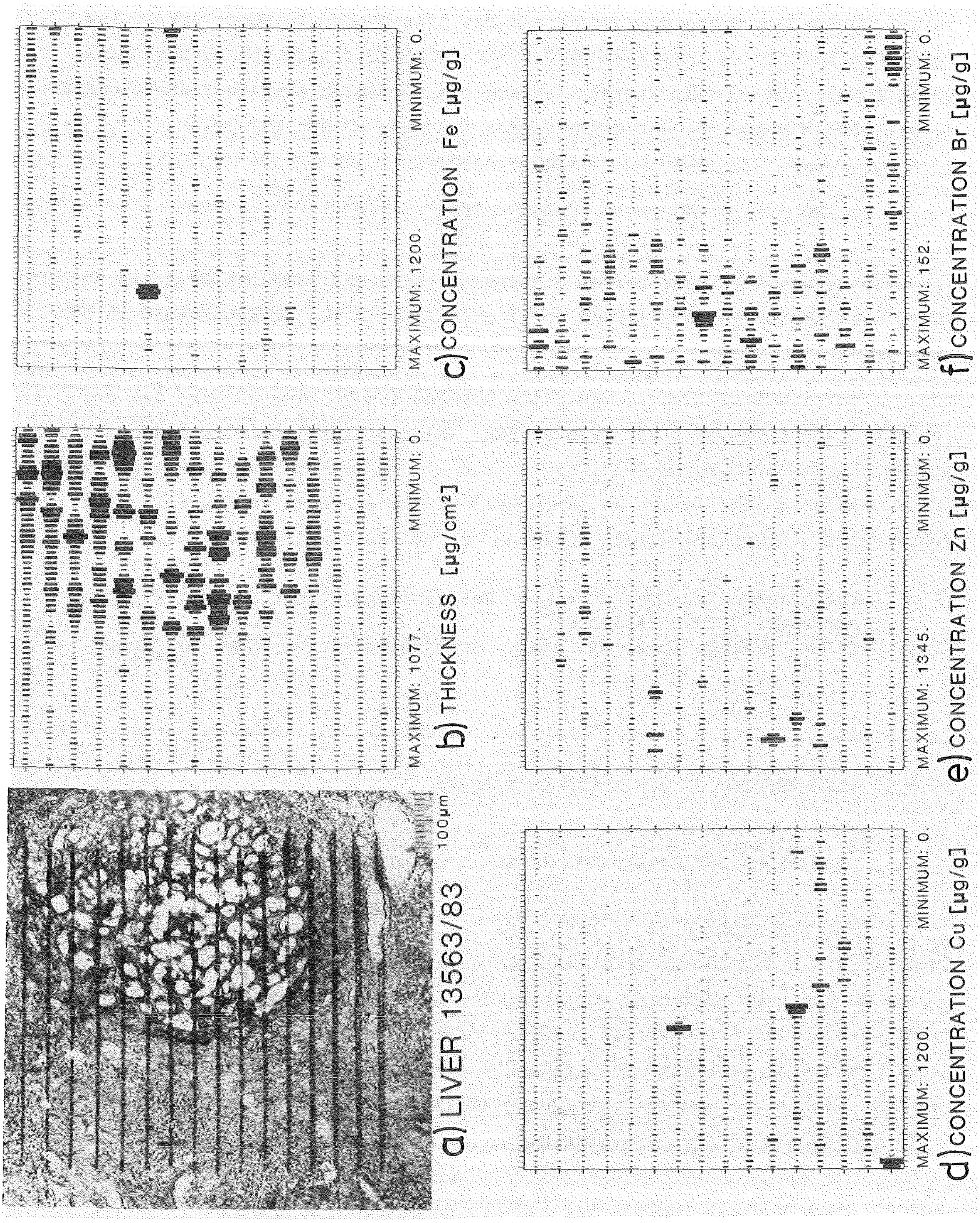

are mounted on Formvar^R backing foils and dried in vacuum for irradiation. The neighbouring slices are brought onto microscopic slices and stained with usual histochemical procedures to identify the structure of the liver lobules. In the ion microprobe setup a 3 MeV proton beam is swept across the samples covering an area ∿ 0.7 x 0.7 mm² centered around the central vein of a lobule. In healthy livers, we find the following average trace element concentrations and concentration ranges (in µg/g of dry matter)

Fe	800	(200 - 1400)
Cu	32	(21 - 46)
Zn	480	(180 - 700)
Br	7	(2 - 16)

In comparison with these values a decrease of Fe and increase of Br is observed within the stroma around the portal area in the neighbourhood of the lobule.

In cirrhotic livers, where the lobules (right side of Fig. 1a) are constricted by stroma (left side of Fig. 1a) and finally become necrotic, these changes are pronounced (Fig. 1c and f). It is interesting to see that Cu is enhanced just in the neighbourhood of the necrotic lobule (Fig. 1d), while Zn is rather completely depleted out of the lobule (Fig. 1e).

+ Fachbereich Gastroenterologie, Medizinische Klinik, Städt. Krankenanstalten, 7300 Esslingen

++ Pathologisches Institut, Städt. Krankenanstalten, 7300 Esslingen

6.4.5 THE STOPPING OF DEUTERONS IN LITHIUM

R. Dierckx[+], W. Kley[+], A. Verga[++], E.V. Benton[+++], J. Buschmann, (1)

The interaction of 52 MeV deuterons with lithium was investigated, in view of the optimization of a lithium target for an intense neutron source based on the d-Li stripping reaction. The experimental results are compared with theoretical calculations obtained from an updated version of the BRAGG code. This code describes in detail the interaction of charged particles with matter. Within the experimental uncertainties the theoretical results are well reproduced by the experiments.

(1) dito, Nuclear Engineering and Disign/Fusion (in press)

+ Joint Research Centre - Ispra Establishment

++ Politecnico di Milano, Milano - Italy

+++ University of San Francisco, San Francisco, U.S.A.

6.4.6 A π^- TRANSPORT CALCULATION APPLIED TO A BEAM FROM A BIOMEDICAL PION CHANNEL

H. Hilgendorff, G. Büche

In the preceding Annual Report distributions of absorbed dose as well as energy deposition spectra were presented which resulted from applications of our π^- transport code PIONDOSE to pencil beams of negatively charged pions. Among the results energy deposition spectra were approved by a comparison to those from a corresponding measurement. In the following we face experimentally determined to calculated isodose contours which have been worked out for one of the 60 beams of the biomedical facility PIOTRON at SIN.

In an earlier experiment (1) trajectories of particles were measured as a function of the beam current settings. Missing additional information like the momentum distribution as a function of the space coordinates was worked out using a beam transport code named TURTLE (2). This way an almost complete set of beam parameters could be used to calculate distributions of absorbed dose within a water phantom. Fig. 1 shows isodose contours for two cuts through the phantom along the beam axis. For matter of comparison experimentally determined isodoses (3) are reproduced within the same frame. From Fig. 1 we state that both systems of isodose contours match remarkably well. It should be stressed that our calculation contains input data like stopping powers, cross sections, yields and spectra of secondary particles etc. that nearly all were approved experimentally and that no fitting procedure related to still unganged parameters (absolute momentum, momentum resolution etc.) was applied. From these statements and those given earlier

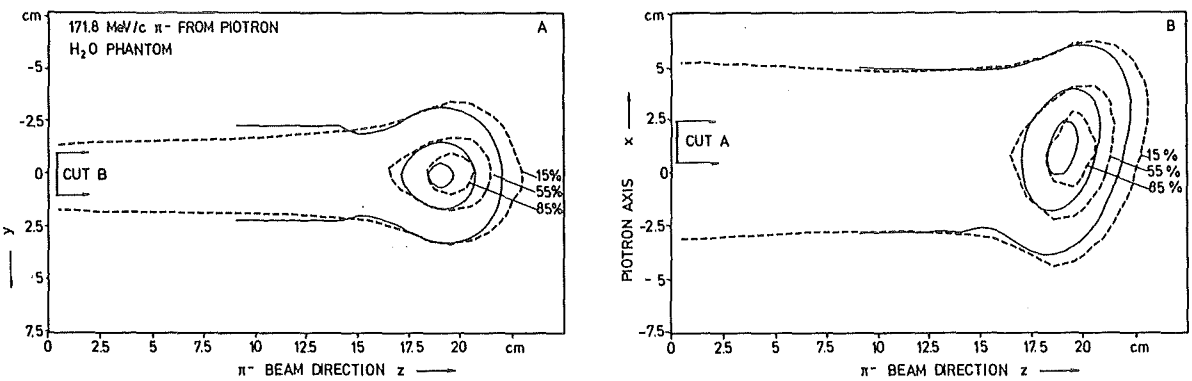

Fig. 1 The absorbed dose from a negatively charged pion beam decelerated within a water phantom. Broken lines are isodoses from a transport calculation, full curves reproduce results from a measurement.

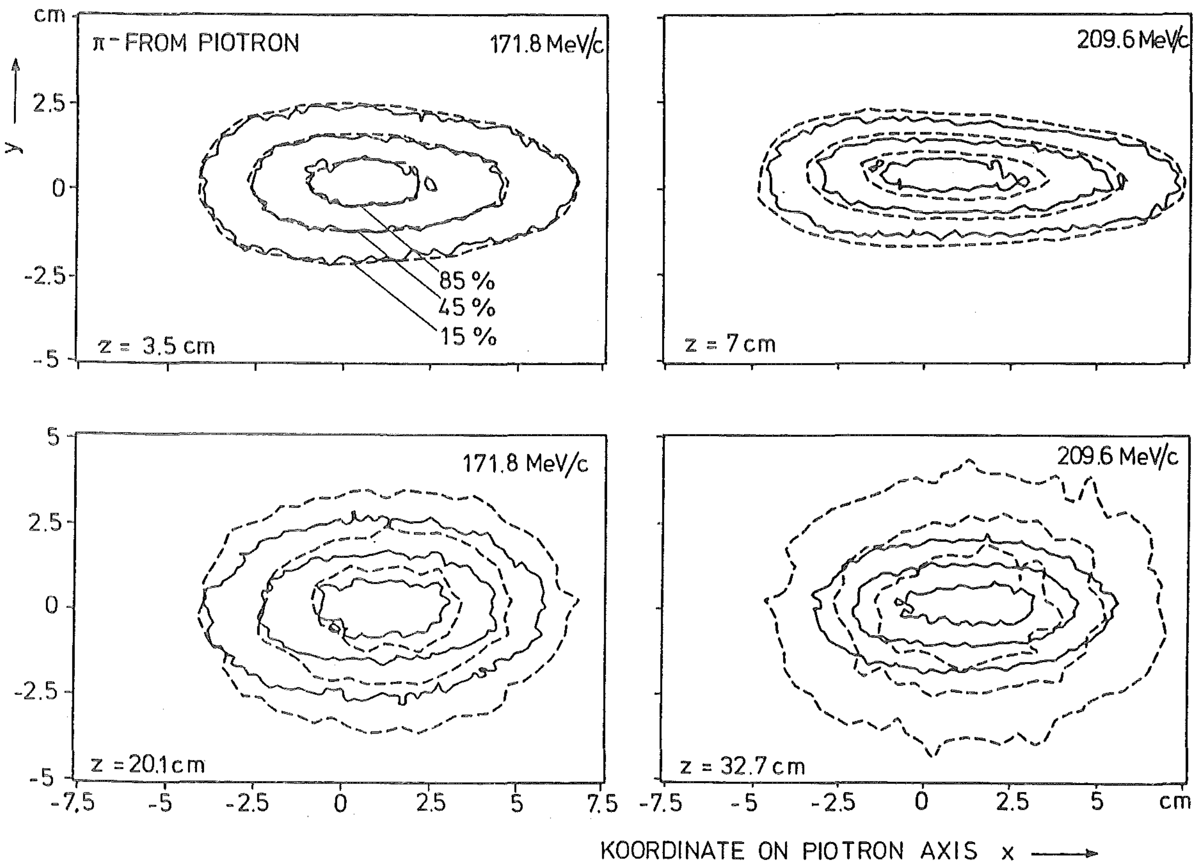

Fig. 2 Contours of absorbed dose in water perpendicular to the beam axis (broken curves) together with distributions of points, where trajectories of particles in air hit the respective planes (full curves).

in connection with the energy deposition spectra one can conclude that the essential physical data necessary for treatment planning procedures are amassed.

Fig. 2 shows a few additional features of the beam. Cross sections of the beam profile for two different momenta and the corresponding isodose contours are plotted for positions just behind the phantom surface (upper half) and that of the Bragg peak. It reveals clearly by the particle distributions that the beam is convergent in the x-direction and divergent in the y-direction. The corresponding isodoses show how convergence of the beam is counterbalanced from scattering and straggling processes of pions during their deceleration leading to a blow up of the beam within the π^- stopping region.

(1) U. Wiedner, Diploma Thesis (Universität Karlsruhe, 1982), unpublished
(2) K.L. Brown, Ch. Iselin, Decay Turtle - A computer program for simulating charged particle beam transport systems ..., Technical Report CERN 74-2 (1974)
(3) E. Pedroni, SIN, private communication (1983)

7. LIST OF PUBLICATIONS

7.1 PUBLICATIONS AND REPORTS

ABELA, R.; BLUEM, P.; GOTTA, D.; KUNOLD, W.; MEISSNER, K.; SCHNEIDER, M.; SIMONS, L.M.
First experimental experience with a cylotron trap.
SIN Newsletter, (1984) Nr. 16, S.65

ADIELS, L.; BACKENSTOSS, G.; BLUEM, P.; BERGSTROEM, I.; FRANSSON, K.; GUIGAS, R.; KOCH, H.; KEREK, A.; MEYER, M.; PAVLOPOULOS, P.; POTH, H.; RAICH, U.; RICHTER, B.; REPOND, J.; SUFFERT, M.; TAUSCHER, L.; TROESTER, D.; ZIOUTAS, K.
Search for narrow exotic states in p annihilations on ^{4}He.
Physics Letters B, 138(1984) S.235

ALMEIDA, J.; KAEPPELER, F.
Neutron capture cross sections of supra(20,21,22)Ne between 5 and 400 keV and the neutron balance in s-process nucleosynthesis.
Boeckhoff, K.H. [Hrsg.]
Nuclear Data for Science and Technology. Proc.of the Internat.Conf., Antwerpen, B, September 6-10, 1982
Dordrecht : Reidel, 1983. - S.948-51

AURES, R.; BISCHOFF, A.; BRADY, F.P.; DOLL, P.; FINCKH, E.; HEERINGA, W.; HOFMANN, K.; KLAGES, H.O.; WILCZYNSKI, J.; ZEITNITZ, B.
Measurement of the spin correlation parameter Asub(yy) for n-p scattering in the energy range up to 50 MeV.
Zeitnitz, B. [Hrsg.]
Few Body Problems in Physics. Proc.of the 10th Internat.IUPAP Conf.on Few Body Problems in Physics, Karlsruhe, August 21-27, 1983. Vol. II
Amsterdam [u.a.]: North-Holland 1984 S.33-34

AURES, R.
Aufbau und Erprobung eines polarisierten Protonentargets.
KfK-3647 (Dezember 83)
Dissertation, Universitaet Karlsruhe 1983

BACKENSTOSS, G.; CIERJACKS, S.; FURIC, M.; IZYCKI, M.; LJUNGFELT, S.; MANKIN, U.; PETKOVIC, T.; SCHMIDT, G.; STEINACHER, M.; ULLRICH, H.; WEBER, P.; WEYER, H.J.; WEYMARN, K.VON
π^{+}/π^{-} absorption in ^{3}He at 120 MeV.
Zeitnitz, B. [Hrsg.]
Few Body Problems in Physics. Proc.of the 10th Internat.IUPAP Conf.on Few Body Problems in Physics, Karlsruhe, August 21-27, 1983. Vol. II
Amsterdam [u.a.]: North-Holland 1984 S.239-42

BACKENSTOSS, G.; IZYCKI, M.; STEINACHER, M.; WEBER, P.; WEYER, H.J.; WEYMANN, K.VON; CIERJACKS, S.; LJUNGFELT, S.; MANKIN, U.; PETKOVIC, T.; SCHMIDT, G.; ULLRICH, H.; FURIC, M.
Isospin dependence of pion absorption on nucleon pairs in ^{3}He.
Physics Letters B, 137(1984) S.329-33

BACKENSTOSS, G.; IZYCKI, M.; STEINACHER, M.; WEBER, P.; WEYER, H.J.; WEYMANN, K.VON; CIERJACKS, S.; LJUNGFELT, S.; MANKIN, U.; PETKOVIC, T.; SCHMIDT, G.; ULLRICH, H.; FURIC, M.
Isospin dependence of pion absorption on nucleon pairs in ^{3}He.
Physics Letters B, 137(1984) S.329-33

BACKENSTOSS, G.; CIERJACKS, S.; FURIC, M.; IZYCKI, M.; LJUNGFELT, S.; MANKIN, U.; PETKOVIC, T.; SCHMIDT, G.; STEINACHER, M.; ULLRICH, H.; WEBER, P.; WEYER, H.J.; WEYMARN, K.VON
π^{+}/π^{-} absorption in ^{3}He at 120 MeV.
Zeitnitz, B. [Hrsg.]
Few Body Problems in Physics. Proc.of the 10th Internat.IUPAP Conf.on Few Body Problems in Physics, Karlsruhe, August 21-27, 1983. Vol. II
Amsterdam [u.a.]: North-Holland 1984 S.239-42

BECK, R.; DICKMANN, F.
Calculation of the momentum distribution of the alpha-deuteron motion in ^{6}Li.
Zeitnitz, B. [Hrsg.]
Few Body Problems in Physics. Proc.of the 10th Internat.IUPAP Conf.on Few Body Problems in Physics, Karlsruhe, August 21-27, 1983. Vol. II
Amsterdam [u.a.]: North-Holland 1984 S.457-58

BEER, H.; MACKLIN, R.L.
The neutron capture cross sections of supra(178,179,180)Hf and the origin of nature's rarest stable isotope ^{180}Ta.
Boeckhoff, K.H. [Hrsg.]
Nuclear Data for Science and Technology. Proc.of the Internat.Conf., Antwerpen, B, September 6-10, 1982
Dordrecht : Reidel, 1983. - S.945-47

BEER, H.; KAEPPELER, F.; REFFO, G.; VENTURINI, G.
Neutron capture cross sections of stable xenon isotopes and their application in stellar nucleosynthesis.
Astrophysics and Space Science, 97(1983) S.95-109

BEER, H.; KAEPPELER, F.; YOKOI, K.; TAKAHASHI, K.
The s-process branching at ^{151}Sm.
The Astrophysical Journal, 278(1984) S.388-95

BEER, H.; WALTER, G.
On the s-process nucleosynthesis of zirconium in S-stars.
Astronomy and Astrophysics, 133(1984) S.317-19

BEER, H.; WALTER, G.
Cosmochronology with the ^{87}Rb/^{87}Sr isobaric pair.
Astrophysics and Space Science, 100(1984) S.243-53

BEKK, K.; NOWICKI, G.; BEKK, P.
Verfahren zur Abreicherung der ^{124}J-Verunreinigungen in ^{123}J-Chargen.
DE-OS 32 02 520 (4.8.1983)

BERDOZ, A.; FAVIER, B.; FOROUGHI, F.; WEDDIGEN, CH.
Measurement of the analysing power of elastic proton-proton scattering at 582 MeV.
Journal of Physics G, 9(1983) S.L261-L265

BLUEM, P.
Proton-antiproton annihilations at rest into $\pi^0\omega$, π^0eta $\pi^0\gamma$ $\pi^0\pi^0$, and π^0eta.
Nuclear Physics B, 228(1983) S.424-38

BLUEM, P.; POTH, H.; SIMONS, L.M.
Measurement of the annihilation cross section at very low energy.
Gastaldi, U.; Klapisch, R. [Hrsg.]
Proc.of a Workshop on Physics at LEAR with Low-Energy Cooled Antiprotons, held at Erice, I, May 9-16, 1982
New York [u.a.]: Plenum Pr., 1984. S.823

BODENKAMP, J.; FRIES, D.C.; MARKOU, A.; SEITZ, E.; BEHREND, H.J.; FENNER, H.; HESSE, W.P.; MIYACHI, T.; MCNEELY, W.A.; SCHROEDER, V.
Cross section and proton antiproton invariant mass distribution of the reaction γproton→proton antiproton proton at 4.7<=Esub(γ)<=6.6 GeV.
Physics Letters B, 133(1983) S.275-78

BRADY, F.P.; DOLL, P.; HANSMEYER, J.; HEERINGA, W.; HIEBERT, J.C.; KLAGES, H.O.; PLISCHKE, P.; WILCZYNSKI, J.
Measurements of the neutron-proton analyzing power between 17 and 50 MeV.
Zeitnitz, B. [Hrsg.]
Few Body Problems in Physics. Proc.of the 10th Internat.IUPAP Conf.on Few Body Problems in Physics, Karlsruhe, August 21-27, 1983.
Vol. II
Amsterdam [u.a.]: North-Holland 1984 S.27-30

BRADY, F.P.; DOLL, P.; FINCKH, E.; HEERINGA, W.; HOFMANN, K.; KLAGES, H.O.; NITZ, W.; WILCZYNSKI, J.
Analyzing power of the elastic n-d scattering from 14 MeV to 50 MeV.
Zeitnitz, B. [Hrsg.]
Few Body Problems in Physics. Proc.of the 10th Internat.IUPAP Conf.on Few Body Problems in Physics, Karlsruhe, August 21-27, 1983.
Vol. II
Amsterdam [u.a.]: North-Holland 1984 S.527-28

BRADY, F.P.; DOLL, P.; HAESNER, B.; HEERINGA, W.; HOFMANN, K.; JANY, P.; KLAGES, H.O.; MAIER, CHR.; WILCZYNSKI, J.
Measurement of the analyzing power of the elastic n-^{3}He scattering up to 50 MeV.
Zeitnitz, B. [Hrsg.]
Few Body Problems in Physics. Proc.of the 10th Internat.IUPAP Conf.on Few Body Problems in Physics, Karlsruhe, August 21-27, 1983.
Vol. II
Amsterdam [u.a.]: North-Holland 1984 S.537-38

BRZYCHCZYK, J.; FREINDL, L.; GROTOWSKI, K.; MAJKA, Z.; MICEK, S.; PLANETA, R.; ALBINSKA, M.; BUSCHMANN, J.; KLEWE-NEBENIUS, H.; GILS, H.J.; REBEL, H.; ZAGROMSKI, S.
Fusion and nonfusion phenomena in the ^{6}Li + ^{40}Ca reaction at 156 MeV.
Nuclear Physics A, 417(1984) S.174-88

CELLO-COLLABORATION
Production of the f_0 meson in photon-photon collision.
Zeitschrift fuer Physik C, 23(1984) S.223

CELLO-COLLABORATION
Limits on spin 0 bosons in $e^+ e^-$ annihilation up to 45.2 GeV C.M. energy.
DESY 84-020 (February 1984)
Physics Letters B, 140(1984) S.130

CELLO-COLLABORATION
Search for new heavy quarks in e^+e^- collisions up to 46.78 GeV in C.M. energy.
DESY Report 84-051 (1984)

CELLO-COLLABORATION
Limits on spin 0 bosons in $e^+ e^-$ annihilation up to 45.2 GeV C.M. energy.
DESY 84-020 (February 1984)

CELLO-COLLABORATION
Measurement of the reaction $\gamma\gamma\to\pi^+\pi^+\pi^-\pi^-$ at PETRA.
DESY-83-081 (September 83)
Zeitschrift fuer Physik C, 21(1984) S.205-18

CELLO-COLLABORATION
Observation of a multiparticle event with 2 isolated energetic muons in e^+e^- interactions.
DESY 84-024 (March 1984)

CELLO-COLLABORATION
On the model dependence of the determination of the strong coupling constant in second order QCD from e^+e^--annihilation into hadrons.
Physics Letters B, 138(1984) S.311-16
DESY 83-127 (December 83)

CELLO-COLLABORATION
New data on semihadronic decays of the tau-lepton.
Zeitschrift fuer Physik C, 23(1984) S.103-09

CELLO-COLLABORATION
Investigation of two photon final states in e^+e^- annihilation at $<\sqrt{s}>=34.2$ GeV.
DESY-82-080 (Dezember 82)
Physics Letters B, 123(1983) S.127-32

CELLO-COLLABORATION
tau branching ratios and polarization limits in e^+e^- interaction at $\sqrt{s}=34$ GeV.
DESY-83-019 (Maerz 83)
Physics Letters B, 127(1983) S.270-76

CELLO-COLLABORATION
Measurement of the tau lifetime.
Nuclear Physics B, 211(1983) S.369-74
DESY-82-056 (August 82)

CELLO-COLLABORATION
Inclusive production of electrons and muons in multihadronic events at PETRA.
Zeitschrift fuer Physik C, 19(1983) S.291-99
DESY-83-034 (Mai 83)

CELLO-COLLABORATION
Experimental study of the hadronic photon structure function.
Physics Letters B, 126(1983) S.391-97
DESY 83-018 (March 83)

CELLO-COLLABORATION
Inclusive γ and π^0 production in e^+e^- annihilation at 14,22 and 34GeV c.m. energy.
DESY-83-066 (Juli 83)
Zeitschrift fuer Physik C, 20(1983) S.207-12

CIERJACKS, S.; HINO, Y.; HOWE, S.D.; RAUPP, F.; BUTH, L.
Differential neutron production cross sections for 590 MeV protons.
Boeckhoff, K.H. [Hrsg.]
Nuclear Data for Science and Technology: Proc.of the Internat.Conf., Antwerpen, B, September 6-10, 1982
Dordrecht[u.a.] : Reidel Publ.Co. 1983 S.383-86

CIERJACKS, S.; LJUNGFELT, S.; MANKIN, U.; PETKOVIC, T.; SCHMIDT, G.; ULLRICH, H.; [KfK-MITARB.]; U.A.
Isospin dependence of pion absorption on nucleon pairs in ^{3}He.
SIN-PR 83/15 (Oktober 83)
Physics Letters B, 137(1984) S.329-33

CIERJACKS, S.; HINO, K.; FILGES, D.; ARMSTRONG, T.W.
Progress report on nuclear data research in the Institut fuer Kernphysik; in Progress report on nuclear data research in the Fed.Rep. of Germany for the period April 1, 1982 to March 30, 1983
NEANDC(E)-242V, FIZ KA--06

CIERJACKS, S.; BEHRENS, H.; [HRSG.]
Progress report on nuclear data research in the Fed.Rep. of Germany for the period April 1, 1982 to March 30, 1983
NEANDC(E)-242V, FIZ KA--06, August 83

DEGITZ, H.; KLEIN, U.; KLUGE, W.; MATTHAEY, H.; WIEDNER, U.
Coulomb-nuclear interference in the scattering of pions on ^{12}C at 76 MeV.
Physics Letters B, 141(1984) S.42-44

DEMBCZYNSKI, J.; REBEL, H.
Fine- and hyperfine structure analysis of the odd configurations in the lead atom.
KfK-3606 (November 83)
Zeitschrift fuer Physik A, 315(1984) S.137-44

DOLL, P.; HAESNER, B.; HIEBERT, J.C.; KLAGES, H.O.; KRUPP, H.; PLISCHKE, P.; WILCZYNSKI, J.; ZANKEL, H.
Analyzing power measurement and phase shift analysis for the n-^{4}He system up to 50 MeV.
Zeitnitz, B. [Hrsg.]
Few Body Problems in Physics. Proc.of the 10th Internat.IUPAP Conf.on Few Body Problems in Physics, Karlsruhe, August 21-27, 1983.
Vol. II
Amsterdam [u.a.]: North-Holland 1984 S.543-44

DUMBRAJS, O.; FROEHLICH, J.; KLEIN, U.; SCHLAILE, H.G.
Analysis of π^{+-}-^{12}C elastic scattering.
Physical Review C, 29(1984) S.581

ENGLER, J.
Status and perspectives of liquid argon calorimeters.
2nd Conf.on Advanced Detectors, Pisa, I, June 3-7, 1983. Invited talk
KfK-3595 (Oktober 83)

ENGLER, J.; KEIM, H.
A liquid ionization chamber using tetramethylsilane.
KfK-3638 (Dezember 83)

ENGLER, J.
Electromagnetic calorimeters using wire chambers. Invited talk.
Wire Chamber Conf., Wien, A, February 15-18, 1983.
Nuclear Instruments and Methods, 217(1983) S.9-18

EYRICH, W.; FUCHS, K.; HOFMANN, A.; SCHEIB, U.; STEUER, H.; REBEL, H.
Direct decay component of the giant-monopole-resonance region in ^{208}Pb.
Physical Review C, 29(1984) S.418-24

FLUEGGE, G.
Search for new particles at PETRA.
KfK-3758 (Juni 84)

GILS, H.J.; REBEL, H.; FRIEDMAN, E.
Nuclear densities of 1fsub(7/2) nuclei from elastic alpha-particle scattering.
KfK-3556 (Dezember 83)

GILS, H.J.
Local density approximation in effective density-dependent αN-interactions.
KfK-3555 (November 83)
Zeitschrift fuer Physik A, 317(1984) S.65-73

GILS, H.J.
The Karlsruhe code MODINA for model independent analysis of elastic scattering of spinless particles.
KfK-3063 1.Suppl. (Dezember 83)

GILS, H.J.; REBEL, H.; FRIEDMAN, E.
Isotopic and isotonic differences between α particle optical potentials and nuclear densities of 1fsub(7/2) nuclei.
Physical Review C, 29(1984) S.1295-1306

GOTTA, D.
X-ray spectroscopy of the antiproton-proton-system in the cyclotron trap.
Gastaldi, U.; Klapisch, R. [Hrsg.]
Proc.of a Workshop on Physics at LEAR with Low-Energy Cooled Antiprotons, held at Erice, I, May 9-16, 1982
New York [u.a.]: Plenum Pr., 1984. S.165-70

GUIGAS, R.; BLUEM, P.; KOCH, H.; MEYER, M.; POTH, H.; RAICH, U.; RICHTER, B.; BACKENSTOSS, G.; PAVLOPOULOS, P.; TAUSCHER, L.; ADIELS, L.; FRANSSON, K.; NILSSON, A.; SUFFERT, M.; ZIOUTAS, K.
Strong interaction effects in antiprotonic $^{6}Li/^{7}Li$ atoms.
Physics Letters B, 137(1984) S.323-28

HAESNER, B.; HEERINGA, W.; KLAGES, H.O.; DOBIASCH, H.; SCHMALZ, G.; SCHWARZ, P.; WILCZYNSKI, J.; ZEITNITZ, B.; KAEPPELER, F.
Measurement of the ^{3}He and ^{4}He total neutron cross section up to 40 MeV.
Physical Review C, 28(1983) S.995-99

HECK, D.
Nuclear microprobe analysis at Karlsruhe.
10th Internat.Congress on X-Ray Optics and Microanalysis (ICXOM), Toulouse, F, September 5-9, 1983
Journal de Physique, Colloque C2, Suppl.au n°2, 45(1984) S.C2/245-48

HECK, D.; ROKITA, E.
Application of the Karlsruhe proton microprobe to medical samples.
3rd Internat.Conf.on Particle Induced X-Ray Emission (PIXE) and its Analytical Applications, Heidelberg, July 18-22, 1983
Nuclear Instruments and Methods, 231(1984) S.606-10

HECK, D.; ROKITA, E.
Local matrix mass thickness determination in scanned micropixe by proton backscattering.
3rd Internat.Conf.on Particle Induced X-Ray Emission (PIXE) and its Analytical Applications, Heidelberg, July 18-22, 1983
Nuclear Instruments and Methods, 231(1984) S.259-62

HEERINGA, W.; MASCHUW, R.
Ein polarisiertes Protonentarget als Anwendung der Karlsruher Kernpolarisationsanlage.
KfK-Nachrichten, 16(1984) S.49-55

HOFTIEZER, J.; MUTCHLER, G.S.; WEDDIGEN, CH.; KONTER, J.A.; MANGO, S.; BERDOZ, A.; FAVIER, B.; FOROUGHI, F.
The spin-correlation coefficient Asub(xz) of the reaction pp→πd for proton energies between 500 and 600 MeV.
Nuclear Physics A, 412(1984) S.273-85

HOFTIEZER, J.; WEDDIGEN, CH.; CHATELAIN, P.; FAVIER, B.; FOROUGHI, F.; PIFFARETTI, J.; JACCARD, S.; WALDEN, P.
The analysing power of the reaction pp→πd for proton energies between 500 and 600 MeV.
Nuclear Physics A, 412(1984) S.286-93

HUETTEN, L.; POTH, H.; WOLF, A.; HAENROTH, H.; HILL, CH.
The electron cooling device for LEAR.
Gastaldi, U.; Klapisch, R. [Hrsg.]
Proc.of a Workshop on Physics at LEAR with Low-Energy Cooled Antiprotons, held at Erice, I, May 9-16, 1982
New York [u.a.]: Plenum Pr., 1984. S.605

JAKI, J.
Bau und Test einer vertifikalen Driftkammer.
Diplomarbeit, Universitaet Karlsruhe 1984

KAPPELER, F.
The status of the sigmaN-curve and the s-process neutron density.
Nuclear Astrophysics: proc.of the 2nd workshop, Tegernsee, June 6-10, 1983
Garching: Max-Planck-Institut fuer Physik und Astrophysik 1983 S.82-85

KILIAN, K.; MOEHL, D.; GSPANN, I.; POTH, H.
Internal targets for LEAR.
Gastaldi, U.; Klapisch, R. [Hrsg.]
Proc.of a Workshop on Physics at LEAR with Low-Energy Cooled Antiprotons, held at Erice, I, May 9-16, 1982
New York [u.a.]: Plenum Pr., 1984. S.677

KLAGES, H.O.; DOBIASCH, H.; DOLL, P.; KRUPP, H.; OEXNER, M.; PLISCHKE, P.; ZEITNITZ, B.; BRADY, F.P.; HIEBERT, J.C.
POLKA - a polarized continuous energy neutron beam source at the Karlsruhe Cyclotron.
Nuclear Instruments and Methods, 219(1984) S.269-74

KUESTER, H.
Investigation of tau pair production at PETRA.
KfK-3610 (November 83)

KUHN, E.; DERON, S.; OTTMAR, H.; KOCH, L.; STOJANIK, B.
Reference values of the solutions used in the KfK K-edge densitometer calibration, task C.2.
JOPAG/11.83-PRG-75

MANGER, D.
Das Programm zur Ueberwachung und Steuerung der Vakuumanlage des Karlsruher Magnetspektrographen 'Little John'.
KfK-3702B (April 84)

MASCHUW, R.
Neutrino physics at the Rutherford SNS.
Allred, J.C. et al. [Hrsg.]
Proc.of the 3rd LAMPF II Workshop, Los Alamos National Laboratory, Los Alamos, N.M., July 18-28, 1983
LA-9933-C (November 83) Vol.I S.405-18

MATHIE, E.L.; SMITH, G.R.; BOSCHITZ, E.; HOFTIEZER, J.; MEYER, M.
Positive pion absorption on deuterium at energies above the 3,3 resonance.
Zeitschrift fuer Physik A, 313(1983) S.108-10

MATHIE, E.L.; SMITH, G.R.; BOSCHITZ, E.T.; MEYER, M.; VOGLER, F.; DAUM, M.; MANGO, S.; KONTER, J.A.
Search for rapid angular and energy dependence of dsigma/dOmega and iT_{11} in large angle π-d elastic scattering.
Physical Review C, 28(1983) S.2558-60

OED, A.; GELTENBORT, P.; BISSOT, R.; GOENNENWEIN, F.; PERRIN, P.; AKER, E.; ENGELHARDT, D.
Amass spectrometer for fission fragments based on time-of-flight and energy measurements.
Nuclear Istruments and Methods, 219(1984) S.569-74

MUELLER, R.; NAQVI, A.A.; KAEPPELER, F.; DICKMANN, F.
Fragment velocities, energies, and masses from fast neutron induced fission of ^{235}U.
Physical Review C, 29(1984) S.885-905

OEHLSCHLAEGER, J.
Die Prozedur BIPLOT zur Plotter-Ausgabe von GS-Bildern.
KfK-3748 (Mai 84)

OTTMAR, H.; EBERLE, H.; MICHEL-PIPER, I.; KUHN, E.
Evaluation of the KfK K-edge densitometer calibration, task C.2.
JOPAC/11.83-PRG-76

PENZHORN, R.D.; WALTER, G.; BEER, H.
Die chemische Fixierung von Kryptonisotopen in Zeolith 5A. Voraussetzung fuer die Messung von 25 keV Neutroneneinfangquerschnitten mit der Aktivierungstechnik.
Zeitschrift fuer Naturforschung, 38a(1983) S.712-18

PLANETA, R.; KLEWE-NEBENIUS, H.; NEUMANN, B.; BUSCHMANN, J.; GILS, H.J.; REBEL, H.; ZAGROMSKI, S.; FREINDL, L.; GROTOWSKI, K.
Investigation of the reaction $^{6}Li+^{40}Ca$ at 156 MeV in a coincidence experiment.
KfK-3642 (Dezember 83)

POTH, H.
A possibility to determine the antiprotonH$^-$ mass difference with stored and cooled antiproton and H$^-$ beams in LEAR.
Gastaldi, U.; Klapisch, R. [Hrsg.]
Proc.of a Workshop on Physics at LEAR with Low-Energy Cooled Antiprotons, held at Erice, I, May 9-16, 1982
New York [u.a.]: Plenum Pr., 1984. S.779

POTH, H.
Physics with antiprotonic atoms.
Gastaldi, U.; Klapisch, R. [Hrsg.]
Proc.of a Workshop on Physics at LEAR with Low-Energy Cooled Antiprotons, held at Erice, I, May 9-16, 1982
New York [u.a.]: Plenum Pr., 1984. S.567

RICHTER, B.; BLUEM, P.; GLOECKNER, M.; GUIGAS, R.; KOCH, H.; KOEHLER, T.; MEYER, M.; POTH, H.; RAICH, U.; [KfK-MITARB.]; U.A.
New results in the search for narrow states in the proton antiproton-system below threshold.
Physics Letters B, 126(1982) S.284-88

SCHATZ, G.
The ^{176}Lu-^{176}Hf s-process chronometer and planned projects with a 4πBGO detector.
Nuclear Astrophysics : Proc.of the 2nd workshop, Tegernsee, June 6-10, 1983
Garching : Max-Planck-Institut fuer Physik und Astrophysik, 1983. - S.71-72

SCHMITT, C.; GUESSOUS, A.; BOCQUET, J.P.; CLERC, H.G.; BRISSOT, R.; ENGELHARDT, D.; FAUST, H.R.; GOENNENWEIN, F.; MUTTER, M.; NIEFENECKER, H.; PANNICKE, J.; RISTORI, CH.; THEOBALD, J.P.
Fission yields at different fission product energies for thermal-neutron induced fission of ^{239}Pu.
IKDA Bericht 84/2 (1984)

SCHNEIDER, H.
Semileptonic decays of c and b quarks.
KfK-3643 (Dezember 83)

SCHWANNER, I.; BACKENSTOSS, G.; KOWALD, W.; TAUSCHER, L.; WEYER, H.J.; GOTTA, D.; ULLRICH, H.
Pionic and muonic X-ray measurements on light isotopes.
Nuclear Physics A, 412(1984) S.253-72

SIMONS, L.M.; WUEEST, J.
A new low level counting system.
SIN Newsletter, No 15(1982) S.NL56-NL60

SMITH, G.R.; MATHIE, E.L.; BOSCHITZ, E.T.; MEYER, M.; VOGLER, F.; DAUM, M.; MANGO, S.; KONTER, J.A.
Measurements of iT_{11} in π-dsub(pol) scattering between 140 and 325 MeV.
Zeitnitz, B. [Hrsg.]
Few Body Problems in Physics. Proc.of the 10th Internat.IUPAP Conf.on Few Body Problems in Physics, Karlsruhe, August 21-27, 1983.
Vol. II
Amsterdam [u.a.]: North-Holland 1984 S.173-76

SRIVASTAVA, D.K.; REBEL, H.
The density dependence of the effective alpha-nucleon force and isoscalar transition rates of nuclei.
KfK-3586 (September 83)
Zeitschrift fuer Physik A, 316(1984) S.225-31

SRIVASTAVA, D.K.; REBEL, H.
Isoscalar transition rates of s-d shell nuclei using a modified implicit folding procedure.
KfK-3708 (Februar 84)

SRIVASTAVA, D.K.; REBEL, H.
Dynamic density dependence of the alpha-nucleon force in folding models of inelastic scattering of alpha-particles.
KfK-3735 (April 84)

SRIVASTAVA, D.K.; REBEL, H.
Evidence for a dynamic density dependence of the alpha-nucleon force in inelastic scattering of alpha-particles.
Journal of Physics G, 10(1984) S.L127-L132

VOGLER, F.; OLSZEWSKI, R.; MEYER, M.; MATHIE, E.L.; SMITH, G.R.; BOSCHITZ, E.; CHAKRAVARTI, S.; DEHNHARD, D.; THIES, M.
Measurement of the $^{12}C(\pi\pi'\gamma)$ ^{12}C (2^+,T=0; 4.44 MeV) angular correlations: a test of the isobar - hole model.
Physics Letters B, 134(1984) S.161-65

WALTER, G.; BEER, H.
The solar mercury abundance.
Astronomy and Astrophysics, 123(1983) S.279-82

WALTER, G.; LEUGERS, B.; KAEPPELER, F.; BAO, Z.Y.; ERBE, D.; RUPP, G.; REFFO, G.; FABBRI, F.
Neutron capture cross sections of the krypton isotopes and the s-process branching at ^{79}Se.
KfK-3652 (Februar 84)

WALTER, G.
Temperatur und Neutronendichte der schwachen Komponente des s-Prozesses.
KfK-3706 (April 84)

WISSHAK, K.; WALTER, G.; KAEPPELER, F.
Self-absorption of neutron capture gamma-rays in gold samples.
KfK-3542 (Juni 83)
Nuclear Instruments and Methods, 219(1984) S.136-40

WISSHAK, H.; KAEPPELER, F.; MACKLIN, R.L.; REFFO, G.; FABBRI, F.
Neutron capture in s-wave resonances of nickel-64.
Nuclear Science and Engineering, 87(1984) S.48-58

WISSHAK, K.; KAEPPELER, F.; REFFO, G.; FABBRI, F.
Neutron capture in s-wave resonances of iron-56, nickel-58, and nickel-60.
Nuclear Science and Engineering, 86(1984) S.168-83

WISSHAK, K.; KAEPPELER, F.
The neutron capture cross section of ^{243}Am in the energy range from 5 to 250 keV.
Boeckhoff, K.H. [Hrsg.]
Nuclear Data for Science and Technology. Proc.of the Internat.Conf., Antwerpen, B, September 6-10, 1982
Dordrecht : Reidel, 1983. - S.215-17

WISSHAK, K.; KAEPPELER, F.
Neutron capture and fission cross section of ^{243}Am in the energy range from 5 to 250 keV.
KfK-3503 (April 83)
Nuclear Science and Engineering, 85(1983) S.251-60

WISSHAK, K.; KAEPPELER, F.; REFFO, G.; FABBRI, F.
Fast neutron capture in actinide isotopes: recent results from Karlsruhe.
Smith, A.B. [Hrsg.]
Fast-Neutron Capture Cross Sections:Proc.of the NEANDC/NEACRP Specialists' Meeting, Argonne, Ill., April 20-23, 1982
ANL-83-4(1983) S.336-45
NEANDC(US) 214L

WISSHAK, K.; KAEPPELER, F.; REFFO, G.; FABBRI, F.
Neutron capture widths of s-wave resonances in ^{56}Fe, supra(58,60)Ni and ^{27}Al.
Smith, A.B. [Hrsg.]
Fast-Neutron Capture Cross Sections: Proc. of the NEANDC/NEACRP Specialist's Meeting, Argonne, Ill., April 20-23, 1982
ANL-83-4(1983) S.417-29
NEANDC(US) 214L

WOLF, A.; HUETTEN, L.; POTH, H.
Magnetic field measurements in the electron cooling device for LEAR.
KfK-3718 (Juni 84)

YOKOI, K.; TAKAHASHI, K.
On the origin of ^{180}Tasupra(m), the rarest naturally occuring isotope.
Nuclear Astrophysics: proc.of the 2nd workshop, Tegernsee, June 6-10, 1983
Garching: Max-Planck-Institut fuer Physik und Astrophysik 1983 S.89-91

ZEITNITZ, B.; [HRSG.]
Few body problems in physics. Proc.of the 10th internat.IUPAP conf.on few body problems in physics, Karlsruhe, 21-27 August 1983.
Vol. I u. II.
Amsterdam [u.a.]: North-Holland 1984

7.2 CONFERENCE CONTRIBUTIONS

6th Internat.Conf.on Hyperfine Interactions, Groningen, NL, July 4-8, 1983

AURES, R.; HEERINGA, W.; MASCHUW, R.; SCHMIDT, F.K.; POSTMA, H.
Brute-force polarized protons.

DESY Seminar, Hamburg, 15.Juli 1983

MUELLER, H.
CELLO contributions for the Brighton conference.

3rd Internat.Conf.on Particle Induced X-Ray Emission (PIXE) and its Analytical Applications, Heidelberg, July 18-22, 1983

HECK, D.; ROKITA, E.
Local matrix mass thickness determination in scanned micropixe by proton backscattering.

HECK, D.
Application of the Karlsruhe proton microprobe to medical samples.

3rd LAMPF II Workshop, Los Alamos National Laboratory, Los Alamos, N.M., July 18-28, 1983

MASCHUW, R.
Neutrino physics at the Rutherford SNS.

12th Internat.Conf.on High-Energy Accelerators, Batavia, Ill., August 11-16, 1983

HUETTEN, L.; POTH, H.; WOLF, A.; HASEROTH, H.; HILL, C.E.
Status of electron cooling device for LEAR.

10th Internat.IUPAP Conf.on Few Body Problems in Physics, Karlsruhe, August 21-27, 1983.

AURES, R.; BISCHOFF, A.; BRADY, F.P.; DOLL, P.; FINCKH, E.; HEERINGA, W.; HOFMANN, K.; KLAGES, H.O.; WILCZYNSKI, J.; ZEITNITZ, B.
Measurement of the spin correlation parameter Asub(yy) for n-p scattering in the energy range up to 50 MeV.

BACKENSTOSS, G.; CIERJACKS, S.; FURIC, M.; IZYCKI, M.; LJUNGFELT, S.; MANKIN, U.; PETKOVIC, T.; SCHMIDT, G.; STEINACHER, M.; ULLRICH, H.; WEBER, P.; WEYER, H.J.; WEYMARN, K.VON
π^+/π^- absorption in ^{3}He at 120 MeV.

BECK, R.; DICKMANN, F.
Calculation of the momentum distribution of the alpha-deuteron motion in ^{6}Li.

BRADY, F.P.; DOLL, P.; HANSMEYER, J.; HEERINGA, W.; HIEBERT, J.C.; KLAGES, H.O.; PLISCHKE, P.; WILCZYNSKI, J.
Measurements of the neutron-proton analyzing power between 17 and 50 MeV.

BRADY, F.P.; DOLL, P.; FINCKH, E.; HEERINGA, W.; HOFMANN, K.; KLAGES, H.O.; NITZ, W.; WILCZYNSKI, J.
Analyzing power of the elastic n-d scattering from 14 MeV to 50 MeV.

BRADY, F.P.; DOLL, P.; HAESNER, B.; HEERINGA, W.; HOFMANN, K.; JANY, P.; KLAGES, H.O.; MAIER, CHR.; WILCZYNSKI, J.
Measurement of the analyzing power of the elastic n-^{3}He scattering up to 50 MeV.

DOLL, P.; HAESNER, B.; HIEBERT, J.C.; KLAGES, H.O.; KRUPP, H.; PLISCHKE, P.; WILCZYNSKI, J.; ZANKEL, H.
Analyzing power measurement and phase shift analysis for the n-^{4}He system up to 50 MeV.

SMITH, G.R.; MATHIE E.L.; BOSCHITZ, E.T.; MEYER, M.; VOGLER, F.; DAUM, M.; MANGO, S.; KONTER, J.A.
Measurements of iT_{11} π-dsub(pol) scattering between 140 and 325 Mev.

Internat.Conf.on Nuclear Physics, Firenze, I, August 29 - September 3, 1983

BACKENSTOSS, G.; FURIC, M.;HUCK, A.; LJUNGFELD, S.; MANKIN, U.; PETKOVIC, T.; SCHMIDT, G.; ULLRICH, H.; WEBER, P.; WEYER, H.J.; WEYMARN, K.VON
π^+/π^- absorption in ^{3}He at 120 MeV.

MENGONI, A.; REFFO, G.; KAEPPELER, F.; WINTERS, R.R.
The calculation of the neutron cross sections for osmium isotopes and their use on the calibration of the Re/Os clock.

WINTERS, R.R.; KAEPPELER, F.; WISSHAK, K.; REFFO, G.; MENGONI, A.
Supra(148,150)Sm: a test for s-process nucleosynthesis.

10th Internat.Congress on X-Ray Optics and Microanalysis (ICXOM), Toulouse, F, September 5-9, 1983

HECK, D.
Nuclear microprobe analysis at Karlsruhe.

15th Summer School on Nuclear Physics, Mikolajki, PL, September 5-17, 1983
x
REBEL, H.
The variation of nuclear charge radii in the vicinity of ^{208}Pb measured by atomic beam laserspectroscopy.

46th Meeting of the Meteoritical Society, Mainz, September 5-9, 1983

BEER, H.; WALTER, G.; MACKLIN, R.L.; PATCHETT, P.J.
On the astrophysical impact of ^{176}Lu, a long lived radioactive relic of stellar s-process nucleosynthesis.

WALTER, G.; BEER, H.; MACKLIN, R.L.
Neutron capture cross section data basis for the analysis of the s-process chronometer Lu-176 /Hf-176.

20th European Cyclotron Meeting, Kernfysisch Versneller Instituut, Groningen, September 6-9, 1983.

BIALY, J.; HEINZMANN, H.; KAPPEL, W.R.; KOEGEL, B.; SCHWEICKERT, H.; THOUW, T.

Computer control for the new compact cyclotron installation in Karlsruhe.

SCHWABE, J.; SCHWEICKERT, H.
Modification of the Karlsruhe isochronous cyclotron.

IAEA Advisory Group Meeting on the Nondestructive Determination of the Isotopic Contents of Plutonium Samples, Wien, A, October 12-21, 1983

OTTMAR, H.; EBERLE, H.; MATUSSEK, P.
Nondestructive isotopic assay on bulk samples of reactor-grade plutonium: a performance evaluation of practical measurement approaches for in-field applications.

Meeting of the Nuclear Physics Division of the American Physical Society, Notre Dame, Ind., October 13-15, 1983

MATHEWS, G.J.; WARD, R.A.; KAEPPELER, F.
Neutron capture cross sections and the stellar nucleosynthesis of neodymium isotopes.

MATHEWS, G.J.; KAEPPELER, F.; WALTER, G.
Stellar neutron capture cross section for supra(46,48)Ca.

Illinois Workshop on Challenges and New Developments in Nucleosynthesis, Williams Bay, Wis., October 19-20, 1983

KAEPPELER, F.
More precise neutron capture cross sections: needs and experimental possibilities.

Workshop on the Physics Program at CELSIUS, Uppsala, S, 7.-9.November 1983

POTH, H.
Aspects of reaction threshold studies.

POTH, H.
Remarks about electron cooling in storage rings

Workshop on Nucleosynthesis, Universite Libre de Bruxelles, B, 8.Dezember 1983

KAEPPELER, F.
Nuclear physics data for stellar s-process nucleosynthesis.

Seminar fuer Kern- und Teilchenphysik, Universitaet Basel, CH, 15.Dezember 1983

GILS, H.J.
Untersuchungen der Kernmaterieverteilung in der 1fsub(7/2)-Schale mittels elastischer α-Teilchen-Streuung.

LAMPF-Meeting on Pion-Nucleus Interactions at Low Energy, Los Alamos, N.M., January 6, 1984

KLUGE, W.
Future experimental programme with the low energy pion spectrometer LEPS at SIN.

MATTHAEY, H.
Status of the low energy pion spectrometer project LEPS.

16.Gasteiner internat.Symp. 'Radioaktive Isotope in Klinik und Forschung', Bad Gastein, 9.-12.Januar 1984

BERBERICH, R.; HANSER, A.; SCHMIDT, E.L.; STEINSTRAESSER, A.; GARTH, H.
Myokardszintigraphie und Bestimmung der relativen Myokardperfusion mit einem reinen Rb-81/Kr-81m-Gemisch.

General Meeting of the American Physical Society, San Antonio, Tex., January 30 - February 2, 1984

SMITH, G.R.; MATHIE, E.L.; BOSCHITZ, E.; OTTERMANN, C.; DAUM, M.; MANGO, S.; KONTER, T.; MEYER, M.; OLZEWSKI, R.; VOGLER, F.
Comprehensive measurements of iT_{11} in πdsupra(+) elastic scattering.

Rencontre de Moriond, LaPlagne, F, 1 Mars 1984

FLUEGGE, G.
Search for new particles at PETRA.

Fruehjahrstagung DPG, Atomphysik, Massenspektrometrie, Quantenoptik, Giessen, 19.-23.Maerz 1984.

ANSELMENT, M.; HANSER, A.; HOEFFGEN, J.; GOERING, S.; MEISEL, G.; REBEL, H.; SCHATZ, G.
Laserspektroskopie an stabilen und radioaktiven Sn-Atomen.

HEFTER, E.F.; REBEL, H.
The relative charge radii of tin isotopes.

Fruehjahrstagung DPG, Kernphysik, Innsbruck, A, 26.-30.Maerz 1984

ALBINSKA, M.; KLEWE-NEBENIUS, H.; PLANETA, R.; GILS, H.J.; BUSCHMANN, J.; ZAGROMSKI, S.; GROTOWSKI, K.; REBEL, H.
The α + ^{40}Ca interaction at 104 MeV(LAB).

ALBINSKA, M.; ALBINSKI, J.; KLEWE-NEBENIUS, H.; REBEL, H.; GILS, H.J.; BUSCHMANN, J.; ZAGROMSKI, S.
Inclusive γ-ray spectra form the ^{6}Li+^{208}Pb interaction at 12-26 MeV/A.

ANSELMENT, M.; HANSER, A.; HOEFFGEN, J.; GOERING, S.; MEISEL, G.; REBEL, H.; SCHATZ, G.
Die Variation der Ladungsradien der Sn-Isotope aus Messungen der Isotopieverschiebung und Hyperfeinstruktur der Sn-Resonanzlinie (lambda=286nm).

AURES, R.; BRADY, F.P.; DOLL, P.; HANSMEYER, J.; HEERINGA, W.; HIEBERT, J.; HOFMANN, K.; KLAGES, H.O.; KRUPP, H.; PLISCHKE, P.; WILCZYNSKI, J.; ZEITNITZ, B.
High precision n - p scattering experiments and new NN phase-shift analyses in the energy range up to 50 MeV.

BECK, R.; DICKMANN, F.; KRUPPA, A.
The cluster model with breathing clusters.

BECK, R.; DICKMANN, F.
Effects of the Pauli principle in quasi-elastic cluster knockout reactions.

BIALY, J.; HEINZMANN, H.; KAPPEL, W.R.; KOEGEL, B.; RUDOLPH, G.; SCHWEICKERT, H.; THOUW, T.J.
Das Rechner-Ueberwachungssystem fuer das Karlsruhe Kompakt-Zyklotron.

BISCHOFF, A.; BRADY, F.P.; DOLL, P.; KLAGES, H.O.; KRUPP, H.
Development and test of MWPC's for neutron induced reactions.

BLUEM, P.; GOTTA, D.; KUNOLD, W.; MEISSNER, K.; SCHNEIDER, M.; SIMONS, L.M.
Erzeugung hoechster Stoppdichten mit einer Zyklotronfalle.

BLUEM, P.; HANCOCK, A.D.; HAUTH, J.; KOCH, H.; KOEHLER, TH.; KREISSL, A.; POTH, H.; RAICH, U.; ROHMANN, D.; SUFFERT, M.; NILSSON, A.; CARIUS, S.; CHARALAMBUS, S.; CHARDALAS, M.; DEDOUSSIS, S.; TAUSCHER, L.; FINDEISEN, C.; REPOND, J.
Erste Ergebnisse vom LEAR Antiproton-Strahl.

BRADY, F.P.; DOLL, P.; HEERINGA, W.; KLAGES, H.O.; KRUPP, H.; WILCZYNSKI, J.
Experimental set-up for the measurement of spin-spin cross sections of various targets for neutrons of 20 - 50 MeV.

BRADY, F.P.; DOLL, P.; HANSMEYER, J.; HEERINGA, W.; HOFMANN, K.; JANY, P.; KLAGES, H.O.; MAIER, C.; WILCZYNSKI, J.
Analyzing power of the elastic n-^{3}He scattering and phase-shift analyses in the n-^{3}He system.

BRADY, F.P.; DOLL, P.; FINCKH, E.; HOFMANN, K.; KLAGES, H.O.; KOIKE, Y.; NITZ, W.; WILCZYNSKI, J.
Measurement of the elastic and inelastic n-d scattering up to 50 MeV.

CIERJACKS, S.; LJUNGFELT, S.; MANKIN, U.; SCHMIDT, G.; ULLRICH, H.; BACKENSTOSS, G.; IZYCKI, M.; STEINACHER, M.; WEBER, P.; WEYER, H.J.; WEYMARN, K.VON; FURIC, M.; PETKOVIC, T.
Pion Absorption im Flug an ^{3}He.

DOLL, P.; HEERINGA, W.; HOFMANN, K.; JANY, P.; KLAGES, H.O.; KRUPP, H.; MAIER, C.; WILCZYNSKI, J.
Measurement of the analyzing power of the elastic n - ^{3}He scattering at low energies.

DREXLIN, G.; GEMMEKE, H.; GIORGINIS, G.; GRIMM, A.; GUMBSHEIMER, R.; HUCKER, H.; HUSSON, L.; KIONTKE, S.; MASCHUW, R.; MOMAYEZI, M.; OTTMANN, K.H.; PLISCHKE, P.; RAUPP, F.; REMANE, E.; REUSCHER, M.; SCHMIDT, F.K.; SCHULZ, R.; SPOHRER, G.; WOCHELE, J.; ZEITNITZ, B.; FINCKH, E.; KRETSCHMER, W.; STAUBER, K.; BOOTH, N.E.; EDGINGTON, J.A.
KARMEN - The Karlsruhe Rutherford medium energy neutrino project.

EHRET, H.P.; SCHWABE, J.; SCHWEICKERT, H.; STARZEWSKI, G.; WIERBA, W.
On the possibility to convert the Karlsruhe Isochronous Cyclotron to an energy variable machine.

ESCHNER, W.; SCHMIDT-OTT, W.D.; GIPPERT, K.L.; RUNTE, E.; BEER, H.; WALTER, G.; KIRCHNER, R.; KLEPPER, O.; ROECKL, E.; SCHARDT, D.
The ß-dacay branch of ^{180}Lu+supra(180m)Hf for evaluation of the r-process nucleosynthesis of supra(180m)Ta.

EYRICH, W.; FUCHS, K.; HOFMANN, A.; MUEHLDORFER, B.; REBEL, H.; SCHEIB, U.; TRESP, M.
Untersuchung von Riesenresonanzen in (^{6}Li, ^{6}Li')- und (^{6}Li,^{6}Li'n)-Experimenten.

EYRICH, W.; FUCHS, K.; HOFMANN, A.; MUEHLDORFER, B.; REBEL, H.; SCHEIB, U.; SCHLOESSER, H.
Untersuchung des γ-Zerfalls der LEOR in ^{90}Zr.

GILS, H.J.; FRIEDMAN, E.; REBEL, H.; BUSCHMANN, J.; DUERRSCHNABEL, D.; HODGSON, P.E.; ZAGROMSKI, S.
Untersuchungen der Kernmaterieverteilungen stabiler Kerne der 1fsub(7/2)-Schale mittels elastischer α-Teilchen-Streuung.

KAEPPELER, F.; WALTER, G.; MATHEWS, G.J.
Stellare Neutroneneinfangraten von ^{46}Ca und ^{48}Ca.

KHAN, S.; KIHM, TH.; KNOEPFLE, K.T.; MAIRLE, G.; RIEDESEL, H.; GRABMAYR, P.; WAGNER, G.J.; BECHTOLD, V.; FRIEDRICH, L.
Die (d,^{3}He)- und (d,t)-Reaktionen an ^{32}S und ^{36}S.

MICEK, S.; GILS, H.J.; REBEL, H.; MAJKA, Z.
Die Streuung von 156 MeV ^{6}Li-Ionen an ^{6}Li.

PFEIFFER, A.; KIHM, TH.; KNOEPFLE, K.T.; MAIRLE, G.; SEEGERT, G.; GRABMAYR, P.; WAGNER, G.J.; BECHTOLD, V.; FRIEDRICH, L.
Ueber die Anregung tief gebundener Lochzustaende im Zr-Bereich durch (d,^{3}He)- und (d,t)-Reaktionen.

PLANETA, R.; KLEWE-NEBENIUS, H.; NEUMANN, B.; ALBINSKA, M.; ALBINSKI, J.; BUSCHMANN, J.; GILS, H.J.; REBEL, H.; ZAGROMSKI, S.; FREINDL, L.; GROTOWSKI, K.
Investigation of the inelastic break-up reaction of 156 MeV ^{6}Li by (light particle, γ) coincidence measurements.

SIMONS, L.M.
Protonium am LEAR.

SMITH, G.R.; MATHIE, E.L.; BOSCHITZ, E.; OTTERMANN, C.; DAUM, M.; MANGO, S.; KONTER, T.; MEYER, M.; OLZEWSKI, R.; VOGLER, F.
Neue Messungen der Vektoranalysierstaerke i T_{11} in der elastischen π - dsub(pol) Streuung.

SRIVASTAVA, D.K.; REBEL, H.
Studies of isoscalar transitions in nuclei with density-dependent forces.

TAUSCHER, L.; ADIELS, L.; BACKENSTOSS, G.; BERGSTROEM, I.; BLUEM, P.; FRANSSON, K.; KEREK, A.; KOCH, H.; PAVLOPOULOS, P.; RICHTER, B.; REPOND, J.; SUFFERT, M.; TROESTER, D.; ZIOUTAS, K.
Experimentelle Beobachtung von Baryonium Zustaenden bei der Antiproton Annihilation in ^{4}He.

WARD, R.A.; TAKAHASHI, K.; YOKOI, K.
The solar abundance of ^{164}Er and the s-process.

WISSHAK, K.; KAEPPELER, F.; SCHATZ, G.
Untersuchungen zum Bau eines 4π Detektors aus Barium-Fluorid zur Bestimmung von Neutroneneinfangquerschnitten im keV-Bereich.

<u>European Conf.on Geochronology</u>, Braunschweig, March 26-31, 1984

TODT, W.; CLIFF, R.A.; HANSER, A.; HOFMANN, A.W.
^{202}Pb + ^{205}Pb double spike for lead isotopic analyses.

<u>Joint Spring Meeting of the Elementary Particle Physics</u> Sections of the Belgische Natuurkundige Vereniging, Deutsche Physikalische Gesellschaft, Nederlandse Natuurkundige Vereniging, Bielefeld, April 2-4, 1984

ACHTERBERG, O.
Search for scalar boson exchange in $e^{+}e^{-}$ annihilation.

ENGLER, J.; FORSTBAUER, B.; KEIM, H.
A liquid ionization chamber using tetramethylsilane (TMS).

HENKES, TH.
Determination of the strong coupling constant in $e^{+}e^{-}$-annihilation into hadrons.

HOPP, G.
Analysis of hadronic events in e^+e^--annihilation with different fragmentation models.

KRUEGER, M.
Search for new heavy quarks in e^+e^--collisions up to 45.22 GeV C.M. energy.

Symp. 'Instrumental Multi-Element-Analysis', Juelich, April 2-5, 1984

HECK, D.; OCHS, A.; KRATT, C.; MAIER, K.P.
Determination of the microscopic trace element distribution in human liver by proton induced X-ray emission.

Erice School 1984. Internat.School of Nuclear Physics, Erice, I, April 8-20, 1984

ZEITNITZ, B.
Neutrino physics at low and medium energies.

Workshop on the Future of Intermediate Energy Physics in Europe, Freiburg, 10.-13. April 1984

POTH, H.
Physics with antineutrinos.

90. Tagung der Deutschen Gesellschaft fuer innere Medizin, Wiesbaden, 29.April - 3.Mai 1984

OCHS, A.; HECK, D.; KRATT, C.; SCHNEIDER, B.; MAIER, K.P.
Protoneninduzierte Roentgenemission zur Spurenelementanalyse in menschlichen Lebergewebsproben.

10th Internat. Conf. on Cyclotrons and their Applications, East Lansing, Mich., April 30 - May 3, 1984.

BECHTOLD, V.; FRIEDRICH, L.; SCHULZ, F.
External ion sources at the Karlsruhe cyclotron.

BIALY, J.; HEINZMANN, H.; KAPPEL, W.R.; KOEGEL, B.; SCHWEICKERT, H.; RUDOLPH, G.; THOUW, T.J.
Computer control for the beamlines of the Karlsruhe compact cyclotron.

EHRET, H.P.; SCHWABE, J.; SCHWEICKERT, H.; STARZEWSKI, G.; WIERBA, W.
Modification of the Karlsruhe insochronous cyclotron to an energy variable machine.

Conf.on the Interactions between Particles and Nuclear Physics,Steamboat Springs,Colo., Steamboat Springs, Colo., May 23 - 30, 1984.

SMITH, G.R.; MATHIE, E.L.; BOSCHITZ, E.T.; OTTERMANN, C.R.; GYLES, W.; LIST, W.; MANGO, S.; KONTER, J.A.; VAN DEN BRANDT, B.; OLSZEWSKI, R.; VOGLER, F.
Search for dybarion in measurements of the πd(pol) system.

Workshop on Coincident Particle Emission from Continuum States, Bad Honnef, 4. - 7. Juni 1984.

DOERR, M.; FETSCHER, W.; GOTTA, D.; REICH, J.; ULLRICH, H.; BACKENSTOSS, G.; KOWALD, W.; WEYER, H.J.
Composite particle emission following π^- absorption in ^{6}Li.

Neutron Interlab Seminar, Braunschweig, 6.-8.Juni 1984

WISSHAK, K.; KAEPPELER, F.
A 4π gamma detector of barium fluoride for neutron capture cross section measurements in the keV range.

CORVI, F.; BRUSEGAN, A.; BASTIAN, C.; WISSHAK, K.
Measurments relevant to the 1.15 keV task force.

Internat.Symp.on Nuclear Excited States, Lodz, PL, June 25-29, 1984

MICEK, S.; REBEL, H.; GILS, H.J.
Inelastic ^{6}Li + ^{6}Li scattering at 156 MeV.

8. PERSONNEL

Head of the Section IK I: Prof. Dr. Bernhard Zeitnitz

Scientific and Technical staff:

Achterberg, O., Dr.
Apel, W.-D., Dr.
Aures, R., DP
Beiner, A.
Bischoff, A.
Deutsch, G.
Dittmann, R.
Doll., P., Dr.
Drexlin, G.
Engler, J., Dr.
Fink, G.
Flügge, G., Prof.Dr.
Forstbauer, B.
Fries, D.C., Prof.Dr.
Fues, W., Dr.
Gamerdinger, K., DP
Gemmeke, H., Dr.
Giorginis, G., Dr.
Grandegger, W.
Grimm, A.
Grosse-Wiesmann, P., DP
Gumbsheimer, R., DI(FH)
Hagert, H.
Henkes, Th.
Heeringa, W., Dr.
Hofmann, K., DP
Hopp, G., DP
Hucker, H.
Husson, L., Ing.
Jany, P.
Jung, J., DP
Keim, H.
Kiontke, S., DP
Klages, H.O., Dr.
Kleinfeller, J., Dr.
Knapp, J., DP
Krüger, M., DP
Krupp, H., DP
Küster, H., DP
Lutz, R.
Maier, Ch.
Maschuw, R., Dr.
Momayezi, M.
Müller, H., Dr.
Nitz, W.
Oexner, M.
Ottmann, K.H.
Plischke, P., Dr.
Ranitzsch, K.H., Dr.
Raupp, F.
Remane, E.
Reuscher, M.
Schmalz, G., DI
Schmidt, F.K., Dr.
Schneider, H., Dr.
Schnell, R.
Schulz, R.
Skacel, H.
Spohrer, G.
Völker, G.
Wilczynski, J., Dr.
Wochele, J., DP
Ziegler, P.

Guest scientists:

Brady, F.P., Prof.Dr., UC Davis, USA
Garrett, R., Prof.Dr., U. of Auckland, NZ
Koike, Y., Dr., RCNP Osaka, Japan

Head of the Section IK II: Prof. Dr. Anselm Citron

Scientific and Technical staff:

Aker, E., DP
Bacher, R., DP
Barth, H.
Blüm, P., Dr.
Borie, E., Dr.
Boschitz, E., Prof. Dr.
Büche, G., Dr.
Cierjacks, S., Dr.
Engelhardt, D., Prof. Dr.
Göring, K. P.
Gotta, D., Dr.
Gyles, W., Dr.
Habfast, C., DP
Hancock, A., Dr.
Hauth, J.
Heitlinger, K.
Hilgendorff, H.
Höhne, A.
Hütten, L.
Jaki, J.
Jödicke, B.
Kärcher, K.
Klein, U., DP
Kluge, W., Prof. Dr.
Kunold, W., DP
Kunze, M.
Koch, H., Prof. Dr.
Köhler, T., DP
Kreissl, A., DP
List, W., DP
Ljungfelt, S., DP
Mathie, E., Dr.
Matthäy, H., Dr.
Metzler, M.
Ottermann, C.R., Dr.
Poth, H., Dr.
Raich, W., Dr.
Rohmann, D., Dr.
Schneider, M., DP
Schnitzler, S.
Simons, L.M., Dr.
Smith, G.R., Dr.
Ullrich, H., Prof. Dr.
Vogel, R.
Weddigen, Ch., Prof. Dr.
Wiedner, U., DP
Wolf, A., DP
Zach, G.

Guest scientists:

Furić, M., Prof. Dr., U. of Zagreb, YU
Garcilazo, H., Prof. Dr., U. of Mexico City, MEX
Petković, T., U. of Zagreb, YU
Simicević, N., DP, U. of Zagreb, YU

Head of the Section IK III: Prof. Dr. Gerhard Schatz

Scientific and Technical staff:

Anselment, M., DP
Beck, R., Dr.
Beer, H., Dr.
Bekk, K., Dr.
Buschmann, J., Dr.
Dennerlein, H.-D.
Dickmann, F., Dr.
Dürrschnabel, D.
Eberle, H., Ing.
Feurer, B.
Friederich, H.M.
Gils, H.J., Dr.
Göring, S., Dr.
Hanser, A., Dr.
Heck, D., Dr.
Heinz, M.
Hoeffgen, H., Dr.
Jelitto, H., DP
Käppeler, F., Dr.
Kunigkeit, G., Ing.
Liewehr, W., DP
Lingenfelder, B.
Matussek, P., DP
Meisel, G., Dr.
Michel-Piper, I., DI(FH)
Müller, H.
Oehlschläger, J., D.-Math.
Ottmar, H., Dr.
Rebel, H.G., Prof. Dr.
Rupp, G.
Schmidt, K.A., DP
Walter, G., DP
Wisshak, K., Dr.
Zagromski, S., DI(FH)

Guest scientists:

Albinska, M., Dr.
Albinski, J., Dr.
Chongkum, S., DP
Corcalciuk, V., Dr.
Dembczynski, J., Prof. Dr.
Kozik, T., Dr.
Kruppa, H., Dr.
Lovas, R.G., Dr.
Naqvi, A.A., Prof.
Srivastava, K.D., Dr.
Yokoi, K., Dr.

Head of the Cyclotron Laboratory: Dr. Hermann Schweikert

Scientific and Technical staff:

Acharya, H.
Assmus, K.H.
Bauer, G.
Bechtold, V., Dr.
Bialy, J., DP
Biber, J.
Blank, R.
Bollmann, E., DP
Dohrmann, H., Ing.
Dressen, R.
Ehret, H.P.
Erbe, D.
Erdel, E.
Ernst, R.
Fehsenfeld, P., Dr.
Fischböck, T.
Foßhag, E., Dr.
Franz, J.
Friedrich, L., Dr.
Gegenheimer, B.
Günther, O.
Haushahn, G., DP
Heger, V.
Heidenreich, K.
Heinzmann, H., D.-Inf.
Herrmann, P.
Hirth, W.
Holler, H.
Huttel, E., Dr.
Kaltenbaek, J.
Kappel, W.-R., Ing.
Kauther, P.
Kernert, N., DP
Kessel, M.
Kirste, E.
Kleinrahm, A., Dr.
Kögel, B.
Maier, W.
Mangold, D.
Mayl, R.
Möllenbeck, J., Ing.
Peters, J.-W., DP
Pfeiffer, R.
Rämer, Ch., Ing.
Ripp, H.
Roth, H.
Sahm, U., Dr.
Schimpf, P.
Schüssler, B.
Schulz, F., Ing.
Seidel, H.
Seidler, M.
Seitz, J.
Seufert, H.
Sheikh, S.
Stöbener, E., Ing.
Thouw, T., Dr.
Uchatius, R.
Uhlemann, S.
Wiss, L.
Ziegler, P.
Zimmermann, H.

Guest scientists:

Braghirolli, A., DCh.
Schwabe, J., Dr.